Quantification of SE Dopant Contrast in Low Voltage Scanning Electron Microscope

Fatima Nouh Zaggout

Submitted in accordance with the requirements for the degree of Doctor of Philosophy

University of York

Electronics Department

2007

Acknowledgements

Several people have helped in various ways during the research work and in the preparation of this thesis. It is a pleasure, with the completion of this thesis to acknowledge the enormous help I received from them.

I would like to thank my supervisor Prof M. M. El-Gomati for introducing me to the surface science and for his advice, support and encouragement during the project.

I would like to thank the staff in the clean room facility for their help and guidance, particularly Jonathan Cremer for his support with the vacuum systems and Mr Malcolm Law for his help and advice.

A special thanks goes to Mr Torquill Wells for his support and teaching me how to run the Vega SEM and the SLEEM, and for his interesting discussion and providing me with a number of useful and constructive suggestions during the whole period of my existing in York.

I am also grateful to Dr Chris Walker for his critical reading of some parts of this thesis and for his help and advice in interpreting the KPM results.

Above all, I would like to offer my sincere thanks and appreciation for the emotional support, and encouragement I have received from my husband Emad and family during the whole period of my studies.

I would like to thank Prof. M. M. El-Gomati for reading the original manuscript.

Finally, I would like to thank the Libyan government for the scholarship award.

Abstract

This thesis is a detailed study of dopant profiling with the Low Voltage Scanning Electron Microscope (LVSEM) using secondary electron signal. This technique has been applied to a wide variety of doped silicon structures.

Although dopant contrast observed in the SEM has been studied over the past decade by a number of researchers, the explanation of the observed contrast remained incomplete due to the high sensitivity of SE to large number of factors in particular the surface structure. Therefore, in order to provide proper understanding of the SE dopant contrast mechanism, SE dopant contrast behaviour has been further investigated by examining the various factors that could affect the SE contrast in LVSEM; the electron beam energy, the electron dose and the surface conditions.

It was found that contrast is altered as a function of beam energy and new SE dopant contrast behaviour was observed in the presence of an oxide layer on the Si surface. The surface structure of the inspected sample has been investigated for the first time with x-ray photoelectron spectroscopy (XPS). As a result an important factor is realised, where the presence of an oxide layer, which is thought to create a kind of metal-oxide-semiconductor structure that generates subsurface electrical fields is proposed and a new model for the contrast arising from such structure has evolved.

The electron dose effect on SE dopant contrast also revealed new contrast behaviour as a function of electron injection level. This behaviour is believed to be dominated by surface state occupation due to oxide adsorption. The process of introducing excess electrons to the semiconductor would imply a movement of the Fermi level. It is found that the results can be divided into two regimes. At low electron dose, the SE emission starts with n doped regions appearing brighter than p^+- type doped regions in the SE image. On the other hand, at high electron dose, p^+- type doped regions brighter compared with n-type doped Si.

The effect of surface barrier height variation on SE dopant contrast by annealing Al/Si diodes at different temperatures has been studied for the first time. the variation of the Schottky barrier height has been detected as either an inverted contrast or an enhanced contrast in the SE imaging. Moreover, Kelvin Probe Microscopy (KPM) has been utilized to measure barrier height changes due to annealing. In addition, annealing effect revealed some changes in the contrast after annealing to 500°C in a forming gas (non evacuated system). These changes have been explained due to molecular adsorption onto Si surface.

These experimental results have provided insights into the contrast mechanism and have enabled a developed contrast mechanism to be proposed. This is based on the sample preparation method and its influence on the secondary electron emission.

Contents

List of figures

Declaration and Publications

The work presented in this thesis is my own, except where the contributions of others have been acknowledged in the main text or by means of references. No part of my thesis has been submitted for any other degree or diploma.
A list of publications arising from the material presented here is given below

1- Zaggout F. and El-Gomati M. "The effect of barrier height variations in Alloyed Al-Si Schottky barrier diodes on secondary electron contrast of doped semiconductors", Proc. of the 14th Conference of Microscopy of Semiconducting Materials, Oxford (2005) pp.523-526

2- El-Gomati M. Zaggout F. Jayacody H. Tear S. and Wilson K. "Why it is possible to detect regions of semiconductors in low voltage SEM: a review and update", Surf. Interface Anal. **37** (2005) pp.901- 911

General Introduction

Developments in ion beam and electron beam lithography have led to the reduction in size of substrates, which has made it possible to fabricate semiconductor devices with features now measured on the nanoscale (i.e that is less than 100 nanometers (nm) in size). Because device performance depends on the precise placement of dopants, application of semiconductors as electric and optoelectronic devices depends critically on their doping profile. Doping a semiconductor with enough free charge carriers at a certain limit, is often the most important challenge for advancing semiconductor-based high technology. Because for Ultra Large Scale Integrated (ULSI) circuits both lateral and vertical device dimensions are of the same order of magnitude, thus, two–dimensional (2D) dopant characterisation is imperative. Dopant profiles are essential for the development of microelectronics and optoelectronics in the process of device production and for failure analysis. Accurate profiles are routinely required for improving device performance and for investigating the fundamental causes of device failure. Therefore, techniques for two-dimensional dopant profiling are being strongly demanded by the semiconductor industry. These techniques must be fast, non-destructive and of high spatial resolution and provide 2D dopant profiles.

In the last decade, a number of techniques have been used to perform dopant profiling such as Secondary Ion Mass Spectroscopy and Capacitance Voltage Profiling etc. However, none of these techniques fulfil the entire upcoming requirement for the semiconductor industry. Therefore, other techniques are being investigated and developed, such as Scanning Capacitance Microscopy and Scanning Electron Microscopy.

The Scanning Electron Microscope (SEM) has been widely used as an analytical instrument capable of providing information regarding the surface topographical features and sample composition, albeit in a qualitative way only. The modern SEMs can be operated at Low voltages (< 5 kV), due to the use of brighter electron sources and more efficient detectors (such as the in-lens type). This mode is recognised as Low Voltage Scanning Electron Microscopy (LVSEM). By operating SEMs with low beam voltage, the generated Secondary Electron (SE) signal has been found to be extremely

sensitive to semiconductor dopant type and level. In this mode the p-doped patterns generally appear brighter than the n-type regions. This is called "SE dopant contrast". This mode does not cause damage to the sample and some authors reported a maximum contrast level at 1keV. Imaging doped semiconductors structures was also demonstrated in the cathode lens equipped Scanning Low Energy Electron Microscope (SLEEM). In this imaging mode, high contrast level was reported at very low electron energies below 100eV. The realisation of a clear contrast from differently doped areas of a semiconductor in the SE image at low voltages has generated much interest in obtaining 2D dopant distributions. Therefore, many models have been developed to explain SE contrast behaviour from differently doped semiconductor regions.

In this thesis LVSEM has been used to obtain dopant distributions of p- and n-type doped Si samples. Careful experiments were carried out to investigate surface effects on the observed contrast in order to provide proper understanding of the contrast mechanism.

Chapter 1 reviews the importance of semiconductor materials, some basic concepts such as semiconductor theory of p-n junctions, how dopants are introduced to semiconductors and the most commonly used characterisation methods to study such samples. In chapter 2 a general overview is given on the SEM, the signals generated as a result of the interaction of the incident electrons with the solid under study and their detection methods. However, discussion will concentrate on the SE theory relevant to the SE dopant contrast mechanisms rather than giving a full account of the operation of the SEM in the different fields.

Chapter 3 addresses the advantages of operating the SEM at low voltages and the many approaches of LVSEM and how these methods have been utilized to study doping profiling. Finally, the previously suggested dopant contrast mechanism models are briefly discussed.

Chapter 4 is a short chapter explaining the differences between the used SEMs, which might be relevant to doping contrast. As large range of surface analysis instruments have been used throughout this thesis; such as x-ray photoelectron spectroscopy (XPS) and Kelvin Probe Microscopy (KPM), this chapter describes the main features of these

instruments and their usage. It also describes the operating conditions of the surface analysis instruments that have been used in the analysis of the surface layer of the studied samples. In addition, section (4.3) describes the structures of the studied samples in this thesis.

Previous research has demonstrated that SE dopant contrast is dependent on the SEM operating conditions. Furthermore, the effect of surface layer on SE images and the difficulty in obtaining repeatable images due to contamination even in high vacuum conditions has been reported. Therefore, in this research, imaging of doped Si was performed in conventional vacuum environment under different operating condition in order to quantify the electron beam energy and electron dose effects on SE dopant contrast. In chapter 5 the experimental findings as a function of the electron beam energy will be demonstrated as well as the effect of oxidation on SE dopant contrast. For the first time X-ray Photoelectron Spectroscopy (XPS) has been utilized to inspect the surface condition of SEM imaged (inspected) samples in order to quantify its contribution to the obtained contrast. While the effect of electron dose on SE dopant contrast will be presented in Chapter 6.

In chapter 7, the effect of a surface adlayer on SE dopant contrast has been further investigated. In addition, altered contrast is demonstrated by changing the barrier height between doped Si and a thin layer of Al by annealing the diodes at different temperatures. Moreover, KPM has been utilised to measure barrier height change due to annealing in order to correlate barrier height variations with SE dopant contrast behaviour.

Finally, in chapter 8 conclusions and suggestions for further work are given.

Chapter 1: Introduction to Semiconductor Dopant Profiling

(1.1) Introduction

Semiconductors have a conductivity range that lies between insulators and conductors and typically ranges from 10^{-8} to 10^{3} S/cm. This conductivity is generally sensitive to temperature, magnetic field, impurity atoms etc. This sensitivity makes semiconductors one of the most important materials that can be used as the building blocks for electronic devices (Sze, 1985).

The importance of semiconductors lies primarily in the great change in their properties when the number of active electrons in the material is altered. The electron density can be controlled with high sensitivity through doping, optical excitation or external electric fields. In addition, the ability to make semiconductors into electronic devices, which can be used as the building blocks for complicated electronic circuits recognizes them as the most important material in the electronics industry. Due to these properties semiconductor devices have found applications in almost all branches of industry and areas of daily life.

In this introductory chapter we consider some basic properties of semiconductors, their conduction processes that are believed to be responsible for SE dopant contrast and the most commonly used methods to introduce dopants to semiconductors. Finally, methods for measuring dopant profiling in semiconductors will be briefly presented.

(1.2) Semiconductors

Semiconductors may be elemental, i.e composed of atoms such as silicon (Si) and germanium (Ge) or compounds that are a combination of two or more different elements such as gallium arsenide (GaAs) and indium phosphide (InP). This thesis will focus on Si as this is still by far the most used semiconductor to date but also to simplify the problem under study. Since the 1960's, Si has become the most widely used semiconducting material for electronics, for the main reasons that; Si devices exhibit low leakage currents and a stable–high quality silicon dioxide that can be grown thermally, which is an essential step in the fabrication of devices. Si is easily doped to form p- and n- type doped regions. There is also an economic consideration; Si is cheap and readily available (Tyagi, 1991).

Si crystallizes in a diamond-like lattice, with each atom bound to its four nearest neighbours by covalent bonds (The covalent bond is formed by sharing of electrons between the bonded atoms). Bonds between neighboring atoms in a semiconductor in general are only moderately strong; therefore, thermal vibrations impart enough energy to some of bound electrons, enabling them to break some bonds and move freely inside the crystal, which leaves behind a hole. Because the band gap of a semiconductor is not as large as that of an insulator, some electrons will be able to move from the valence band to the conduction band, leaving a hole in the valence band. If an electric field is applied, both electrons in the conduction band and the holes in the valence band will gain some energy and conduct electricity. Band to band transition is determined by the semiconductor bandgap energy (E_g). The variation of bandgap for Si with temperature is given by

$$E_g(T) = 1.17 - \frac{(4.73\times10^{-4})T^2}{(T+636)} \quad \text{eV} \qquad (1.1)$$

where T is the temperature in Kelvin (Sze, 1985).

At room temperature and under normal atmosphere, the value of the bang gap for Si is 1.12eV (Sze, 1985).

(1.3) Intrinsic Semiconductors

An intrinsic semiconductor contains very low levels of impurity atoms compared to the thermally generated electrons and holes. In an intrinsic semiconductor the number of electrons per unit volume in the conduction band (n) is equal to the number of holes per unit volume in the valence band (p), that is

$$n = p = n_i \qquad (1.2)$$

where n_i is the intrinsic carrier density or carrier concentration (Sze, 1985)

The energy band diagram of an intrinsic semiconductor is shown in figure (1.1). The figure shows the valence band (E_v), the conduction band (E_c), the energy band gap(E_g) and the Fermi level (E_F), which is generally lies very close to the middle of the band gap in an intrinsic semiconductor. The Fermi level is defined as the energy level at which the probability of occupation by an electron is exactly one half. The work function of a material (Φ) is defined as the energy required to release an electron from the Fermi level to the vacuum, and is typically a few eV for most elements. The ionization energy

(E_i), is the difference between E_{VAC} and E_V, i.e the energy required to release an electron from the top of the valence band to the vacuum level.

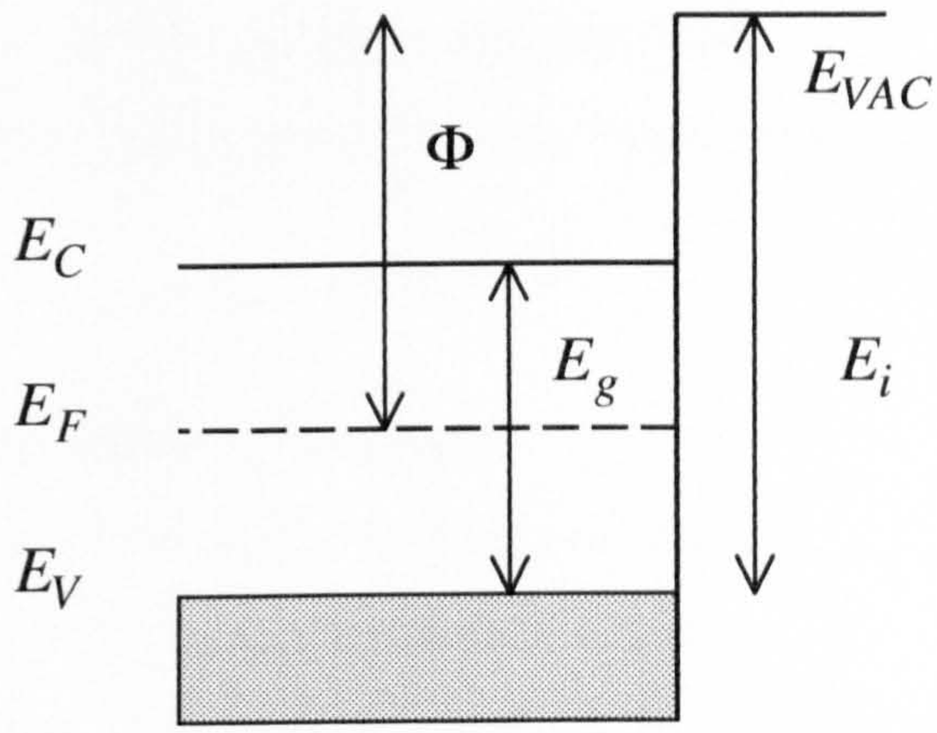

Figure (1.1) Energy band diagram of an intrinsic semiconductor.

(1.4) The Doping of Semiconductors

When a semiconductor is doped with impurities, the semiconductor becomes extrinsic. Dopant atoms may be donors or acceptors. If the dopant atom adds a negative charge carrier (electron) to the conduction band of the semiconductor, it is called a donor and the semiconductor becomes n-type material (i.e. an abundance of electrons in the semiconductor in comparison to holes), resulting in electron current in an applied electric field. Similarly, if the dopant atom creates a positive charge (hole) in the valence band, it is an acceptor because the acceptor atom accepts an extra electron from the valence band, in this case hole current will then dominate in an applied electric field. If both donors and acceptors are present in different concentrations in the same material, the uncompensated carriers will dominate the current.

In n-type material for complete ionization of the dopants, the Fermi level is approximately given by

$$E_C - E_F = kT \ln\left(\frac{N_C}{N_D}\right) \qquad (1.3)$$

where N_D is the concentration of donors

N_C is the conduction band effective density of states

k is Boltzmann constant

The Fermi level is moved towards the conduction band.

Similarly, in p-type material the position of the Fermi level can be calculated from

$$E_F - E_V = kT \ln\left(\frac{N_V}{N_A}\right) \qquad (1.4)$$

where N_A is the concentration of acceptors.

N_V is the valence band effective density of states.

The Fermi level is moved towards the valence band.

The above two equations are applicable only if the doping level is not very high (Sze, 1985). For very highly doped material, the Fermi level can lie within the conduction or valence bands. Although equations (1.3) and (1.4) do not allow $E_F > E_C$ or $E_F < E_V$, in general the change of the Fermi level is dependent on the doping concentration, the type and the temperature. So these equations are useless for describing the position of the Fermi level of degenerate semiconductors (Sze, 1985).

Doping concentration above about 10^{18} cm^{-3} is considered degenerate at room temperature. Degenerately doped silicon contains a proportion of impurity to silicon in the order of parts per thousand. Most of the samples have been used in this study includes degenerately doped regions.

(1.5) Electrical properties of semiconductor surfaces

(1.5.1) Fundamental Concepts

Introduction of dopant atoms to an intrinsic semiconductor results in introducing impurity energy levels within the bandgap but very close to the energy band that corresponds with the dopant type. In other words, donor impurities create states near the conduction band while acceptors create states near the valence band. In addition, the termination of the periodic structure of a semiconductor at its surface results in dangling bonds, which may form localized electronic states within the semiconductor bandgap or a double layer of charge known as a surface dipole. The formation of surface states induces charge transfer between bulk and surface that results in a non-neutral region in

the bulk referred to as the surface Space Charge Region (SCR).

(1.5.2) Gap States

The ideal crystalline semiconductor, results in the appearance of allowed energy bands separated by forbidden energy gaps. The probability of finding an electron in the allowed bands in any unit cell is equal due to the perfect three-dimensional translational symmetry. However, semiconductor termination eliminates this symmetry in the direction perpendicular to the surface. Therefore, the unit cells next to the surface are in general not equivalent to the bulk cells and localized surface states may arise.
The formation of localized surface states includes; dangling bonds, i.e. formation of surface atoms with no upper atom to bind to, surface reconstruction or relaxation, i.e. a change in the position or chemical bonding configuration of surface atoms which minimizes the surface energy (Kronik and Shapira, 1999).

Because of the difficulty in calculation of surface states or interface states, for practical purposes, the electrical and optical behaviour of surface states is characterized by a set of surface states related parameters which may be determined experimentally. These parameters are; the surface state density N_t,(measured in states per unit area), electron and hole occupation n_t and p_t (measured in charge carriers per unit area).

$$n_t = \frac{N_t}{1 + g_t \exp[(E_t - E_F)/kT]} \qquad (1.5)$$

where $n_t + p_t = N_t$

E_t is the surface state energy,

and g_t is the degeneracy factor of the surface state.

(1.5.3) Surface Space Charge Region (SCR)

The created surface states within the gap induce carrier transitions that result in a charge found in surface states in the vicinity of the surface supplied by the underlying bulk. Therefore the carrier density in the vicinity of the surface is expected to deviate from its equilibrium value and result in a surface space charge region (SCR). The surface space charge can be found in three different regimes: (a) Accumulation, where the majority carrier concentration at the surface is larger than its value in the bulk, (b) Depletion,

where the majority carrier concentration at the surface is smaller than its equilibrium value, (c) Inversion where the majority carrier concentration at the surface is smaller than the minority carrier concentration at the surface.

According to the Poisson equation, the relationship between the electric potential and the electric charge is given by:

$$\frac{d}{dx}\left(\varepsilon_s(x)\frac{dV(x)}{dx}\right)=-\rho(x) \qquad (1.6)$$

where x is the coordinate, V(x) is the electric potential, ρ (x) is the charge density in the SCR and $\varepsilon_s(x)$ is the dielectric permittivity of the semiconductor (Kronik and Shapira, 1999).

A non–equilibrium carrier density implies a non zero electric field and potential. This means that even under equilibrium conditions, the surface potential is different from the electric potential for quite some distance in the bulk. Hence the semiconductor bands are bent in the vicinity of the surface.

(1.5.4) Semiconductor Surfaces (Surface Dipoles)

At a free semiconductor surface, electrons of the localized surface states spill out into the vacuum, creating a negative charge in the region just outside the surface, whereas the region just inside the surface is left with a net positive charge (Zangwill, 1988). Therefore, the separation of positive and negative charges over atomic distances creates a microscopic dipole. This dipole creates an electric field that retards further electron emission into the vacuum. i.e the created field works as a barrier opposing electron transfer into the vacuum. As a result electrons reaching the surface are repelled by the negative charge outside the surface and then attracted by the positive charge inside the surface. This barrier is called the potential surface barrier, which is the major contribution to the work function. The dipole contribution is affected by dangling bonds and surface reconstruction, whereas the number of dangling bonds is different on different crystal orientations, therefore the work function depends on the crystal face.

(1.6) The doping Process

The fabrication of semiconductor structures began with the growth of the substrate. Since dopant introduction to semiconductor is a crucial step in the fabrication of a

working device, a number of processes are used to precisely introduce dopants into the semiconductor. Diffusion and ion implantation are the two main processes used to introduce controlled amounts of dopants into semiconductors. They are used to dope selectively the semiconductor substrate to produce either n- or p-type regions.

In the diffusion method, impurities are typically diffused by placing the semiconductor wafers in a furnace and passing an inert gas, which contains high concentration of the desired impurity on the surface through windows etched in the protective barrier layer. The temperature usually ranges between 800 and 1200°C for Si. Boron is the most popular dopant for introducing a p-type Si, while Arsenic and Phosphorus are used as n-type dopants. These three elements have been selected due to their high solubility in Si in the diffusion temperature range. The exact dopant profile depends on the temperature and diffusion time.

More precise control of the impurity atoms, particularly for modern devices made of thin active layers, can be achieved with ion implantation. In this method a high-energy ion beam impinges into a semiconductor substrate, implanting the desired dopant atoms. Typical ion energies are between 30 and 300 keV. After implantation, the material is annealed to reduce lattice damage and to activate the dopant. The required annealing temperature is lower than that required in the diffusion process.

Localization of the doped region may be achieved by growing a thin layer of oxide on the substrate wafer to form a mask. Later, selected regions of the mask can be etched using lithography and chemical solutions. After that dopants are introduced through the etched windows and exposed to the substrate. The remainder masked layer of oxide may affect the SE dopant contrast if this surface has been inspected in the SEM, this effect will be studied in chapter 5 and chapter 6.

Both diffusion and ion implantation are used for fabricating discrete devices and integrated circuits because they complement each other (Jaeger, 1988). For example, diffusion is used to form a deep junction while ion implantation is used to form a shallow junction. The substrates in this work were doped by the diffusion method.

Also dopants can be introduced into the semiconductors by growing Epitaxial Layers on top of the substrate either by Chemical Vapor Deposition (CVD) or Molecular Beam

Epitaxy (MBE). In a CVD system the substrate wafer is supported in a susceptor, which is rotated and heated to a relatively high temperature while gaseous sources are introduced. These gaseous mixtures of host atoms and dopant atoms adsorb onto the surface to find their proper positions within the crystal lattice.

In the MBE processes, the substrate wafer is placed on a rotating plate and kept in temperature ranges between 673 and 1173K. Sources of host atoms and a dopant are stored in a separate effusion ovens that are heated to specific temperatures to give a desired evaporation rate. The thermally evaporated atoms and molecules impinge on the substrate and epitaxial growth occurs. The relative evaporation rate of each source determines the dopant concentration.

Although very precise atomically abrupt layers can be grown With CVD or MBE, diffusion and ion implantation are more effective to selectively incorporate dopants into semiconductors.

After dopants are introduced to a semiconductor, it is crucial to evaluate the doping profiles. It is reported that dopant distribution depends on the method used to introduce them to the semiconductor. For example, an annealing stage following ion implantation process may broaden the doping profile by diffusion of the dopants outside the desired regions. If dopant introduction processes are followed by further thermal oxidation, the dopants near the surface may diffuse through the oxide and escape into the ambient. Therefore, dopants will be redistributed during thermal treatment.

The incorporation of dopants into semiconductors by ion implantation or diffusion are presently well-understood processing steps for the formation of 1D structure, since reliable measurement techniques exist for their characterization. However, when implantation and diffusion are performed through a mask (a sharp corners window), into the substrate, not only vertical but also lateral diffusion occurs during the thermal treatment. Hence, the final doped region will consist of cylindrical or spherical edges. The reduction in size of the devices in ultra large scale integration (ULSI) technologies implies that the resulting lateral extension needs to be controlled very carefully. Since the lateral diffusion and vertical dopant distribution are in the same order of magnitude, the techniques used to determine the dopant distribution must also have nanometer resolution in both directions. In the next section we address the commonly used main techniques to measure the dopant distribution.

(1.7) Dopant Profiling Techniques

The Semiconductor Industry Association (SIA) has defined the needs for dopant profiling techniques, which need to be fast, non-destructive two-dimensional profiling at sub-10nm spatial resolution with high detection sensitivity for dopants in the range $10^{16}cm^{-3}$ to $10^{20}cm^{-3}$. This capability is crucial for the development, optimization, and understanding of future ULSI processes and devices.

There are many characterization methods available for semiconductor dopant profiling, many of these spurred by the SIA roadmap. However, the majority of them are capable of providing only one-dimensional (1-D) dopant profiles such as Secondary Ion Mass Spectroscopy (SIMS), Capacitance–Voltage Probe (CVP), Spreading Resistance Profiling (SRP) and many scanning probe microscopy based techniques which detect different interactions with the samples. Some methods have been extended to provide 2D profiles. However, obtaining 2D profiles in this method requires complicated sample preparation technique such as etching and staining and laborious data deconvolution methods and hence time consuming. Also, the obtained spatial resolution and sensitivity is limited by the sample preparation method. Scanning Probe methods such as Scanning Tunneling Microscopy (STM), Scanning Capacitance Microscopy (SCM) and Atomic Force Microscopy (AFM) involve direct inspection of the dopant distribution and can provide 2D dopant profiles with good spatial resolution. However, special sample preparation is still required for many probe methods and their sensitivity is dependent on tip deconvolution algorithm in order to obtain the correct 2D dopant profiling.

Recently, Electron Holography in the Transmission Electron Microscope has also been reported as a very high resolution technique for 2D profiling of semiconductors, however it is destructive and unsuitable for online inspection. A brief review of the most commonly used techniques follows.

(1.7.1) Secondary Ion Mass Spectroscopy (SIMS)

SIMS is one of few techniques capable of mapping the dopant concentration directly. This is due to its excellent elemental sensitivity (<ppm). In this method, the sample under inspection is bombarded with heavy ions such as Ar^{+}, of energy (1-20) keV, the ionized sputtered atoms are then analysed in a mass spectrometer. This technique

measures the atomic concentration of dopants as a function of depth into the sample, with high depth resolution of ~0.2 nm while the lateral resolution is determined by the ion beam optics (Heimbrook et al, 1996).

The main advantage of SIMS is that it has excellent sensitivity to dopant concentration as low as $10^{12}cm^{-3}$ and it can be applied to any semiconductor material with an accuracy of ±10% (Goeckner et al, 2000). Therefore, it has been used to calibrate profiles obtained by other dopant characterization techniques. Moreover, this detection method is not affected by the existence of surface contamination such as carbon and oxide. On the other hand, SIMS is an intrinsically destructive technique. Sputtering leave craters in the material as well as ion implantation and lattice damage therefore, the atomic mixing off ions and the target material will yield an incorrect composition profile.

SIMS has been used to obtain 2D dopant profiles (Dowsett et al, 1992 and Cooke et al, 1994). SIMS beam at various angles are used to profile the unknown dopant distribution. A polysilicon layer covers the samples and the polysilicon is beveled at the required angle such that the SIMS beam is perpendicular to the bevel. Because SIMS is a destructive technique, several identical samples are required. The various SIMS profiles can therefore be used to extract the 2D profile (Subrahmanyan, 1992). The sensitivity was estimated to be comparable to that of 1D SIMS. Due to its destructive nature SIMS method is still a 1D profiling technique.

(1.7.2) Transmission Electron Microscopy (TEM)

TEM techniques provide the sub 10 nm resolution required to characterize microstructure and chemistry, however conventional intensity images reveal little or no information about local concentration of dopant atoms. Although TEMs do not allow the dopant atoms to be directly observed, they have been applied successfully for 1D dopant profiling to obtain iso-concentration.

The use of TEM to image 2D dopant profiles is based on the enhancement of the contrast between areas with different dopant concentration. It employs two ways of chemical methods for delineating the p-n junction. The first referred to as chemical staining, where the junction is decorated with metal depositions using the principle of galvanic displacement reaction. In this way the change of contrast is due to the large

strain, which results from the difference in size between the substitutional dopant atoms and the Si atoms they replace. The second method referred to as chemical etching, in this way, selective etching techniques are used to preferentially etch the p-type region. The resulting contrast can be due to a thickness difference and a change of lattice parameters that is based on the use of etchants with dopant concentration dependent etching rates.

The chemical staining technique was applied for the first time by Sheng and Marcus (1981) to observe an n-type region in a TEM. These authors have decorated a Si device with copper, but they found that the grain size of the deposits was too large (~0.1μm) preventing the precise location of the junction. Therefore, most recent TEMs rely on chemical etching.

Chemical etching takes place by oxidation and reduction reactions, a commonly used solution for selective etching is a mixture of Nitric (HNO_3) and Hydro Fluoric (HF) acid. Since the etching process is sensitive to dopant concentration, etching produces surface topography at the p-n junction which can be readily imaged using TEM.

Although TEM is a high resolution characterization tool to examine the chemically etched p-n junction, particularly at high magnification, the difficulty in determining the absolute concentration from the TEM cross-section is still reported, as there is no direct measurement of the concentration level. Furthermore, its accuracy for identifying a p-n junction without relying on other techniques such as SIMS and SRP is rather poor (Heimbrook, 1996).

Since the accuracy of the obtained dopant profile depends on the sample preparation technique such as concentration of etching solution, etching time and volume of solution on the sample, careful sample preparation techniques are required. And in order to avoid the difficulties in handling thin fragile samples prepared by chemical etching, it was suggested to use focused ion beam (FIB) for these types of delineation studies. Chemical etching/staining can be used for different materials such as Si and compound semiconductor such as GaAs and InP.

In order to overcome the difficulties in determining the absolute concentration and to

benefit from its high resolution, several modes were incorporated into this technique to get more quantified data. Recently, electron holography has been extended to quantify the electrostatic potential across a Si p-n junction as it is biased electrically in situ in the TEM. Electron holography is an interference–based TEM technique, which can be used to record the phase shift of a high-energy electron wave that has passed through a sample. The resulting phase image can be analyzed to determine the electrostatic potential within the specimen, from which the local charge density can be calculated using Poisson's equation. In this method samples are prepared for TEM examination by using FIB workstation. Great care is taken during sample preparation to minimize the implantation of Ga ions into the sample by exposing the area of interest to the focused beam of Ga ions only at a glancing angle to its surface.

Electron holography images the doping indirectly through electrostatic potential redistribution caused by charge carriers. The images show a clear contrast between n- and p-type doped regions. In general p-type doped areas appear darker than n-type regions.

The main problem related to this investigation method is connected with the specimen preparation that can give rise to the measurement of artefacts due to sample charging and surface dead layers (Rau et al, 1999).

Several attempts have been introduced later to image thin specimens using a scanning transmission electron microscope (STEM) with high angle annular detector (HAAD). This method allows one to distinguish in very thin specimens (less than 5 nm) all the dopant material, however the description of the dopant profile is based on the knowledge of the number of dopant atoms.

Merli et al (2002) have developed a new strategy, which is based on incoherent bright field (BF) imaging at low energy in a SEM operating in transmission mode. The image is formed using the signal produced by the SE resulting from the conversion of transmitted electrons (TE) on a converter and collected by the standard Everhart-Thornley detector. This strategy is presented in chapter 3.

In spite of the above-mentioned difficulties, TEM continues to be used as a dopant profiling method because of its higher resolution compared to many other techniques.

(1.7.3) Scanning Probe Microscopy (SPM)

All SPM techniques are based on the ability to position various types of probes in very close proximity with extremely high precision to the sample under investigation. These probes can detect electrical current, atomic and molecular forces, electrostatic forces or other types of interactions with the sample. Scanning the probe laterally over the sample surface and performing measurements at different locations can obtain detailed maps of surface topography or other properties. The obtained properties can then be analysed as a measurement of the dopant concentration within the semiconductor. The resolution of the SPM is only limited by the sharpness of the tip of the probe used, the accuracy with which the probe can be positioned, surface conditions and the nature of the property being detected. Most methods are limited to p-n junction delineation or provide a semiquantitative image of the differently doped regions. However, recent developments of SPM have shown that the techniques can provide useful information (De Wolf, 2000). In general SPMs can provide sensitivity varying from few angstroms to tens or hundreds of nanometers. The basic SPM characteristic techniques will be reviewed below.

(1.7.3.1) Scanning Capacitance Microscopy (SCM)

The scanning capacitance microscope (SCM) provides a direct method for mapping the dopant distribution in a semiconductor device on a 10 nm scale. In this technique, the sample or the metallic AFM tip is covered with a sufficiently thick insulator layer (in most cases oxides), such that this contact forms a metal–insulator–semiconductor MIS capacitor. By monitoring the capacitance variations as the probe scans across the sample surface, one can measure a 2D carrier concentration profile. If no dielectric layer is used, the tip–sample contact forms a metal–semiconductor M-S structure and one has a so-called Schottky contact. This approach increases the debate about the physical processes that are responsible for signal generation.

Since the total tip–sample capacitance is large compared to the capacitance variations due to different carrier concentrations; SCM is being used to measure the capacitance variations of the sample in comparison to the degree of doping and of the insulator thickness (Basnar et al, 2001) and not the absolute capacitance values. The authors investigated the dependence of the SCM signal on the oxide thickness as well as the

dopant concentration and they have shown a good correlation with conventional MOS theory for the decrease of the capacitance signal with increasing insulator thickness and with increasing dopant concentration.

Most SCMs are based on contact-mode AFM with a conducting tip, and an essentially independent capacitance measurement in parallel. The capacitance between the tip and sample is measured by using a high frequency capacitance sensor, based on a 915 MHz oscillator driving a resonance circuit that is tuned in part by the external capacitance to be measured. High-quality probe tips and surfaces are critical for obtaining accurate measurements of two-dimensional dopant profiles. An extensive review of SCM for 2D dopant profiling is given by Williams (1999).

Since the measured capacitance signal is proportional to the tip interaction area, shrinkage of the tip size will improve the spatial resolution, but also reduce the sensitivity of the capacitance measurement. Reducing the thickness of the oxide layer can increase the sensitivity of the carrier concentration. The response of SCM is not necessarily monotonic with concentration but does depend on the applied experimental conditions as well. The SCM results are extremely sensitive to sample preparation and to the preparation procedure chosen. Furthermore, tip erosion limits the qualitative reproducibility of the SCM data (Basnar et al, 2001). In addition, the accuracy of 2-D carrier profiles that can be extracted from SCM images of doped Si depends on the model used to interpret the SCM differential capacitance data (Kopanski et al, 2002).

(1.7.3.2) Scanning Tunneling Microscopy (STM)

The scanning tunneling microscope is a very surface sensitive SPM technique, which requires a conductive surface. The most direct STM-based dopant profiling method is to simply count the number of dopant atoms appearing in or near the surface atomic plane. Examples are given by Johnson and co-workers (1993), who clearly resolved individual Be and Zn dopant atoms in a cleaved Ga (110) surface. In this method, the negatively charged dopant atoms are attractive to holes and appear in the STM image as protrusions. However, dopant atom counting has not been reported for Si substrates. Further, dopants at the surface and one atomic layer below the surface only could be distinguished from each other and from dopants further below the surface. Despite these

basic limitations, cross sectional STM offers several methods for high-resolution analysis.

Modern STM has been used for p-n junction delineation by detecting differences in tunneling current characteristic between n- and p-type doped materials. The conductive tip induces band bending at the surface; hence the tunneling current depends on dopant type and concentration. By incorporating Current Voltage spectroscopy it is possible to identity differently doped regions and depleted regions.

Feenstra and co-workers (1992) carried out the first detailed imaging and spectroscopic studies of GaAs p-n junctions, observing electronically induced topography. However, such STM measurements on Si can not normally be operated in air due to the presence of the native oxide. It is clear that if the native oxide is removed through sample heating to relative high temperatures ~1000 °C, the dopant distribution is disturbed. Therefore, one has to use in situ cleavage to generate a fresh sample cross-section, which is only possible along certain crystal directions due to the difficult cross-section preparation. The structure of interest must thus be oriented exactly in that direction, limiting the flexibility of the technique. Additionally, it is not always possible to determine the carrier profile with respect to the mask edge and mask shape since the STM cannot image the oxide position due to the requirement of a conductive surface

Despite these complications, 2D junction delineation of cross sectioned Si based structures has been performed for the first time by Kordic and co-workers (1991). Si cross-sectional structures were cleaved in air and UHV and Scanning Tunneling Potentiometry (STP) was used to resolve the location of the junction. Further, they measured differences in tunneling current in p-type, depleted and n type regions for various voltages applied to the junctions. The application of STP is limited because most of the active devices are surrounded by an insulator.

Yu and co-workers (1992) used current imaging tunneling spectroscopy (CITS). In this technique, the sample surface is scanned with a fixed current value I_o for a specific voltage V_o at each point, a current–voltage spectrum is measured. Variations in electronic structure across the sample produce variations in the current voltage spectra; these variations can be revealed by the formed current images. Further, they studied potential distributions in Si (001) p-n junctions by monitoring a threshold voltage for

the onset of tunneling in the sample. They have been able to determine the shape of the conduction band edge profiles in these junctions. In addition, by using CITS method under UHV conditions and cleaning the tip in situ by electron bombardment, it was possible to image the source and drain junction on cleaved hydrogen passivated cross section Si MOS structure with a spatial resolution on the order of 10nm.

(1.7.3.3) Kelvin Probe Force Microscopy (KPFM)

KPFM is a high resolution and highly sensitive potential imaging method. This technique is capable of imaging surface potential differences between probes and samples. A conductive tip is scanned in the none contact AFM mode while an ac voltage is applied to it. This voltage results in an electrostatic field, which causes an oscillation of the cantilever at the same frequency. This force vanishes when the potential difference between the tip and sample is zero. By changing the dc bias voltage on the tip, the sample's surface potential can be measured. The semiconductor bulk potential varies depending on the dopant concentration and the dopant type, and it is directly related to the dopant concentration. It is possible, therefore, to infer the local dopant concentration by measuring the lateral surface potential, although the sensitivity is limited. Henning et al (1995) and Tanimoto et al (1996) have achieved a qualitative 2D carrier profiling of Si structures by applying this mode. This method is presently sensitive to changes in dopant concentrations from~ 10^{15} to 10^{20}/ cm^3, in 2D at size scale below 100nm. Measurements are fast, and require little sample preparation. They are repeatable, and reproducible to the extent that changes in probe tip do not affect the measurements significantly. However, the sensitivity to small concentration changes and the application towards quantitative profiling are limited by surface charges and KPFM calibration against absolute doping concentration remains to be further demonstrated (De Wolf et al, 2000).

In this thesis KPM has been incorporated to measure potential barrier height between thin layer of Al and p-n doped Si as will be introduced in chapter 7.

(1.7.3.4) Scanning Spreading Resistance profiling (SSR)

SSRP is a simple method capable of providing or measuring active dopant

concentration. This technique determines the carrier profile based on the sequential measurement of the resistance between two metal probes placed on a bevelled semiconductor surface. The probes are spaced less than 20 μm apart and a low voltage ~5 mV is applied between them. Resistance is measured as the tips are stepping down the bevelled surface. The flowing current (I) through the probes spreads out radially into the semiconductor is measured and using the relation $V=IR_{sp,}$ the spreading resistance (R_{sp}) is calculated. Then the resistivity of the semiconductor (ρ) is measured at each location (or at different points) using the equation

$$R_{sp} = \frac{\rho}{2\pi r} \qquad (1.5)$$

where r is the radius of the probe.

The data obtained must be calibrated against known samples and the carrier type (p- or n-) must be determined by another method (Heimbrook et al, 1996).

The resolution of this method is limited by the size of the probe tip and the magnification provided by the bevel. Hence, a good depth resolution of nm scale is possible by using high magnification with small bevels (typically 15′-60′) on the sample which provides an expanded view of the depth distribution (Vandervorst et al, 1992). The method is very sensitive to electrically active dopant concentration over the range10^{11} to $10^{21}cm^{-3}$. Similar to other probe methods the sensitivity is affected by the finite geometrical size of the tip. Since SSRP is a comparative method, sample preparation and conditioning of the probes are critical for reproducibility (Heimbrook et al, 1996). The carrier type n or p must be known or measured by different method.

The main problem with the conventional SSRP technique is that it cannot be applied directly to determine lateral profiling due to the large separation between the probes (20-40μm) and the size of the probe imprints (2μm). Recently, AFM tip has been proposed to acquire 2D profiling, in this technique the resistance is measured between a sharp conductive AFM tip and a large contact connected to the back of the sample. Due to its similarity to SSRP this technique is named nano SRP (De Wolf et al, 1996).

(1.7.3.5) Capacitance Voltage profiling (CV)

CV profiling is a well-developed technique that is capable of providing qualitative data.

In this technique the capacitance between a reverse biased semiconductor sample and a metallic probe tip is measured by applying a dc voltage to the semiconductor. Therefore, a depleted region is formed between the sample and the tip. The capacitance is measured by varying the applied voltage to the metal contact. Since depletion region capacitance between the sample and metallic tip is inversely proportional to the doping concentration, the direct density is directly extracted from the slope of the C-V curve then converted into a depth profile by calculating the depletion region width from the measured capacitance (Vandervorst et al, 1992).

This method can be fast and non-destructive, and sensitive to dopant levels as low as 10^{14} cm^{-3} which means is not as sensitive to low doses as SSRP. The sensitivity of the capacitance sensor used to measure the capacitance affects the CV measurements. Further, the spatial resolution is limited by the calculated depletion region width.

Although CV profiling extended to acquire 2D profiles by incorporating more than one electrode (tip) in several places on the sample, it is still widely used as a 1D profiling technique due to the large number amount of capacitance versus voltage data that has to be analysed in order to deduct the 2D profiling. The main disadvantage of 1D CV profiling is that the resolution is limited by the Debye length in low doped regions and it is insensitive to highly doped regions (Schroeder, 1990). The scanning capacitance microscope (SCM) is one such method for 2D profiles. However profile extraction from large amount of data need to be considered.

Based on all the methods described, it is clear that none of the available techniques fulfills all the upcoming requirements and can be applied on any arbitrary semiconductor structure. All 1D-based techniques require a special test structure, making them less flexible as compared to the SPM-based methods. However, most of the SPM methods have a low performance on Si due to the difficult cross section preparation, particularly if the technique is a very surface sensitive. In addition, the small field of view of SPM techniques also proves a time limiting factor for a large wafer inspection.

(1.7.4) Dopant Profiling With the SEM

The Scanning Electron Microscope (SEM) has been extensively used over the past

years and it is considered one of the most important examination methods to study doping profiles in a non-destructive inter-operational check. This technique is 2D doping profiling, fast and simple, and involves very little sample preparation. Further, this method does not require any data convolution to obtain 2D dopant profiling. This technique provides measurement with a microscope resolution (i.e. the instrument used), high magnification and great depth of field, thus enabling us to observe specimens well at the nanometer scale.

In the 1970's Lifshin, Aven and Sawyer have reported secondary electron (SE) dopant contrast in the SEM. Years later, Farrow et al (1991) while studying InP/InGaAsP, have observed anomalous SE dopant contrast that could only result from differences in dopant concentration. Ogura et al (1991) studied GaAs/AlGaAs superlattice structure and they were the first to carry out Backscattered Electrons (BSE) and SE imaging in a high resolution field emission SEM. BSE images have shown a good correlation with the supperlattice structure. Further, GaAs layers have shown a higher brightness in the BSE image which has been attributed to the higher average atomic number of GaAs. However, SE imaging was not in good correlation with the superlattice structure due to the appearance of a higher number of layers in the SE image. In addition, a contrast reversal between the p- and n-type regions (dark compared to bright appearance) has been observed when the beam voltage is varied between 25keV-3keV which complicated the interpretation. Hence interpreting SE images has not been successful. Although Ogura et al (1991) did not interpret the SE dopant contrast successfully; they were the first to observe higher contrast in the SE images collected at low beam voltages.

Ogura's study followed by Takahashi et al (1993), who studied doped Si structure for the first time in a SEM capable of operating at low voltage (1.5keV). For the first time they observed Arsenic implanted n-type regions appeared darker than the p-type substrate. They attributed the origin of contrast to the electron channeling effect. However, contrast has been observed from doped Si that has been annealed. The annealing process reduces any crystallinity variations between the implanted and non-implanted regions of the semiconductor. Furthermore, contrast has been observed from diffused Si devices and structure that have no crystallinity variations between the dopant diffused and non diffused areas. Therefore, the observed contrast cannot be

attributed to electron channeling effects.

In order to understand doped semiconductor regions behaviour in the SEM (the aim of this study), we need firstly to understand the signals generated in the SEM, their detection method, the advantages of operating the SEM at low voltages and reflection of utilizing LVSEM in studying dopant profiling in the SEM.

(1.8) Aims of this study

The aim of this dissertation is to provide clarification of dopant profiling in LVSEM through additional investigations in order to provide more understanding of the contrast mechanism. This will be achieved with a number of carefully devised experiments that address surface effects on SE dopant contrast. The research is mainly concentrated on studying the factors that affect the contrast in the Low Voltage Scanning Electron Microscope (LVSEM); the experimental conditions such as electron beam energy and electron dose. In addition, the surface effects, using a wide range of doped silicon structures (Si). These experiments includes imaging a large range of Si structures at different accelerating voltages, electron dose injection level effect on the SE dopant contrast, barrier height change effect on the contrast by annealing at different temperatures.

Chapter 2: Scanning Electron Microscopy and Generated Signals

(2.1) Introduction

In the scanning electron microscope, electrons from a thermionic or field emission cathode are accelerated by voltage applied between a cathode and an anode. The generated focused electron beam is scanned over the sample under inspection. Electrons which are produced due to the interaction processes within the sample are then collected with a suitable detector. These signal electrons carry much information, hence it can be used to analyse the sample surface topography or its composition. By varying the energy of the primary electrons, the interaction volume with the solid will be different. This in turn affects the energy distribution of the re-diffused electrons within the solid and hence these will affect the scattering cross sections of various generated signals.

This chapter will briefly review the SEM technique and discuss the different signals generated in the SEM focusing on the secondary electron (SE) emission theory. As a knowledge of the dependence of the SE yield on surface tilt, material and beam energy and their angular and energy distribution is essential for proper interpretation of SE dopant contrast (or image contrast), these basic concepts will be introduced.

(2.2) Scanning Electron Microscope Signals

When an electron of energy E_p impinges on the surface of a solid specimen and penetrates into the specimen to a finite depth R of the order 0.1-10μm that depends on its energy and target density, it suffers multiple scattering events with the atoms of the specimen. The interaction between the incident electrons and the solid sample in the SEM produces a spectrum of electrons with energies varying from zero up to that of the incident beam energy as shown in figure (2.1).

The interaction of the electron beam with the atoms in the specimen can be divided into elastic and inelastic scattering events. As a result, several forms of signals at or near the specimen surface are generated. The signals generated are Backscattered electrons, Secondary electrons, Auger electrons, Characteristic X-rays and photons of various energies. Suitable detectors are normally used to collect a given signal and the latter is usually amplified and displayed for further processing. These signals can be analysed to provide the required information, such as its composition, its crystallographic structure, its, morphology and many other characteristics.

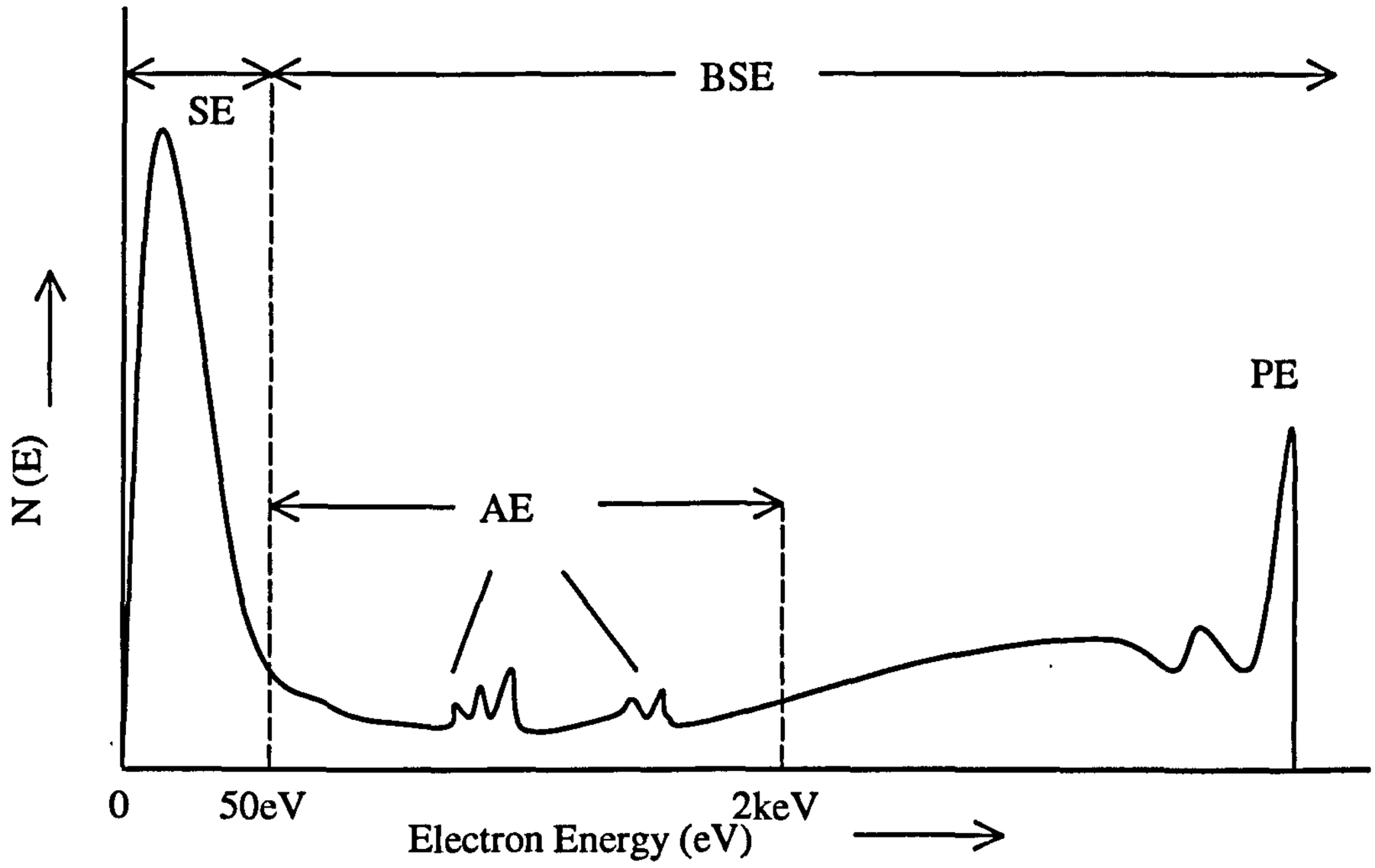

Figure (2.1) Energy spectrum of electrons emitted from a solid surface bombarded with electrons of energy E_p, (Reimer, 1985).

(2.3) Electron Range and Excitation Volume

When primary electrons impinge into the specimen, electrons will travel a finite distance depending on the electron energy and the target density. Incident primary electrons will lose energy gradually as they diffuse into the specimen after scattering. Therefore a lateral spreading will also occur. Due to the lateral spreading in addition to the vertical spreading, the interaction volume is formed, where all SEM signals are generated. The interaction volume is found to have dimensions of several micrometers with the depth substantially greater than the width and to have a distinctive pear shape. The electron range is defined as the average distance traveled by an electron along its trajectory. The electron range in microns (μm) is given by the formula (Goldstein et al 1981).

$$R_{KO} = \frac{0.0276 A E_o^{1.67}}{\rho Z^{0.889}} \qquad (2.1)$$

where, E_o is the primary electron energy (keV)

Z is the atomic number of the target.

A is the target's atomic weight (g/mol) and

ρ is the target's density (gcm^{-3})

The range of a 1kV primary electron beam incident on Si is approximately 32nm while for electron beam energy of 10kV, the range increases to ~1.5 μm. Figure (2.2) shows schematically the most important interaction processes and their information volumes. Auger electrons and secondary electrons are generated very close to the surface, while backscattered electrons and X-rays are generated from the bulk of the specimen. The three most important signals in a SEM are secondary electrons, backscattered electrons and x-rays.

(2.4) Secondary Electrons

Secondary electrons are conventionally defined as those emitted with energies less than 50 eV. These electrons are ejected from the sample when the primary electron moves inside the target and starts interacting inelastically with the orbital electrons of the target atoms. As a result of this interaction, a few electron volts are transferred from the incident electron to the orbital electrons, especially to those in the valance band of the target atoms. This energy excites the orbital electrons to be ejected from the atom and some of them move towards the surface.

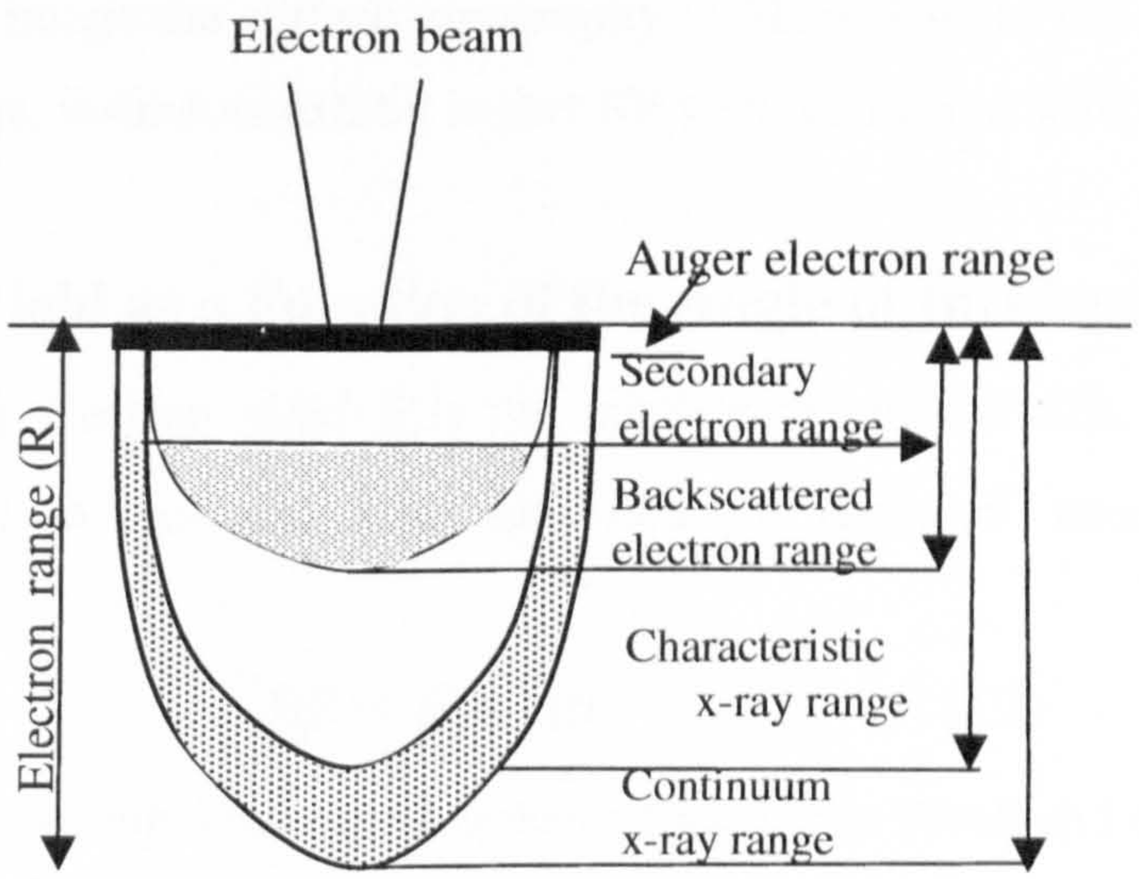

Figure (2.2) Schematic diagram of the interaction of an electron beam in a bulk sample showing different signals generated as a result of this interaction.

If the energy of these electrons is sufficient to overcome the surface potential barrier, which is usually several electron volts, then they can escape from the surface.

(2.4.1) Escape Depth of SE

The escape probability of a SE produced at distance x from a surface decreases as $e^{-x/\alpha}$ where α is the escape depth. For metals $\alpha \approx 0.5$-1.5nm and increases to the order of 10nm for carbon, for insulators $\alpha \approx 10$-20 nm (Reimer, 1985), with a maximum of 75nm (Seiler, 1983). Because of this small depth SE is the most important signal emitted from the surface to image the surface topography in SEM. Due to the large escape depth of SE in insulators, insulators exhibit higher SE yield compared with metals.

(2.4.2) SE Yield as a Function of the Angle of Incidence

The secondary electron yield δ is the number of emitted SEs per incident primary electrons (PE). δ increases with specimen tilt angle θ according to the secant distribution

$$\delta(\theta) = \delta_o \sec(\theta) \qquad (2.2)$$

where δ_o is the SE yield measured at normal incidence ($\theta=0$) and θ is measured relative to the surface normal (Seiler, 1983). The increase of δ with tilt angle is attributed to the small escape depth of SEs. The deeper the penetration distance of the PE within the escape depth, the higher the SE yield. Thus, SE emission is enhanced at the edges of features where the angle between the PE and the surface normal is increased. At lower beam energies, if the penetration depth is smaller than the dimensions of the features, only the edges of the feature appear bright. The angular distribution of emitted SEs is a cosine distribution about the surface normal. Since SEs emitted from surfaces that are tilted towards the SE detector will be collected more efficiently than those emitted away from the detector, the SE topographical contrast depends on the position and efficiency of the SE detector.

(2.4.3) SE Yield as a Function of Incident Energy

Measurements of δ at primary energies in the range 1-100keV (Reimer, 1985) show a decrease with increasing primary energy which can be represented by the equation

$$\delta \propto E^{-0.8} \lambda \sec(\theta) \qquad (2.3)$$

where λ is the inelastic mean free path. The above equation describes the dependence of the yield on the primary beam energy and tilt.

The behaviour of δ as a function of beam energy is shown schematically in figure (2.3). The general shape is the same for all materials. The plot indicates that δ rises with increasing energy, reaching a peak δ^m slightly above unity at E_{PE}^m, with a further increase in beam energy, then δ decreases and passes through unity again. The maximum yield in the plot can be understood by considering the SE cross section, the penetration depth of the beam and the SE escape depth. The E_p^m typical range for metals varies from 100 to 800eV and for insulators varies from 300 to 2000eV (Seiler, 1983). In general δ shows a peak ~2-3keV then decays rapidly with increasing primary beam energy. The maximum value of SE yield occurs when the electron range is nearly 5 times the inelastic mean free path (Seiler, 1983).

(2.4.4) SE Signal in the SEM

There are four types of SEs that are normally produced in electron probe instruments; SE1 generated due to the direct inelastic scattering between the incident electron beam with target orbital atoms, SE2 generated by backscattered electrons (BSEs) exiting the target through the SE escape region. Both these types of SE1 and SE2 are useful in SE dopant imaging since they both are generated within the specimen surface. However, for high resolution scanning electron microscopy, the first source is beneficial while the second source adds noise to the signal (Goldstein et al, 1981). Further it is possible with SE2 to image features below the surface beyond the escape depth of the SE and it shows some sensitivity to the atomic number of the target atoms (Seiler, 1983).

Seiler (1983) has found that the probability of SE2 emission is higher than SE1 due to the lower mean energy of BSEs compared with PEs which increase its ability to generate SEs compared with PEs. The total SE yield δ is the sum of those SEs generated by the PEs and the BSEs

$$\delta = \delta_{PE} + \eta\, \delta_{BSE} = \delta_{PE}(1+\beta\eta) \qquad (2.4)$$

where δ_{PE} is the yield of SE1, $\eta\delta_{BSE}$ the yield of SE2 and $\beta=\delta_{BSE} / \delta_{PE}$

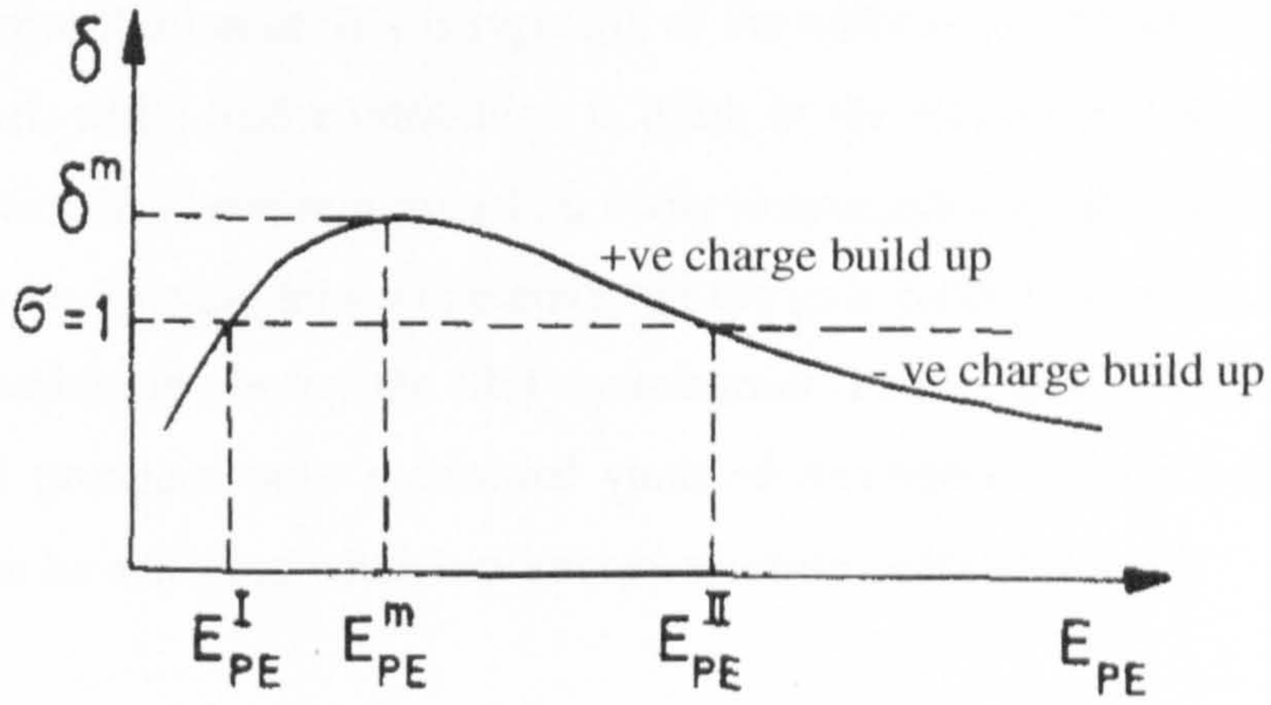

Figure (2.3) SE yield δ as a function of E_{PE} (Selier, 1983).

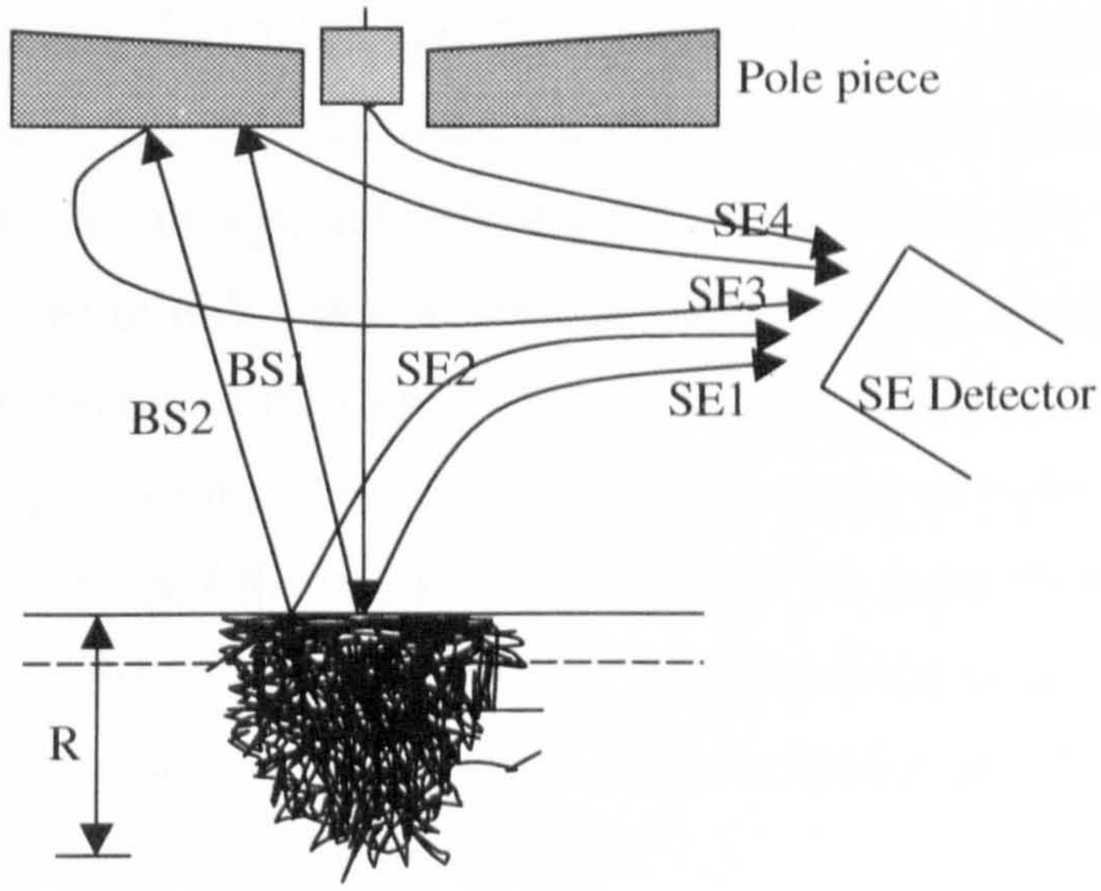

Figure (2.4) Different types of SEs generated in the SEM (Joy, 1984)

The third type is SE3s, which are called tertiary electrons, and originate as a result of BSEs hitting the pole piece of the microscope column or its specimen chamber walls. Finally, direct scattering of the incident electrons from the column's objective aperture produces the SE4 contribution.

The relative contribution of SE4 is typically of the order of 2-10% of the total secondary electron signal, while SE3 contribution is often in the range 10-50% (Joy, 1984). The SE4 contribution has been minimized on many instruments by placing the final aperture before the probe-forming lens while covering the pole piece face by an aluminum plate coated with carbon to control the SE3 contribution (Peters, 1982). This layer is largely absorbed and produces only a minimal yield of secondaries. Thus a higher signal to noise ratio can be achieved when low energy electron beams are used.

(2.4.5) Secondary Electron Detection

There are two types of detectors that can be used to detect SEs in the SEM; Everhart-Thornley detector (E-T) and the in-lens detector. E-T detector is the most widely used system for SEs detection and is shown in figure (2.5). The generated secondary electrons are collected by a grid biased between +100V and +300V placed close to the sample. The SEs that pass through the collector grid are accelerated to the scintillator which is normally biased to 6kV-10kV at the conductive coating, which can be a thin evaporated film of aluminium of the order of a few tens of nanometers thick. When the SEs hit the metal, they cause the phosphorous to emit a pulse of light; its intensity is proportional to the energy and the number of the SEs. This pulse flows down into a phosphorous to emit a pulse of light; its intensity is proportional to the energy and the number of the SEs. This pulse flows down into a photomultiplier tube (PMT) to amplify and convert it into an electron pulse (Reimer, 1985).

The second important detector is referred to as the in-lens detector or through the lens detector (TLD). This is normally placed inside the objective lens of the electron column and therefore collects SEs from immediately over the scanned area of the sample. The SEs are focused by an electric field to pass through the lens pole piece into the collector. (Burton, private communication).

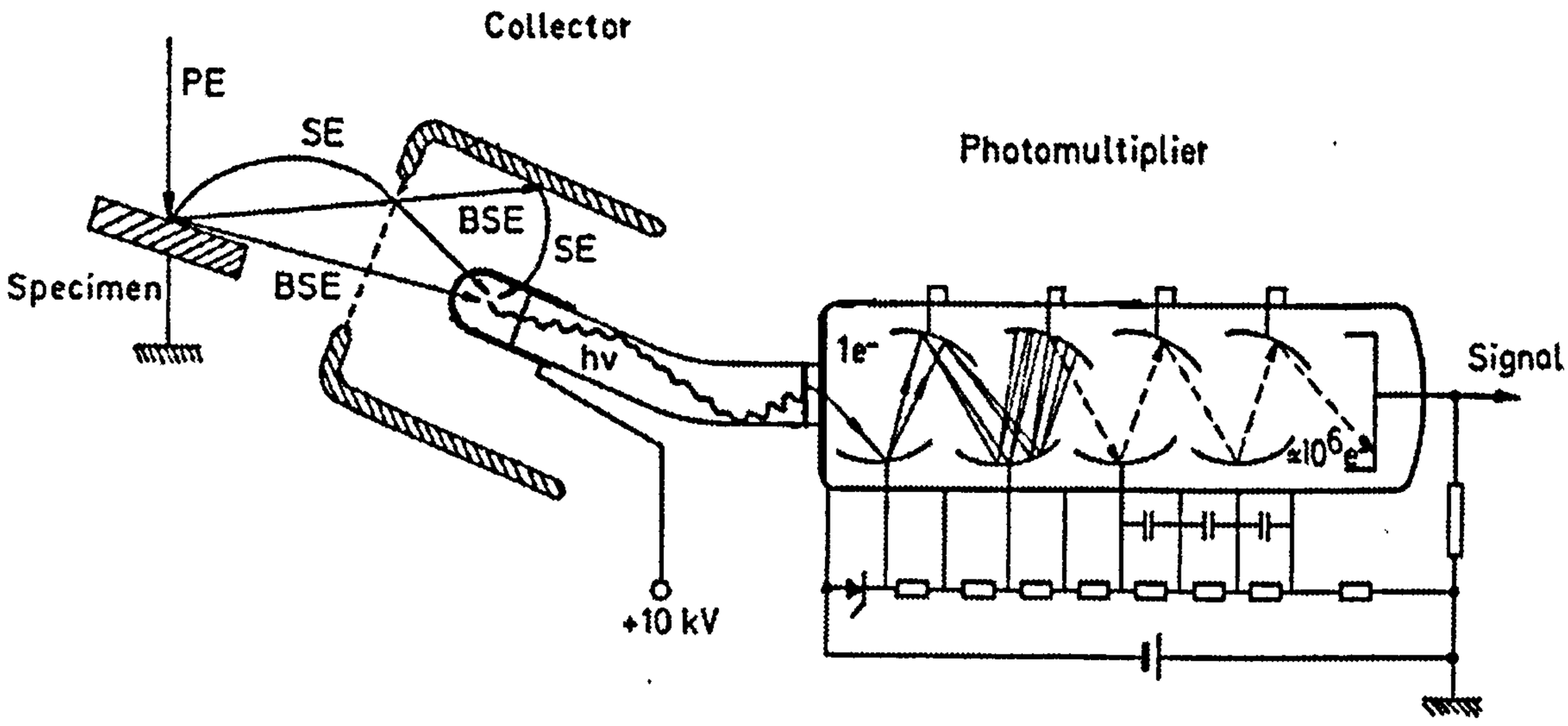

Figure (2.5) Everhart-Thornley detector (Reimer, 1985).

The main disadvantage of E-T detector is that it attracts a proportion of the SE3 and SE4 electrons thus increasing the noise of the image. Although the in-lens detector suppresses SE3 and SE4 types and it shows efficiency in collecting SE1 and SE2, the main disadvantage of this method is relatively small field of view (Joy, 1996).

(2.4.6) SE Contrast in the SEM

Different SE yields of adjacent object elements causes contrast brightness between the corresponding elements. The difference in intensity ΔI between two-object elements must be greater than the signal to noise ratio (S/N). There are different types of contrast in the SEM. In this study only contrast due to differences in SE yield caused by differently doped regions is considered. The dopant contrast in this report is determined by the following relation

$$C_{A/B} = \frac{I_A - I_B}{256} \qquad (2.5)$$

where; I_A is the secondary electron intensity from object A.

I_B is the secondary electron intensity from object B.

256 is the number of grey levels (Jayakody, 2003).

(2.5) Backscattered Electrons

Backscattered electrons are described as those which leave the specimen surface with energies greater than 50 eV after they have penetrated the specimen and suffered a number of elastic and inelastic scattering events. The backscattered electrons are divided into: primaries (PE) which leave the specimen without any loss in their energies (i.e. after going through a number of elastic scattering events), second is diffused electrons which leave the specimen with a greater loss of energy and third are Auger electrons (AE) which have an energy related to the specimen material. The importance of the BSE signal in the SEM is mainly due to its dependency on the specimen atomic number Z. Dependence of BSE yield on the atomic number is shown in figure (2.6). This dependence on the atomic number allows the regions of a specimen of different atomic number to be distinguished particularly at high electron beam energies, whereby in BSE image an area that consists of higher atomic number material will appear brighter compared with lower atomic number material.

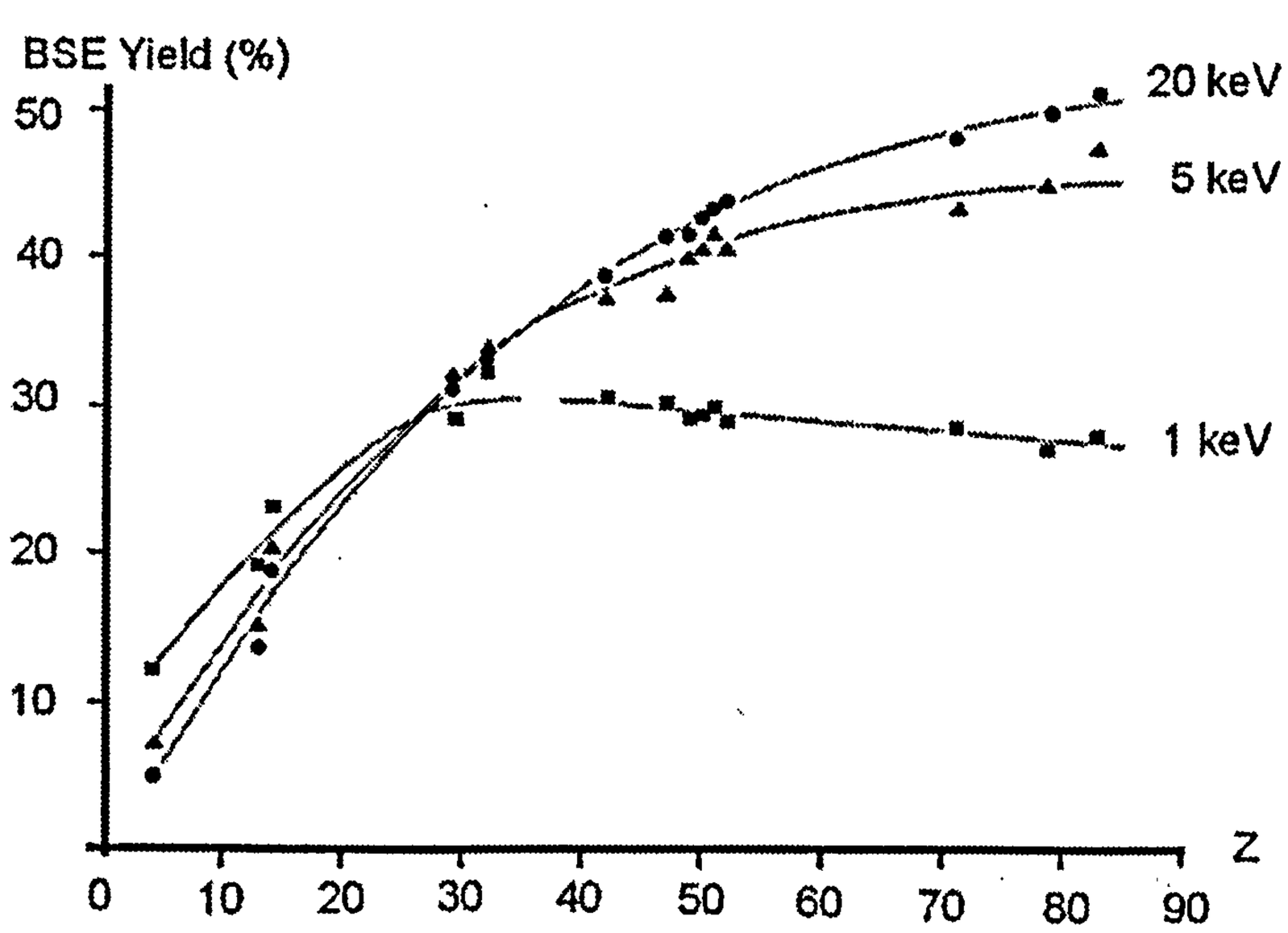

Figure (2.6) BSE yield variation as a function of atomic number for three different primary beam energies (Reimer, 1980). It is clear that BSE yield increases as the atomic number increases for high beam energies. However, for low beam energies, the BSE yield decreases due to contaminant effect on the signal.

Due to their high energy BSEs follow straight-line paths, it is necessary to use a large solid angle of collection and a suitable detector is placed above the sample to detect all the generated electrons. If BSEs are collected by the E-T detector, this signal will appear as a constant noise source in the image. BSEs can be detected using a channel plate detector or semiconductor detectors, which amplify the number of BSEs that impinge on the detector surface.

Two specialised detectors are used to detect BSE both of these detectors sit directly beneath the objective lens and cover large surface area to maximize collection efficiency

(2.5.1) Scintillator Detectors

These comprise a scintillator (phosphor) with a light pipe and a photomultiplier, which are distinguished by a fast response time and a high gain, which makes them suitable for use at TV rates. However, these detectors are bulky and may restrict the working distance of the microscope.

(2.5.2) Solid State Detectors

This detector consists of Si p-n junction that forms electron-hole pairs when a BSE impinges its surface. A reverse bias which is applied to the detector separates the electron hole pairs giving rise to a detectable current. This detector is much smaller than a scintillator detector and cheap to make. On the other hand, its response is rather slow which makes them unsuitable for operation at TV scan rates.

(2.6) Characteristic X-rays

Apart from the above signals, when an electron strikes an atom in the sample, direct inelastic scattering process generates X-rays. The inelastic scattering process can release a bound electron such as from the K shell. Another electron from a higher energy level, say L_1 shell, falls into the vacant position and an X-ray photon is ejected which has energy equal to the difference between these two states. The ejected photon has a characteristic energy which differs from element to element.

$$\text{X ray energy } h\nu = hc/\lambda = E_K - E_{L1} \qquad (2.6)$$

Where; h is Planck's constant

ν is the frequency of x ray photon

c is the speed of light

λ is wavelength of the emitted x- ray

E_K is electron energy in shell K and

E_{L1} is electron energy in shell L_1

The wavelength of the emitted spectra is a characteristic of the specimen composition, thus it can be used for elemental analysis. Generated x-rays can be detected with a suitable detector and display against the wavelength λ, thus elemental and structural information can be collected from the specimen under inspection. From the relative intensities of the X-rays, quantitative analysis can be made. However, it is not suitable for the chemical analysis for small dimensional structures due to the large generation volume where the X-rays come from. Furthermore, this method is not very surface sensitive technique for the same reason of the X-ray generation volume. Most commercial SEMs are equipped with an x-ray analyser of the energy dispersive type. Figure (2.7) gives a basic representation of the mechanism.

The reverse process of x-ray generation is the x-ray photoemission spectroscopy (XPS), which can also be used as an elemental analysis technique. In this method the specimen is bombarded by x-rays, electrons are then generated and leave the specimen. These electrons have discrete energies depending on the sample composition. The process is shown schematically in figure (2.7), which depicts two possible photoelectron emissions, following core ionisation for Si. These photoelectrons have a small escape depth of the order of 3nm (Ambridge et al, 1985). Therefore, they can be used to identify the elements present in the specimen surface.

X-ray

Photoelectrons

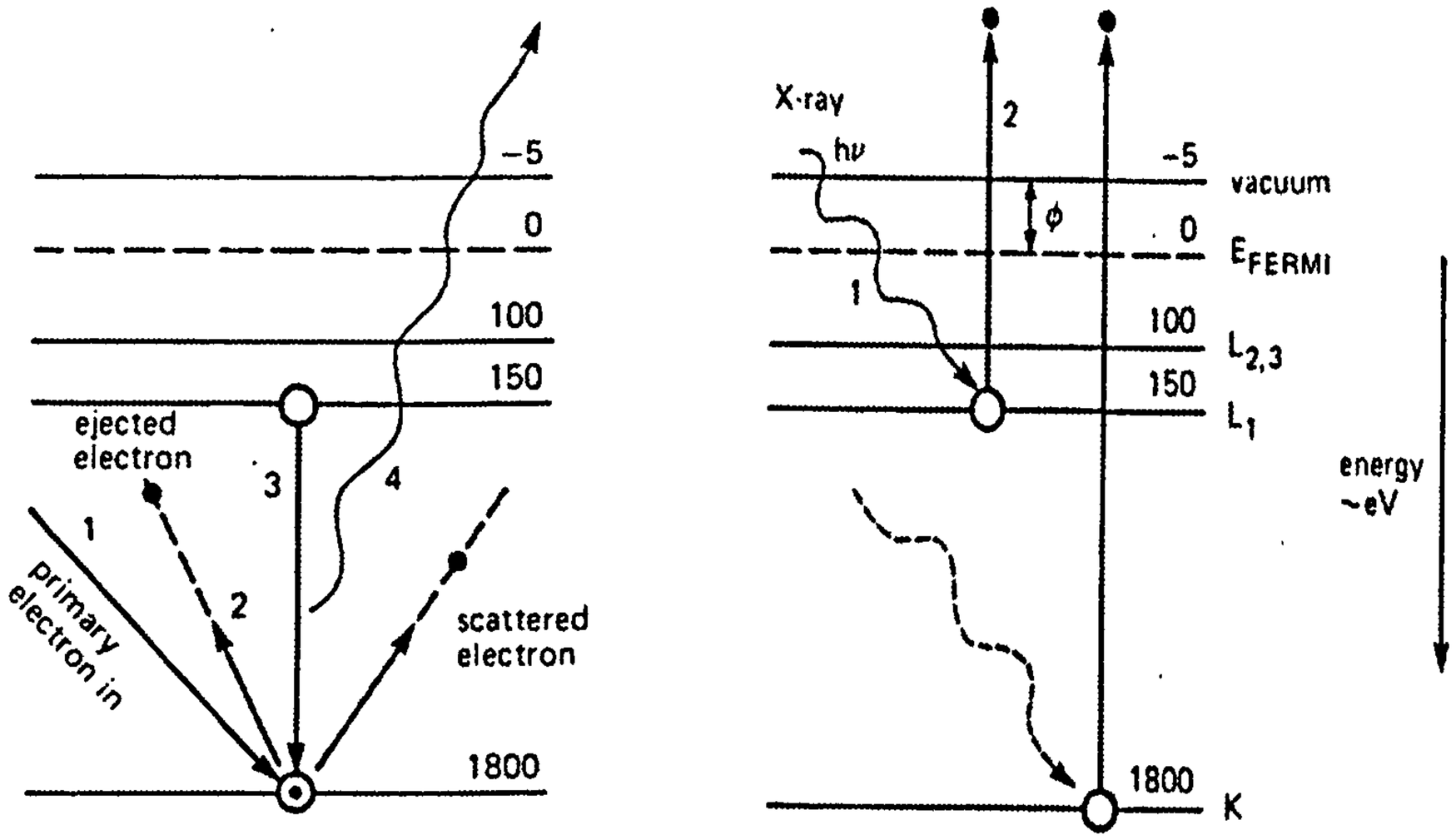

(a) (b)

Figure (2.7) Process for the generation of characteristic emission from atoms in Si; (a) Generation of characteristic X-rays. (b) The generation of photoelectron spectroscopy (XPS) two possible emissions are shown (Ambridge et al, 1985).

(2.7) Auger Electrons

Auger electrons are generated as part of the inelastic scattering process of electrons interacting with a solid sample. When a primary beam of electrons is incident upon the surface of a specimen, its interaction with the surface atoms may result in removing an electron from a target atom (say the K shell) and the atom will be raised from its ground state due to the generated hole in an inner shell. The ionised atom will then fill this core hole with an electron from a higher energy level, say the L_1 level, by losing its surplus potential energy (equal to the difference in binding energies between these two levels, i.e E_K- E_{L1}). This energy difference can either be emitted as x rays or transferred to another electron in a higher or the same electron level L_2. If the energy is transferred to another electron, this electron is released as an Auger electron. The process of an Auger emission is shown schematically in figure (2.8)

The Auger electrons therefore have energy approximately equal to the energy difference between the two shells involved in the transition.

The approximated kinetic energy (KE) of an Auger electron generated due to this transition is given by

$$KE = (E_K - E_{L1}) - E_{L2,3} \qquad (2.7)$$

This equation has been used in the early days of AES to calculate the Auger energies. However, it gives only an approximate value because after the creation of the initial K core hole the remaining electrons become more tightly bound to the nucleus, due to the extra positive charge of the atom. Because of this, as well as the difficulty in determining $E_{L2,3}$, an approximation value of the kinetic energy of the emitted Auger electron is given by

$$KE=E_K^{Z}- E_{L1}^{Z}-E_{l2,3}^{Z+1} \qquad (2.8)$$

This expression was approximated by Siegbahn et al (1967).

By replacing the binding energy of the level $L_{2,3}$ for an atom of atomic number Z, with the corresponding binding energy of an atom of atomic number (Z+1).

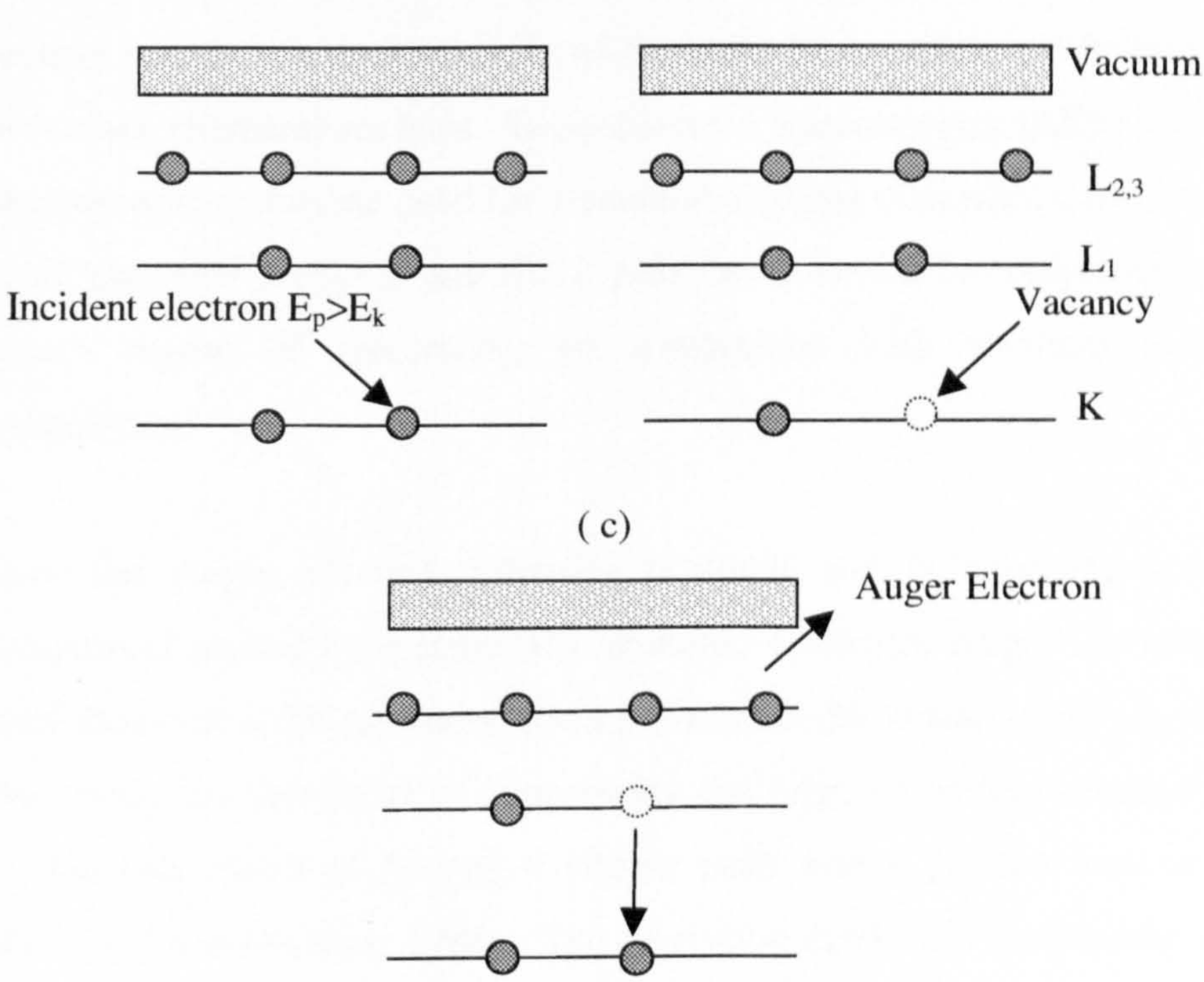

Figure (2.8) Electron energy levels diagram depicting a $\mathbf{KL_1L_{2,3}}$ transition.

(a) A primary electron of energy Ep creates a vacancy in the **K** shell.

(b) An electron from $\mathbf{L_1}$ shell fills the vacancy created in the **K** shell.

(c) The excess energy (E_k-E_{L1}) is given to an electron from $\mathbf{L_{2,3}}$ which allows it to be emitted.

Auger electron emission is efficient in filling core holes with low binding energy. Thus, the Auger process giving rise to relatively low kinetic energy Auger electrons, which then have a short mean free path (Woodruff and Delchar, 1986). Due to their short mean free path only Auger electrons that are generated near the surface can emerge to the vacuum. Auger electron spectroscopy is based upon the measurement of the kinetic energies of the emitted electrons. Each element in a sample being studied will give rise to a characteristic spectrum of peaks at various kinetic energies. Because the Auger electron energy is a characteristic of the atom from which it is released, it can be used for surface chemical analysis. Auger Electron Spectroscopy (AES) is a surface-sensitive spectroscopic technique used for elemental analysis of surfaces; it offers high sensitivity for all elements except H and He. It provides quantitative compositional analysis of the surface region of specimens, by comparison with standard samples of known composition.

Since the Auger electron intensity is small and is superimposed upon the high background caused by inelastically scattered electrons, Auger electron spectra are also often shown in a differentiated form to increase the visualisation of small Auger peaks. This mode has the virtue of suppressing the large secondary electron background and has the side effect of turning a simple peak into a positive and negative excursion (Woodruff and Delchar, 1986). The derivative dN(E)/dE is obtained by superimposing a small sinusoidal potential modulation on the analyzer pass energy and synchronously detecting the current passed through the analyzer (McGuire,1979).

(2.8) Auger Electrons Detection

Auger electrons have discrete exit energies; therefore they can be detected by analysing the energy distribution of all the emitted electrons from the sample. The electron spectrometers have been used to separate electrons with different energies. In principle, the energy analysers can be of magnetic or electrostatic type. However, electrostatic fields are preferred to deflect electrons according to their energy, where the number of Auger electrons detected can be plotted against their energy to obtain an Auger electron spectroscopy (AES). The electron spectrometers were developed in the 1960s, when Ultra-High Vacuum (UHV) technology became commercially available.

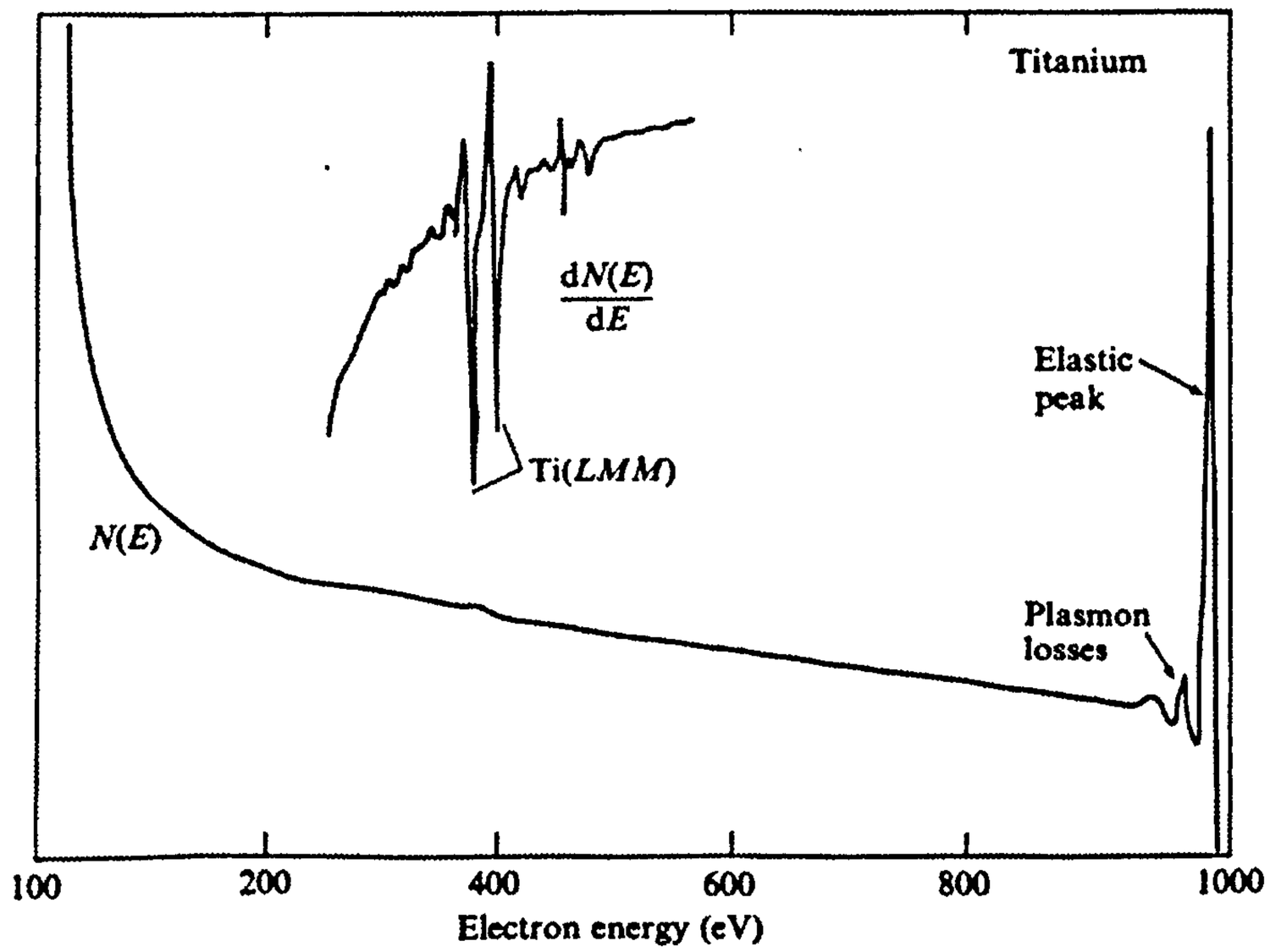

Figure (2.9) N(E) and dN(E)/dE for electrons emitted from a Titanium target with incident electron beam energy 1keV (Park and Den, 1977).

The most widely used electrostatic energy analysers are Cylindrical Mirror Analyser (CMA) and Concentric Hemispherical Analysers (CHA), which will be briefly reviewed below.

(2.8.1) The Cylindrical Mirror Analyser (CMA)

The Cylindrical Mirror Analyser consists of two concentric cylinders of radii r_1 and r_2 that are placed coaxially with each other. The inner cylinder is held at ground potential, and the outer cylinder is set to a negative potential (-V). By adjusting the outer cylinder potential, electrons in a small energy window will pass through the analyser. This arrangement allows electrons of a given energy which are generated on the axis of the CMA to be refocused after deflection by the electrostatic field, at a point which is determined by their energy and direction. A schematic of the CMA is shown in figure (2.10).

The relationship between the focused electron energy and instrument parameters is given by:

$$E_o = \frac{Ke}{\ln(r_2 / r_1)} V \qquad (2.9)$$

where E_o is the energy of the focused electrons, e is the electron charge, K is the CMA characteristic constant and $K=L/r_1$ with L the distance between the analyser's focal point S and the output focal point F. V is the outer cylinder voltage, r_1 and r_2 are the inner and outer cylinder diameters, respectively.

The energy resolution of an electron spectrometer is defined as the ratio of the width of the energy spread after analysing ΔE to the energy E of the peak maximum $\Delta E/E$. ΔE is usually measured as the full width at half maximum (FWHM) intensity of a selected peak-usually the elastic peak is used since it is a well-defined peak.

The energy resolution of the CMA is related to the CMA parameters as follows

$$\Delta E/E = 0.18(w/r_1) + 5.5/4(\Delta\alpha)^3 \qquad (2.10)$$

where w is the aperture width of the inner cylinder (equal for the entrance and the exit apertures) (Sar-El, 1967).

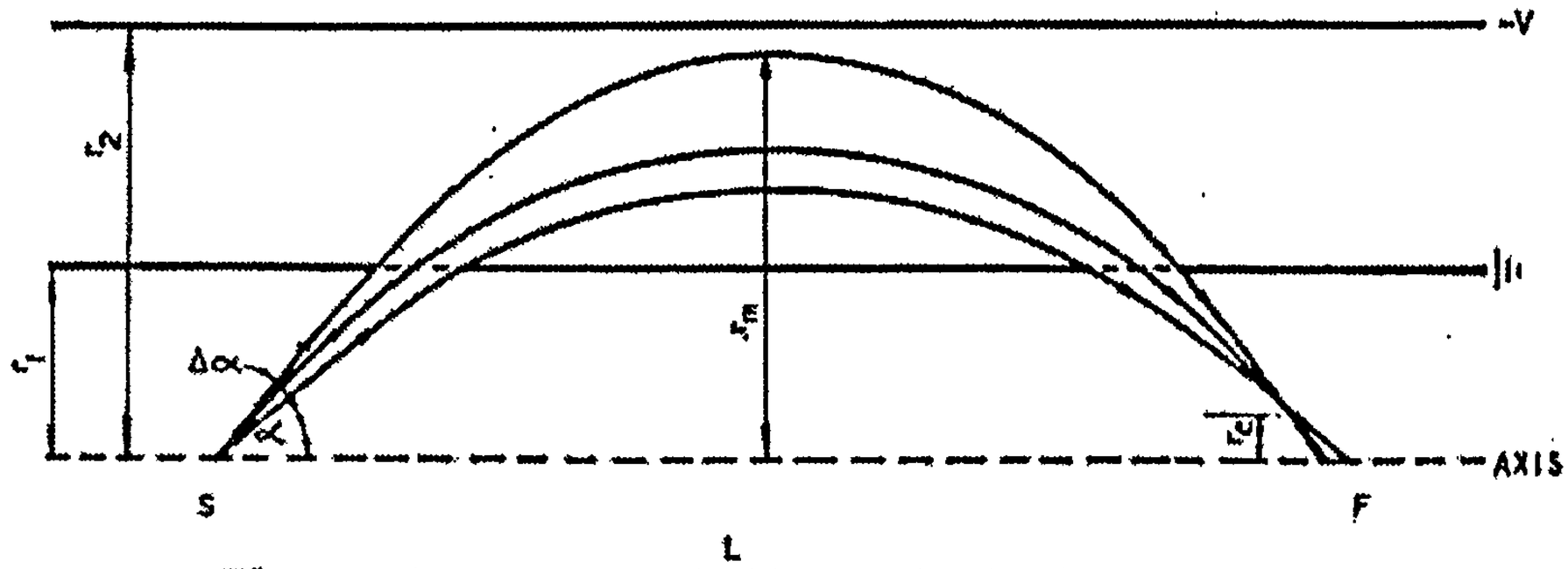

Figure (2.10) Schematic diagram of the CMA, showing the trajectories of the emitted electrons from the sample under investigation that placed at S. Electrons emitted within an angular range $\pm \Delta\alpha$, travel through a mesh-covered aperture and are refocused at F where the distance between S and F is denoted by L. (Briggs and Seah, 1996)

The CMA has excellent collection efficiency and high signal to noise ratio can be achieved. Also it has a high transmission value (Woodruff and Delchar, 1986). However, it is sensitive to the movement of the sample along the analyser axis. Further, it is reported that secondary electrons are generated by collision with the CMA may reach the detector and contribute to the noise (Seah, 1985). Also, the electron energy spectra produced from a CMA are non-linear. This means that the electron transmission rises with increasing beam energies. Consequently, collected spectra are explicitly defined as the E N (E) as opposed to N (E) spectra.

(2.8.2) Concentric Hemispherical Analyser (CHA)

The Concentric Hemispherical Analyser consists of two hemispherical concentric shells of inner radius R_1 and outer radius R_2. A potential difference, ΔV, is applied between the two surfaces such that the outer sphere is negative and the inner positive. Between the spheres there is an equipotential surface of radius R_o. The entrance and exit slits lie on a diameter and are centred at a distance R_o from the centre of the curvature.

Since the two hemispheres are held at different potential V_1 and V_2, an electric field is generated between the hemispheres. Potentials V_1 and V_2 can be adjusted so only electrons with a certain energy range, entering the CHA, will be caused to move in a curved trajectory and reach the exit aperture F, as shown in figure (2.11). Remaining electrons hit the hemisphere will not get detected. Together with lens system takes electrons from the sample and injects them into the analyser. Electrons that passed the exit aperture can be detected using a suitable detector. The base resolution is given by

$$\Delta E/E_o = S/2R_o + \alpha^2/4 \qquad (2.11)$$

where E_o is the energy of electrons entering the analyser at an angle α to the slit normal and S is the slit width equal at the entrance and exit.

The main advantages the CHA has over the CMA are much better access to the sample (i.e is not sensitive to the sample positioning) and the ability to vary analyser resolution electrostatically without changing physical apertures. In addition, the CHA is a narrow band-width analyser, since it only allows electrons within a certain energy range to move on a circular orbit and reach the detector.

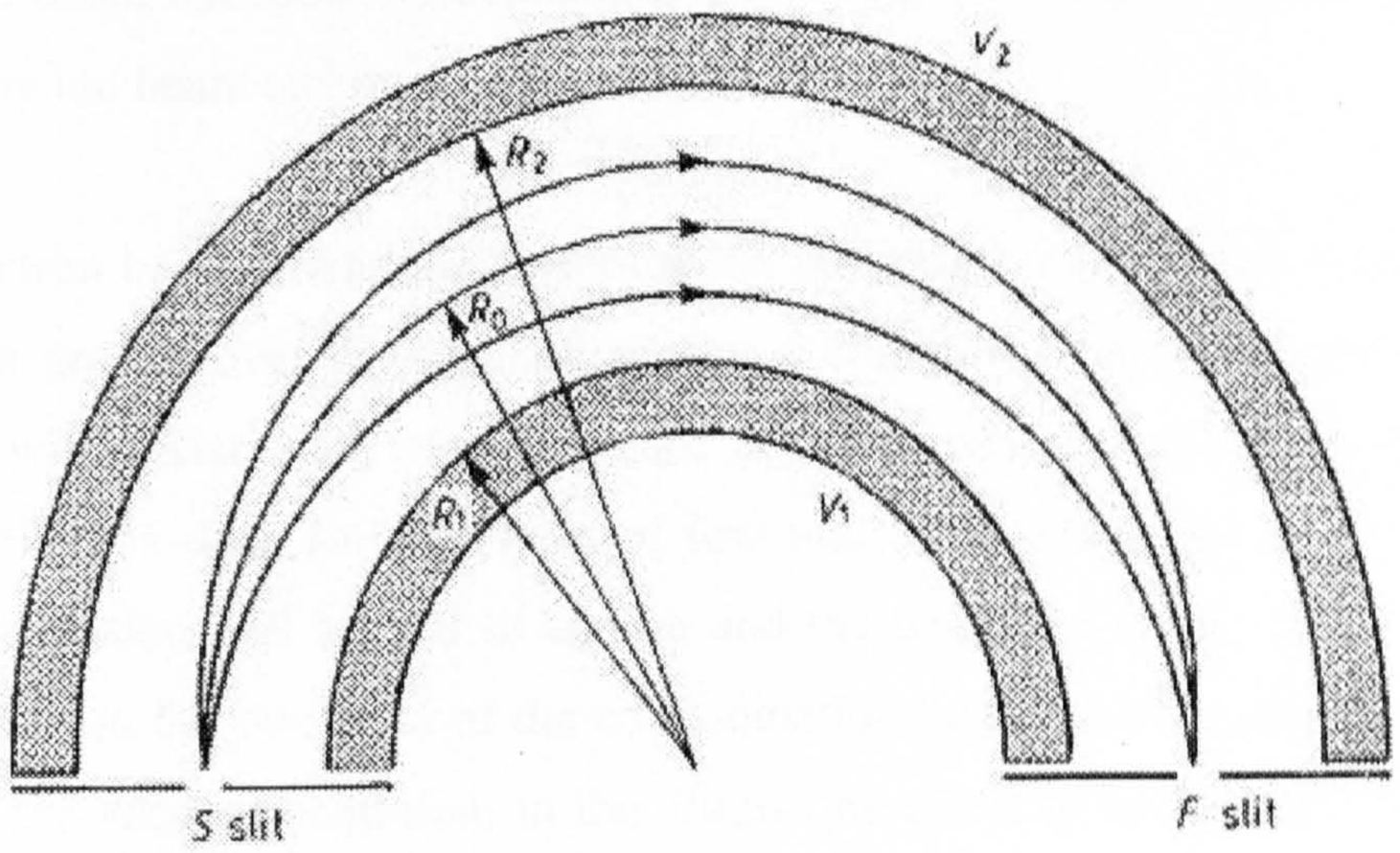

Figure (2.11) Cross-sectional view of the CHA (Briggs and Seah, 1996).

Having passed through the analyser, the electrons of a particular energy are spatially separated from electrons of different energies; hence various detectors are used to detect these electrons such as a micro channel plate (MCP) or a multi channel detector.

(2.9) Contamination in the SEM

The presence of hydrocarbon molecules on the specimen surface is virtually unavoidable during inspection in the SEM. These molecules are formed in the vacuum of the microscope due to the partial pressure of hydrocarbons or silicon oils from the diffusion pump and the grease of vacuum seals and finger marks. Furthermore, hydrocarbons are already deposited on the specimen during handling it in the air, so the best way to avoid hydrocarbon deposition is cleaving the sample in ultra high vacuum (UHV) or by ion beam etching inside the UHV.

During electron beam irradiation, hydrocarbon molecules are cracked, which results in carbon film growth over the scanned area or a contamination needle grows up when irradiation with a stationary electron probe at a thickness depending on the scanning time, and electron dose and is almost of few nm. Since SE signal is of short escape depth, SE emission will be that of carbon and the irradiated areas. Therefore, the SE yield depends on the thickness of the contamination layer which is affected mainly by changes in the vacuum condition. In this thesis, the effect of surface contamination on SE dopant contrast will be discussed in detail.

Chapter 3: Dopant Profiling in the LVSEM and Related Mechanisms

(3.1) Introduction

Low Voltage Scanning Electron Microscopy (LVSEM) has become one of the most important tools in studying semiconductors and in biological science where a decrease in the electron range reduced charging and radiation damage during inspection, and an increased topographic contrast are desired. Some advantages of operating the SEM at low electron energies were recognised since the early days of SEM. However, its use has been increased only recently due to overcoming the difficulties connected with achieving high resolution low voltage microscopy.

Although the dopant contrast in the SEM was reported in 1970's for the first time, the research did not gain much momentum until the work of Perovic in 1995. Since LVSEM can provide high resolution (<5nm) and high signal levels, this improvement has generated much interest in acquiring 2D dopant profiling. Perovic has utilized LVSEM to image doped GaAs and Si structures. Since that time, this area of research has been given more attention due to the progress that has been made in developing the LVSEM.

This chapter describes the advantages of operating SEM in low and very low energy mode and the methods that have been applied to obtain this mode are described. It also shows reflection of utilizing LVSEM and Scanning Low Energy Electron Microscopy (SLEEM) mode on the SE dopant contrast. Further, this chapter will review several SE dopant contrast mechanisms in the SEM.

(3.2) Difficulties Connected with Achieving Low Voltage Microscopy

Generally, at low voltages, the electron optical performance of the SEM deteriorates due to both the reduced brightness of the electron source and the increased aberrations of the electron optics. Therefore, the SEM signal strength and resolution are degraded. In addition, low beam energy electrons take long time to travel along the optical column compared with high beam energy electrons. This makes low energy electrons more susceptible to spurious dc and particularly ac electromagnetic field throughout the column. This field causes misalignment of the beam, and even for the objective lenses of the best design, the spot size starts to increase steeply, owing to diffraction aberration (Frank et al, 1999), which can cause distortion in the image.

Moreover, the detection of signal electrons without affecting the primary beam performance becomes difficult at low voltages due to collecting the primary beam electrons by the positively biased grid the and hence this collecting field will retard the resolution by distorting the probe. The effect of the collecting field becomes more pronounced when the beam energy is reduced below 5keV (Pawley, 1990). Thus, a long period of instrument development was needed to overcome the main difficulties which can be categorized as follows;

- Low source brightness.
- Increased aberrations.
- Increased sensitivity to stray fields.
- Defocusing of the probe by SE collecting field.

Operating SEM at low voltages means overcoming poor instrumental performance in obtaining high spatial resolution and signal electron detection. LVSEM has and still is witnessing intensive activity in both directions. The high spatial resolution is obtained due to the recent developments in ultra high vacuum systems thus making it easy to use higher brightness electron sources of the field electron emitter and Schottky type, which are increasingly replacing conventional thermionic sources. An example of this development is achieving small probe diameters with sufficient probe current to form an SEM image of comparable signal to noise ratio to conventional large probe diameter SEM's that are now commercially available (Ogura et al, 1991, El-Gomati et al, 2005).

Apart from the improvement in electron sources and high brightness FE guns, software packages that can analyse complex electron optical systems have been incorporated in developing LVSEM. As a result of these advancements, it is possible to obtain low voltage electron beams (<5keV) with very high resolution (<5nm) for routine exploitations (Mullerova et al, 1992).

(3.3) Advantages of Low Voltages Electron Microscopy

When low energy primary electrons impinge on the specimen surface, they penetrate a short distance and the interaction volume with the solid is decreased. As a consequence the production of SEs is restricted to a smaller area nearer to the surface which results in;

(3.3.1) Increased SE Yield

Since the SEs escape depth is < 20nm regardless of the incident beam energies, when low beam energy (< 5keV) is used the interaction volume becomes comparable to the SE escape depth. Thus the majority of SEs are generated due to the direct inelastic scattering of the primary incident beam (SE1) in the immediate surface region and leads to an increase of the SE yield. The variation of the total SE yield with the beam voltage is shown in figure (2.3). Therefore the signal to noise ratio (SNR) of this signal is increased at low electron beam energies. Furthermore, at low and very low beam energies, the generated SEs can escape to be detected within a few nanometers of the sample surface where the beam interaction occurs; this gives the SE signal very high resolution. Where the intensity of the SEs in the SEM is a very sensitive function of the doping concentration, it is possible to map p-n junctions and study the dopant contrast at low energy electron beam where the SE intensity is maximised. Therefore, the obtained SEs will carry useful information about any surface doped regions, i. e. the obtained information is more localised.

(3.3.2) Reduced Charging

Insulators and semiconductor samples charge heavily when irradiated by an electron beam in SEM even when using a conductive surface layer. This charge accumulation results in unstable imaging conditions and loss of resolution due to the defocusing of the primary beam spot (Joy, 1988). However, the charging of these materials can be reduced and even eliminated with using low voltages, as schematically shown in figure (2.3). There are many methods that have been used to eliminate or reduce sample charging which involve using (different) gases environment, however imaging in low beam energy is the most effective way in imaging non conductors and semiconductors without special sample preparation techniques.

(3.3.3) Reduced Specimen Damage

In semiconductor devices, radiation damage can occur due to the accumulation of space charge inside the insulating surface layer and also due to surface recombination states near the interface between semiconductor and surface coating (Reimer, 1985). This is explained as follows: all integrated Si devices include insulating layers such as SiO_2 and Si_3N_4 to isolate conductive pads from the semiconductor. Therefore, when an electron

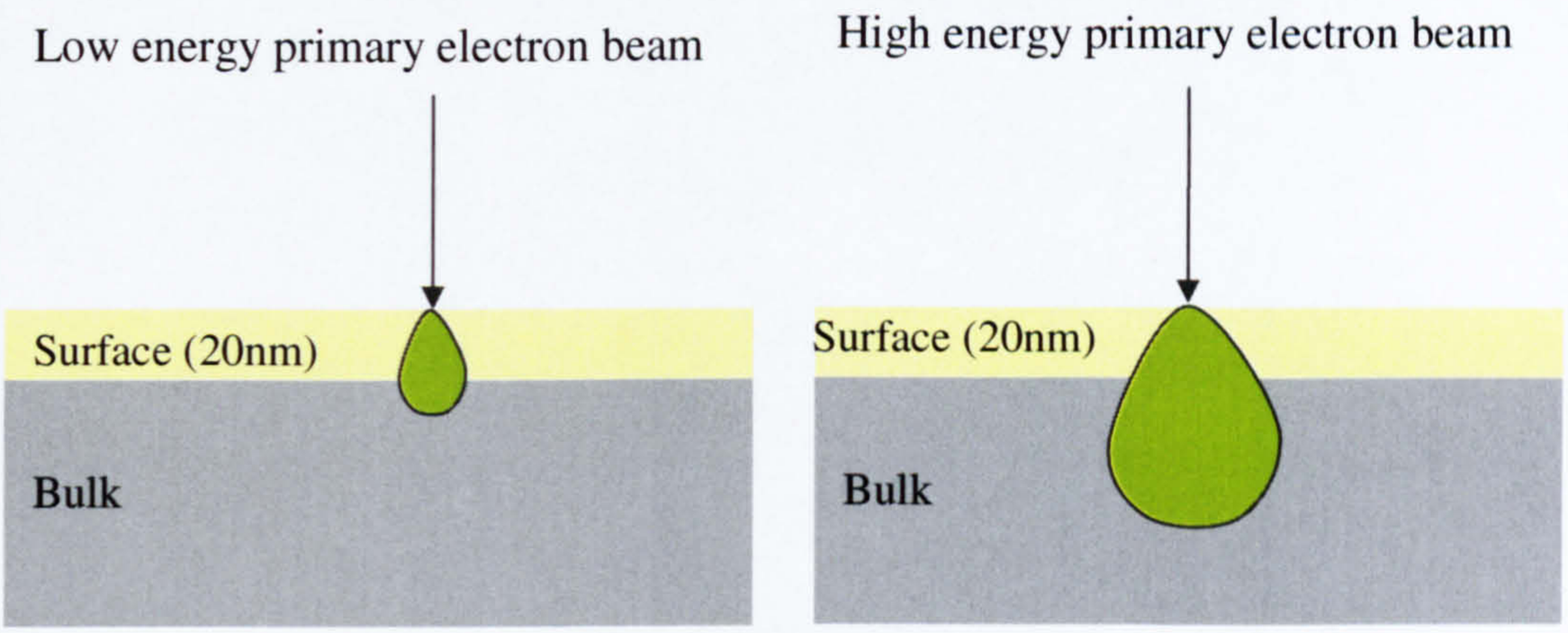

Figure (3.1) Schematic illustration of the interaction volume in SEM and low voltage SEM.

beam irradiates such a device, electron–hole (e-h) pairs are generated in the insulating layer. Whereas electrons can move easily as they have a faster mobility compared to holes which accumulate inside the insulting surface layer. Thus a device with such coating ends up with a positive charge. However, applying a negative voltage during electron irradiation can dissipate charge collection; hence damage is reversible in a device with a SiO_2 surface layer. On the other hand, damage is irreversible for Si_3N_4 layers because it contains large concentration of traps for electrons and holes; hence no charge is built up.

Apart from charge accumulation, electron irradiation can create surface recombination states near the Si-SiO_2 interface. These surface states increase the surface recombination velocity; hence influence all dependent device parameters that may lead (attribute) to broken and rearranged bonds at the interface.

Another effect of high beam energy irradiation, is that if the electron energy is increased to a few hundred keV, elastic scattering results in energy transfer to nucleus of the order of 10-30 eV. This may shift an atom from a lattice to another interstitial site. However this effect will not occur at the low electron energies used in the SEM.

For semiconductor devices, radiation damage can be minimised by utilising LVSEM, imaging at low beam energies below 5keV reduce the effects of charge accumulation and formation of recombination states.

(3.4) Approaches for Low Voltage Electron Microscopy

Apart from the above advantages and due to the rapid improvements in ultra high vacuum systems, FE guns and software packages that can analyse complex electron optical systems have opened the avenues for different designs of low voltage microscopes (Mullerova et al, 1992). The different approaches to obtain low voltages can be divided into two different approaches; the first involves utilising the improvements of the electron optical performance of the column such as increasing gun brightness, aberration correction elements and incorporating complex signal detection methods which do not affect the primary beam spot size (diameter). The second approach is to use a retarding electrostatic field to reduce the landing energy of the primary electrons. This can be done by either using an electrostatic lens or biasing the sample to a negative potential. The latter method is known as the cathode lens method.

The main advantage of this method is that the electron beam is focussed at its original high energy. i.e with relatively low aberrations and then within the cathode lens is decelerated to a landing energy continuously adjusted by the specimen bias (El-Gomati et al, 1997).

(3.4.1) The Cathode Lens

The cathode lens is of great interest in retarding field microscopy. It is usually formed by a cathode held at a negative potential and by an anode at ground potential. Figure (3.2) shows schematic diagram of the cathode lens. The retarding field between the specimen (cathode) and the anode (objective pole piece) acts as a lens for the primary electrons. The primary beam of electrons which is usually operated in the energy range 10-20 keV in conventional SEM are decelerated to the specimen by the negative potential which is finely adjustable. Therefore, the landing energy of the decelerated beam ($E_{L)}$ is given by the difference between the primary beam energy and the applied cathode potential.

$$E_L = E_P - E_U \qquad (3.1)$$

E_L is the energy with which electrons strike the specimen, E_P is the primary beam energy and E_U is the applied voltage to the specimen. The cathode lens principle allows one to vary the energy of electrons in a wide energy range making it is possible to achieve primary electron beam energy approaching zero eV.

Signal electrons generated upon the primary beam impact are accelerated back, opposite to the direction of the primary electron direction. Hence a suitable detector must be replaced within the cathode lens field to collect as many electrons as possible without allowing them to escape through the detector bore.

The spherical and chromatic aberration coefficients of the cathode lens can be approximately given as

$$S_{CL} \approx - C_{CL} \approx l\,(E_L/E_P) \qquad \text{for } E_L << E_P \qquad (3.2)$$

According to this relation, the aberration coefficient decreases as the landing energy falls for a fixed l and primary beam energy E_P, which is what we need in order to achieve the small spot size at low energies (or keep the beam spot size). Although the resolution achieved is better than that in LVSEM, it depends on the quality of the final objective lens.

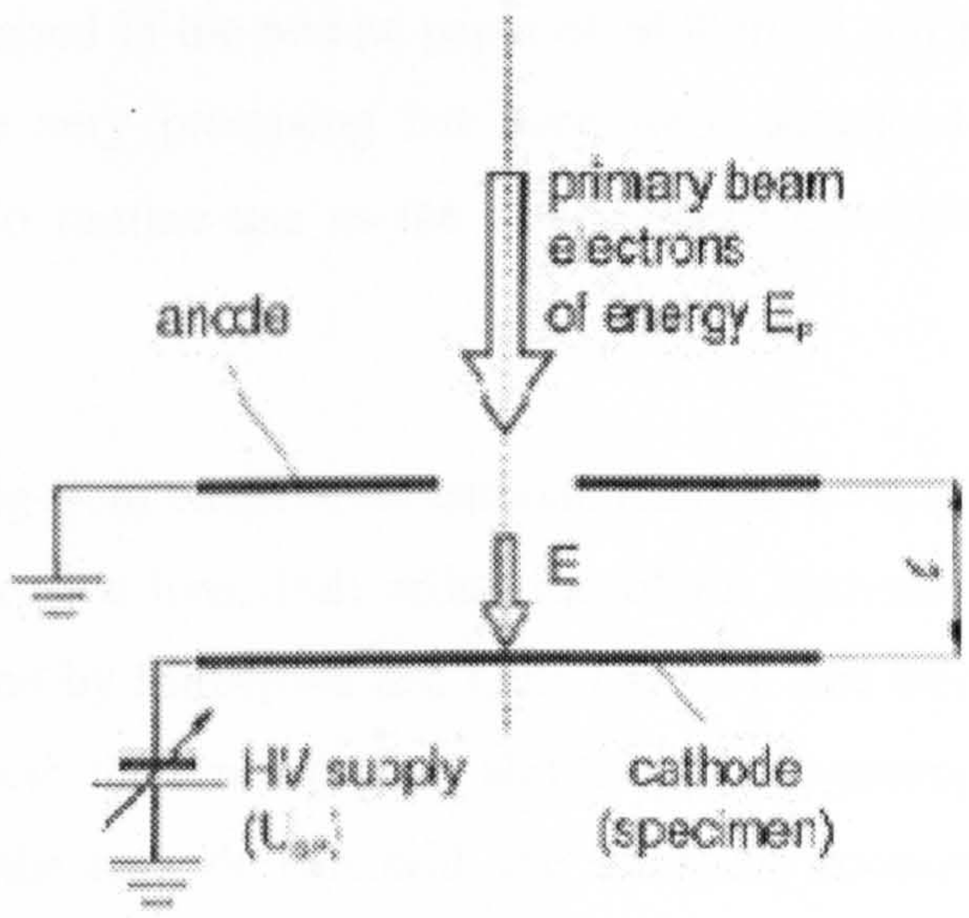

Figure (3.2) Schematic diagram of the cathode lens, *l* is the distance between the anode and cathode of the cathode lens (Müllerová, 1999)

Because the cathode lens forms only a virtual image, a focusing lens has to be used. However, the major advantage of using a cathode lens is that one can reduce the incident electron energy to units of eV. The electron optical properties of the cathode lens have been extensively studied (Lenc et al, 1992). More details about the cathode lens and about the cathode lens in combination with the focusing lens can be found in (Paden et al 1968, Lenc et al 1992 a, b and Frank et al 1999).

During the last three decades, many attempts were made to utilise retarding-field optical elements in SEM for purposes of improving the resolution at low energies. These attempts are summarised in the review paper of Müllerová and Lenc (1992a). Some of these attempts were very promising but none were advanced enough to bring this version of SEM into routine use as the Low Energy Electron Microscopy (LEEM) method.

As a special retarding-field element the cathode lens has been introduced into the SEM as a part of its objective lens. Full utilisation of the cathode lens in the SEM was experimentally proved by Müllerová and Lenc (1992b). The theory of the cathode lens takes into account both the uniform field and the anode opening field and particularly the combination of the cathode lens with the necessary focusing lens was developed (Lenc and Müllerová, 1992a,b). Preliminary image series were published which exhibited a consistent quality throughout the energy scale down to a nearly zero landing energy of electrons (Müllerová and Frank, 1993), and the basic imaging parameters were quantitatively verified (Müllerová and Frank, 1994). The cathode lens equipped SEM is capable of holding the image resolution near to the nominal one, down to the lowest energies, as is the case in LEEM. This method has been applied recently for low energy imaging of non-conducting and semiconductor specimens (Frank et al 1991, Müllerová 2001, Frank et al 2001). The cathode lens principle has been utilised successfully for the design of SLEEM for the first time at the University of York, El-Gomati et al (1997), where, a combination of scanning Auger and SLEEM is developed in order to develop a super surface analysis machine and to overcome the problems of using either of these methods alone. El-Gomati and Wells (2001 a,b) have utilised the UHV SLEEM mode for imaging doped semiconductor regions, the converted cathode lens mode allowed the incident electron beam energy to be varied from 1-1000eV with <1μm resolution. The principle scheme of the combined CMA electron gun with built in

detector for acquiring SLEEM signals is shown in figure (3.3). Frank et al (2000) have imaged doped semiconductor regions in the SLEEM mode at very low landing energies down to 0.5 eV.

For the work presented in this thesis, dopant imaging was performed in a commercial Vega SEM that has been adopted to operate in the SLEEM mode using the cathode lens principle. A brief view of the method is given in the next section.

(3.4.2) Adaptation of Vega SEM to Cathode Lens Mode

In this work, the Vega SEM was converted to cathode lens mode by placing a cathode lens below the final objective lens. The complete conversion involved also the use of a stable high voltage power supply to bias the sample, and means to isolate the sample from the sample holder. This way allowed scanning low energy electron imaging down to energies approaching sub-10 eV.

To detect electrons in SLEEM mode a scintillator detector is situated above the specimen in the field of the cathode lens. This scintillator is connected to a light pipe. The detector consists of a scintillating disc (YAG crystal) with a central bore and a light pipe that feeds a photomultiplier. This disc acts as the anode of the cathode lens and the objective aperture. The disadvantage of this method is that some of the electrons escape through the detector bore. Although reducing the bore diameter that reduces the portion of escaped signal electrons, it reduces the available field of view as well. Figure (3.4) shows an adaptation of conventional SEM to cathode lens mode with a YAG crystal detector.

(3.5) Dopant Profiling in LVSEM

Perovic et al (1995) studied several semiconductor multilayer heterostructures of Si and GaAs in both cross-sectional and oblique plan-views at low voltages (0.5-1 keV). They investigated n-i-p-i Si heterostructures with As doped Si with concentration 3×10^{20} cm^{-3} (n-type doped Si) and B doped Si with concentration 8×10^{18} cm^{-3} (p-type doped Si). This study was the first attempt to try to explain the origin of the SE contrast from dopants in Si. They found that p-type doped regions exhibit bright contrast relative to the intrinsic Si background as shown in figure (3.5).

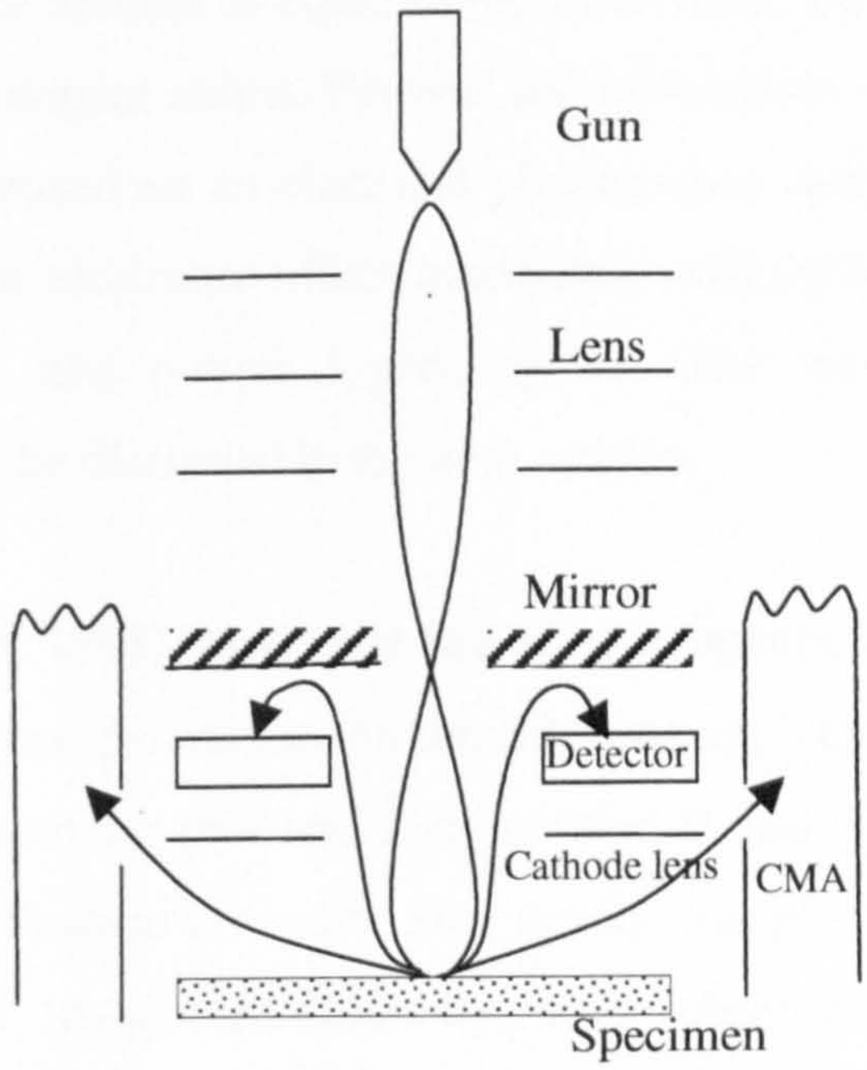

Figure (3.3) The principle scheme of the combined CMA electron gun with built in detector for acquiring SLEEM signals (El-Gomati et al, 1997).

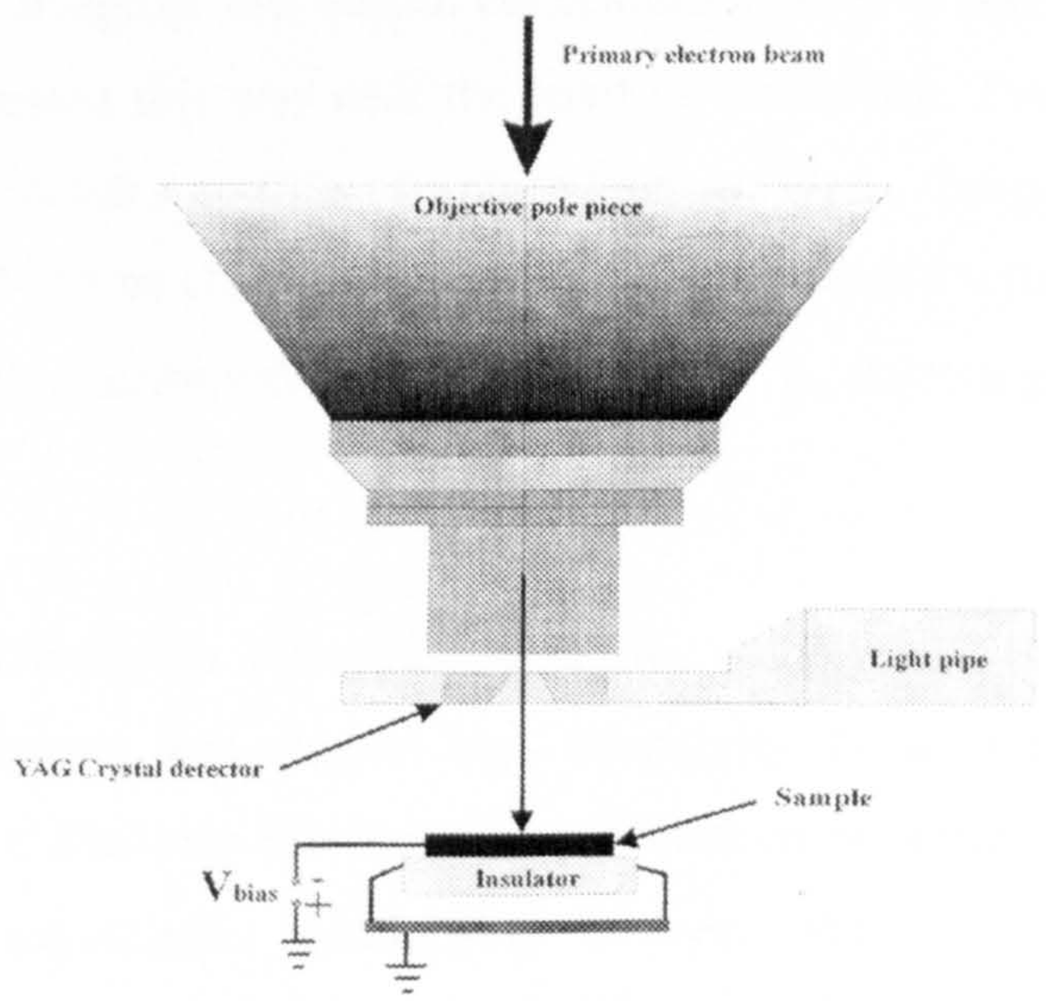

Figure (3.4) Adaptation to cathode lens mode with a YAG crystal detector (Frank et al, 1998)

In addition, they found that SE imaging of p- and n-type doped GaAs heterostructure have shown higher SE contrast from p–type doped areas in comparison with n-type doped regions. Also, they have shown that the dopant contrast is due to electrically active dopants, whose amount is equal to the free-carrier concentration, rather than the chemical number of dopant atoms. Perovic and co-workers (1995, 1998) were the first to propose a model based on an electrical phenomenon where they interpreted the SE dopant contrast as an electronic effect associated with different surface induced band bending between n- and p-type doped regions. The various contrast mechanisms proposed to date will be discussed in the next section.

Venables et al (1996, 1998) have used doped Si structures in a FESEM to investigate the effect of microscope parameters on the SE imaging. This was the first ever attempt to quantify the SE contrast profiles. They studied P and B diffused Si p^+/n and n^+/p patterns. Similar to Perovic's results, they found that p^+-diffused areas again appear brighter in the SE image. Additionally, they observed higher contrast at low accelerating voltages (around 1keV) when a through-the-lens detector was employed. However, similar SE contrast has not been observed from n^+/p junctions. This group has addressed the spatial resolution and sensitivity of the LVSEM by demonstrating its ability to detect SE image of low dopant concentration level as low as $4\times10^{16}cm^{-3}$ for B doped Si and suggested this was near the limit of sensitivity. They reported a spatial resolution of the intensity profile of approximately 17nm. Turan et al (1996) have shown that FESEM can be effectively used to map electrically active dopant profiles in two dimensions with a sensitivity as low as $2\times10^{16}cm^{-3}$ by detecting contrast of B doped regions in Si.

In spite of the difficulty in reproduction of the absolute SE contrast from similar samples, this technique has shown high sensitivity to a wide range of dopant concentration levels. Studying the contrast as a function of dopant concentration levels depicts a rough logarithmic relationship between the SE contrast and dopant concentration level in the range from $4\times10^{16}cm^{-3}$ to $3\times10^{20}cm^{-3}$ as shown in figure (3.6). This result was also verified for a larger range of doping concentrations by Elliot et al (2002).

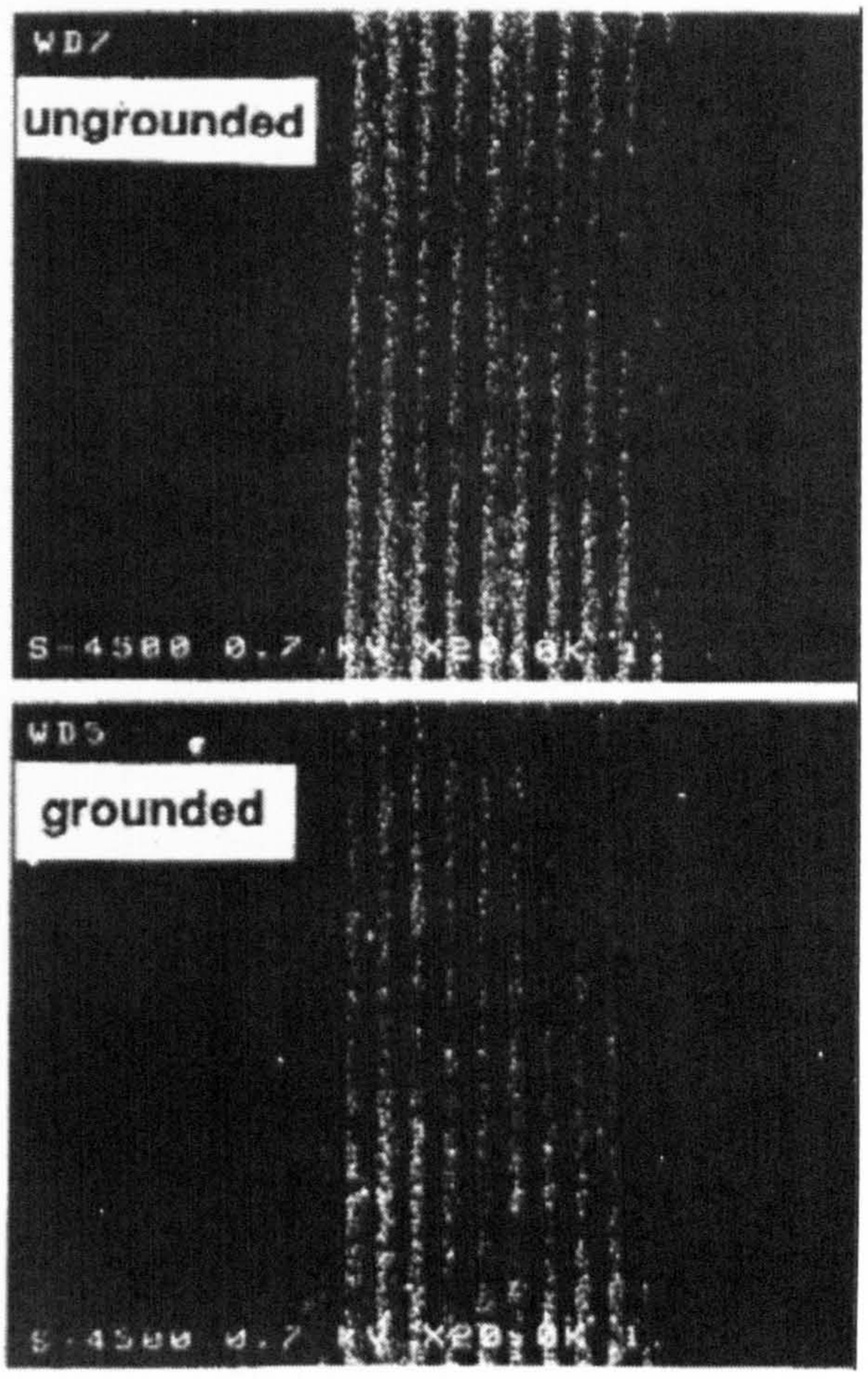

Figure (3.5) SE image of B and As doped n-i-p-i hetero structure taken at 0.7 keV in a FESEM using upper SE detector (Perovic et al, 1995).

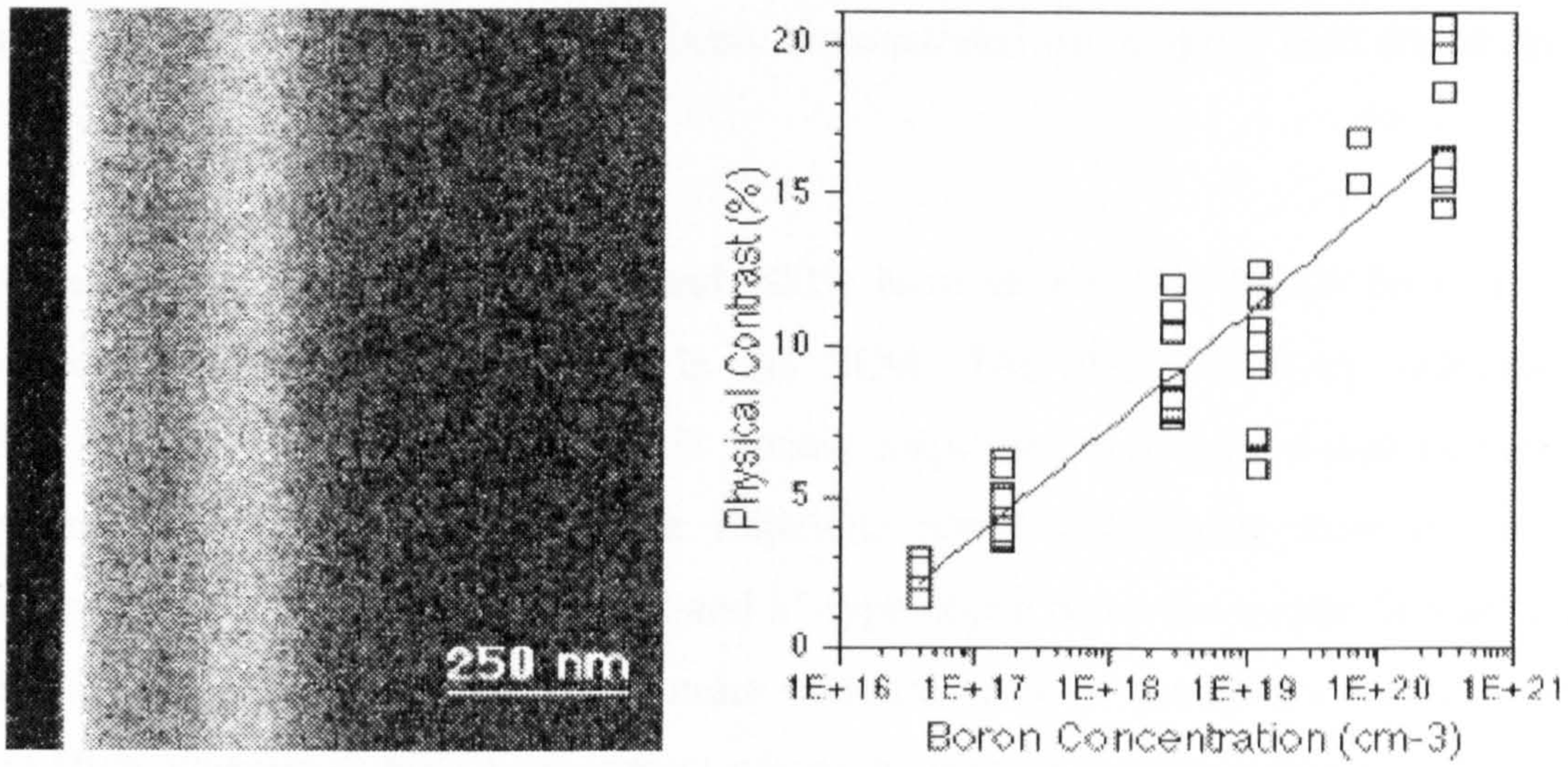

Figure (3.6) SE image of a boron doped test structure and boron concentration vs SE contrast measured from several test structures (Venables et al, 1998).

A higher contrast has been observed from Si samples treated with Hydro Fluoric acid compared with just cleaved samples (Sealy et al, 2000). Elliott et al (2001) has also found that contrast is enhanced after dipping Si sample in Ammonium Fluoride solution. Elliott et al (2001; 2002) have carried SE imaging observations by examining the SE contrast of doped Si samples at different temperatures and of biased p-n junctions in order to investigate the built in potential effect on the SE dopant contrast. The high sensitivity of the LVSEM was demonstrated by observing contrast from p-type doped Si with dopant concentration level as low as $8\times10^{15}cm^{-3}$. The ultimate spatial resolution of the LVSEM has been demonstrated by imaging 1nm doped layers (Elliot et al, 2002)

El-Gomati et al (2000, 2001, 2004 and 2005) have studied SE dopant contrast as a function of possible contamination in the SEM. The effect of work function of hydrocarbon layer deposited on the Si during inspection has been tested further by depositing candidate metals of work functions lower and higher than that of Si. Observation of p^+-type doped patterns and n^+-type doped Si on the n-type Si was made in LVSEM and in the SLEEM both under standard vacuum conditions and also in an Ultra High Vacuum (UHV) environment where the sample surface was examined in the Auger electron spectrometer. This group related the SE dopant contrast to surface structure.

Jayakody (2003) has carried out new experiments to clarify surface effects on the contrast. He has studied doped Si samples in the SLEEM, and observed higher contrast at very low energies (few eV). He also compared SE dopant contrast obtained with a sample exhibiting a hydrocarbon layer and then after cleaning the sample surface with ion beam, in UHV. Jayakody found that the existence of a thin carbon layer on the imaged sample surface has enhanced the obtained contrast.

Merli et al (2002) have developed a new strategy based on incoherent bright field (BF) imaging at low energy in a SEM used in transmission mode. The image is formed using the signal produced by the SE resulting from the conversion of transmitted electrons (TE) on a converter and collected by the standard E-T detector. The converter used is a circular disk, covered with MgO smoke, a material providing a SE yield of about 1 for a wide range of electron energies (1-30keV)(Reimer; 1998). This material covers an Al

disk centred on the optical axis of the microscope. The experimental setup is shown in figure (3.7)

In this method SE profile versus distance for the multilayer has shown dependence of the SE intensity of the different regions on the atomic number, whereby multilayers with higher atomic number appear brighter in the profile as should occur for a BF image. Also in this technique layers of 2 ML are visible, their width is equal to the convolution of the layer size with the probe size.

Merli et al (2002) suggests that it is possible to deduce dopant profile information, with the resolution of the probe size using BF images and operating in transmission at low energy in SEM. In such a case, the image profile can be considered the convolution of the dopant profile with the beam profile. The experiment has been performed with As implanted Si with two different doses. Then the As implanted dopant profiles have been simulated with Monte Carlo computer code that has been previously developed for the simulation of backscattered electron images. The obtained dopant distribution is shown in figure (3.8). This figure shows the peak concentration at a depth between 15 and 20nm.

In this method, the detected dopant concentration is very high and the resolution of this method is equal to the spot size of 6nm. However, the resolution and the sensitivity can be improved by incorporating Schottky or field emission sources as the microscope cathode.

SE dopant contrast from differently doped n-type regions of low dopant concentration in commercial LVSEM is extremely low; therefore, such regions can not normally be detected. It was reported by Jayakody (2003) that depositing thin layers of C, Cr and Ni onto Si surfaces that were in-situ cleaned by ion bombardment have enhanced the obtained contrast. Schonjahn et al (2002) have demonstrated that energy filtering of SEs enhanced the contrast of differently doped n-type regions. This is attributed to contrast dependence on the shift of energy spectra from n and p regions rather than the secondary electron yield differences.

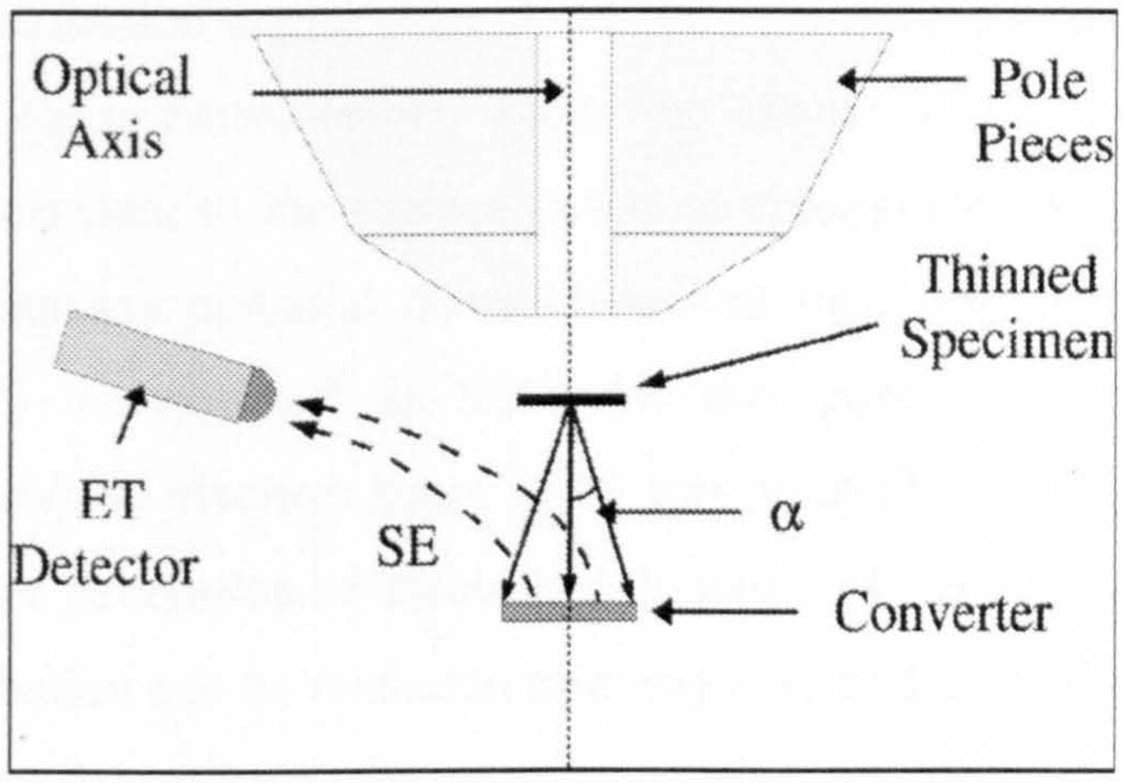

Figure (3.7) Scheme of the experimental setup used for BF STEM imaging (Merli et al, 2002).

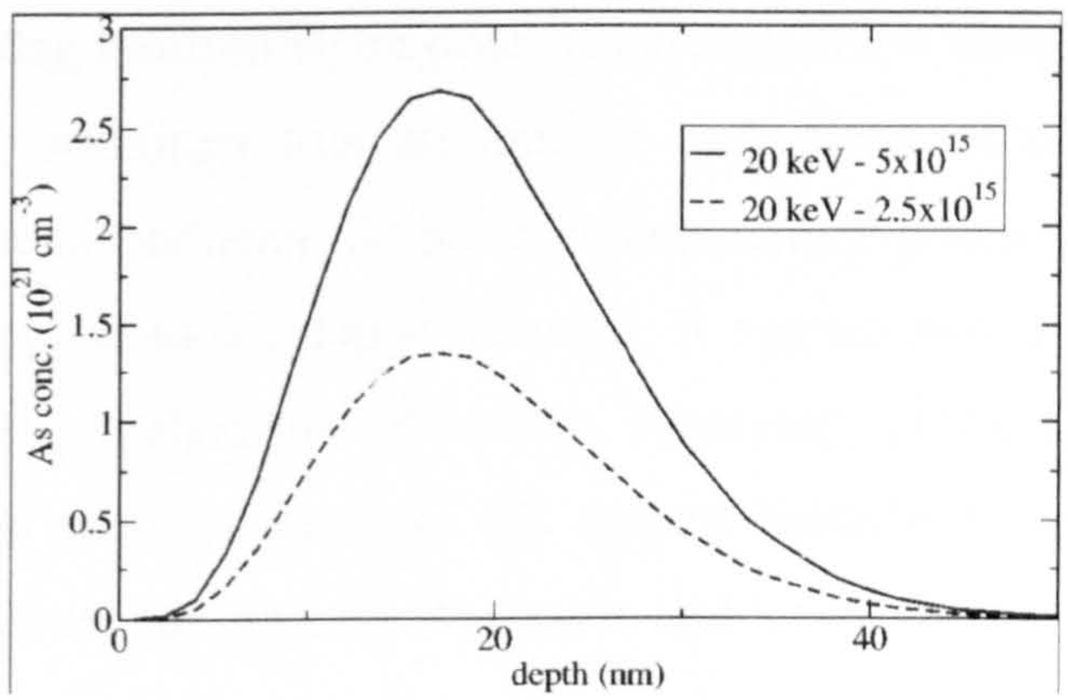

Figure (3.8) As concentration vs depth in the implanted silicon specimens.

Thomas et al (2004) have studied effect of electron beam injection in the SEM on surface potential of p- and n-type doped Si. It is found that during electron beam bombardment, a local surface potential change influencing electron beam technique due to generated carriers during inspection, since it changes beam properties and sample properties. The distribution of the generated carriers is calculated using semiconductor equations. This distribution causes a local change in surface potential due to presumed movement of the quasi Fermi level. Since the change of the average quasi-Fermi energy level is equivalent to the surface potential change (or has the same functional dependence), the surface potential distribution was measured with a scanning probe microscope (SPM) incorporated in SEM for this purpose. The surface potential distribution produced by electron beam in Si can be attributed to diffusion processes that take place after generation of electron-hole pairs. Moreover, it was observed that the potential distribution can be related to minority carrier distribution. For n-Si, there is a depletion of holes for positive and an accumulation for negative cantilever voltages. On the other hand, for p-type doped Si there is an accumulation of electrons for positive voltages that has been calculated and a depeletion for negative voltages.

However, SE imaging was not collected during inspection. In addition no information was reported regarding electron beam dose which may affect charge distribution within the semiconductor. Although this attempt to understand effect of electron beam injection in doped semiconductor did not correlate surface potential distribution during electron beam inspection to SE dopant contrast, it opened new avenues to understand SE dopant contrast mechanism. Whereby observing potential variations during inspection is almost more relevant to SE dopant behaviour from surface potential measurements in thermal equilibrium (Tanimoto and Vatel, 1996).

The LVSEM of dopant profiling using the SE signal is sensitive to the doping concentration levels and it became superior to many competitive methods. Therefore, this technique has become a useful tool for qualitative analysis of p-n junctions. However, this method is still largely qualitative and instrument dependant. In addition to the difficulties in reproducing the SE images in the LVSEM due to the high sensitivity of surface contamination, it has not yet been accepted by industry as a 2D dopant profiling technique for ULSI. And in order to be accepted, a full understanding of the SE contrast mechanism is required for quantitative analysis of the SE image

contrast. For this purpose, and due to the growing use of SE imaging in the SEM to map doped semiconductors, various descriptions have been developed to explain this phenomenon. The next section will demonstrate the main mechanisms which explain the contrast.

(3.6) Review of the Dopant Contrast Mechanism

The SE contrast observed from doped regions of semiconductors is electronic in nature, since the amount of impurity atoms in the range 10^{16} to 10^{19} atoms/cm^{-3} of Arsenic or Boron doped Si is 0.00002 to 0.02 percent respectively, the contrast from doped areas can not be attributed to compositional difference in the doped regions. There are three existing mechanisms that have been developed to explain the SE dopant contrast. These are:

(3.6.1) Band-Bending and SE Dopant Contrast

If any semiconductor surface is cleaved in air, this results in the introduction of crystal atomic energy levels in the forbidden gap, referred to as surface states. Surface states also arise through impurities and these surface states are referred to as extrinsic surface states (Rhoderick and Williams, 1988). The presence of surface states modifies the electron energy levels at the surface. Surface states may possess electronic charge, which results in the energy bands bending upwards in n-type material and downwards in p-type material and pinning the Fermi energy within the band gap.

For n-type semiconductors, electrons lying near the bottom of the conduction band will be captured by surface states, producing a positive space charge layer near the surface. This means a depletion region of width W is formed near the surface. The resultant charge flow creates an electrostatic dipole layer that retards the emission of secondary electrons generated as a result to interaction of the primary beam electrons with valence electrons in the near surface region. As a result to this dipole, the electron energy in the bulk is lower than the surface by qV_{bb} which is the amount of band bending.

A similar situation occurs for p-type material. However, a positive charge distribution results in the surface with a negative charge distribution extending into the depletion region. Thus, this electric field will accelerate SEs to the surface in p-type and the

electron energy in the bulk is higher than the surface by qV_{bb}. Figure (3.9) presents band-bending on n-type and p-type semiconductors. The internal electric fields responsible for the band-bending are of opposite sign for p-type and n-type material.

Perovic et al (1995) proposed that SE dopant contrast resulted from these electric fields, which accelerated SEs to the surface for p-type and repelled SEs back into the bulk for n-type. Therefore, p-type materials would appear brighter in the SE image than n-type.

(3.6.2) Patch–Fields and SE Dopant Contrast

Many of the related studies of SE dopant contrast have explained the observed contrast due to the differences in the work functions which caused patch field effects. It was suggested that the shape of the surface potential barrier that affect the SE emission is altered by patch fields. To understand this effect, consider a small region of low work function material, A, surrounded by higher work function material B, as shown in figure (3.10a)

When the materials are brought together, the Fermi level will equalise through the transfer of electrons and the surface charge will be redistributed. The A material will be left positively charged and B material will be negatively charged. Due to this distribution, an electric field called a patch field will form just outside the crystal to keep the sample overall electrically neutral. This field works as an additional potential barrier where the SEs emitted from material A must overcome to escape the surface. The height of the barrier is equal to the difference between the two work functions (ϕ_B-ϕ_A). Thus, material A will appear darker than material B when they are brought in contact. This model is only correct, if region A is much smaller than region B but no experimental evidence is presented. It is not clear in the literature the patch field potential barrier effect if region A is comparable in size with region B (Elliot, 2001).

Patch field effect on SE emission has been studied by Futamoto et al (1985). Sealy et al (1997) detailed description of the effect of the patch field effect on SE emission from differently doped semiconductor regions. It was suggested that due to generated external patch field, the resulting ionisation energy would then become lower for p-type material than n-type. This is discussed in the next section

(a) n-type

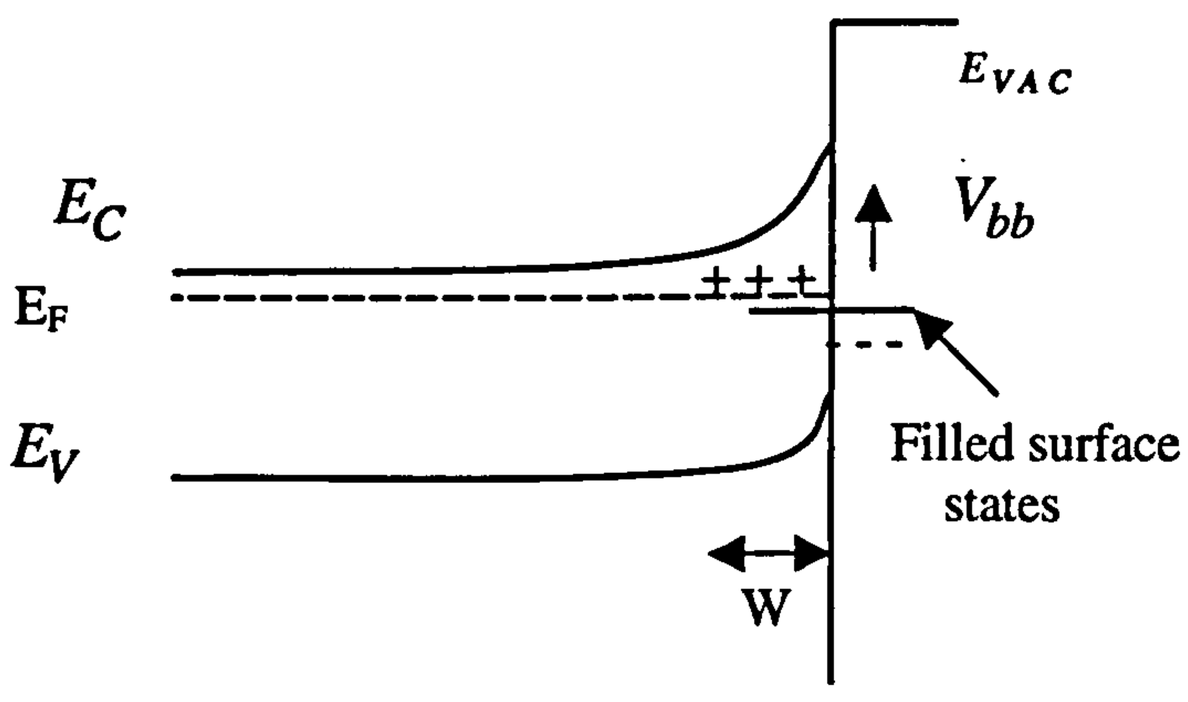

(b) p-type

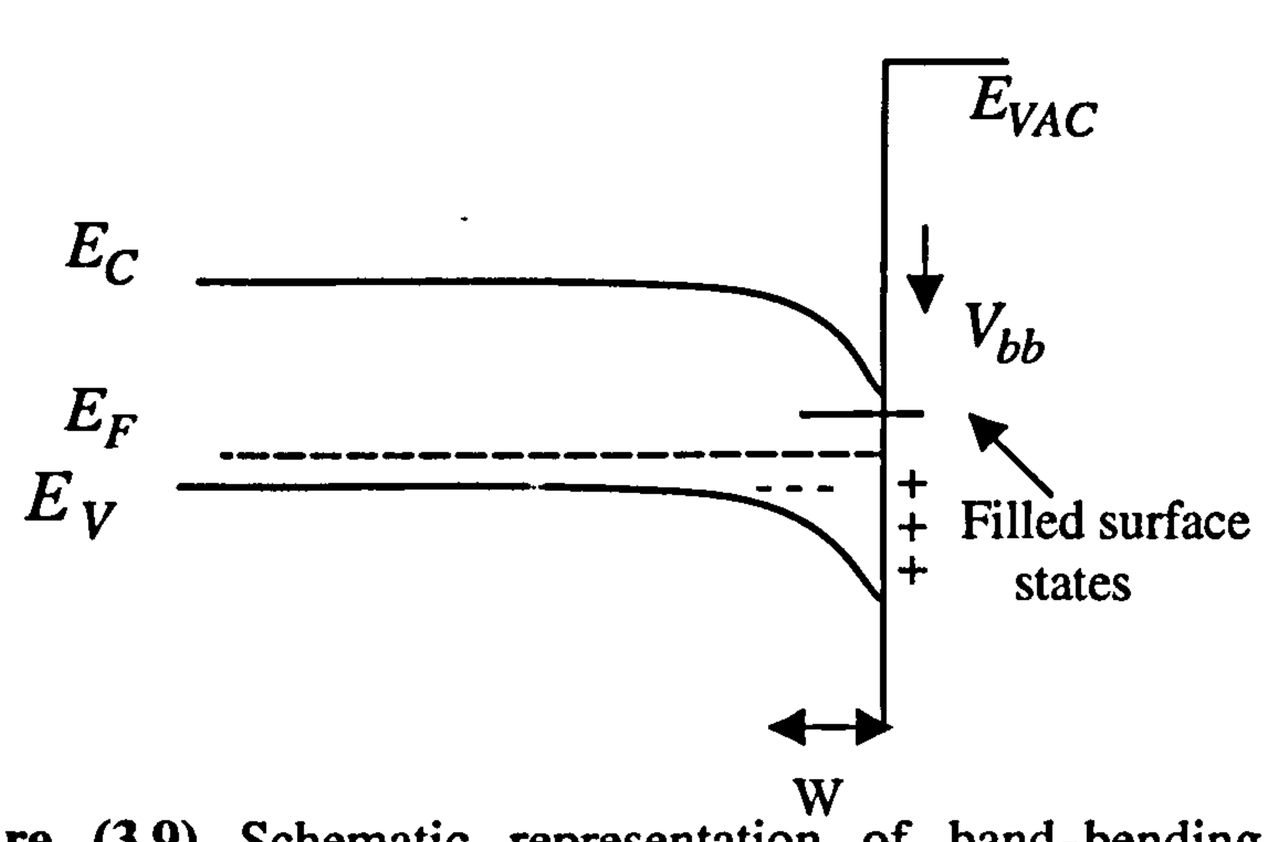

Figure (3.9) Schematic representation of band–bending on (a) n-type (b) p-type semiconductors. E_C, E_V and E_F are the energy levels of conduction band, valence band and Femi level respectively. E_{VAC} is the energy of the vacuum level and W is the depletion region extension into the semiconductor from the surface.

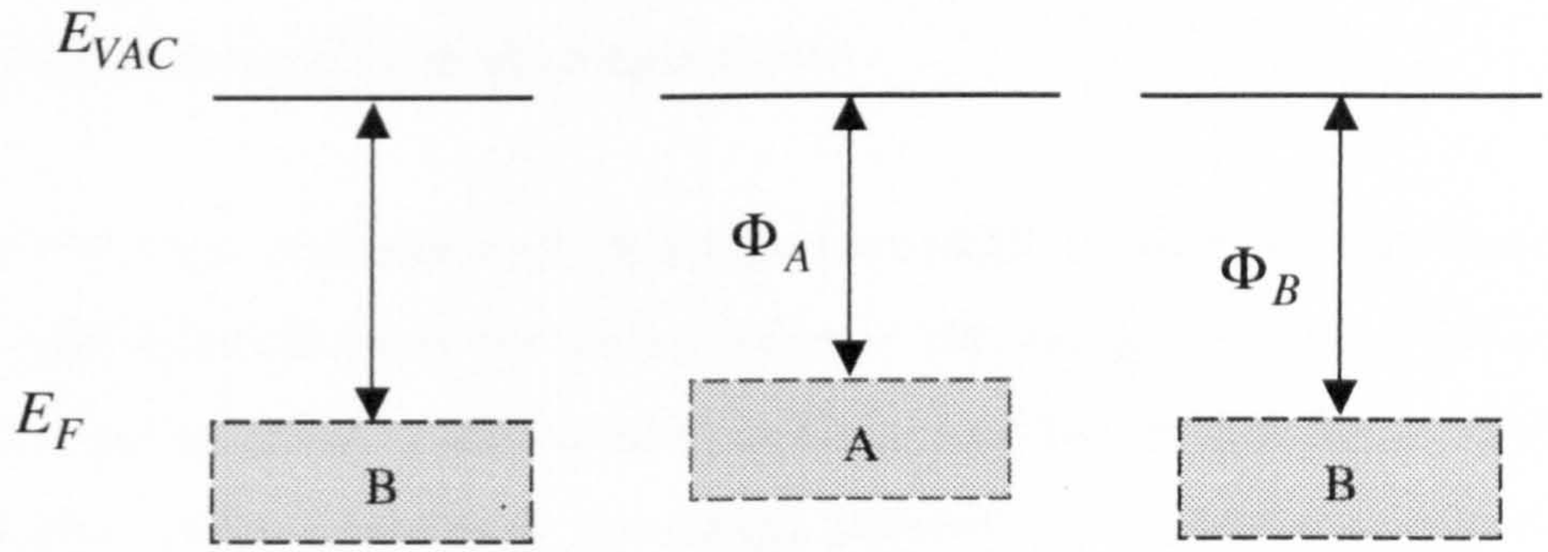

(a)

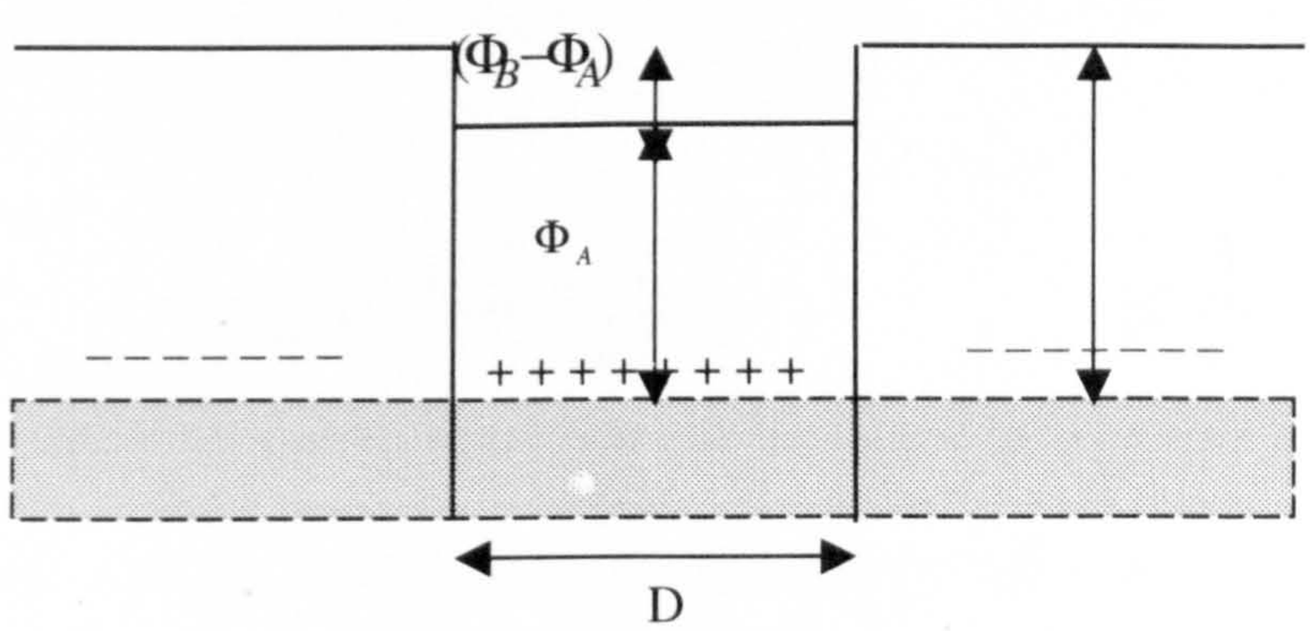

(b)

Figure (3.10) Energy band diagrams for a thin region of low ϕ material A surrounded by a higher ϕ material B when (a) the materials are separated.

(b) the materials are brought into contact.

(3.6.3) Ionization Energy and Patch Fields Contrast

One of the main models that have been developed to understand the SE dopant contrast phenomenon is based on the work of Howie, Castell and Sealy (2000), who related contrast to electron ionization energy and patch fields. In this model, the authors considered the observed contrast as corresponding to a clean semiconductor surface, possibly with some layer of surface states.

Due to the low occupation of the conduction band and surface states in semiconductors, the most relevant value for SE emission is the energy difference between the nearly fully occupied states at the valence band edge and the vacuum level, which is called the ionization energy. However, the energy required for SE emission within the bulk of a crystal not only depends upon the ionization energy but also upon other interior conditions and upon the conditions at the surface.

At equilibrium, the Fermi levels are aligned, but the energy bands are bent across the depletion region and a built–in voltage (V_{bi}) results. The built-in voltage is determined by the acceptor and donor concentration relative to the intrinsic carrier density (Sze, 1981)

$$V_{bi} = \frac{k_B T}{q} \ln\left(\frac{N_A N_D}{n_i^{\,2}}\right) \qquad (3.3)$$

Sealy suggests that the effect of the built-in voltage on the dopant contrast is equivalent to the external patch field generated by the electrostatic dipole at the junction. Due to charge redistribution across the junction, Sealy has proved mathematically that an external patch field must exist outside the specimen generated by the electrostatic dipole at the junction. According to existence of this external field, SE from the p-side region require an energy E_p to be collected, whereas for a SE to be collected from the n-side requires an energy of $E_n+\Delta E_n$.

An electron from the n-side requires more energy for emission than electron from the p-side by ($1/2V_{bi}$) to surmount the barrier (Sealy, 2000). Figure (3.11) presents a schematic of the band structure of a p-n junction and it shows effects of the interior

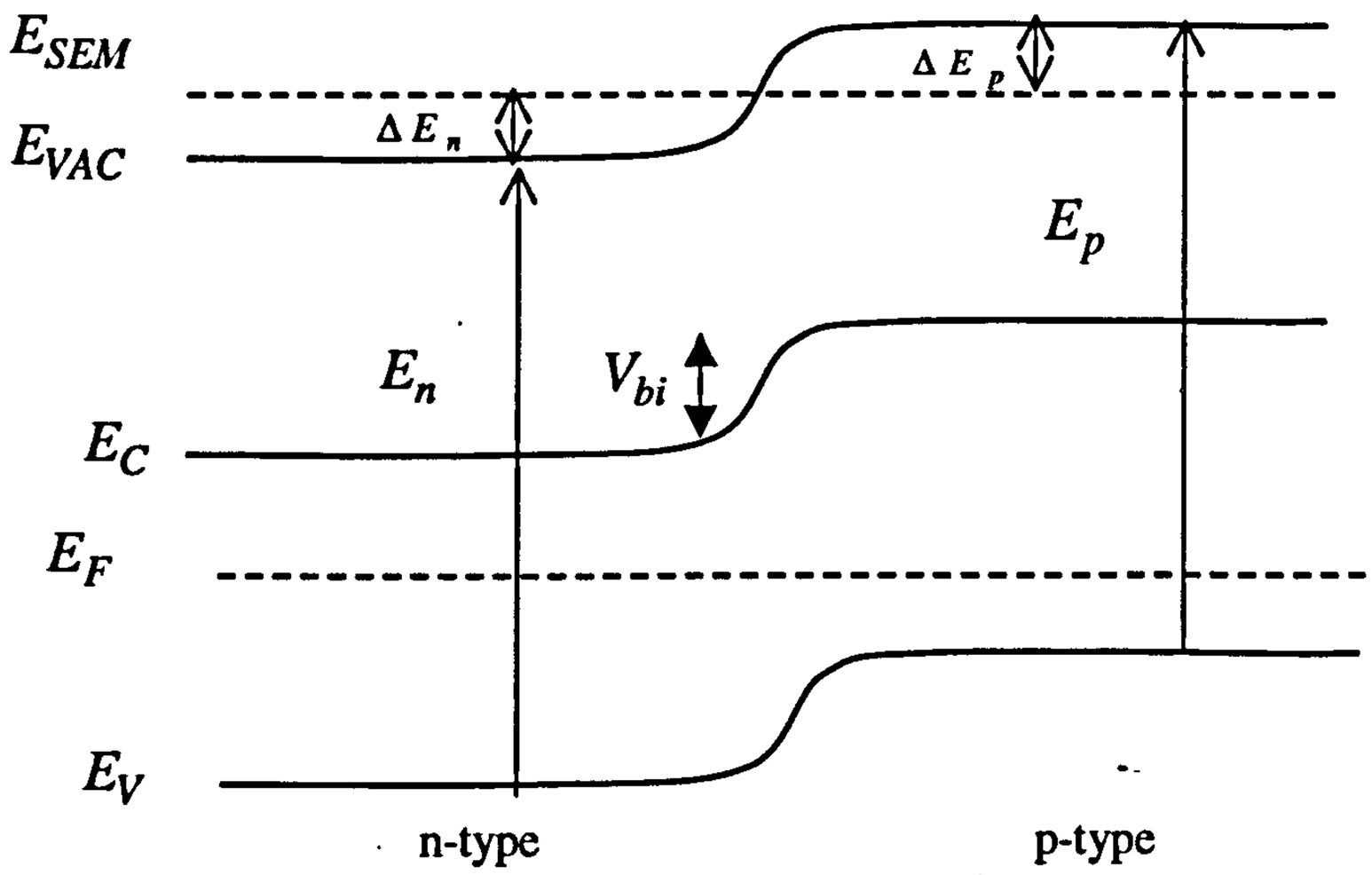

Figure (3.11) Schematic representation of the band structure of a p-n junction. For SE emission from p-type to E_{VAC} an amount of energy E_p is required, compared to $E_n+\Delta E_n$ for n-type. This variation in energy gives rise to the SE contrast (Sealy et al, 2000).

structure and the external conditions on the required energy of SE emission within the junction.

According to Sealy's theoretical model (2000) for the case of a p-n junction, the energy required to take an electron from the valence band to the vacuum level is independent of the dopant concentration and unaffected by band bending at the surface. In addition, the contrast mechanism exhibited in the SE imaging between differently doped regions arises from the difference in energy required for electron emission from these regions and they suggested to call it ionisation energy contrast. It was also reported by the same authors that contribution of band bending due to surface states is less dominant compared to band bending due to effect of the built in potential of the junction. Furthermore, band bending induced by surface states decreases the contrast, because surface states tend to pin the Fermi level towards the centre of the energy gap, and as a consequence, this effect reduces the difference in ionization energy between p- and n-type doped areas.

Elliott (2002) has carried out experiments to study the effect of built in potential on the contrast by examining the contrast at different temperatures and after surface H-passivation treatment. Also she studied the contrast at a Si p-n junction, as the junction was forward and reverse biased.

Mullerova et al (2002), reported the drawback of this model in detail. We can summarise the weak points as follows:

1- In the basic low density of the surface states, the SE emission is considered solely from the valence band, and the contributions of the conduction band are neglected.

2- The energy required to move an electron from the top of the valence band to the vacuum side of the surface double layer is assumed to be independent of dopant concentration; i.e. the patch fields act between regions of different densities of the surface dipoles.

3-The Authors of this model expected that a small p-type region surrounded by n-type should lose its contrast, though without presenting any experimental evidence. Further, this model is unable to explain the n^+/n contrast and p^+/n^+ contrast.

(3.6.4) Metal-Semiconductor (M-S) Contact

Although the above studies acknowledging that there is likely to be a thin surface film of contaminants of unknown composition and thickness formed during sample inspection in the SEM, they did not take into account the effect of this film on the SE mission when interpreting the obtained results. M-S contact model takes into account the influence of the surface layer on the obtained contrast. This model related the observed contrast to the existence of a thin surface layer of hydrocarbons of a thickness dependent on the specimen preparation and the vacuum environment in the microscope used.

When the electron beam strikes the specimen surface, the hydrocarbons quickly crack to form a carbonaceous layer which has quasi-metal properties. This layer was suggested, and using Auger electron spectroscopy for surface analysis, confirmed experimentally by El-Gomati and Wells to be graphitic. This layer can be several nanometers thick. Thus, the observed contrast can be interpreted as governed by a metal-semiconductor junction. The specimens used to confirm this model consisted of p^+(B) doped patterns on n-type silicon and n^+(As) on n-type silicon. Since the carbon work function ϕ_M is about 5.1eV, somewhat higher than that for Si ($\phi_S \approx 4.9$eV), i.e. $\phi_M > \phi_S$, and for n-type it is known, a double layer charge will be formed on the surface where Schottky contact is formed on the n-type, thus lowering SE emission. On the other hand, an Ohmic contact is formed on the p^+-type and so the electrons will pass with lower resistance. Figure (3.12) is a schematic of the band structure of a metal- semiconductor contact in the case of $\phi_M > \phi_S$ for both p-type and n-type.

In case of p^+ and n^+ doped regions, Ohmic contacts will therefore form, but with different degeneracy. Related to the differences of the Fermi level positions, the secondary electron emission will be different in these two cases with the n^+ region being generally higher than the p^+ region. Experiments related to this model demonstrated that the SE contrast from the n^+ -type is brighter than that from the n-type regions, and also indicated that the obtained contrast follows the pattern $C_n^+ > C_p^+ > C_n$ (El-Gomati et al, 2001).

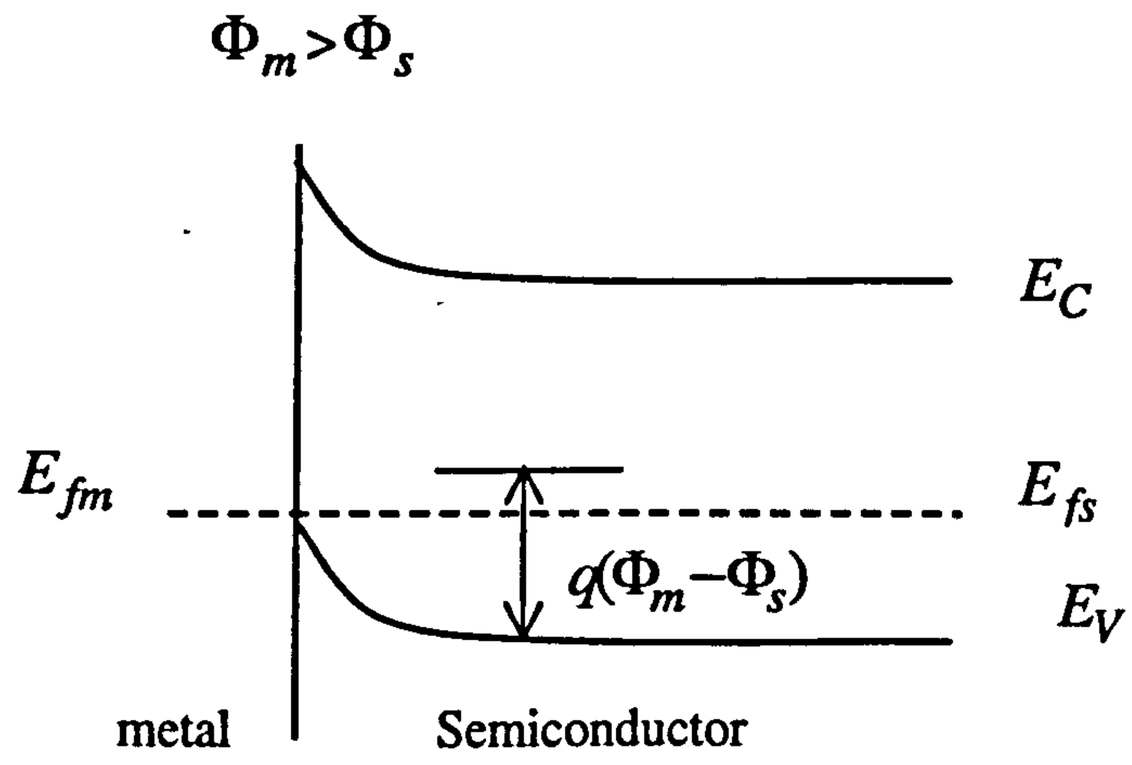

(a)

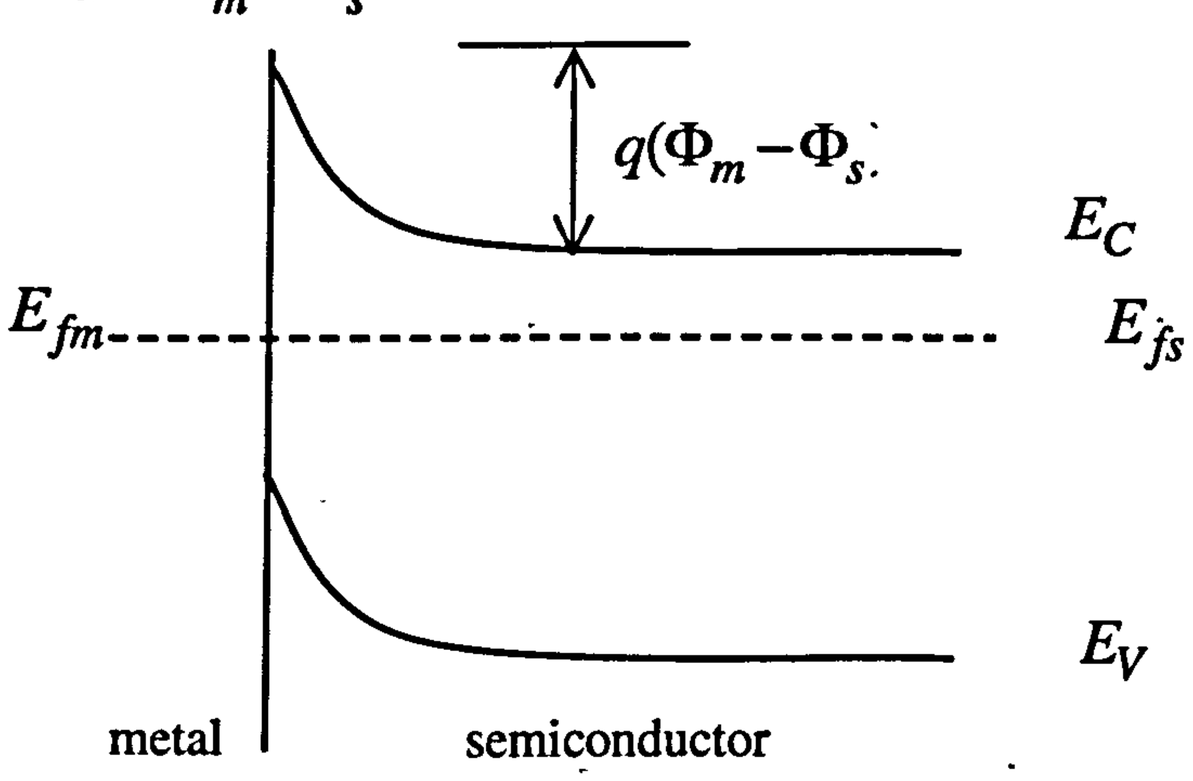

(b)

Figure (3.12) The energy band diagram of metal to semiconductor contact depicting the case for a metal work function greater than that of the semiconductor. This results in (a) an Ohmic contact on the p-type region and (b) a Schottky contact on the n-type region (El-Gomati et al, 2001).

In short, this model assumes the surface structure will affect the SE emission from the specimen and that it should be taken into account. It also shows the power of combining AES and SEM to analyse the surface structure to study doping contrast but in the long run. Therefore, it has to rely on the SEM alone.

Moreover, this model predicts that when differently doped materials for example, p^+ and n silicon are coated with metals of work functions both higher and lower than that of silicon, both signs of p^+/n contrast can be obtained and the structure contrast will be inverted. This prediction has been confirmed by means of nickel and chromium over-layers, where the contrasted from the same doped Si was inverted (El-Gomati et al, 2001).

(3.6.5) Further Comments on the SE Dopant Contrast Mechanism

An additional suggestion about the origin of the SE dopant contrast has been made by Frank et al (2006). As mentioned previously, the possible contrast influencing factors include the release of signal electrons, their motion in the subsurface or above surface electric fields and and their passage through the surface potential barrier (Frank et al, 2006). And one additional factor has not been mentioned is that the absorption of hot electrons on their way to the surface. An attempt has been made to explain the p/n contrast in the light of this factor. Photoemission electron microscopy has been used to generate low energy electron emission in this case, whereby, photon absorption is a more straightforward mechanism for generating low-energy electron emission rather than the scattering of primary electrons. It is suggested (Frank et al, 2006) that the p/n contrast is primarily related to local differences in the absorption of hot electrons along their trajectory toward the surface by generating e-h pairs. Below a certain energy threshold, such inelastic collision prevents both the scattered and the excited electrons from escaping the target and leaves time for their recombination with holes inherent to the p-type, so that the ionized acceptors become unbalanced and the p-type area is negatively charged. This explanation is expected to be valid in the interpretation of image contrasts formed by secondary electrons. However, the application of this mechanism for reliable quantitative mapping remains a task for further research.

(3.7) Summary

The scanning electron microscope is a natural choice for imaging doped semiconductor structures since mid 1990s if operated at low voltages after the significant advanced development in its capability for the study of material structure. LVSEM is witnessing intensive activity in obtaining high spatial resolution and signal electron detection. The LVSEM using the SE signal is sensitive to the doping concentration levels and type and the authors generally agreed that the p-type semiconductor is brighter than the n-type semiconductor. Due to the growing use of SE imaging in the SEM to map doped semiconductors, various descriptions have been developed to explain this phenomenon. However, the exact interpretation of the SE dopant contrast remains questionable, in particular as regards the measurement of the dopant concentration.

Chapter 4: Experimental Set Up

(4.1) Introduction

Most of the experiments reported in this thesis were performed on a Vega SEM. However an FESEM was used for the results reported in chapter 6; to study electron dose effect and scanning speed effect on SE dopant contrast. In addition, some results were obtained from the Vega SEM after converting it to the Scanning Low Energy Electron Microscopy (SLEEM). This is a short chapter explaining the differences between the SEMs used, which might be relevant to doping contrast. As a large number of Si samples were examined throughout this thesis, this chapter also describes the structures of these samples. Due to the large range of surface analysis instruments that have been used throughout this dissertation such as XPS and KPM, this chapter also describes some specific details of XPS and the processing methods (operating conditions) that have been adopted for the analysis of sample surface layers, in addition to the main features of these instruments.

(4.2) Equipment used in this Thesis

(4.2.1) SEM and FESEM

Two SEMs were used in this thesis, Vega SEM and Serion FESEM. There are major differences between these SEMs that influenced the magnitude of the dopant contrast measured by each of them; the vacuum level of the microscope specimen chamber, the electron gun and the SE detection system.

The Vega SEM has a thermionic emission gun of a heated tungsten filament type. The chamber is pumped with a turbomolecular pump to approximately 4×10^{-3} Pa (~10^{-7} Torr ~ 4×10^{-5}mbar). In the thermionic emission gun, electrons overcome the work function ϕ by thermionic excitation then accelerated toward the anode.

The Serion has a thermally assisted Schottky emitter. The vacuum in the chamber is ~10^{-4} Pa, while the vacuum in the column is a UHV. Since the tip of such emitter must be kept under UHV so that ion bombardment from the residual gas does not destroy it (Reimer, 1998). Therefore, the column is pumped down to1.7×10^{-10} Torr better than 10^{-6} Pa. In an electron gun, electrons emitted from the tip are accelerated between the cathode and anode. FEGs require two anodes the first regulates the field strength at the tip and hence emission current. The second anode accelerates the electrons to the final

kinetic energy which can range from 0.1 keV to 30 keV.

The Schottky emitter has a tip radius (0.1- 1.0 μm). This tip is made of W (100) and coated with ZrO to lower ϕ from 4.5 to 2.8 eV. This reduction allows electrons to overcome the ϕ at a temperature of 1800K. Schottky emitter operates on the principle that an applied high field (~10^6 V/cm) at the cathode further decreases the work function to ~ 0.4 eV (Reimer, 1998). However, Schottky emitters require thermal energy to enable electrons of overcoming the barrier. To avoid destroying the tip, similar to cold FEGs, Schottky emitters must be kept under an UHV.

The advantages of the FEG emitters come from their small energy spread ΔE (full-width half maximum) of the emitted electrons and the gun brightness (β) which is defined as the current (ΔI) passing through an area (ΔS) into a solid angle ($\Delta\Omega$) (Remier, 1998). In Schottky emitters these are 0.6 eV and 5-10 x10^8 Am^{-2}, respectively (El-Gomati, private communication). Small energy spread is desirable to reduce chromatic aberrations at the cross over in the lens, and a large gun brightness to increase the electron beam current at the specimen (Goldstein et al, 1981). Another advantage of FEG is the high gun brightness even at low accelerating voltages compared with low brightness of thermionic emitters.

Furthermore, the small energy spread of FEG emitters, results in a smaller diameter of the virtual source (3-15nm) which needs only one demagnifying lens to attain electron probe diameters below 1.0nm (Remier, 1998). Some properties of tungsten thermionic emitter, Schottky emitter and FEG are summarised in table (4.3)

Both the Vega SEM and Serion FESEM can be operated at low voltages which made it suitable for the work carried out here.

Both Vega SEM and Serion FESEM are equipped with a standard in chamber E-T detector. The Serion FESEM is also equipped with a through-the-lens detector. In this work, the Vega SEM was also operated in the SLEEM mode by converting it to the cathode lens mode by placing a cathode lens below the final objective lens. The complete conversion has been shown in section (3.4.2). This way allowed scanning low energy electron imaging down to energies approaching sub-10 eV. To detect electrons

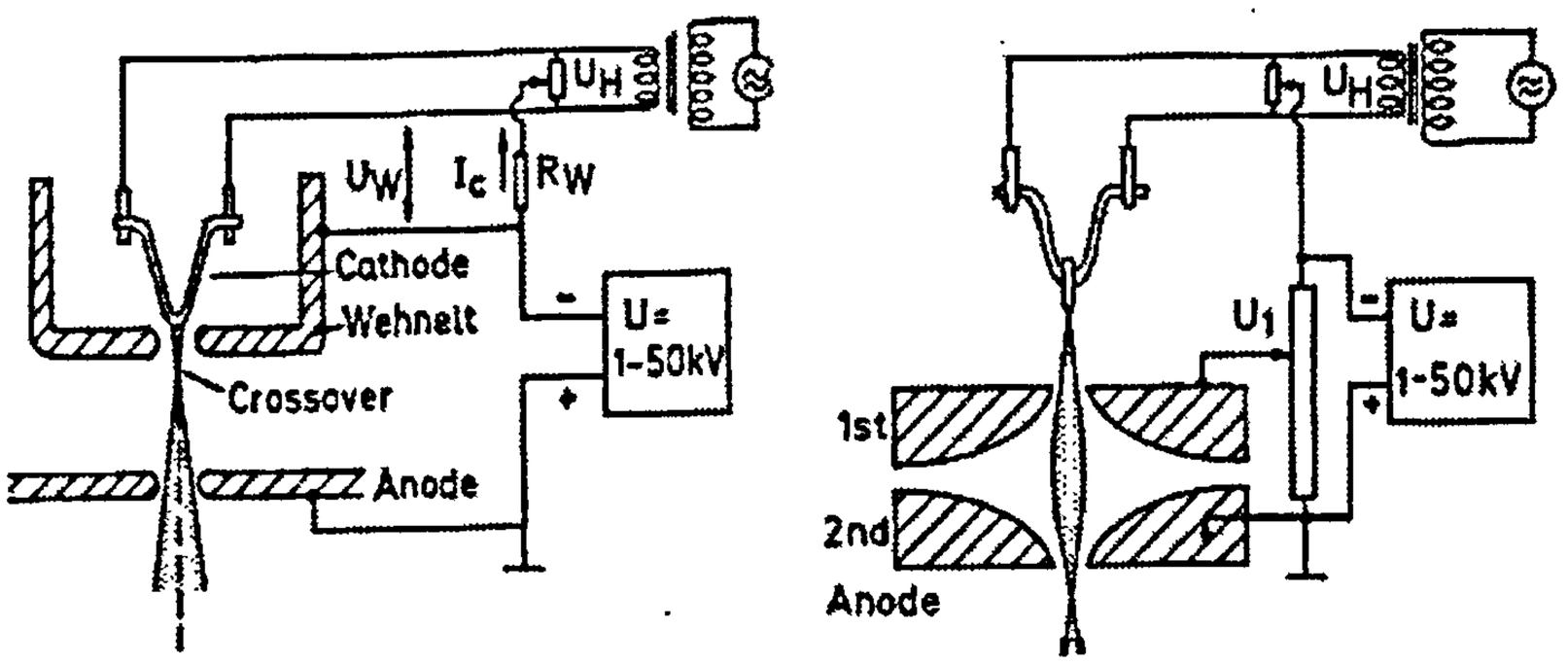

Figure (4.1) a- Thermionic gun. b- Field emission gun

The thermionic gun consisting of cathode, Wehnelt cup and anode and the field emission gun of the Butler type (Reimer, 1998).

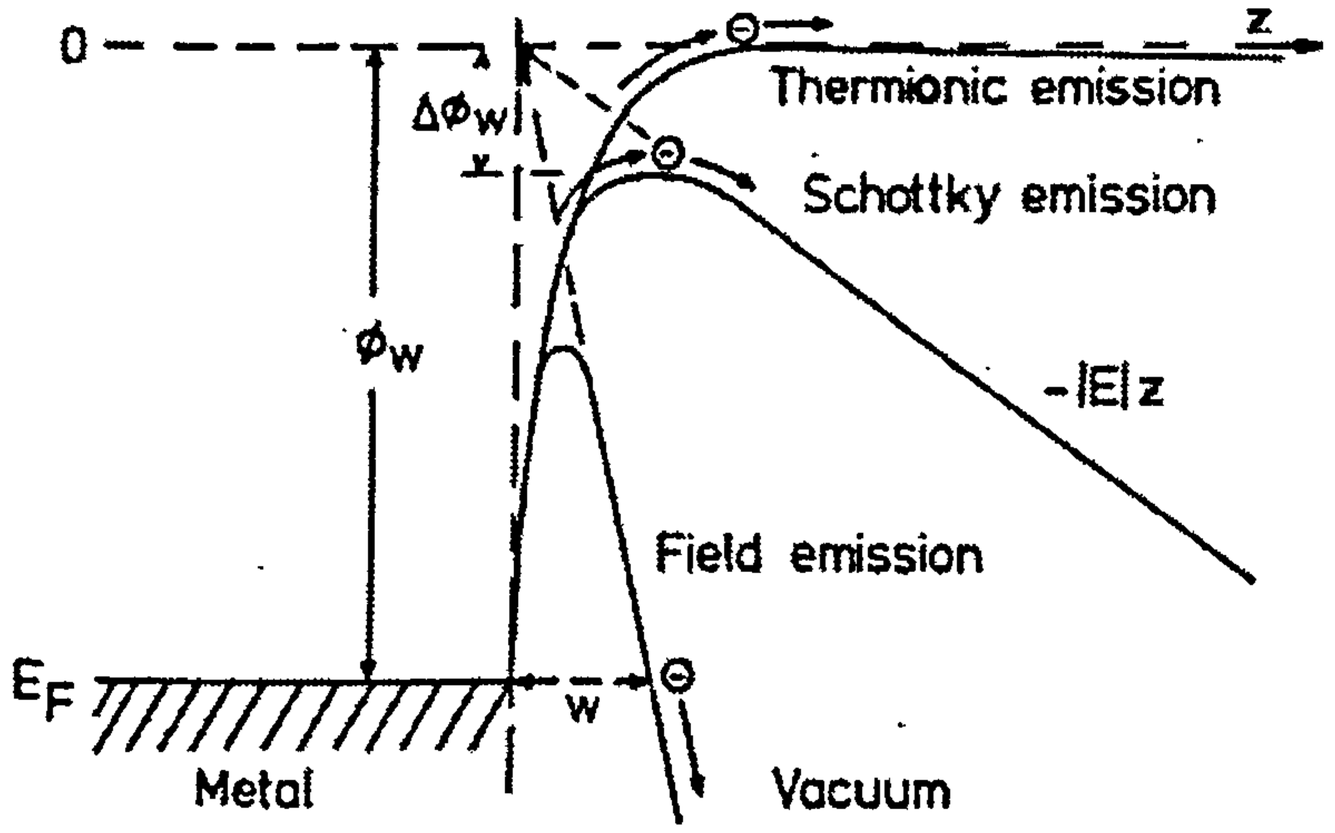

Figure (4.2) Potential barrier at the metal- vacuum boundary for thermionic, Schottky and field emission (Reimer, 1998).

	Thermionic (Vega)	Schottky (Serion)	FEG
Material	W (100)	W(100) coated with ZrO	W(111) or W(100)
Tip radius (μm)	10-200	0.3	0.1- 0.5
ΔE (eV)	1-3	0.6	0.3
β ($Acm^{-2}sr^{-1}$)	10^5	10^8	10^8 -10^9
Diameter of Virtual source (μm)	25-100	0.015-0.020	0.003-0.015
Operating temperature (K)	2700	1750 - 1850	300

Table (4.3) Comparison of some properties of a tungsten thermionic emitter, a Schottky emitter and a FEG.

in SLEEM mode, a YAG scintillator detector is situated above the specimen in the field of the cathode lens.

Most of the work described in this thesis was carried out in high vacuum conditions ($<10^{-3}$ Pa). However, in order to overcome contamination problems during metal deposition on a clean semiconductor surfaces, using UHV system is necessary.

In order to analyse the surface structure of some samples, XPS spectrum were also measured for some samples. XPS have been obtained in the Chemistry department, at the University of York by Dr C. Wilson.

(4.2.2) X- ray Photoelectron Spectroscopy (XPS)

The principle of XPS has been mentioned in chapter 2, before looking at the results of applying XPS to study surface structure of some doped Si regions, it is useful to consider briefly the basic concepts of XPS which define some parameters of the technique. The sample is kept in vacuum, is irradiated by x-ray photons. The radiation is obtained from x-ray tube, UV discharge lamp or a synchrotron source. The photon energy $E = h\nu$ can be absorbed by an electron in an atom of the sample. If the photon is of sufficient energy for ionization, it will release an electron with kinetic energy E_k (figure 2.7b). If the ejected electron did not suffer any further inelastic collision, the kinetic energy will be conserved by the electron until it leaves the sample. Then the electron kinetic energy can be measured to a high precision by an electrostatic analyser. The electron kinetic energy can be extracted according to Einstein conservation law

$$E_K = h\nu - E_b^F - \Phi_{Spectrometer} \qquad (4.2)$$

Where E_b^F is the photoelectron binding energy in the solid.

$\phi_{Spectrometer}$ is the work function of the spectrometer (known constant for the system).

The number of photoelectrons detected at a given energy is counted and displayed versus the electron binding energy (or electron kinetic energy). As a result XPS spectrum shows some sharp and intense peaks. Hence the ejected photoelectrons from the atom have different kinetic energies according to their electronic level and the type of the atom they come from, photoelectron spectra allow an elemental analysis of the

target (Grasserbauer et al, 1991). This technique is hampered by its high surface sensitivity; therefore it has been incorporated in this research to estimate the composition and thickness of the surface layer. The diagram below shows a real XPS spectrum obtained from a Pd metal sample using Mg Ka radiation.

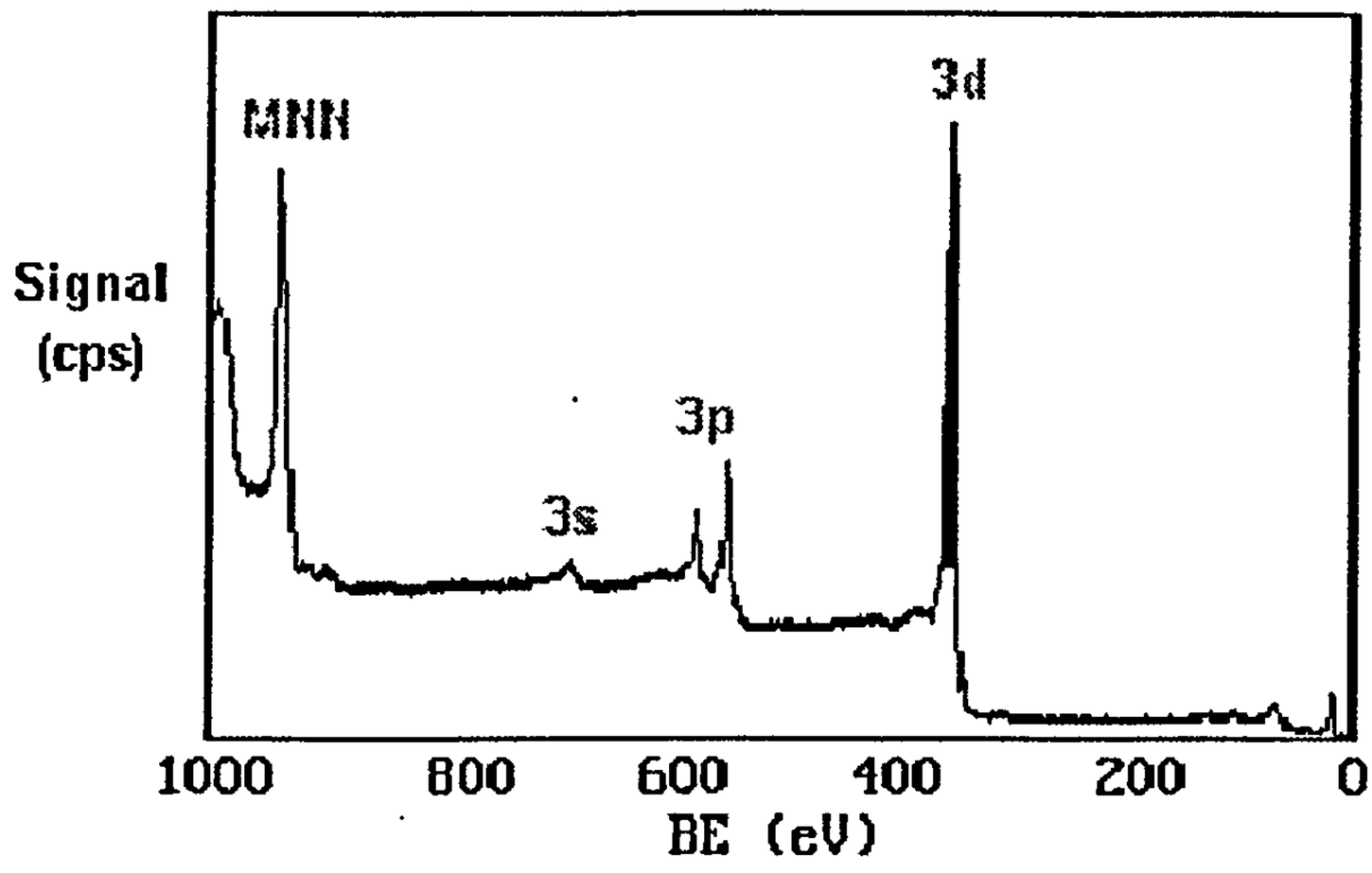

Figure (4.4) Real XPS spectrum obtained from a Pd metal sample using Mg Ka radiation, showing emission from levels 3s, 3p and 3d. It is also showing an Auger peak arising from X-ray induced Auger emission.

(http://www.jhu.edu/~chem/fairbr/surfacelab/xps.html).

The XPS instrument used in this work is a Kratos Analytical XSAM 800. The XPS vacuum system is pumped down to obtain a base pressure of the order of 10^{-4} Pa. The x-ray radiation is obtained from an x-ray tube with magnesium anode which gives lines at 1254 eV. This energy is sufficient for ionization of core levels in many elements. Angular resolved XP measurements were performed using a 120 μm diameter analyser aperture, analyser pass energy of 20 eV and an X-ray power of 144 W. An estimation of the surface layer thickness of carbon and oxide was determined from analysis of the angular-dependent intensity variation of both the oxide and elemental Si components.

(4.2.3) Kelvin Probe Microscope

(4.2.3.1) Principle of Operation

The Kelvin probe Microscope is one of the oldest techniques for determining relative changes in work functions by measuring the work function difference between two materials forming the two sides of a parallel plate capacitor. Kelvin probe is extremely sensitive to changes in contact potential difference (cpd) between a reference material and a sample to less than 0.001 V. The changes in contact potential difference can be wholly ascribed to changes occurring at the sample surface and can be expressed in different ways: contact potential, Fermi-level, work function, surface potential, surface dipole, etc (Kronik and Shapira, 1999).

Prior to connection the metals are electrically neutral, no macroscopic electrical fields arise, and the two metals share the same local vacuum level. A schematic band diagram of two metals in such an arrangement is shown in figure (4.5-a). Upon short-circuiting the metals, i.e. bringing them into contact, charge must flow from the metal with smaller work function to the metal with larger work function until equilibration of the Fermi levels is achieved (Figure (4.5-b)). As in any parallel plate capacitor, this charge transfer results in an electric field in the gap between the two plates and a drop in the local vacuum level across this gap. This potential energy drop is equal to the difference in the work functions of the two metals. The corresponding potential drop is usually known as the contact potential difference (CPD).

In order to determine the CPD, it was suggested that the CPD may be measured directly by applying an external dc bias, equal and opposite to the CPD. As shown in figure (4.

5-c), the Fermi levels on both metals differ by V_{CPD}, just as in the isolated case (figure (4.5-a)). No charge exchange between the metals need take place and the capacitor is discharged. Therefore, the applied bias which discharges the capacitor is measuring the CPD of the structure in question.

If the spacing between the two plates is varied while the plates remain connected under bias, the resulting capacitance change should induce a change in the capacitor charge and hence a current in the external circuit. This current can be zero if and only if the capacitor is discharged. Thus, the CPD may be easily measured by determining the external bias for which no external currents are observed upon changing the spacing between the plates.

In Lord Kelvin's original experiments, moving the capacitor and measuring the resulting charge exchange with an electrometer required several minutes for a single CPD determination. Few years later, the vibrating capacitor Kelvin probe technique was introduced, in which the capacitor is vibrated periodically so that a steady state ac current develops in the capacitor. This current is easily monitored continuously. Thus, the dc bias is adjusted until the ac current is vanished. This approach increases the measurement sensitivity drastically since the measured ac voltage may be considerably amplified. Moreover, the measurement time is reduced from several minutes to several seconds. As a result, it has become the standard setup.

(4.2.3.2) Scanning Kelvin Probes

In this mode the probe is scanned across the sample, and it maps lateral variation of the CPD, hence local surface potential may be obtained. With advanced designs, probe resolutions of several microns on both axes have been achieved with a voltage resolution of several tens of mV by incorporating a flattened tip to several μm (MaÈckel et al, 1993). The probe is actively maintained at a distance of about 50 nm from the surface. The distance control makes it possible to use the microprobe for topographic mapping as well. A higher resolution was reported by Nabhan et al (1997) who claimed a record lateral resolution of ~100 nm and a voltage resolution of several mV.

The successful use of a scanning Kelvin probe requires very careful attention since it is

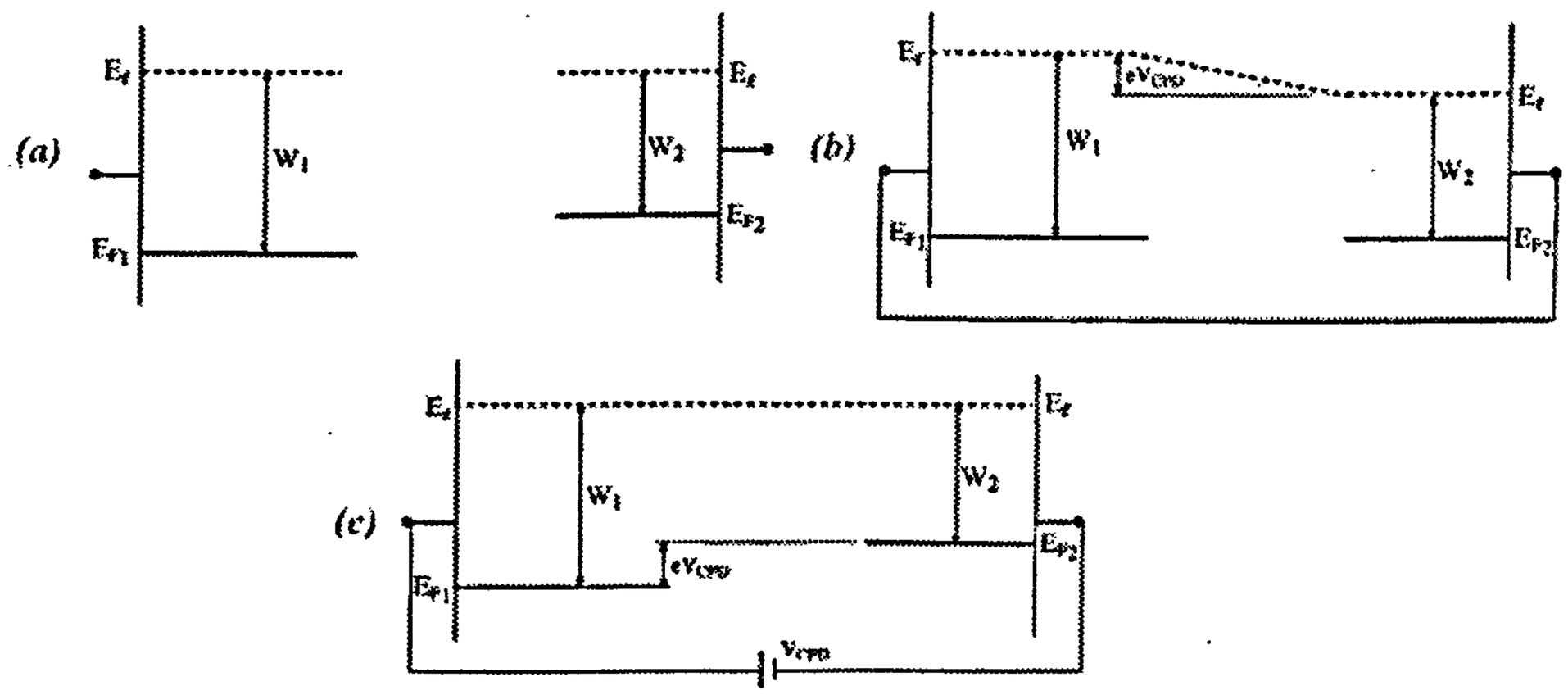

Figure (4.5) Schematic band diagram of a parallel plate capacitor formed from two different metals, with the two plates: (a) isolated, (b) short-circuited, (c) connected through a DC bias equal and opposite to the contact potential difference (Kronik and Shapira, 1999).

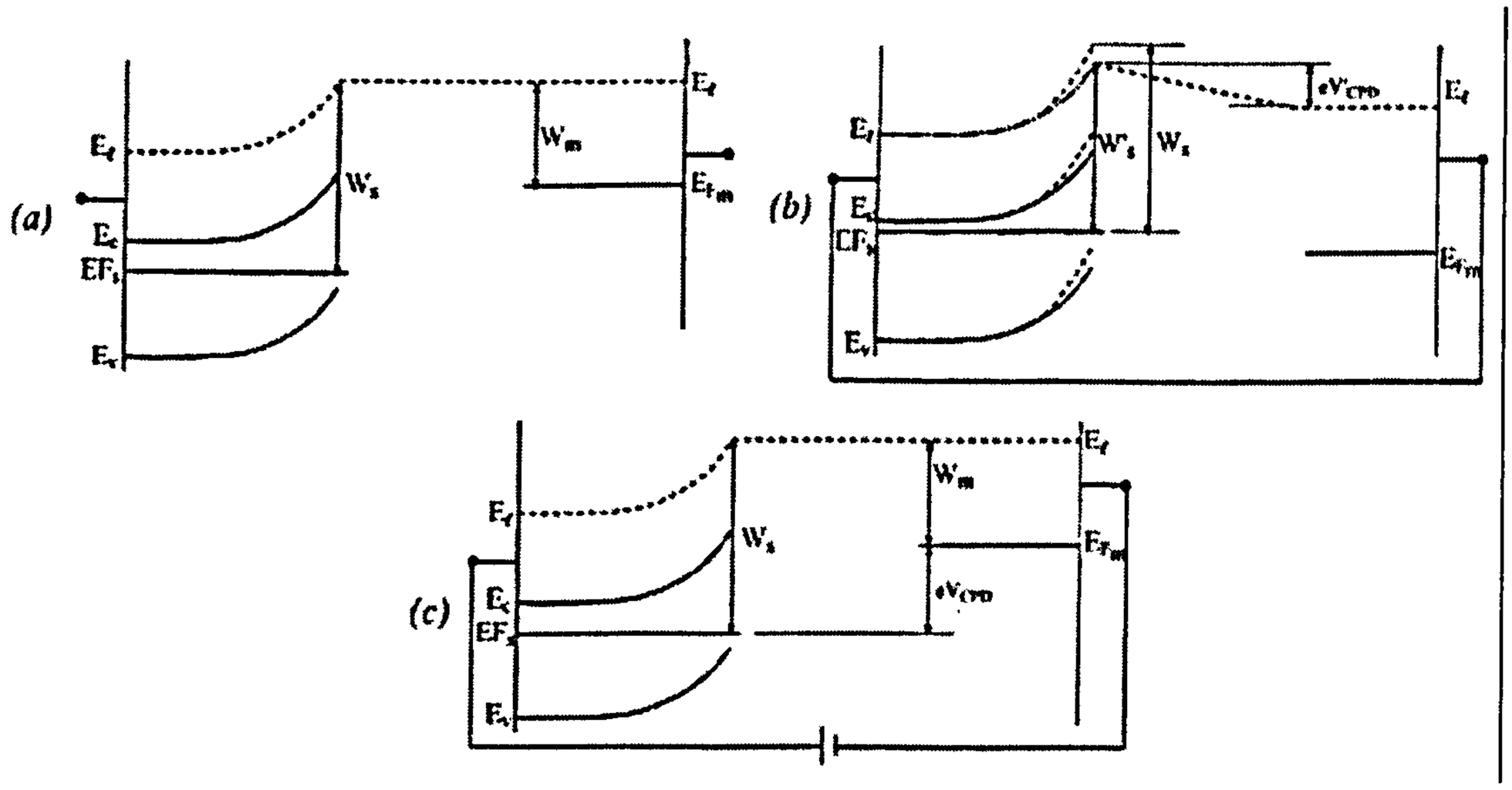

Figure (4.6) Schematic band diagram of a parallel plate capacitor formed from a metal and a semiconductor, with the two plates: (a) isolated, (b) short-circuited, (c) connected through a DC bias such that the capacitor is discharged (Kronik and Shapira, 1999).

particularly prone to many of the difficulties of Kelvin probe operation explained above. For more details about difficulties in running KPM, the reader is referred to some of the excellent available literature on KPM by Kronik and Shapira (1999).

(4.2.3.3) How Does the Scanning Kelvin Method Work?

The plates are electrically connected via an external "backing" potential. When this potential is zero, a contact potential difference, V_{CPD}, exists between the plates due to the difference in the work functions (ϕ) of the inner plates surfaces. By definition,

$$e\, V_{CPD} = \Delta\phi \qquad (4.3)$$

where e is the electronic charge. Setting the external potential to create a potential difference between the plates induces a charge on the surfaces of the plates proportional to the capacitance of the plates. Because one plate is being oscillated relative to the other, the value of the capacitance is also a function of time. The KP signal is the current that flows between the plates as charge moves from one plate to the other due to motion of the probe.

At the point where the external potential = $-V_{CPD}$, the circuit is balanced, meaning the electric field between the plates vanishes, and the induced charge is zero so the current vanishes. This is the balance and at this point CPD is equal to the applied backing potential. Furthermore, if changes in the balance condition have been detected, adsorption effects on the work function can be monitored.

KPM system is used to map the distribution of potentials on a surface. Using KPM, the contact potential barrier between a metal and a semiconductor is usually evaluated by calculating local potential difference between the metal and the semiconductor. Therefore, the contact potential measured by KPM is the difference of the surface potentials on the metallic film and semiconductor substrate with respect to the reference electrode. The contact potential calculated in this way is expected not to be affected by surface effects such as the adsorption on the metallic film.

The reported potential barrier measurements (section 7.5) were taken by KP Technology, Edinburgh, UK. The system used is SKP 5050 system. This system uses

sharp tips of approximately 50 and 30 μm and is able to scan 1-2 mm on the sample surface without any problems. Spatial resolution with the Kelvin method is approximately the tip size.

(4.3) Materials

Three Si samples used for the experiments in this dissertation, referred to as; ISI, SRL and Durham samples. In all of these samples dopants were introduced to n-type Si substrate by diffusion. The ISI samples were provided by the Institute of Scientific Instruments (ISI, Brno Check Republic) and consist of n-type Si phosphor doped to a level ~ 1×10^{15} cm^{-3}. They were patterned with p^+- doped (10^{19} cm^{-3} Boron doped) and the depth of the doping was about 5 μm.

The SRL sample used was kindly supplied by Shimadzu Research Laboratory Ltd (UK) and consists of n-type Si (~10^{15} cm^{-3}) doped with As to $2.5\times10^{20}cm^{-3}$ forming n^+ regions to depth of 0.25 μm and Boron to a level of 8×10^{19} cm^{-3} forming p^+ regions to depth of 0.3 μm.

Finally, the Durham Si sample were kindly prepared by the Engineering Department at Durham University. Sample was made in the form of Boron-diffused patterns at a temperature of ~1000 K into a phosphor-doped n-type silicon (111) substrate. The doping concentration of the n-type substrate is about $10^{18}cm^{-3}$, while the p^+ areas had a carrier concentration of ~$10^{19}cm^{-3}$ and the depth of the doping was about 3 μm.

Chapter 5: Effect of Beam Energy on SE Dopant Contrast

(5.1) Introduction

In order to achieve a quantitative procedure towards full understanding of the dopant contrast mechanism, it is crucial to have a comprehensive knowledge of the set of key experimental parameters that affect the observed contrast in the SEM. If such a model can be developed then the SEM technique can be accepted by the SIA. Hence, semiconductor industry users will start looking for practical guidelines in using the SEM as a dopant profiling method. Previous studies (Perovic 1995, Venables 1997, Sealy 2000, Elliot 2001, El-Gomati 2001, Jayakody 2003, Kazemian 2003) have shown that the dopant contrast observed in a SEM is dependent on a number of parameters. The parameters that have been studied can be divided into three groups as follows:

1-Material type, which includes semiconductor type, band gap, doping type and concentration level.

2-Specimen surface conditions, some of which depend on specimen preparation, such as the presence of surface contaminants and oxides and the vacuum quality in the SEM which may result in metal-semiconductor contacts.

3-Microscope operating parameters, such as accelerating voltage, electron dose, exposure time, detector type, working distance and SEM resolution.

The aim of this chapter is to further investigate electron beam energy effect on SE dopant contrast in order to provide proper understanding of the SE contrast mechanism. The influence of beam energy on the measured SE dopant contrast values of different Si structures is studied. In spite of the difficulty in preparing semiconductor surface for controlled adsorption studies, the effect of beam energy on SE dopant contrast has been studied for a Si surface with an existing thin layer of adsorbed oxide onto the surface. In addition, a new model has been developed to identify oxide effect on SE dopant contrast.

In this chapter, most of the presented work on SE imaging of Si has been performed with a Tescan Vega SEM (a commercial microscope). The specimen chamber pressure of this microscope is ~ 4×10^{-3} Pa. Therefore at such a pressure, an induced hydrocarbon layer must exist. This microscope is equipped with a thermionic emission filament. Due to the difficulty in operating thermionic electron guns at low voltages, it was converted into the SLEEM mode by inserting a cathode lens detector. As mentioned before, this configuration allows one to reduce the beam voltages down to very low values without

sacrificing the gun brightness or the resolution significantly. In addition to the Tescan Vega SEM, a Serion FESEM has been used to investigate electron beam energy effect on the contrast.

The experiments were performed on differently doped p^+, n^+ and n Si structures with accurate in-situ measurements of the incident electron beam current in the Vega SEM. It is found that sample charging or contamination substantially affects the contrast. Effect of microscope accelerating voltage combined with sample surface contaminations will be discussed in detail in this chapter using different SE detectors. In order to inspect the surface condition and quantify its contribution to the obtained contrast, XPS has been utilised to analyse the surface structure after imaging (section 5.4). The proposed SE contrast mechanism at different beam energies is introduced (section 5.6).

(5.2) Sample Preparation for SE Imaging

Semiconductor samples that are transported in air, or those that have their surfaces treated outside the vacuum system, normally end up with several monolayers of foreign atoms residing on the surface; e.g O, C and H. Since the SE contrast can be affected by the oxide layer as it can charge up during electron beam bombardment, hence the oxide layer must be removed to eliminate the charging effects during inspection. Moreover, when imaging is performed at low voltages, the SE signal becomes very surface sensitive. Therefore, it is crucial to clean the semiconductor surface before loading it for inspection.

Sample preparation for SEM inspection involves either cleaving in air or wet chemical etching. A Si sample cleaved in air is expected to build a thin layer of native oxide (SiO_2) on the surface within a relatively short time. A widely used method to remove the Si native oxide layer is chemically etching the sample surface in a dilute Hydro Fluoric acid (HF). This etching will remove the surface oxide without etching the underneath Si. In addition, the HF passivates the surface dangling bond with Hydrogen and hence prevents more oxide growth (Burrows et al, 1988). However, more recent studies have shown that it is possible to grow a native oxide on HF treated Si surfaces at room temperature due to handling the sample in air (Morita et al, 1990, Angermann et al, 1994)

All the used samples in this study feature dopants diffused into Si. Each sample was

ultrasonically cleaned with high purity Isopropanol Alcohol (IPA) to remove any small particles that may exist on the surface. These were then etched in HF:H_2O =1:5 to remove any naturally grown oxide. Following IPA cleaning and etching, the samples were transferred into the SEM and vacuum chamber pumped down.

(5.3) Beam Energy Effect on SE Dopant Contrast

The specimen used in this work is ISI Si(111) sample. The depth of the patterned doped regions was about 5 μm. This depth is quite sufficient to confine the electron penetration to be within the doped region during plan-view observation even with 10 keV electrons.

Firstly, the cleaned specimen was examined in the Vega SEM. Signs of the p^+/n contrast were clearly observed in the range 500 eV to 5 keV of the incident electron beam energy. Throughout the work presented in this thesis an identical method was followed to evaluate contrast magnitude. In each case, the SE signal from the specimen was measured in the form of multiple line-scans where the data were collected and averaged under computer control. Then the dopant contrast was determined according to relation (2.5).

Figure (5.1) shows a series of SE images of similarly etched samples at different beam energies. As can be seen, the p^+ areas appear brighter relative to the n-type Si substrate in the range 500 eV up to 2 keV and then the contrast reduces around 2 keV. However, for higher beam energies the contrast is inverted. In the range of energy 2.5 keV and upward, p^+ regions appear darker than n-type regions.

The maximised contrast at low accelerating voltages can not be related to an increase in BSE yield because this leads to an increase in the SE intensity from the two layers by the same factor and consequently it does not lead to increase in the contrast.

Initial analyses of results indicate that samples that show such behaviour may have a residual layer of very thin oxide on their surface. In order to ascertain this belief, the sample was then further etched with 10:100 HF:H_2O solution in order to remove the native oxide layer completely from the surface. It was then transferred back into the Vega SEM.

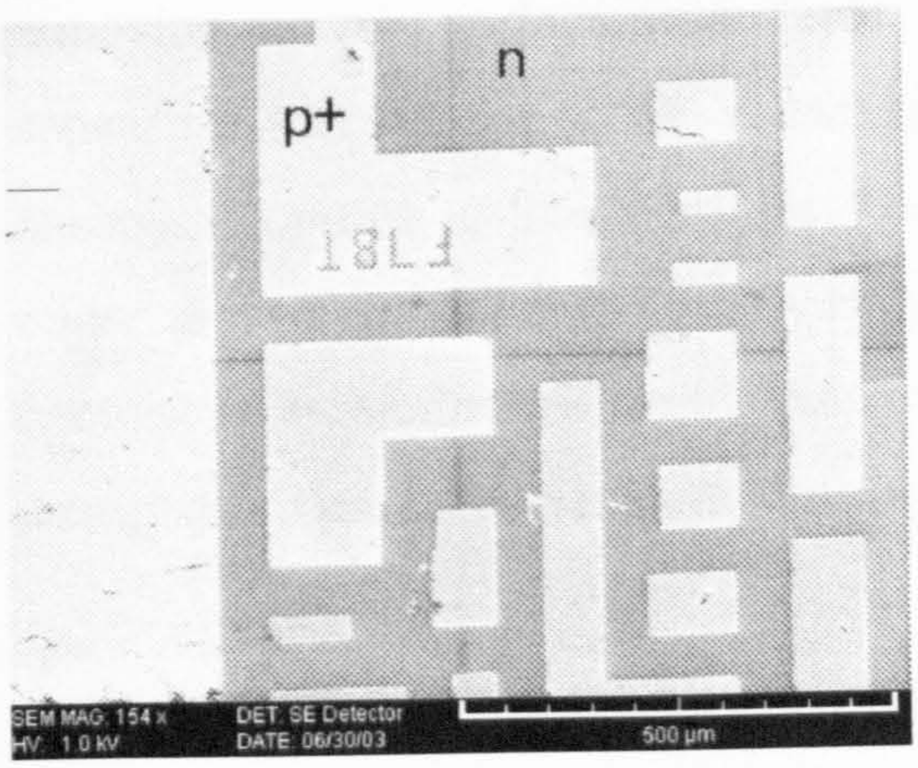

1keV

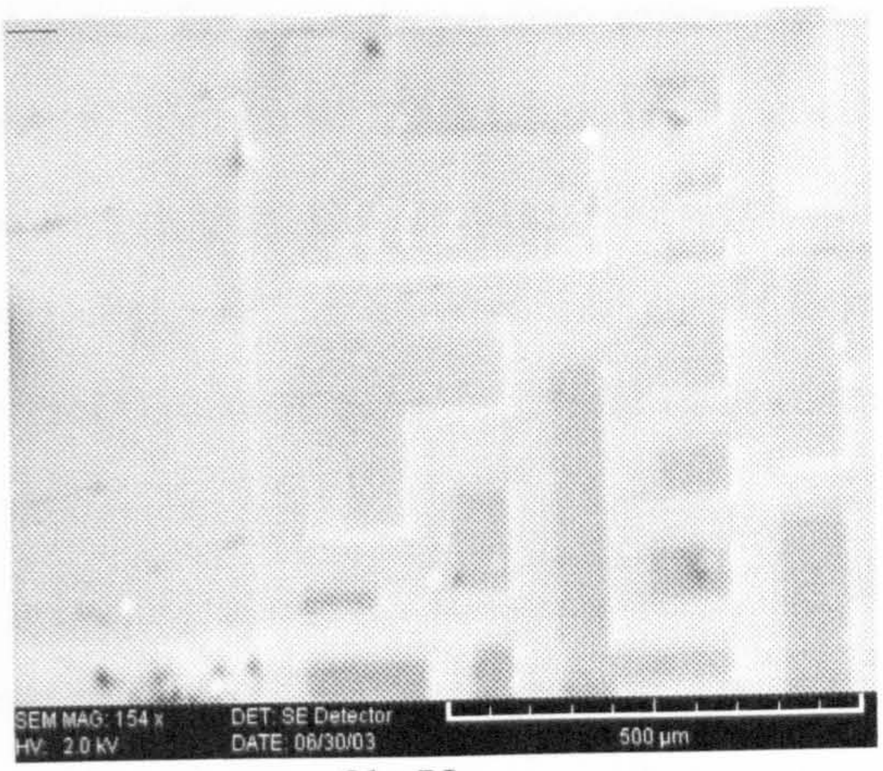

2keV

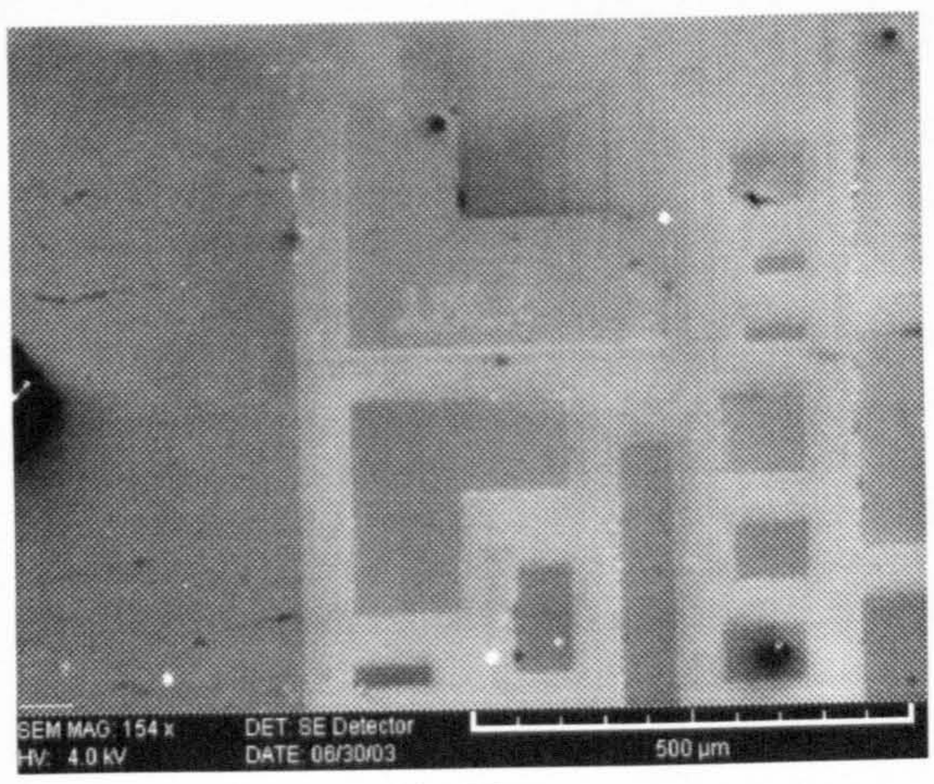

4keV

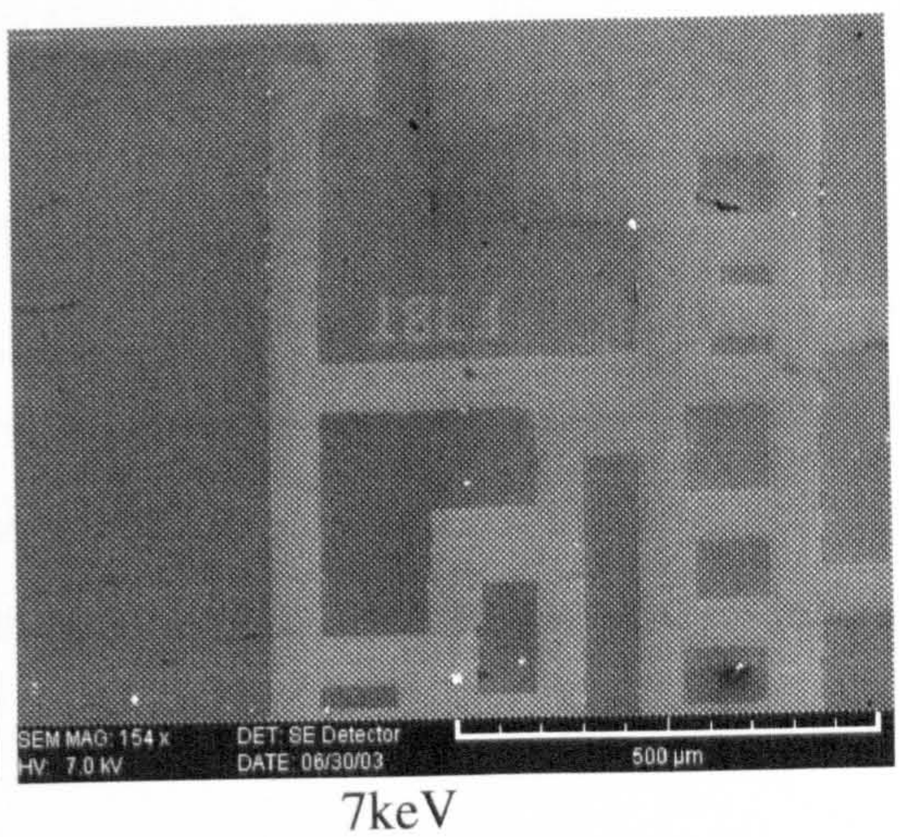

7keV

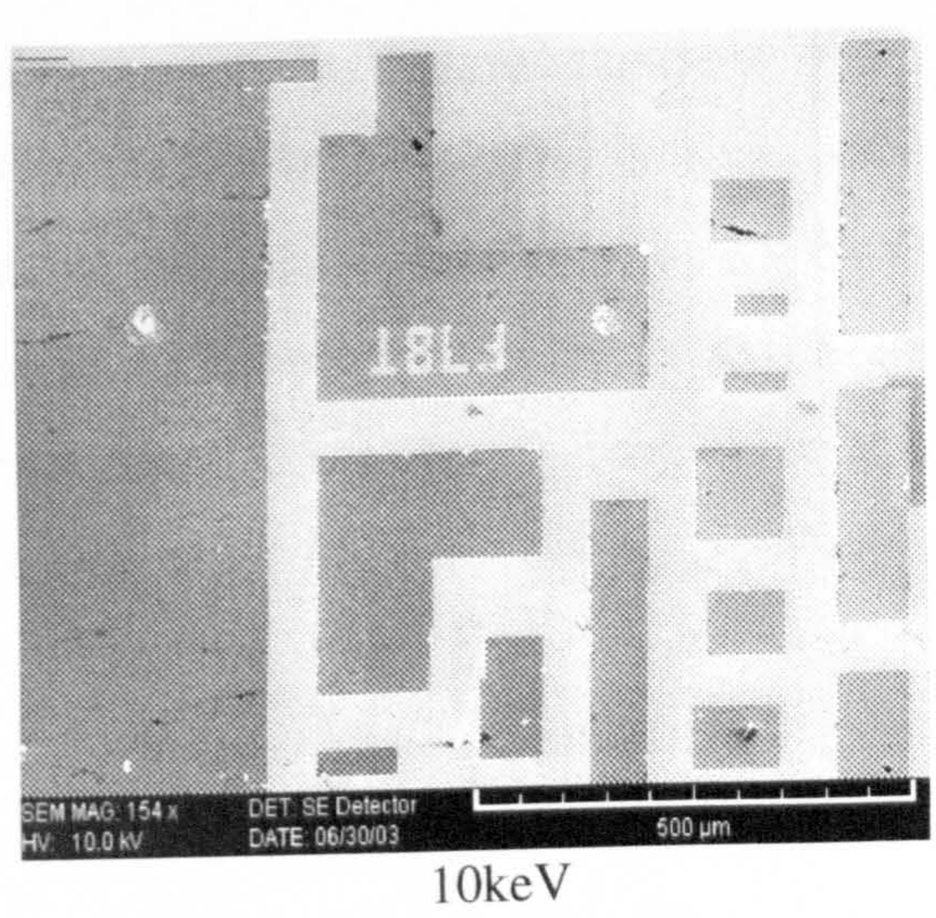

10keV

Figure (5.1) SE images of ISI sample collected from E-T detector at different beam energies.

Figure (5.2) shows SE images of ISI sample at different accelerating voltages after removing the thin surface oxide layer. As can be seen from this series, the p^+ areas appear brighter relative to the n background. However for higher beam energies, the observed contrast is low. This result confirms that the contrast between differently doped regions is not carried out by BSEs and the effect of very thin oxide layer on SE contrast is ascertained whereby the contrast reversal as a function of incident beam energy disappears after removing this layer.

A comparison between the calculated contrast levels before and after extra etching as shown in figure (5.3), show that the maximum contrast level is shifted to lower beam energy in existing an oxide layer at ~700 eV. In addition, the maximum contrast level is enhanced before extra etching (or reduced after extra etching). This observation can be explained by the fact that the produced SEs have been generated within different surface structures. Whereby before extra etching, there is almost a thin layer of oxide above Si surface. Therefore, at low beam energy SEs are generated within the oxide layer. Since SEs generated within oxide layer have higher escape depth than those generated within Si. As a result, higher SE emission and then higher contrast level are obtained from the sample before extra etching.

Another fresh ISI sample was cleaned ultrasonically in IPA then dipped in HF solution before inspecting in the Vega SEM, SE images collected of this sample show inversion of contrast obtained at relatively high beam energy >1500 eV (i.e similar to figure 5.1). The sample was then left in a drawer in the clean room environment for few months, and then inspected in the Vega SEM. The obtained SE images in this case show only an inverted contrast for a wide range of beam energy (1-10keV) as shown in figure (5.4).

In order to study the beam energy dependence more quantitatively, another sample (SRL type) that contains p^+ and n^+ doped areas was used to image in the Vega SEM converted to operate in the SLEEM mode. The substrate was n-type silicon doped with a phosphorous. Following the HF cleaning the sample was transferred into the Vega SEM and the sample chamber pumped down to a base pressure of 4×10^{-3} Pa before imaging was performed. Imaged areas were selected whereby p^+ and n^+ contrasts could be obtained relative to the n-type area. The cathode lens aperture was ~ 300 μm.

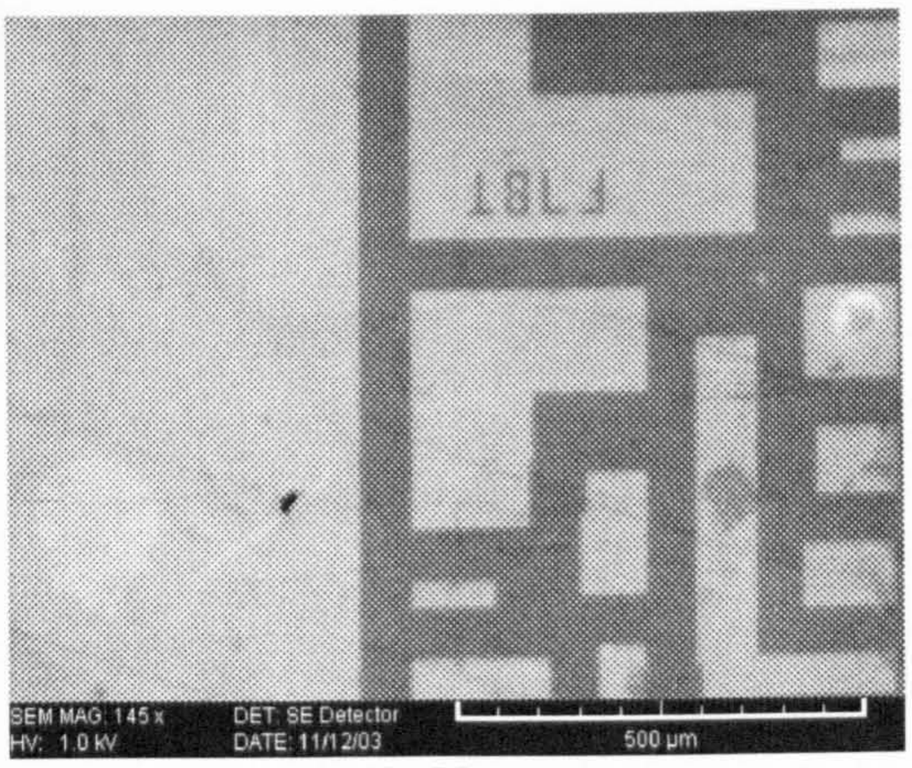

1keV

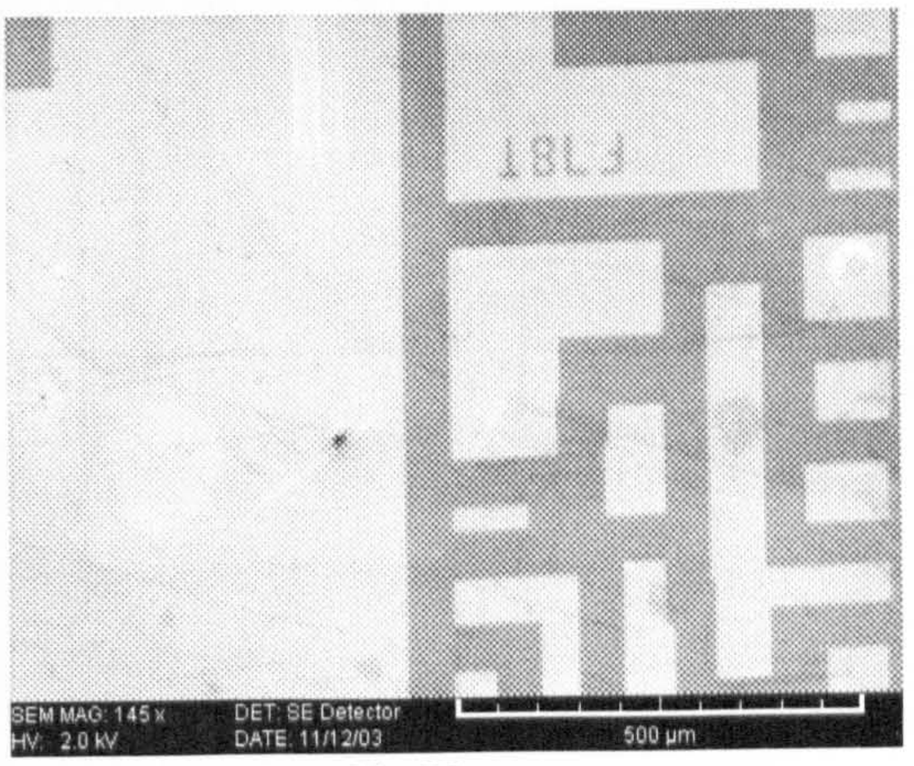

2keV

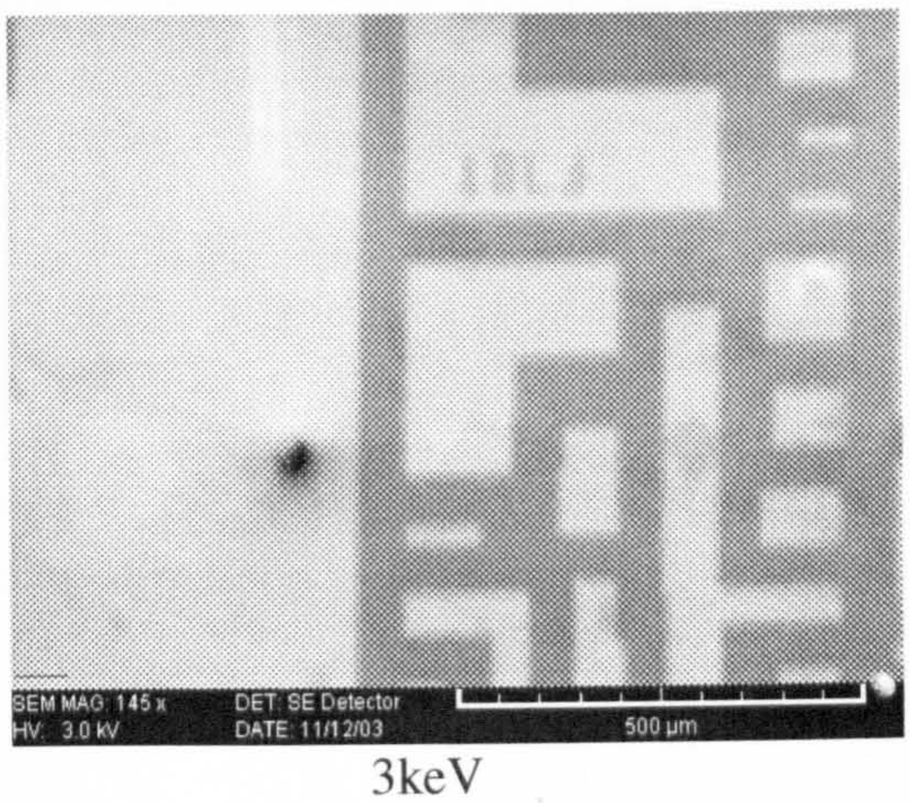

3keV

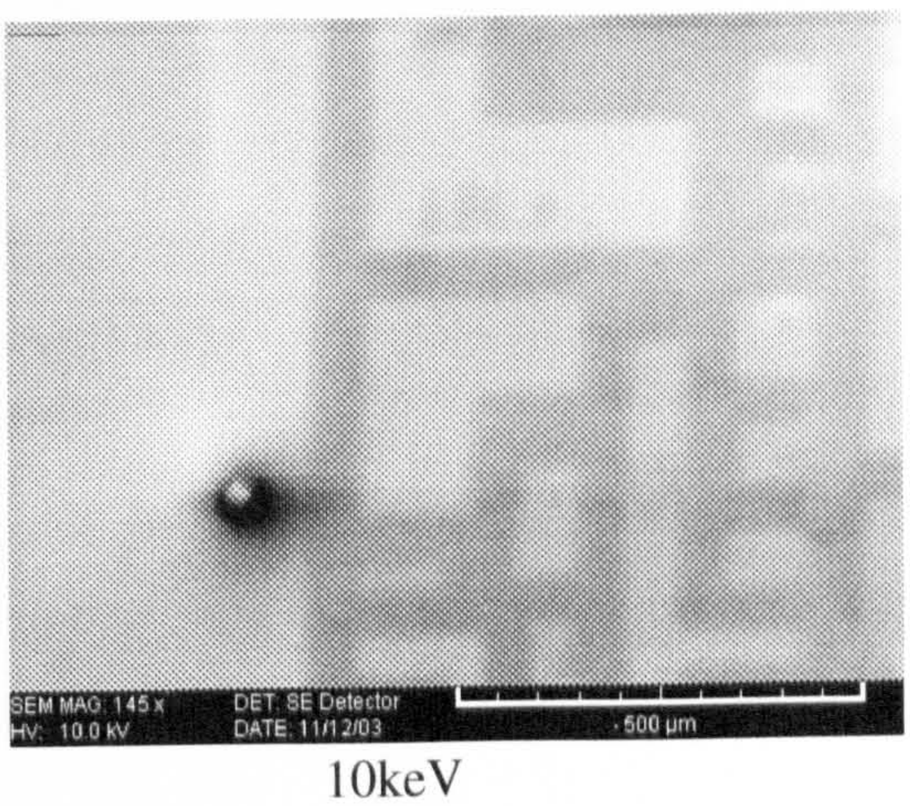

10keV

Figure (5.2) SE images of ISI doped Si sample after extra etching collected at energies indicated, showing low contrast level at high beam energies.

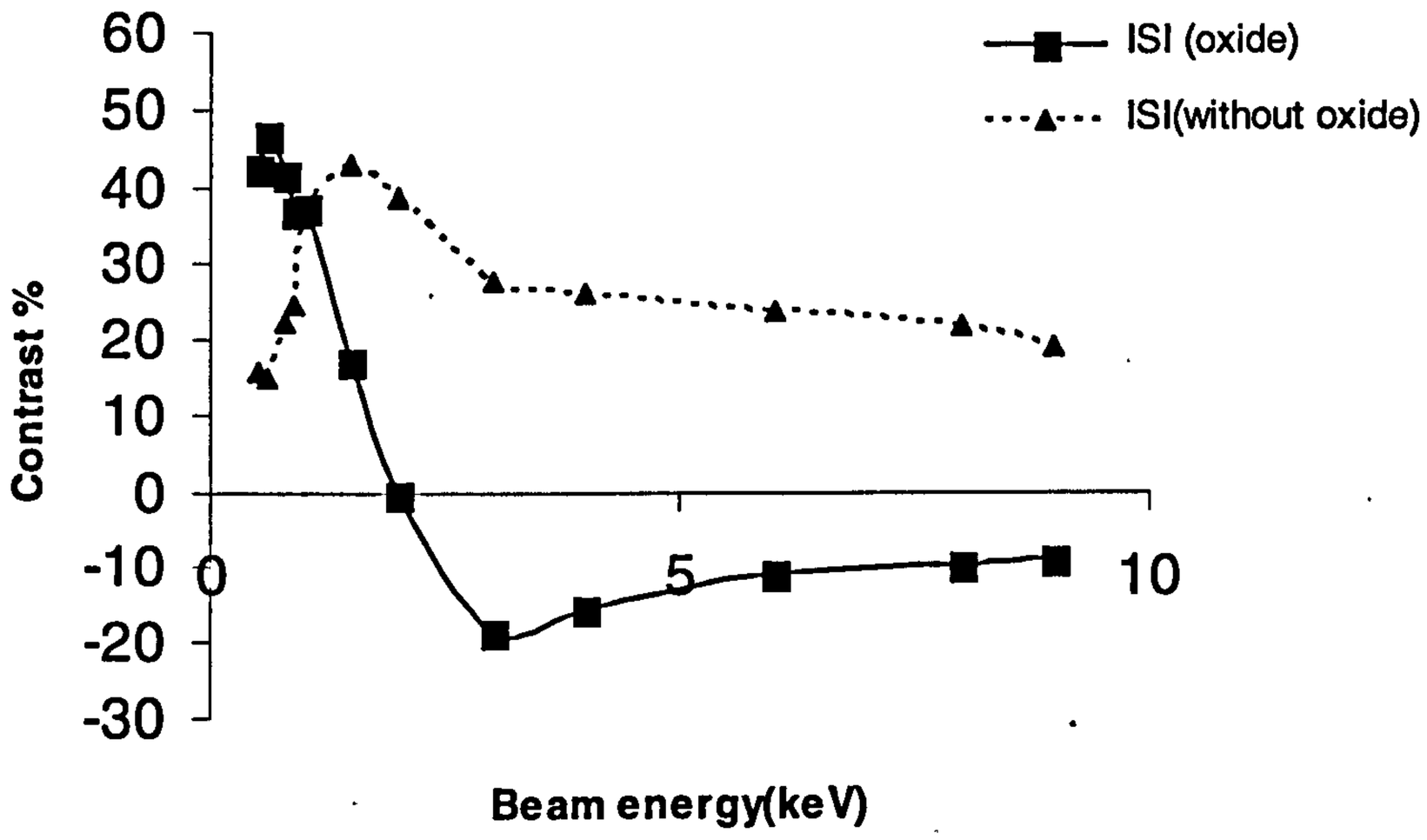

Figure (5.3) The contrast of p^+ doped regions relative to the n areas at different beam energies with and without a surface oxide layer. The contrast was calculated for the series of images collected at different beam energies according to the formula (2.5).

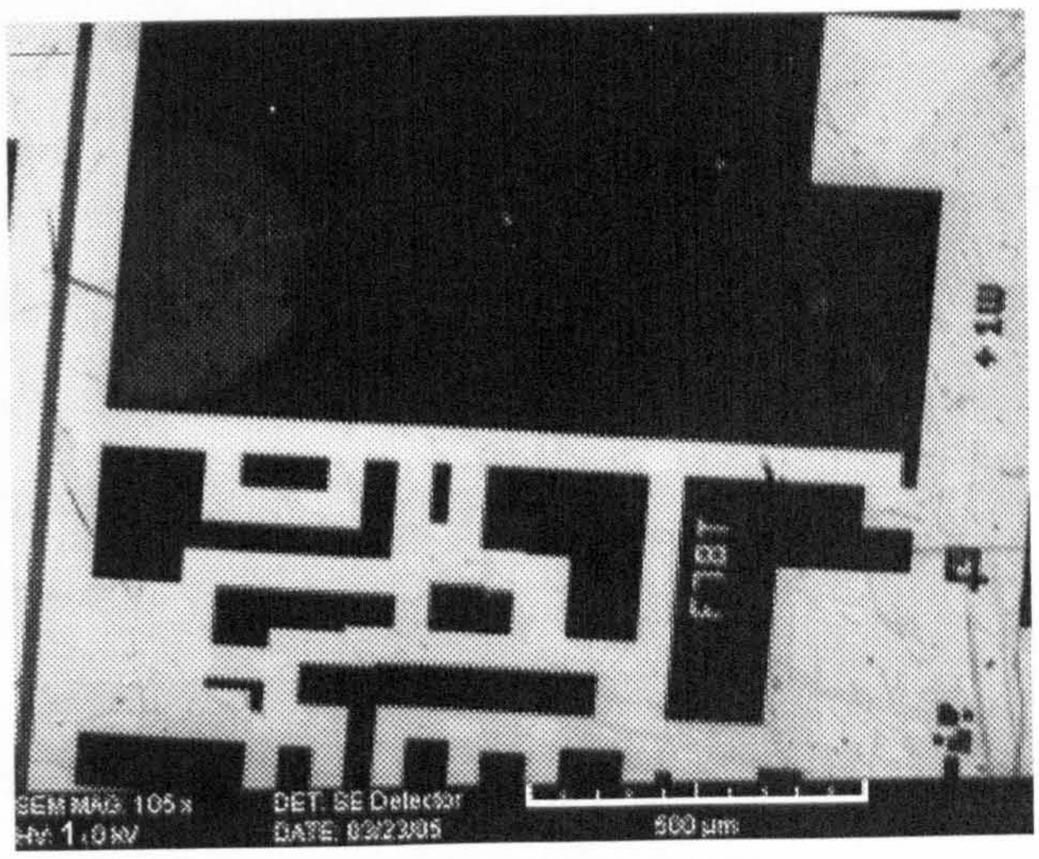

1 kV

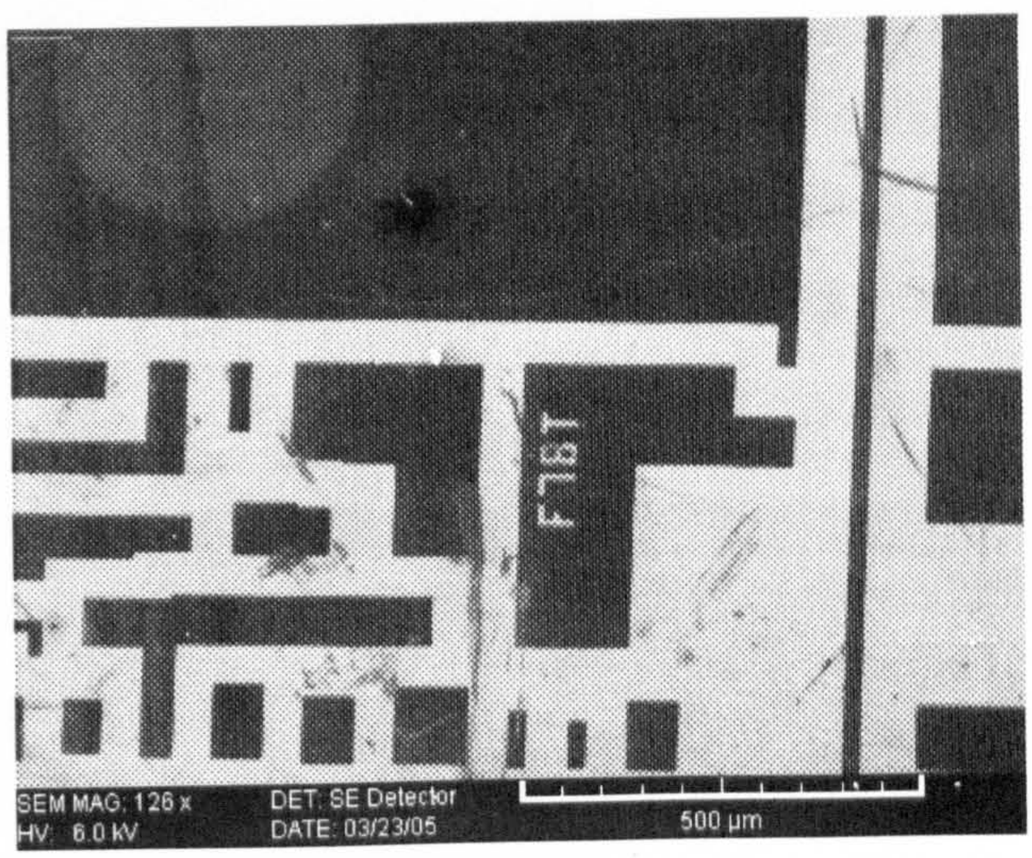

6 kV

Figure (5.4) SE images show inverted contrast at different beam energies, after being left in the clean room environment for few months.

Therefore, due to the limited field of view, only a small area of the specimen was imaged.

The primary beam energy of the microscope was set at 10 keV, and then the landing energy of the beam was reduced by increasing the sample bias voltage using a stable high voltage power supply unit. When the sample bias voltage is changed, image refocusing and astigmatism correction were needed. Changing of the contrast parameters would affect the contrast dependence on the beam voltage and hence complicate the attempt to quantify the contrast. However, this effect can not be eliminated. Images were acquired digitally and collected as 512×384 pixel images with 256 grey level intensities. These images allow calculating average pixel brightness from differently doped regions, and hence allow accurate quantification of the SE contrast.

As shown in figure (5.5) and figure (5.6), the contrast starts to appear from both p^+ and n^+ areas relative to the n-type areas for beam energy <10 keV. SE images indicate that at low and very low beam energy, both n^+ and p^+ regions appear brighter than the n-type areas. Moreover, the observed contrast p^+/n is higher than the contrast n^+/n. Further increase of the beam energy causes an inverted contrast whereby n^+ and p^+ regions appear darker than n-type areas. Thus a contrast reversal can be observed from both p^+- and n^+-type areas relative to the n-type areas at high energies >1.5 keV. The calculated contrast values are shown in figure (5.6). This figure shows that the inverted contrast of n^+/n structure is obtained at slightly higher beam energy than the required energy to obtain inverted contrast of p^+/n.

Similar observations have been made using the E-T of the Vega SEM as shown in figure (5.7). This rules out any effects due to angular emission as seen by Schonjahn et al (2003). This result confirmed Jayakody's result. However, Jayakody (2003) did not report a contrast reversal from p^+ relative to n-type areas. In addition, the inverted contrast in Jayakody's experiment was obtained after treating the sample with HF and NH_3F prior to imaging. In all cases, polycrystalline Silicon (poly-Si) areas appear brighter due to charging caused by a thin oxide layer underneath the poly-Si layer. The appearance of brighter p^+ and n^+ areas at very low energies was also observed under

Landing energy	n^+/n	p^+/n
9000 eV	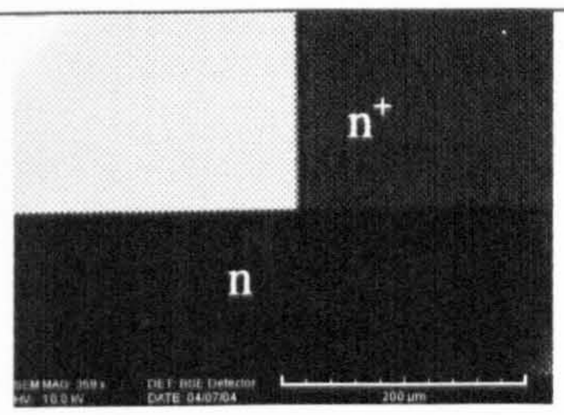	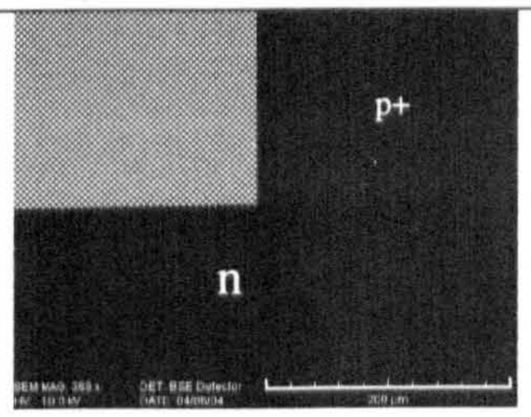
6000 eV	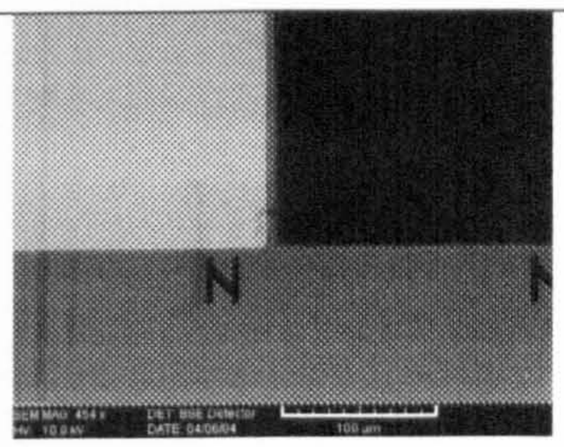	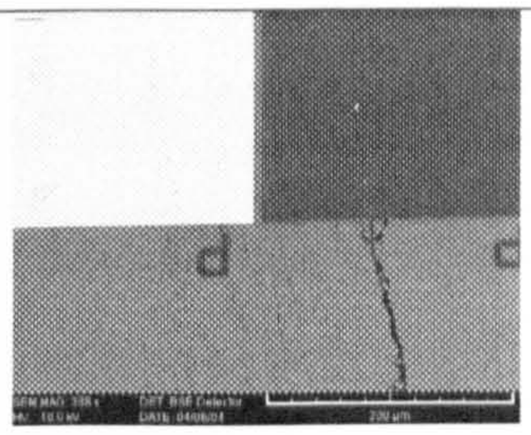
1000 eV	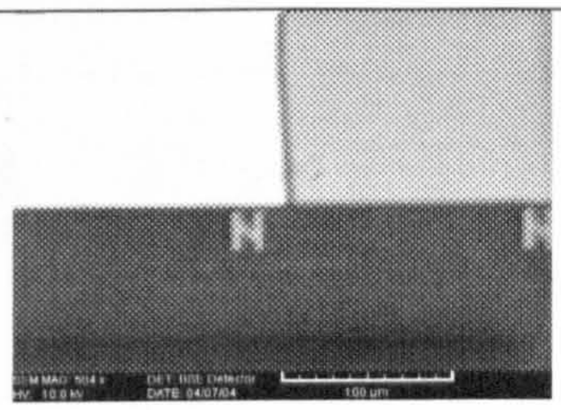	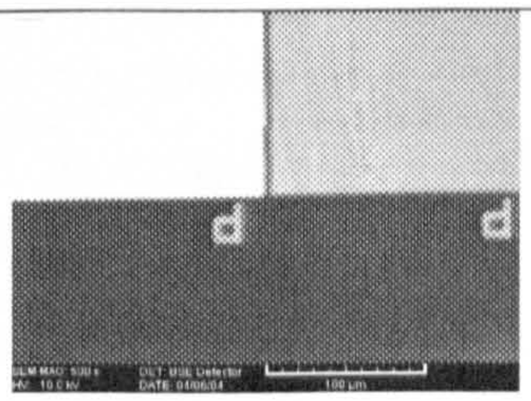
400 eV	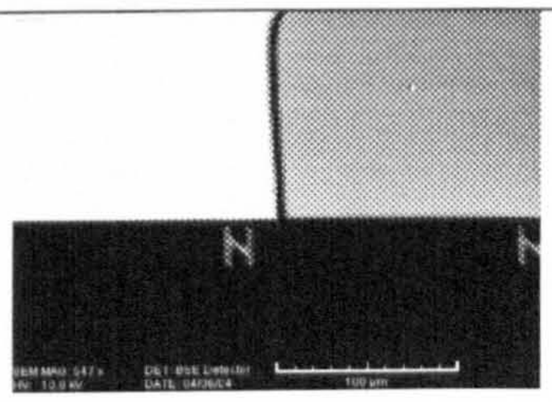	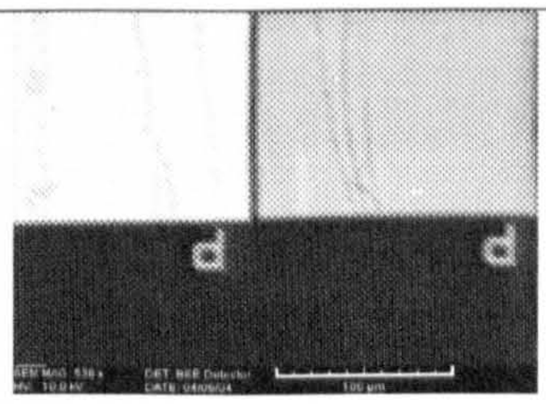
280 eV	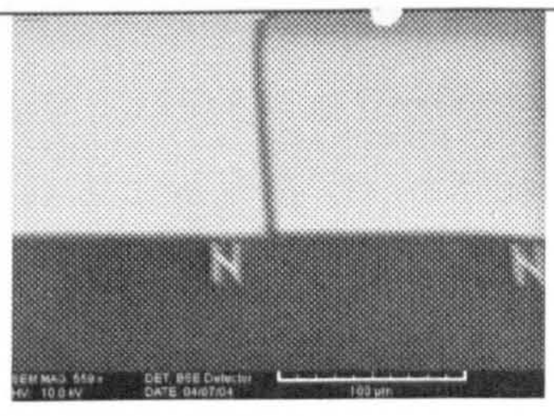	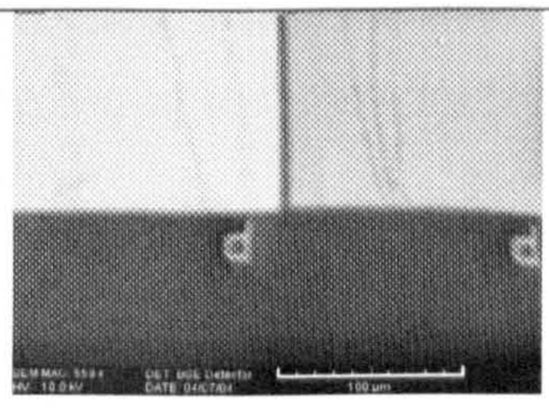

Figure (5.5) Series of images collected at high, low and very low energies in the SLEEM mode.

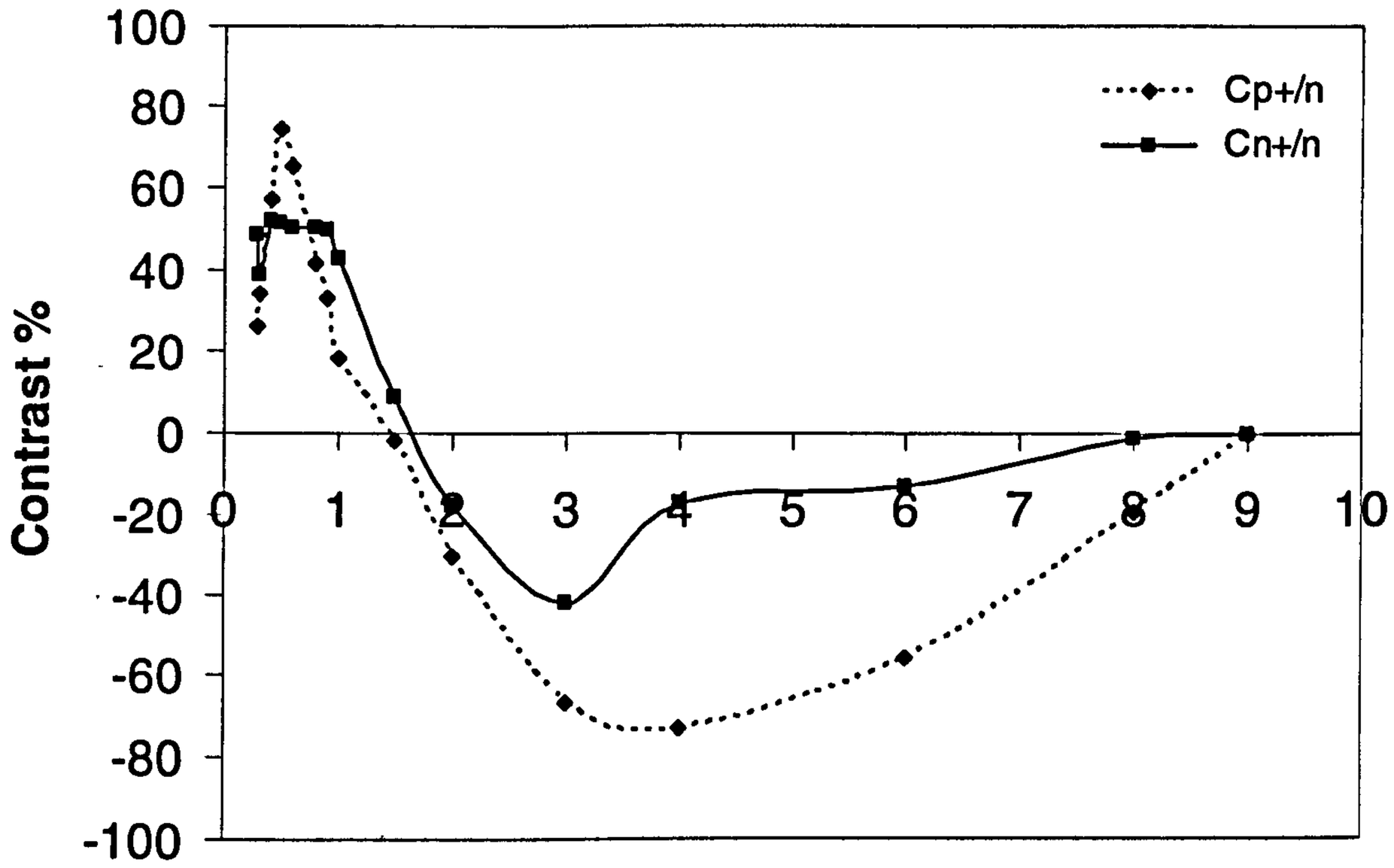

Figure (5.6) Contrast as a function of beam energy obtained from SRL sample collected in the SLEEM mode. Obviously inverted contrast of n^+/n structure is obtained at slightly higher beam energy than the required energy to obtain inverted contrast of p^+/n.

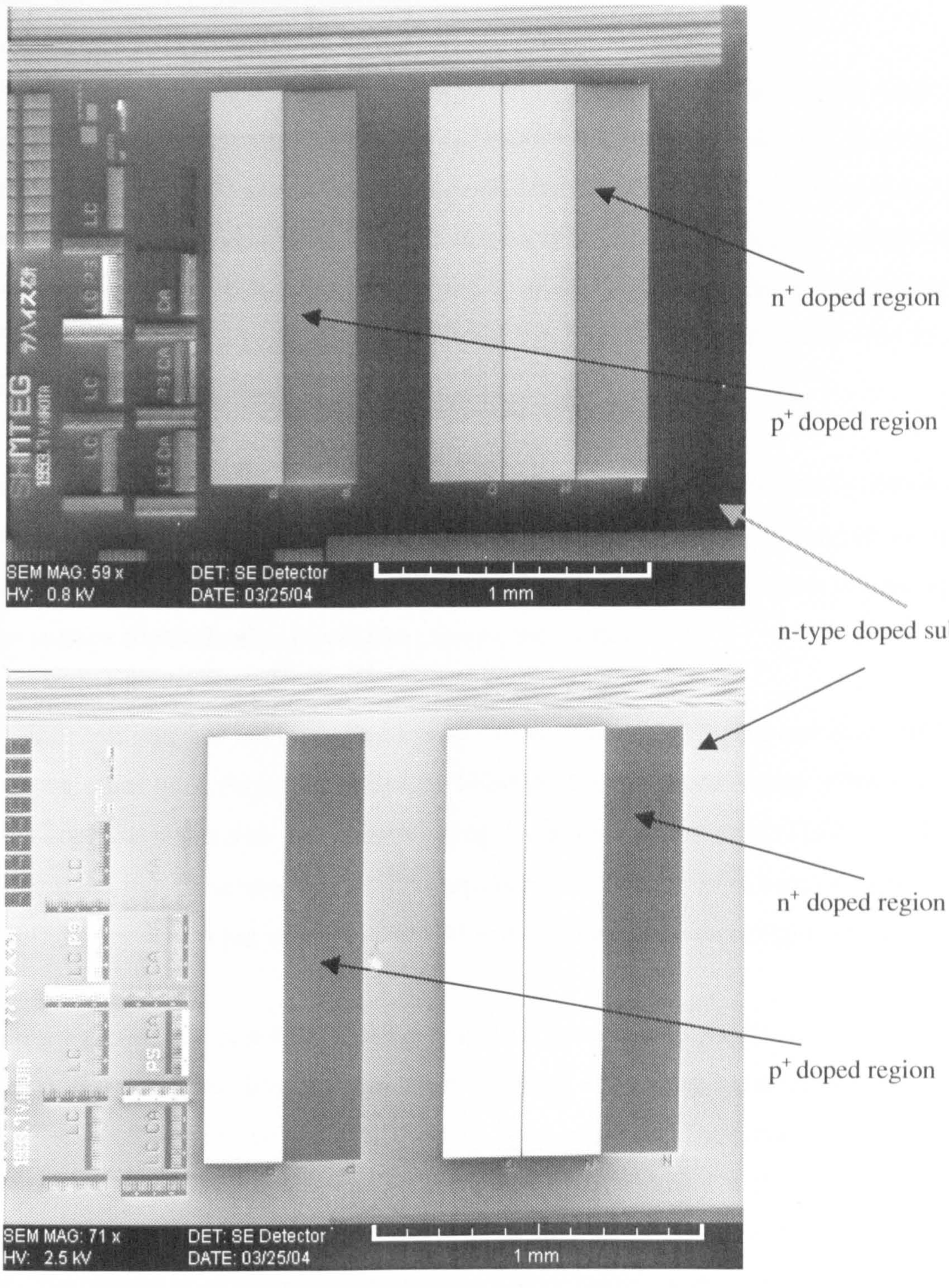

Figure (5.7) Showing usual contrast using E-T detector, in Vega SEM at 800 eV then an inverted contrast at 2500 eV.

UHV conditions with the single lens electrostatic column (El-Gomati, 2001). However, the observed contrast level was lower than that in this study. In addition, it was not clear whether the sample surface has been cleaned in situ before inspection or not.

The appearance of brighter p^+ and n^+-type regions relative to the n-type areas is expected at low energies and can be explained using the m-s contact model. According to this model, since p^+ and n^+ are degenerate, therefore the metal to semiconductor contact will be Ohmic, but with different degeneracy. On the other hand, a Schottky contact will be formed between n-type Si and C adlayer. Therefore, the energy required for SE emission from an n-type area is higher than that required to release SEs from both p^+ and n^+ doped regions.

Although until this stage there is no explanation to understand the inverted contrast at high beam energy (>2keV), the fact that the contrast alteration is dependent on the electron beam energy suggests that this is a function of the beam interaction volume and on the surface contamination layers that exist on the surface.

In order to test whether the inverted contrast can be obtained in higher resolution SEM, SRL sample has been inspected in Serion FESEM to study beam energy effect on SE dopant contrast. Collected SE images using both In-lens detector (TLD) and E-T detector show that an inverted contrast is observed at relatively high beam energy (> 2 keV). SE images collected in Serion FESEM using TLD are shown in figure (5.8).

SE images shown in figure (5.9) indicate that at very low beam energies (800eV) p^+ and n^+ doped regions appear brighter than the n-substrate. Increasing beam energy causes a contrast reversal that can be observed from p^+ areas relative to the n areas at ~1.2 keV. However, the n^+ areas and n areas do not show clear contrast at this beam energy. Moreover, increasing beam energy causes n^+ to appear darker than the n areas at ~ 2keV. This means n^+/n contrast is inverted at higher beam energy compared with p^+/n by an energy shift $\leq$ 800 eV. The variation of the SE image due to increasing the accelerating voltage can be explained due to the increase of the interaction volume combined with internal fields within the surface structure or due to rise of electron-hole

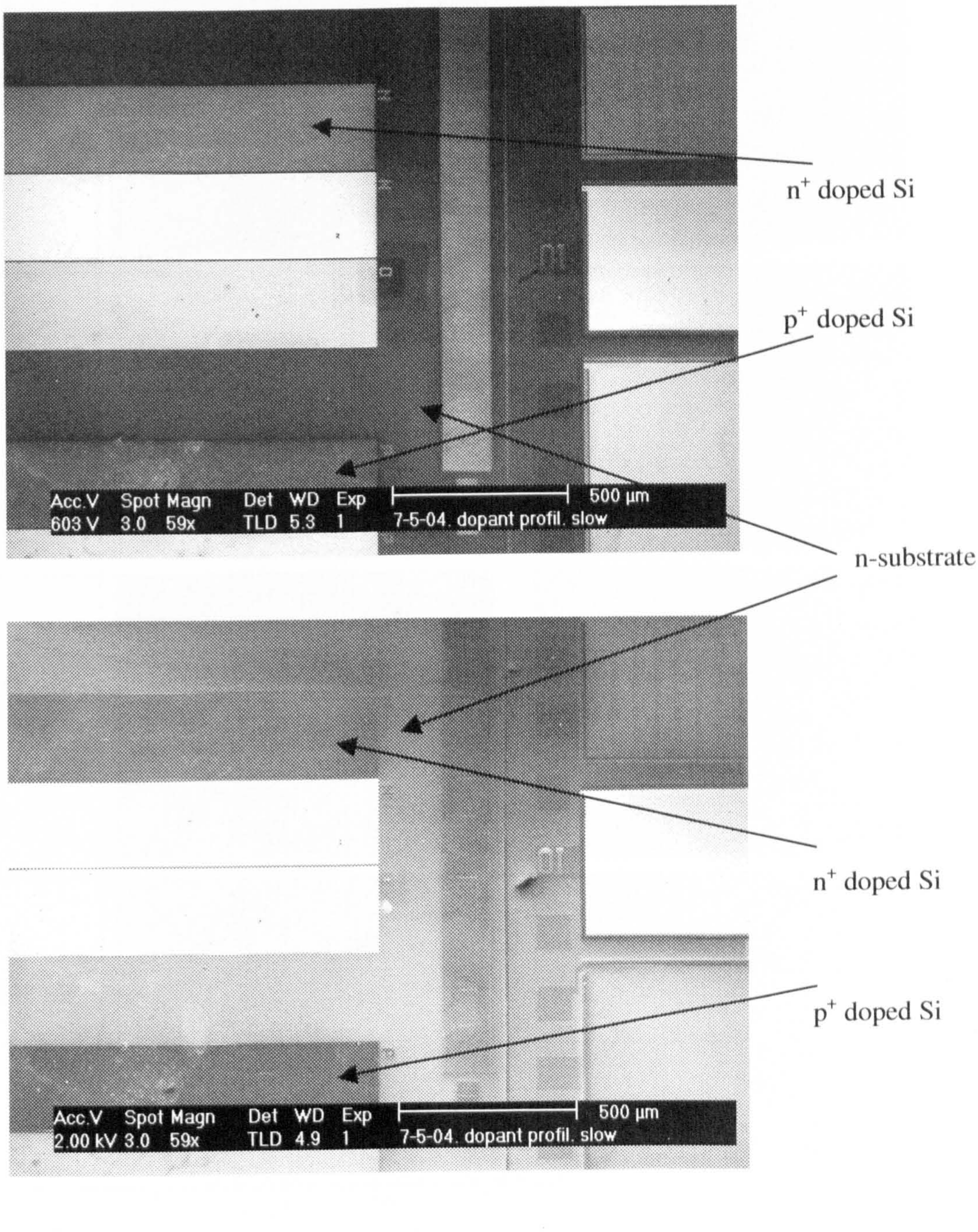

Figure (5.8) SE images collected using In-lens detector in Serion FESEM, at 0.6 keV and 2 keV accelerating voltage respectively, an inverted contrast is shown at 2 keV.

Beam energy	n^+/n	p^+/n
800 eV	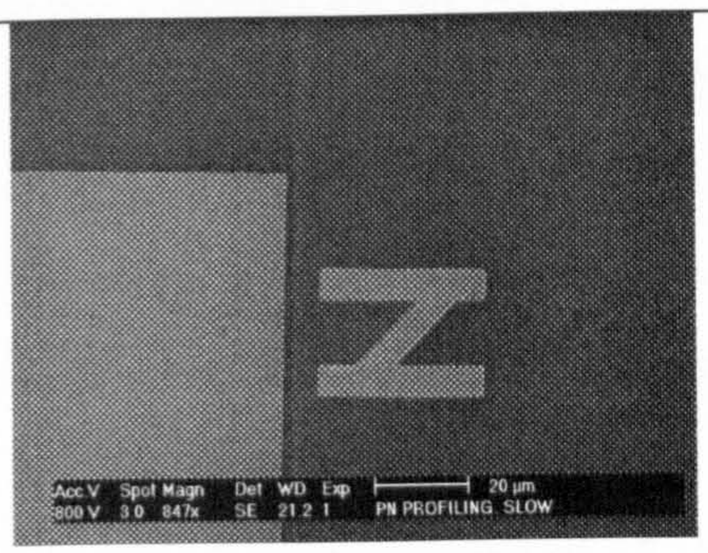	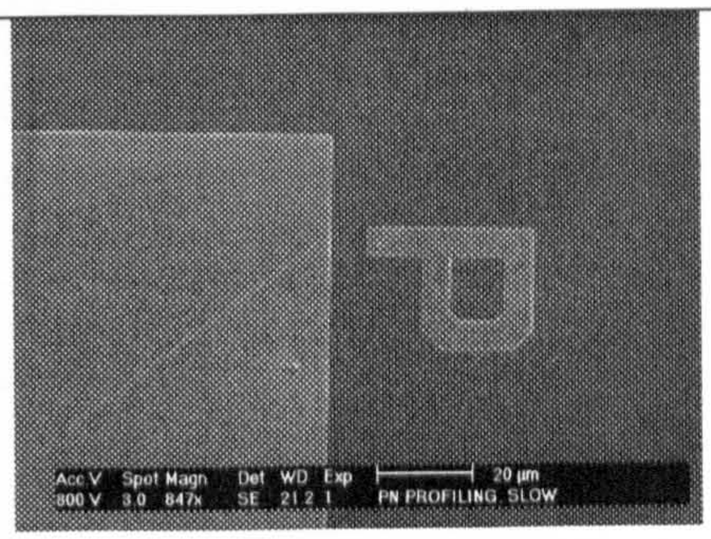
1200 eV	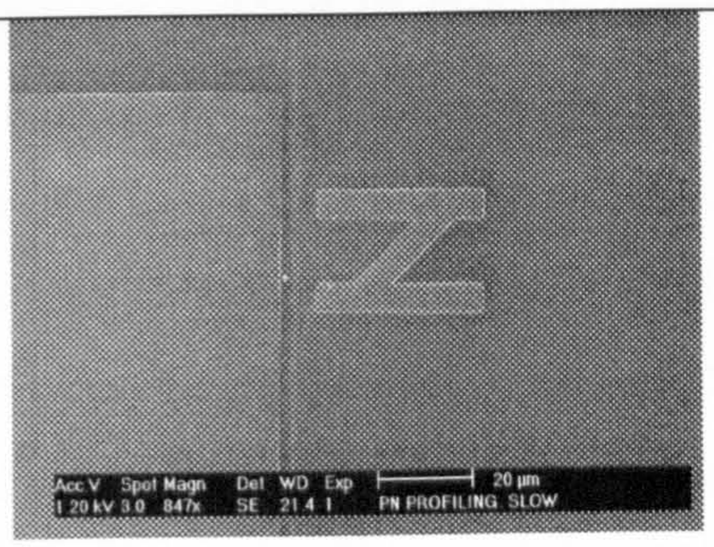	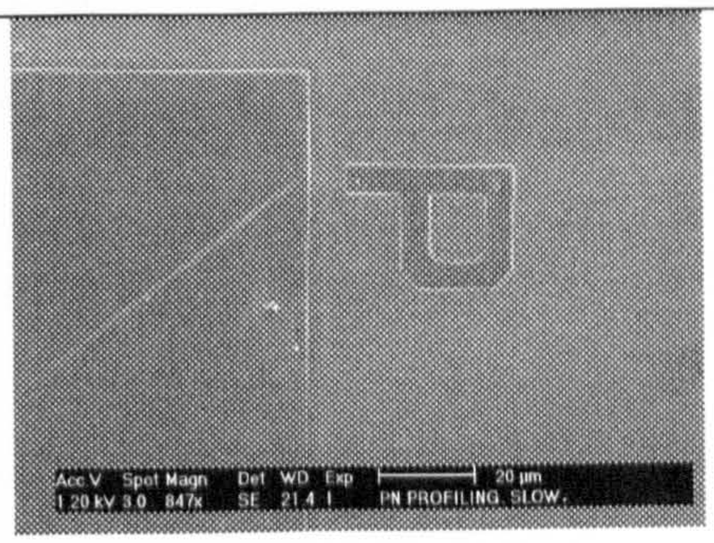
1500 eV	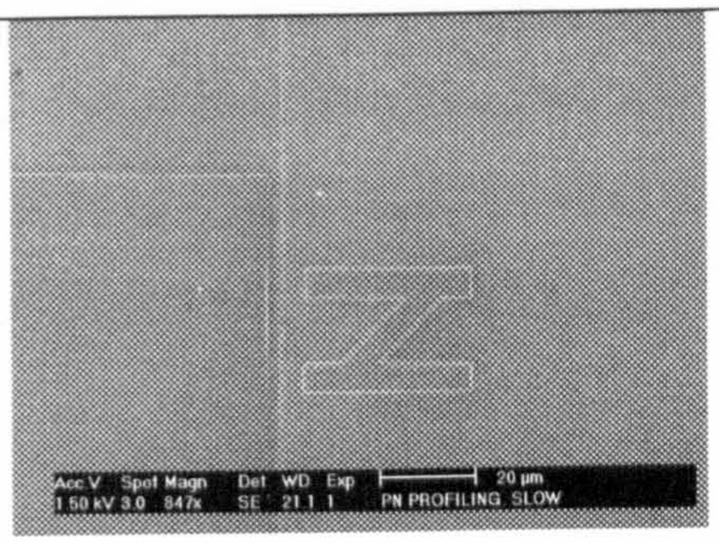	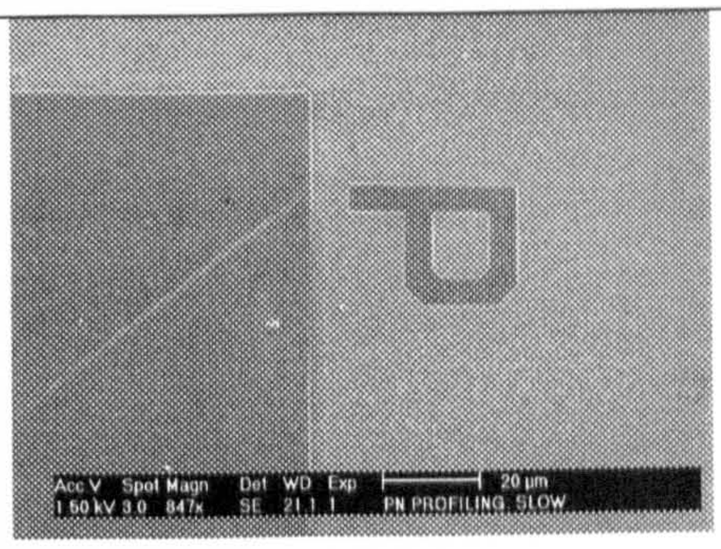
2000 eV	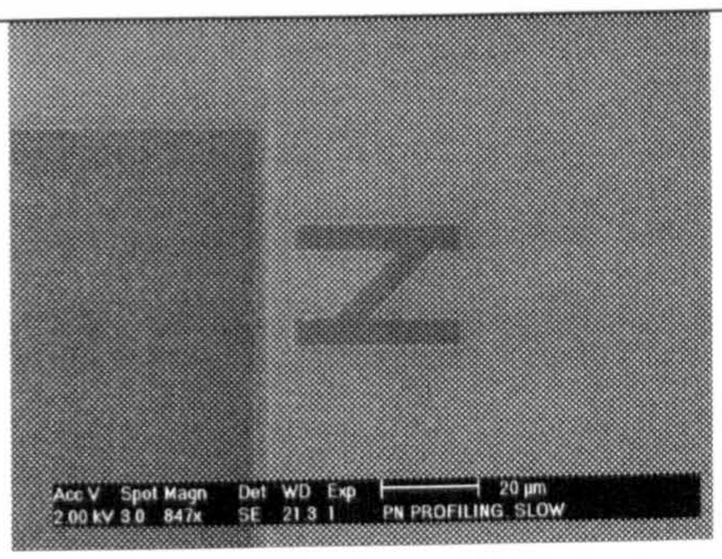	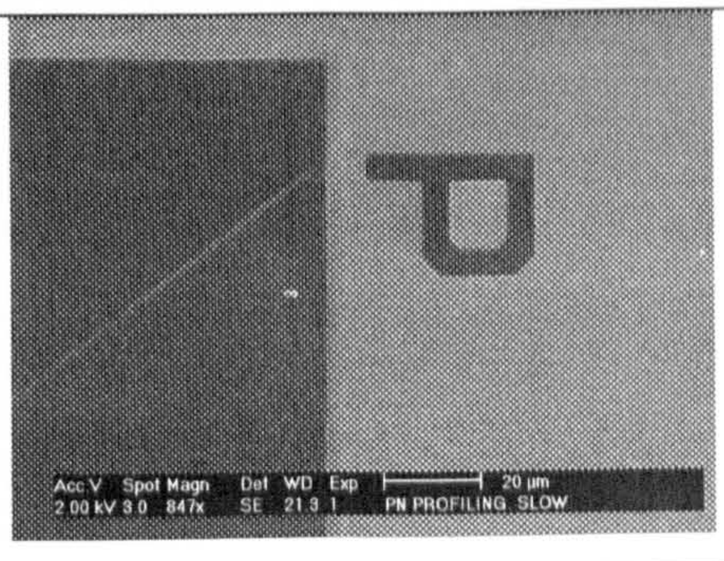

Figure (5.9) Series of SE images collected in Serion FESEM using E-T detector, showing an energy shift of the lower beam energy required to obtain an inverted contrast of n^+/n and p^+/n structures.

pairs generated. However, SE images collected of ISI sample after long etching in HF predicts that presence of an oxide layer on the surface causes the inverted contrast.

The reversal of SE contrast produced due to increase of the accelerating voltage was noticed by Ogura et al (1990) in comparing SE and BSE images of GaAs /AlAs super lattice structure. However, they considered the SE images may not correspond to the real structure in spite of the appearance of the topographic contrast. Hence, no explanation was given to the inverted SE dopant contrast.

It is possible that the contrast reversal of p^+ and n^+ at high beam energies (>2 keV) can be explained due to the existence of a thin layer of oxide sandwiched between the semiconductor and the carbon adlayer i.e. (MOS). This is an important observation that needs surface investigation of doped semiconductors in order to obtain further information to aid our understanding of the contrast mechanism. XPS is a widely used surface examination technique and has been utilised in this study to provide very surface sensitive information of doped Si surface structure. The next section will present results from XPS studies of SRL sample surface.

(5.4) Estimation of the Surface Layer by XPS

The suspicion that samples showing contrast reversal may have a residual layer of natural oxide has led to the use of XPS to estimate the composition and thickness of the surface layer. Data was collected from the sample using a magnesium x-ray source with characteristic energy of 1253.6 eV and a total spectrum acquisition time of about 0.2 sec. Figure (5.10) shows the photoelectron spectra from this sample. The spectrum shows the existence of carbon and oxygen on the surface. The oxygen peak is higher than the carbon peak implying that it is thicker. These carbon molecules and oxygen adsorbates are adsorbed on the sample surface when the wafer was handled in air after cleaning, before being inserted into the UHV.

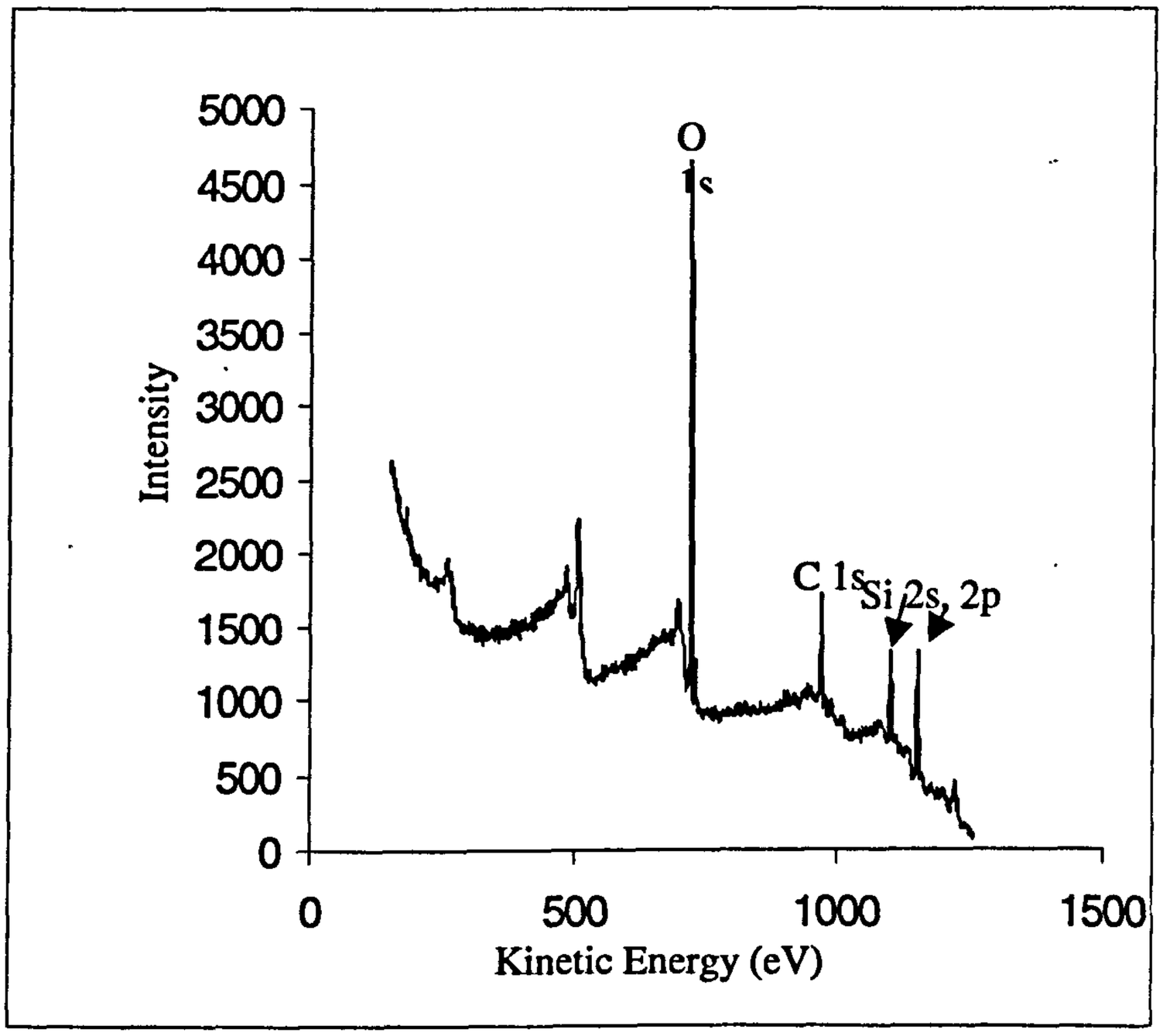

Figure (5.10) XPS spectra from p^+ doped region of SRL sample.

In order to clarify formation of silicon oxide into the sample, spectra were recorded at normal and 60 degree emission using a 120 micron diameter analyser aperture, analyser pass energy of 20 eV and x-ray power of 144W. Wide scan spectra were recorded with analyser pass energy of 160eV. Quantification of spectra was performed following correction of peak areas for the atomic relative sensitivity factors of O 1s (0.736), C 1s (0.318), and Si 2p (0.371). All spectra were energy referenced with respect to the C (1s) at 285 eV.

The photoelectron analyser rotation effect is illustrated in figure (5.11), which presents photoelectron spectra from the Si2p level for the oxidised sample. For two different collection angles, normal emission (θ =90) and grazing angle (θ =60). The relative intensities of the two Si2p signals –assigned to the silicon oxide and to the Si element are increased. At normal emission; it was possible to detect an oxide /element with a ratio of 1.5, a value that increases to 2.4 at the grazing collection angle. The angular dependent of the XPS allows the thickness of the oxide layer to be estimated by using the escape depth of Si 2p level and O 2p level which their values are 1.9 nm and 1.45 nm, respectively. The thickness of the surface layer is about 3 nm composed of about 3-4 mono-layers of oxide and 1-2 mono-layers of carbon. Angular analysis confirmed that the carbon is on top of the oxide. Thus, when this sample is inserted into the SEM environment a carbon deposition will increase the carbon thickness and ends with MOS structure.

(5.5) Discussion

SE imaging of p^+ and n^+ doped regions of Si with an existing thin layer of oxide sandwiched between the semiconductor and the carbon adlayer has shown new contrast behaviour. XPS examination of the surface has shown it to be covered with an oxide (SiO_2) layer of few monolayers in thickness and with a carbon film on the top. The thickness of the carbon adlayer depends on the SEM vacuum quality, as can be inferred from the brightness of scanned areas in SEMs. Although prior to imaging the Si surface was chemically cleaned with HF, during the exposure to air a native oxide layer has grown on the surface. The presence of native oxide on the surface of the semiconductor produces interface states whose nature and density depends only on the oxide-semiconductor combination (Tyagi, 1991). If this layer is very thin (ca. 0.5-2 nm), its

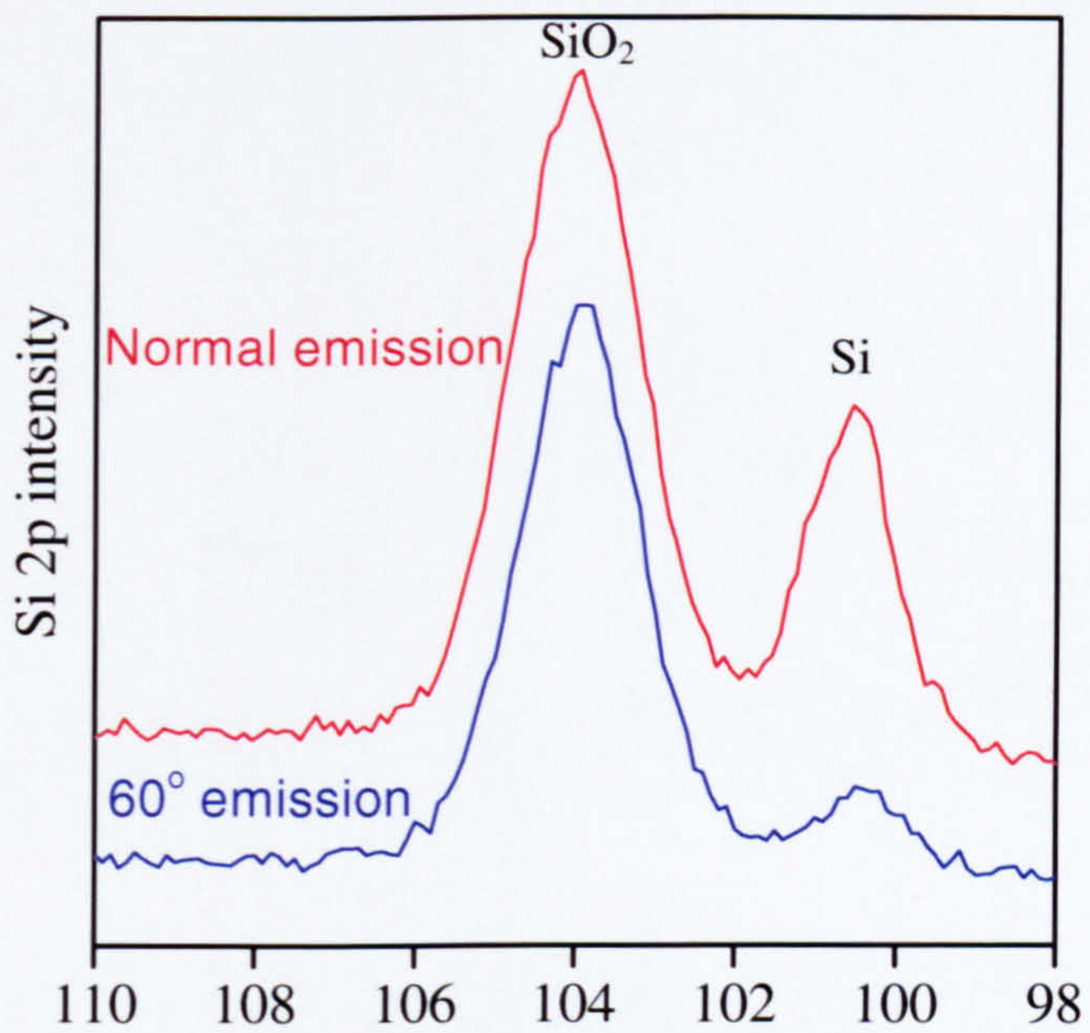

Figure (5.11) Photoelectron spectra of the Si 2p level for SRL sample covered with 2-3 monolayers of oxide. At 60^{o} collection angle, more intensity signal from the oxide is detected, the ratio between SiO_2 peak and Si peak at the different grazing angles are used to calculate the oxide layer thickness.

presence would prevent intimate contact between the Si and the C layer (or any metal film), whereas, the oxide layer suppresses the tunneling of C electrons into the forbidden gap of Si. This is important since covalently bonded semiconductors, such as Si, have a low heat of reaction and tend to react readily with the metal to produce chemical defects in the interfacial region (Jayakody, 2003). Furthermore, such a thin oxide layer is assumed to be charge free (Tyagi, 1991). However, this study shows that if the oxide layer was ~ 2nm thick, then it can not be ignored. Therefore, the presence of oxide charges on doped Si regions may affect SE emission.

Considering the above findings, it is possible to understand the reversal of SE contrast as a function of the electron beam energy in terms of variations of the penetration depth R of the incident electrons within the MOS structure. Therefore the SE emission within the MOS structure can be affected by the sub-internal electric field caused by charge redistribution to form MOS structure. Apart from charge distribution within the MOS structure, oxide charges may influence SE emission as well.

(5.6) SE Contrast Mechanism in the Presence of an Oxide Layer

The above explanation of MOS formation and the effect of the observed SE contrast can be demonstrated in energy band diagrams adopted from Sze (1985). Figure (5.12) depicts the energy band diagrams for p^+, n^+ and n doped Si forming MOS structure with metal of work function higher than that of Si such as in the case of carbon.

Consider the case of a metal of work function $\phi_m > \phi_{Si}$, and p^+ doped Si, when these are brought into contact with the presence of an oxide layer on the surface, the Fermi level must be constant and the vacuum level must be continuous. To accommodate the work function difference, the semiconductor bands bend up as indicated in figure (5.12a). Thus, the metal is negatively charged and the semiconductor surface is positively charged and both charges are adjacent to the oxide layer. So, an electric field is created within the metal-oxide-semiconductor system (MOS diode). Since electrons are depleted at the semiconductor surface, very few electrons are present in the conduction band. Therefore, the source of SEs generated from p^+ (at low and very low beam energy not far from thermal equilibrium) is considered as the electron energy level below the valence band. The energy required to release SEs from p^+ is labelled as Ep^+.

On the other hand, in the case of a metal of work function $\phi_m > \phi_{Si}$, and n doped Si brought to form a MOS structure, the metal is positively charged and negative charge appears on the semiconductor side, causing bands to bend downwards. Since electrons are accumulated at the semiconductor surface, thus the created electric field is opposite to that in the previous case. In this case there are two sources of SEs, one source is from impurity states just above the valence band and the second source depends on doping concentration within the valence band, figure (5.12b).

The n^+ doped Si is similar to that of the n-type, whereas a negative charge accumulates on the Si side. However, the accumulated charges on n^+ doped Si surface and hence the created electric field on highly doped regions are higher than those on n-doped Si surface. Thus (at low and very low beam energy), the source of SEs is considered as the energy levels just above the conduction band and Fermi level, figure (5.12c).

The figure (5.12) shows the different energies required to raise an electron from the densely populated band of the semiconductor to the vacuum level within the MOS formation. It shows contribution of both valence band and conduction band electrons in the SE signal. As can be seen, the energy required to release SEs from n-type Si is the highest. Furthermore, the energy required for SE emission from p^+ and n^+ is comparable. Thus, the SE contrast from $p^+$and n^+ areas will be higher than n areas.

The previous energy band diagram works well at thermal equilibrium and during impinging the MOS structure with very low and low energy electron beam. However, applying high voltage electron beam is expected to cause variations in the energy band bending. Increasing beam energy is probably equivalent to biasing the metallic top layer with a negative voltage ($V<0$) caused by excess negative charge build up on the surface of the samples (Stewart, 1934). The negative potential of the surface can reach very high values up to the potential of the electron gun (Seiler, 1983). In the case of n and n^+ doped regions, since bands bend downward (Sze, 1985), thus applying a negative potential (estimated to be >1.0 kV) leads to the ideal flat band condition in n-type Si due to attracting holes to the Si-Oxide interface which recombine the accumulated negative charge gradually. While slightly higher voltage is required to get the flat band condition in n^+ doped region to compensate the larger accumulated charges here. Increasing the

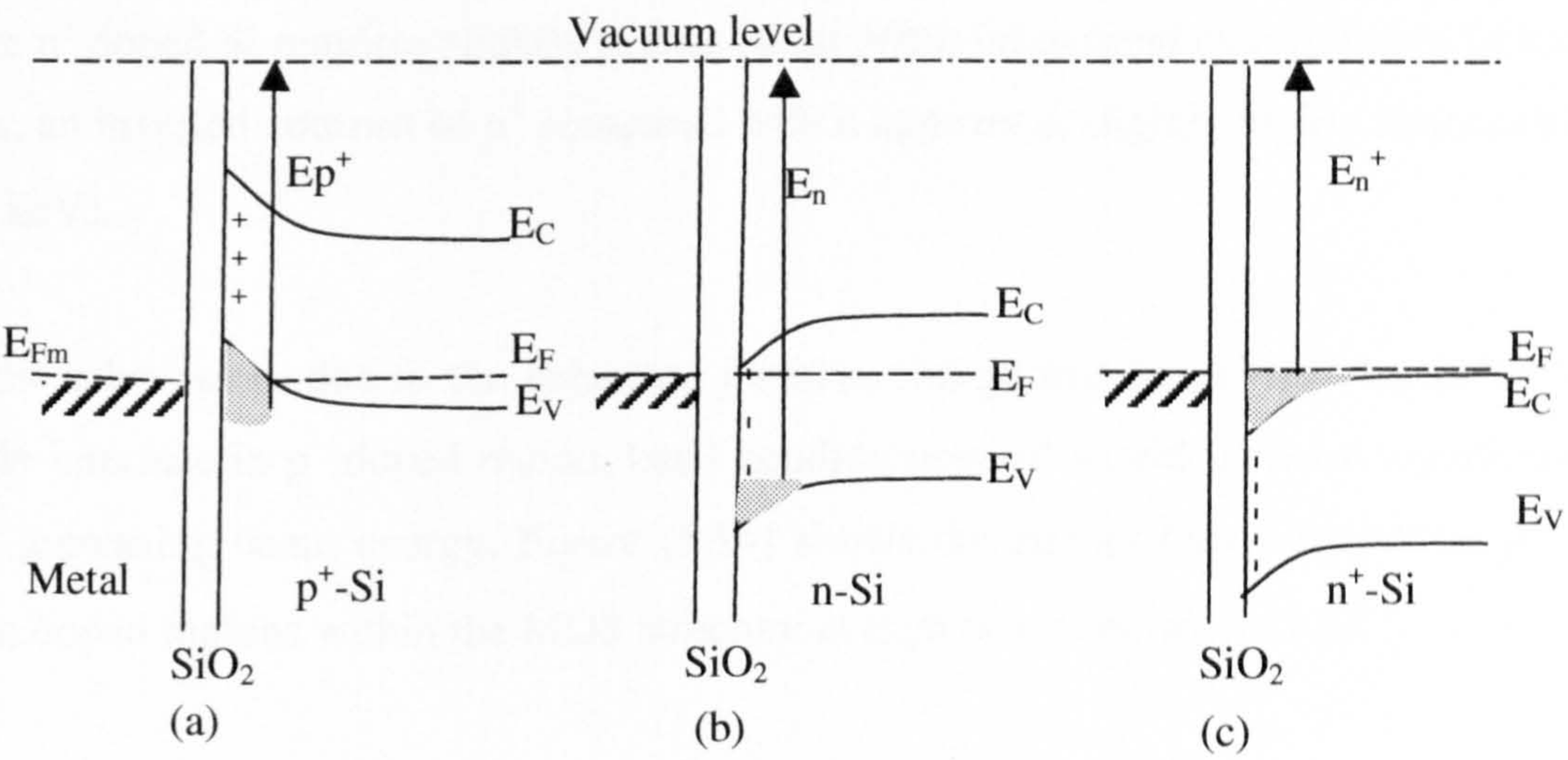

Figure (5.12) The Energy band diagram of a MOS diode formed between doped Si and metal layer of work function larger than that of Si ($\phi_m > \phi_S$), in thermal equilibrium, (a) p^+-doped Si. (b) n-doped Si. (c) n^+- doped Si. ϕ_m = Metal work function, E_V = Valence band, ϕ_S = Semiconductor work function, E_C = Conduction band, E_F = Semiconductor Fermi level and E_{Fm} = Metal Fermi level. E_p^+, E_n, and E_n^+ are the energies required to release SEs from p^+, n and n^+ doped Si regions respectively.

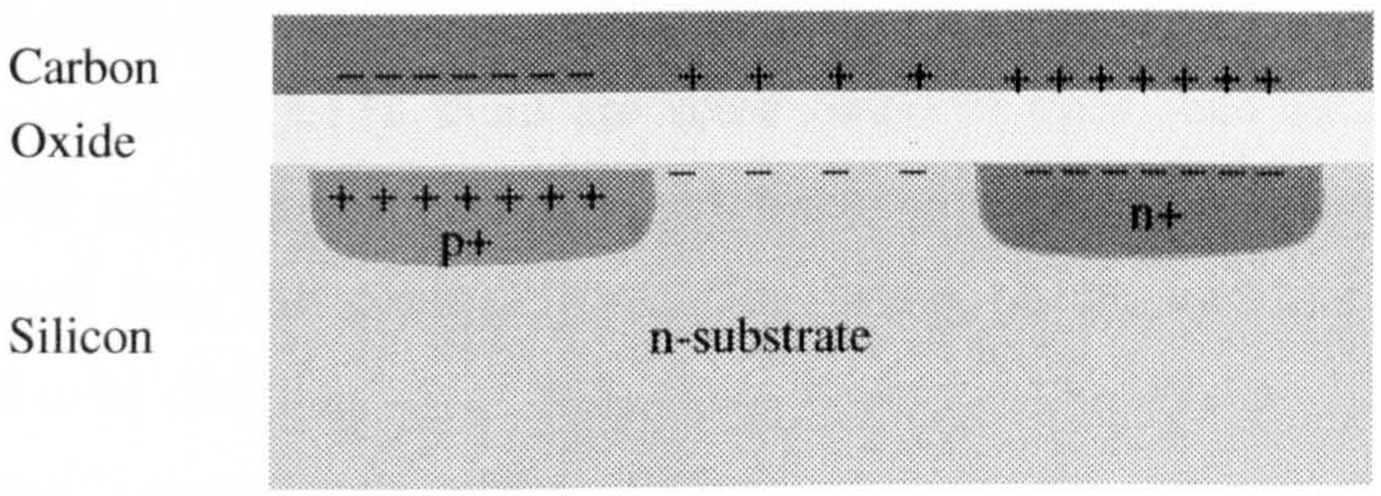

Figure (5.13) The cross section structure of the MOS structure and the charge distribution within the different layers at equilibrium. (This applies at the low and very low energy condition).

applied negative voltage to the metal layer would bend the bands near the semiconductor surface upward due to accumulation of holes near the oxide semiconductor interface. Therefore, the energy bands bend upward in n-type Si at beam energy ~1.2keV. As a result n appears brighter than p^+ at high beam energies (≥1.2keV), while n^+ doped Si requires slightly higher beam potential to bend energy bands upward. Thus, an inverted contrast of p^+ compared with n appears at slightly higher beam energy (≥ 2 keV).

On the other hand, due to the enhanced positive charge that accumulated near the Si-Oxide interface in p^+ doped region, band bending upward would increase significantly with increasing beam energy. Figure (5.14) shows the energy band diagram of p^+, n^+ and n doped regions within the MOS structure at high beam energy (≥ 2 keV).

In the explanation given above, the SE contrast has been related to the different energies required for SE emission of p^+, n^+ and n doped areas due to the MOS structure formation. The SE source has been regarded as the valence band and conduction band electrons within the SE-escape-depth, λ_{SE}. The fact that SE dopant contrast depends on beam energy suggests that the particular contrast mechanism is dependent on the beam interaction volume. Therefore, it is possible to understand SE contrast behaviour due to increasing interaction volume as beam energy increases, taking into consideration oxide charges effect on SE emission.

In addition to the created electric field caused by the oxide layer at thermal equilibrium as shown in figure (5.13), there are some oxide charges such as interface-trapped charges, the oxide trapped charges and fixed oxide charges that could affect SE emission and then the contrast level. The origin of the interface charge (Q_{it}) is considered to be dangling bonds of Si atoms located at the interface between the oxide layer and the Si crystal surface (Sze, 1985).

The oxide-trapped charges (Q_{ot}) are associated with defects in silicon dioxide; these charges can be created by high energy electron bombardment. The traps are distributed inside the oxide layer. The related process of these charges can be removed by low temperature annealing (Sze, 1985).

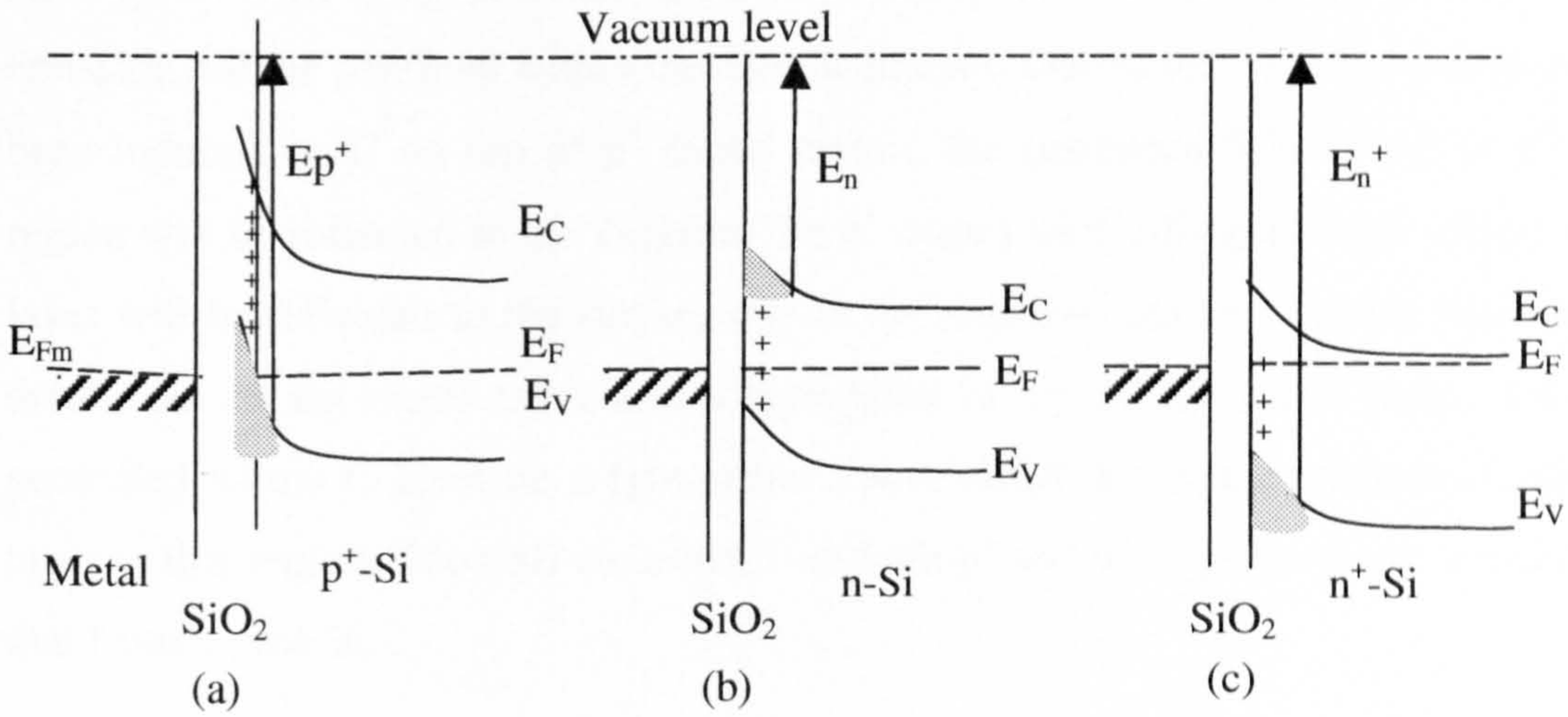

Figure (5.14) Energy band diagrams of a MOS diode formed between doped Si and metal layer of work function larger than that of Si ($\phi_m > \phi_S$), show the upward bending of the energy bands caused due to positive charge accumulation at the Si surface after impinging with high energy electron beam (≥ 2 kV), (a) p^+-doped Si. (b) n-doped Si. (c) n^+-doped Si.

The fixed–oxide charge (Q_f) is located within the Si-SiO_2 interface, this charge is positive in p-type Si (Sze, 1985), and negative in n-type Si (Munakata et al, 2000). Moreover, on n^+-doped well, due to the strong electric field on the highly doped region, the negative charges may be driven out of the oxide layer by the electric field (Munakata et al, 2000). Thus, this negative charge will accumulate above the metal positive charge. Charge distribution according to MOS structure, in addition to oxide charges that may affect SE emission charge distribution within the investigated sample can be presented as shown in figure (5.15).

At very low PE, the penetration depth R is small, thus the interaction volume and SE emission will be confined within the carbon adlayer. Due to the negative charge that has been induced on C on top of p^+ doped region, the generated SEs on top of p^+ doped region will be reflected to the vacuum. On n^+ doped well, SEs generated within surface layer will be reflected to the surface due to the negative charge of oxide that has been driven out of the oxide layer and accumulated in top of the metal layer, while SEs generated within C layer on n-type suffer lower effect due to the positive charge of C layer in this region. Thus SE emission from both p^+ and n^+ doped regions is higher than that from n-type Si.

With increasing beam energy, the primary beam penetrates the oxide layer so, SEs generated in this layer are affected by the electrostatic field as follows; On p^+, the generated SEs are retarded by the negative charge of the C layer, thus SE emission within this area reduces. On the other hand, SE emission on n-type does not change a lot, and SE emission from n^+ is reduced this appears as a reduced contrast around 1.5 keV up to 2 keV.

With increasing the energy of the incident electron beam ≥ 1.2 keV, SE emission form p^+ goes down compared with a slight increase of SE emission from n-type. This appears as an inverted contrast between p^+ doped region and n-substrate. Since increasing beam energy increases the penetration depth, and whereby SE emission from n^+ doped region is reduced at 2keV. Then this can be explained due to the influence of negative charge present on top of n^+ on SE generated within this area. Thus, inverted n^+/n contrast occurs at slightly higher beam energy, compared with inverted contrast of p^+/n by energy shift ~ 500- 800eV. Moreover, irradiating the oxide layer with such high energy

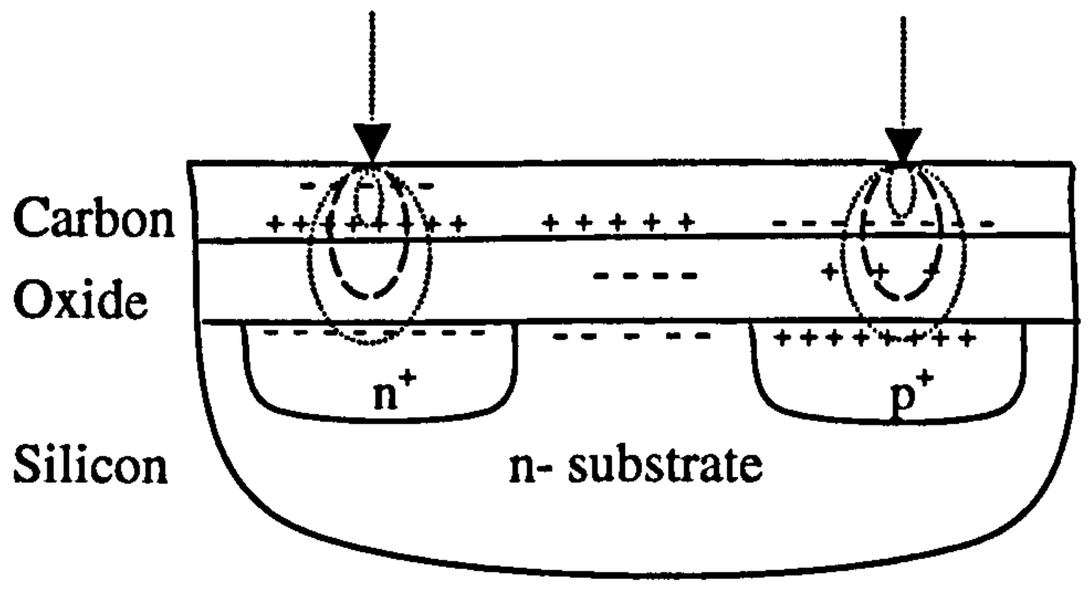

Figure (5.15) Variation of the interaction volume within MOS structure. Notice charge distribution within the MOS structure. In addition to the negative charge that accumulated on top of the C layer above n^+ doped region, this charge may be driven out of the oxide layer by the high electric field created between n^+ doped region and C adlayer.

will create more trapped oxide charges associated with oxide defects. This produces more charges within the oxide layer and may contribute into contrast inversion. Therefore the contrast reversal of p^+ and n^+ with respect to n doped Si can be attributed to the difference in the energy required for SE emission from the three doped areas at different accelerating voltages.

In order to confirm the analysis above, the variation of SE intensity of both p^+ and n doped regions of ISI sample as a function of electron beam energy have been measured and displayed in figure (5.16). This figure shows that the variation of SE intensity emitted from p^+ doped Si is higher than those emitted from n-type Si. This can be explained due to the strong electric field that affects SE emission from p^+ doped region compared with low electric field that governs SE emission from n–type Si.

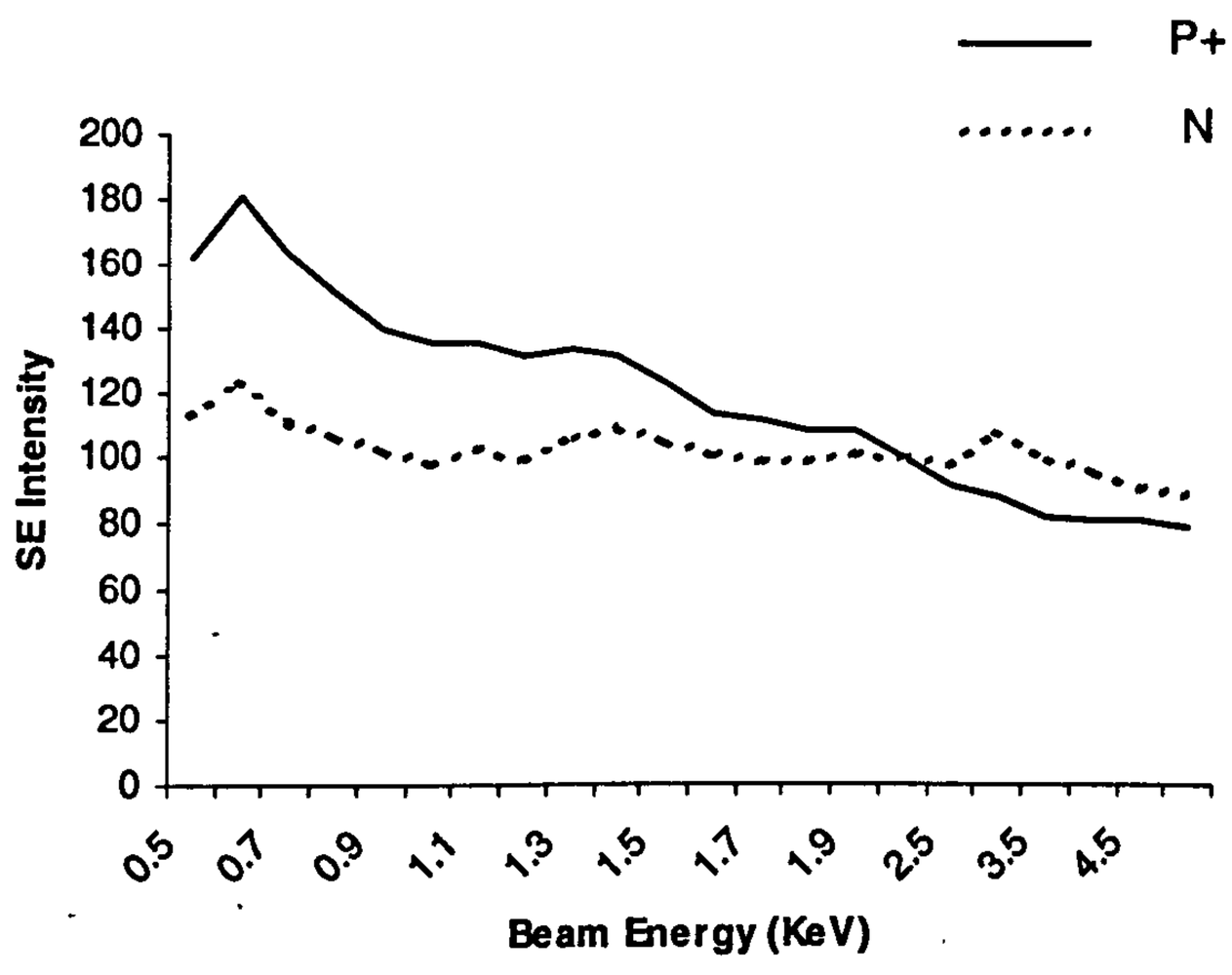

Figure (5.16) Variation of SE intensity as function of beam energy, measured from ISI sample.

(5.7) Conclusions

In this chapter, results from SE imaging of different Si structures in a Vega SEM and a Serion FESEM are presented. Further SE imaging of the same structures has been observed in the low energy and very low energy Vega SEM operated in the cathode lens mode. The contrast dependence on the beam energy, the detection method and the contamination effect have been investigated. It has been demonstrated that the maximum SE contrast from doped Si is obtained by imaging at very low beam energy regime (≤ 1 keV).

A contrast from n^+ and p^+ doped Si was observed at low and very low beam energy and it is reversed above 1.5 keV. An inverted contrast of ISI and SRL samples has been observed although these samples are prepared in accordance with similarly used methods by others. SE imaging using different SE detection methods has shown that n^+/ n contrast has inverted at slightly higher beam energy compared with inversion contrast of p^+/ n. Surface analysis of one of these samples (SRL) using XPS has shown surface layer of about 3 nm composed of about 3-4 mono-layers of oxide and 1-2 mono-layers of carbon. In addition, XPS angular analysis confirmed that the carbon is on top of the oxide. The information gained about the chemical and elemental composition of the surface layer has been combined with results from SE imaging to provide a proper interpretation of the contrast behaviour at low and very low beam energy. The data from the present study clearly identify oxide effect on SE dopant contrast. Moreover, the data also supports the proposed model by El-Gomati (2000) considering the high sensitivity of the obtained contrast to semiconductor surface structure.

According to the observations in this study, the variation of SE emission and hence contrast inversion is attributed to sub-internal electric field within MOS structure. It also predicts that the contrast must be dependent on thickness of metal layer and oxide layer. Although the oxide layer is always present at the surface, electrons can easily tunnel through it if it is very thin (0.5-1 nm). Therefore, the m-s contact governs the SE emission. On the other hand, if the oxide layer was thick, the inverted contrast can be seen even at low beam energy as shown in figure (5.4). In the extreme case i.e when the oxide layer is much thicker (i.e. few microns), the contrast may be masked as reported by Jayakody (2003). While if the carbon layer was thicker than in this study, the reversal of contrast will be shifted to higher beam energy.

The next chapter will present electron dose effect on SE contrast by using more than one technique in order to evaluate the complex problem in quantifying dopant profiling. The changes of the energy bands that affect the SE emission with existing an oxide layer will be discussed in details after presenting electron dose effect on the contrast.

Chapter 6: Effect of Electron Dose Injection on Doping Contrast of Si p-n Junctions in LVSEM

(6.1) Introduction

In most of the previous studies of dopant contrast it has been found that the magnitude of the doping contrast measured in the LVSEM is dependent on the microscope operating parameters such as: the specimen working distance, exposure time, accelerating voltage, magnification, beam current and scan time. Therefore, in order to achieve a comprehensive understanding of the dopant contrast mechanism, it is crucial to study the experimental parameters that affect the observed contrast in the SEM. Although these parameters have been studied by a number of researchers (Venables 1997, Sealy 1997, 2000, Elliot 2001, Kazemian 2003), these authors did not carry out a systematic investigation as it will be reported upon here. It is the aim of this chapter to show that experimental conditions like magnification, scan speed and electron beam current incident on the Si sample have a rather large influence on the observed contrast values. Furthermore, the aim is also to provide proper understanding of electron beam injection effect on SE contrast and compare these results with those in the literature.

The effect of electron dose injection on the magnitude of SE contrast has been carried out in this chapter using clean Si samples and in the presence of an oxide layer adsorbed into the Si surface. In addition, the optimum conditions for these parameters are investigated in order to enable reliable quantification of the technique. Apart from electron dose effect on SE contrast, the effect of the specimen working distance has been studied in this chapter as well. Results will be considered in terms of m-s contact combined with adsorption effect on the contact.

Apart from Vega SEM, Serion FESEM has been used to investigate electron dose effect on the contrast.

In most of the previous studies, SE dopant investigations carried out using freshly cleaved surfaces, however in this study only patterned surfaces of Si have been investigated. Moreover, in all Si samples dopants were introduced by diffusion a long time before starting this study. Therefore adsorption effect on these surfaces even in best cleaning conditions can not be ignored unless it was cleaned in-situ (i.e under UHV conditions).

(6.2) Review of the Literature

The electron dose can be defined as follows:

$$\text{Electron dose} = \left(\frac{\textit{beam current}}{\textit{unit area}}\right) \text{(dwell time)} \qquad (6.1)$$

Sealy et al (2000) have studied the electron beam current effect on SE contrast and found that the contrast increases with decreasing beam current. This result has been explained in three possible ways. Firstly, in terms of the patch field model, where a high beam current incident on a p-n junction will create thousands of electron-hole pairs. Then a current will be induced across the p-n junction by the electron beam. A greater reduction in the built-in voltage results from a larger beam current. According to the patch field model, this would decrease the contrast.

Secondly, high beam current incident on semiconductor produces electron-hole pairs within the specimen surface in a region defined as the generation volume. If the concentration of the generated carriers exceeds the doping concentration of this region, then this area could appear to be effectively intrinsic and the contrast between p-and n-type regions might be lost.

Finally, as the beam current increases, it is possible that the surface band bending is decreased until a flat band condition is approached. A reduction in surface band bending would imply that the contrast level should increase, but Sealy did not observe contrast rise experimentally. Sealy et al (2000) have reported that band bending reduces the contrast and flat band condition increases it.

Kazemian et al (2003) have thoroughly investigated the electron dose effect on SE contrast. Equation (6.1) is used to evaluate electron dose, whereby for a constant magnification, the dose increases with increasing scan time per line, and for a constant scan time, the dose increases with increasing magnification. Therefore, the minimum electron dose effect on the contrast was studied at the shortest scan times as well as low magnifications. This resulted in the highest SE intensity difference at the minimum electron dose. As the magnification increases above 30,000×, the SE intensity difference between the n- and p- type regions is reduced. The pronounced result was explained as a

consequence of charging according to the built in-voltage model. The built in-voltage across the p-n junction gives rise to higher SE intensity from the p-region than from n-region (Sealy et al, 2000). This voltage, however, will be affected by electron-hole pairs generated by the primary electron beam in the space charge region. The generated carriers then recombine with the fixed ionized dopant atoms in the space charge region leading to a reduction of the built-in voltage.

(6.3) Electron Dose Effect on SE Dopant Contrast

In this study, electron dose effect on contrast has been studied in three ways. Firstly, for a constant beam current, and a constant scan time per line, the dose increased with increasing magnification. Secondly, for a constant magnification and scan time, increasing beam current increases electron dose. Finally, for a constant magnification and beam current, electron dose increased with using slow scan speeds. Since the number of emitted electrons from the specimen per incident electron depends on the primary beam energy, SE images were collected at the same accelerating voltage. In order to minimise charging effects in Si, SE images were collected at 1 keV or at lower beam energies.

The experiments were performed on the ISI, Durham and SRL samples with accurate measurements of the beam current in the Vega SEM.

(6.3.1) Magnification Effect on SE Dopant Contrast

The SE images were taken from freshly cleaned ISI and Durham samples using accelerating voltage of 1 kV at a working distance of 19 mm and beam current =2 nA at two different scan speeds; 7.8×10^{-3} s/line and 117.7×10^{-3} s/line using an E-T type detector.

From the results shown in figure (6.1) obtained from ISI sample, it can be seen that, when the electron dose increases with increasing the magnification up to 20 kx, the contrast is reduced. After this magnification value the contrast is almost constant. Plot of contrast collected from the Durham sample (Figure (6.2)) shows that contrast is reduced with increasing magnification. Both plots are showing that the highest contrast can be obtained at low magnification. This can be explained in terms of the built in

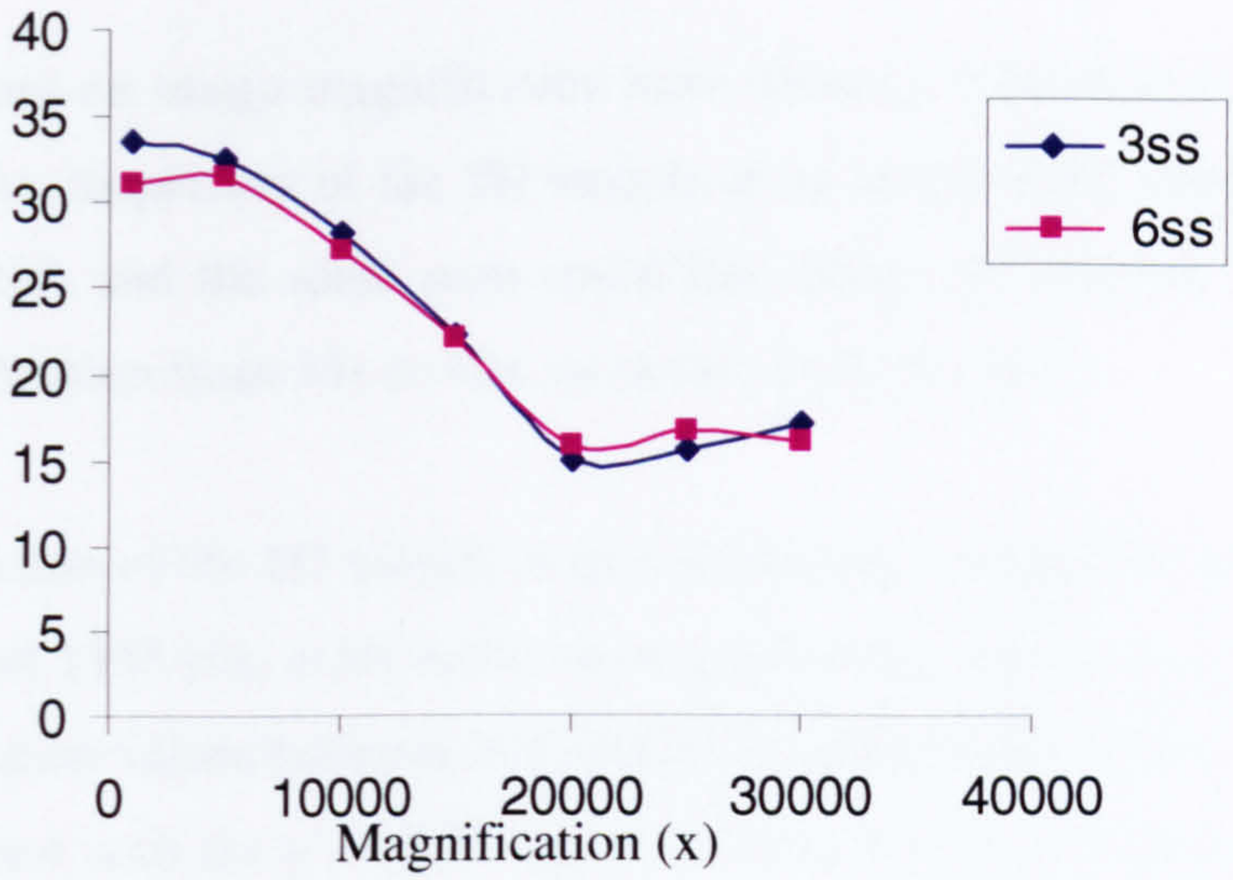

Figure (6.1) The graph shows dopant contrast as a function of magnification for ISI sample at 3ss=7.8×10^{-3} s/line and 6ss=117.7×10^{-3} s/line.

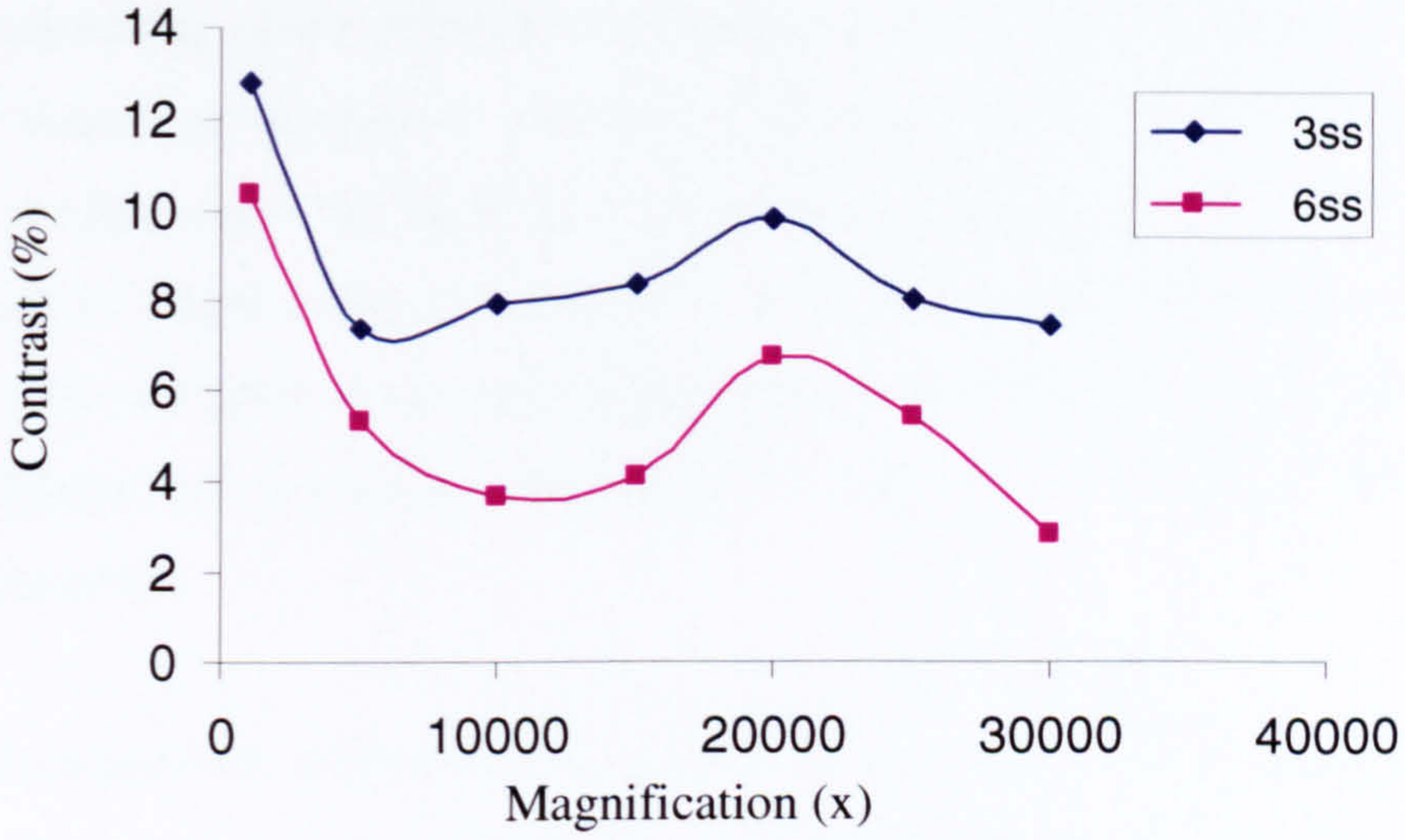

Figure (6.2) Contrast as a function of magnification for the Durham sample at two different scanning speeds.

voltage model, whereby increasing electron dose by increasing magnification results in a reduction of the built in voltage, hence a reduction of contrast.

Further observations on image magnification have shown a reversal of contrast in some cases. For example, inspection of the ISI sample at an accelerating voltage of 1 kV, at beam current = 2nA and the same scan speed has shown an inverted contrast due to increasing magnification from 34x to 49x, as shown in figure (6.3).

In addition, inspection of the ISI sample at an accelerating voltage of 1 kV, and at lower beam current about 1165 pA, at the same scanning rate has shown an inverted contrast at small magnification values between 40x and 200x, where n doped areas appear higher brightness compared with the p^+ doped regions. However a usual contrast is obtained at higher magnification values.

Investigating the same sample at higher magnification values; 300 x, 400 x, 500 x to 1000 x, has shown that a reversal of contrast can be obtained at beam current ≈312 pA i.e higher magnifications require lower beam current to obtain unusual contrast at the same accelerating values. Moreover, at magnification values higher than the previously reported values, no reversal of contrast is obtained regardless of the value of the beam current, neither does the contrast vanish. This dependence of the contrast on the magnification values is not so clear, but it is likely to be a result of the variations of the electron dose whereby at low magnifications inverted contrast is obtained even at high beam currents and increasing magnification requires lower beam current to get an inverted contrast.

Initial investigations of this behaviour have shown that; the inverted contrast at low electron dose can only be obtained in the presence of an oxide layer whereby extra cleaning in HF gets rid off the inverted contrast as shown in figure (6.4). Therefore, the inverted contrast as a function of magnification can be explained to be due to the variations of electron dose combined with the effect of residual thin layer of oxide adsorbed onto the Si surface.

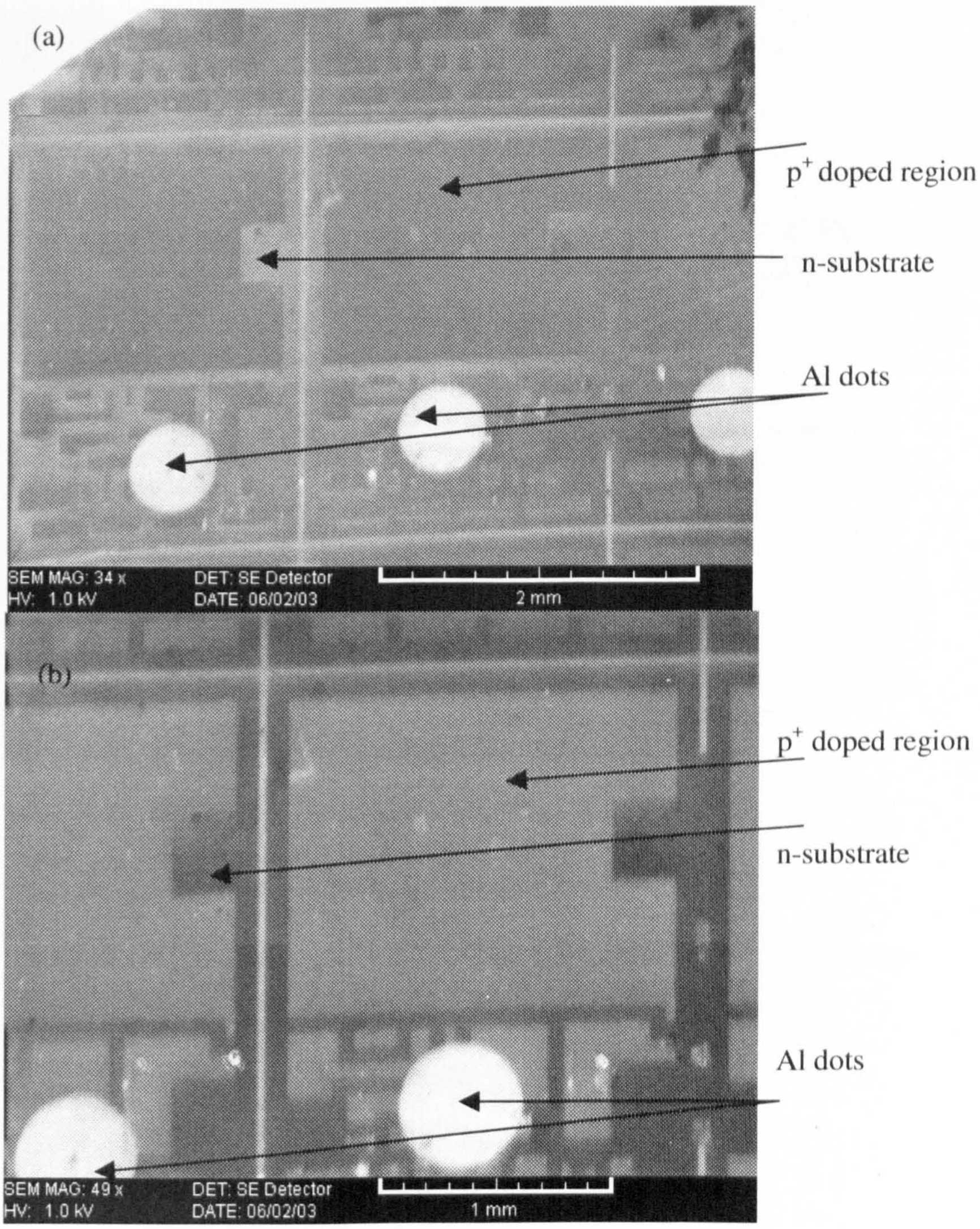

Figure (6.3) SE images collected from ISI sample show inverted contrast at small magnification (34 x) in (a), and normal contrast at higher magnification values (49 x) in (b), notice that these images were collected at the same scan speed and the same beam current. Al dots appear bright in both images.

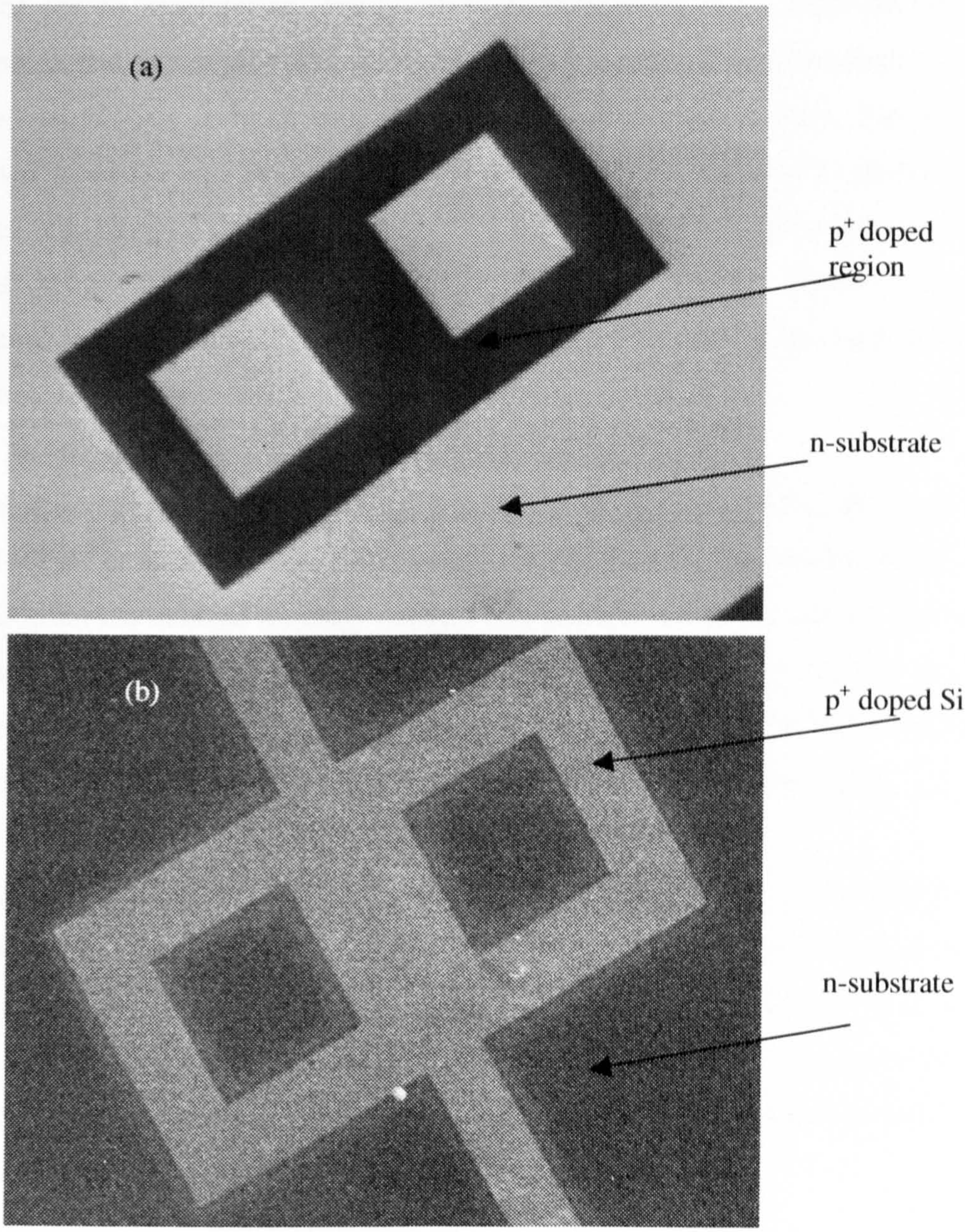

Figure (6.4) SE images collected of ISI at low electron dose, (a) after normal cleaning, the image is showing inverted contrast whereby p^+ doped region appear dark and n doped Si appear bright. (b) After extra cleaning in HF, normal contrast is obtained after removing the oxide layer.

(6.3.2) Beam Current Effect on SE Dopant Contrast

There is an increase of contrast with increasing beam current obtained through the E-T detector for an accelerating voltage of 1kV. This result was confirmed by imaging different doped Si samples (ISI, Durham) in the Vega SEM. In contradiction to Sealy's results, the highest contrast was observed for higher beam current. Plot of contrast collected from ISI and Durham Si samples as shown in figure (6.5) shows increased contrast at high beam currents. This result is also confirmed in figure (6.6) that showing two SE images of ISI sample collected at 171pA and 2090pA. Whereby, the highest difference in the SE intensity between p^+ and n doped regions is observed at high beam current.

The increased contrast at higher beam current can be explained using the band bending model (Sealy et al, 2000). The beam current is expected to alter band bending. At high beam current the induced minority carriers will be captured by the surface potential well produced by the bent bands. The charge on the trapped minority carriers will tend to compensate for the trapped surface charge and hence reduce the band bending. The reduction in surface band bending is expected to increase the contrast level.

In order to investigate the adsorption effect on SE contrast, some ISI samples have been cleaned in IPA and then in HF solution, where a thin layer of oxide is likely to be left on the surface. These samples have been imaged in the Vega SEM at different beam currents. The obtained images indicate that an inverted contrast appears at low beam current compared with the usual contrast that appears at higher beam current as shown in figure (6.7).

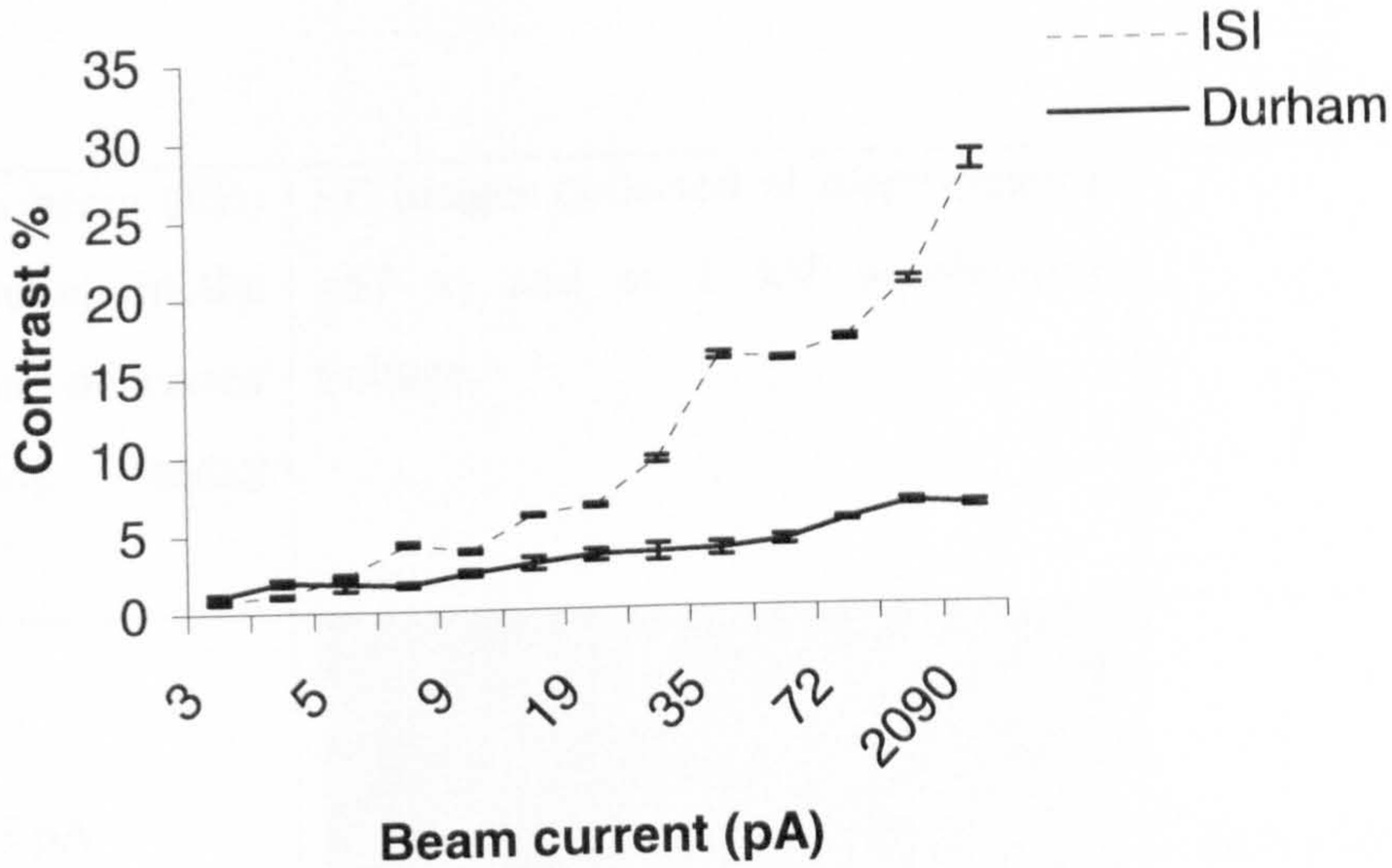

Figure (6.5) Contrast as a function of beam current, calculated from digitally collected SE images from the ISI sample and from the Durham sample.

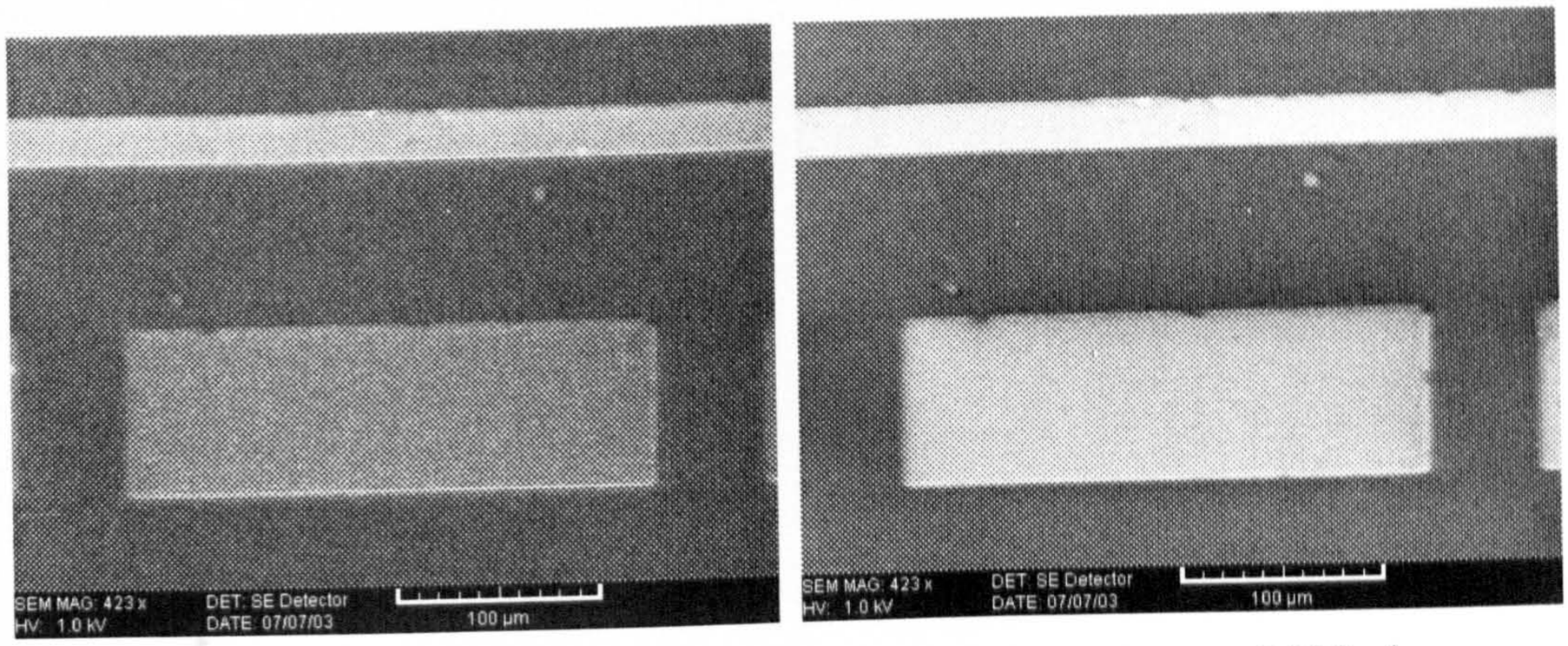

(a) beam current = 171 pA

(b) beam current = 2090pA

Figure (6.6) Showing two SE images of ISI sample collected at two different currents, obviously p^+/n contrast is higher at higher beam current.

The electron beam (EB) current incident on the sample was measured in-situ using faraday cup.	SE images collected at magnification =57 x, and at 1 kV accelerating voltage.	
(a) EB = 35 pA	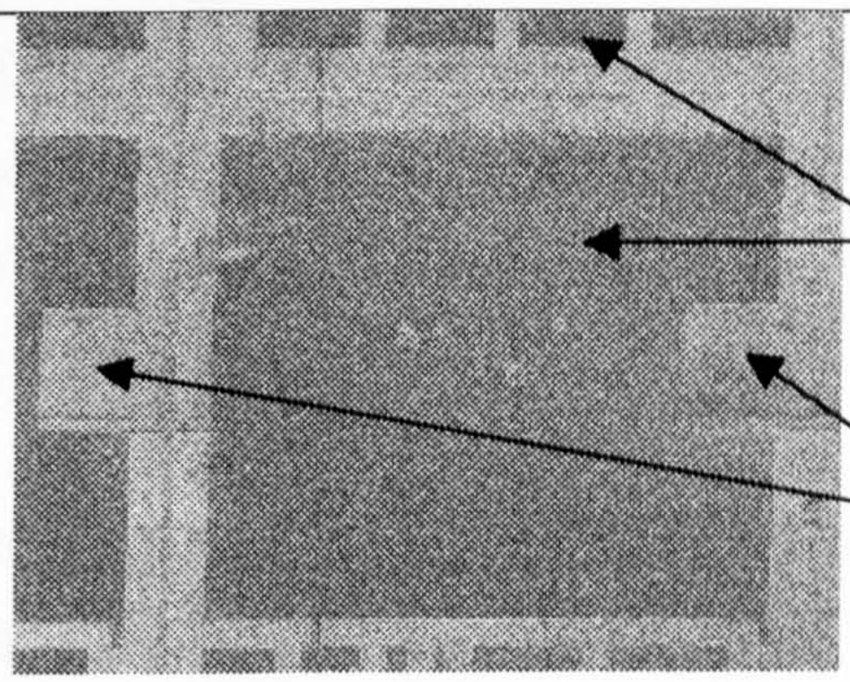	dark p^+doped regions bright n substrate
(b) EB = 171 pA	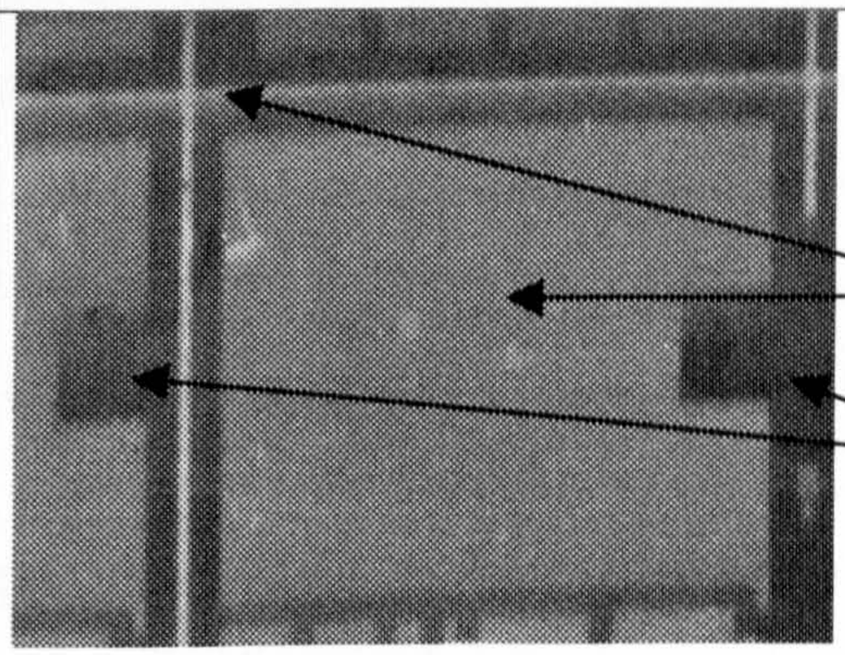	bright p^+doped regions dark n substrate

Figure (6.7) Beam current effect on the SE contrast. (a) shows the appearance of an inverted contrast whereby the n-type substrate is brighter than the p^+-type doped areas as indicated by the arrows. As the beam current is increased by a factor of 5x the contrast is inverted to the normally obtained case as shown in (b) even though the image has approximately the same magnification and at the same scan speed.

(6.3.3) Scan Speed Effect on SE Dopant Contrast

A Durham Si(111) sample has been used to study the scan speed effect on the contrast. It is found that the contrast is almost constant as shown in figure (6.8). However, ISI sample has shown that the contrast is enhanced at fast scan speeds as shown in figure (6.9).

Inspection of the ISI sample at different scan speeds has shown similar interesting behaviour to the obtained behaviour by using different magnifications and different beam currents. This is shown in figure (6.10). The images of this figure were collected with a beam current of 2090 pA, at the same magnification and the same WD, but at different scan speeds. The shown images indicate that the contrast is inverted at fast scanning rates whereby p^+ regions appear darker than n substrate. However, a normal contrast appears at slower scan speeds.

In order to test electron dose effect on ISI sample, the Vega SEM was operated at the minimal magnification (34 x) and at beam current 1165pA (2pc), it was found that at all fast scan speeds an inverted contrast is obtained, while the normal contrast is obtained only at low scanning rates starting from 455.73×10^{-3} sec/line. Moreover increasing beam current to 2090pA (1pc) allows one to obtain inverted contrast at fast scanning rates, while the normal contrast in this case can be obtained at slightly faster scanning rates compared with the previous case starting from 177.18×10^{-3} sec/line and slower. This dependence of the contrast on the scan speed value is complimentary to its dependence on magnification and beam current. This behaviour can be understood simply as following increasing the electron dose by increasing the beam current require a faster scanning rate to obtain a normal contrast at the same magnification.

The required minimal dose to obtain a normal contrast in the Vega SEM with existing thin layer of oxide can be calculated according to equation (6.1) to be about 3360 e/line(μm^2).

In the course of studying scan speed effects on SE imaging of doped Si structures, SRL Si samples have been inspected as well. This sample was inspected in the Serion FESEM instrument at low keV.

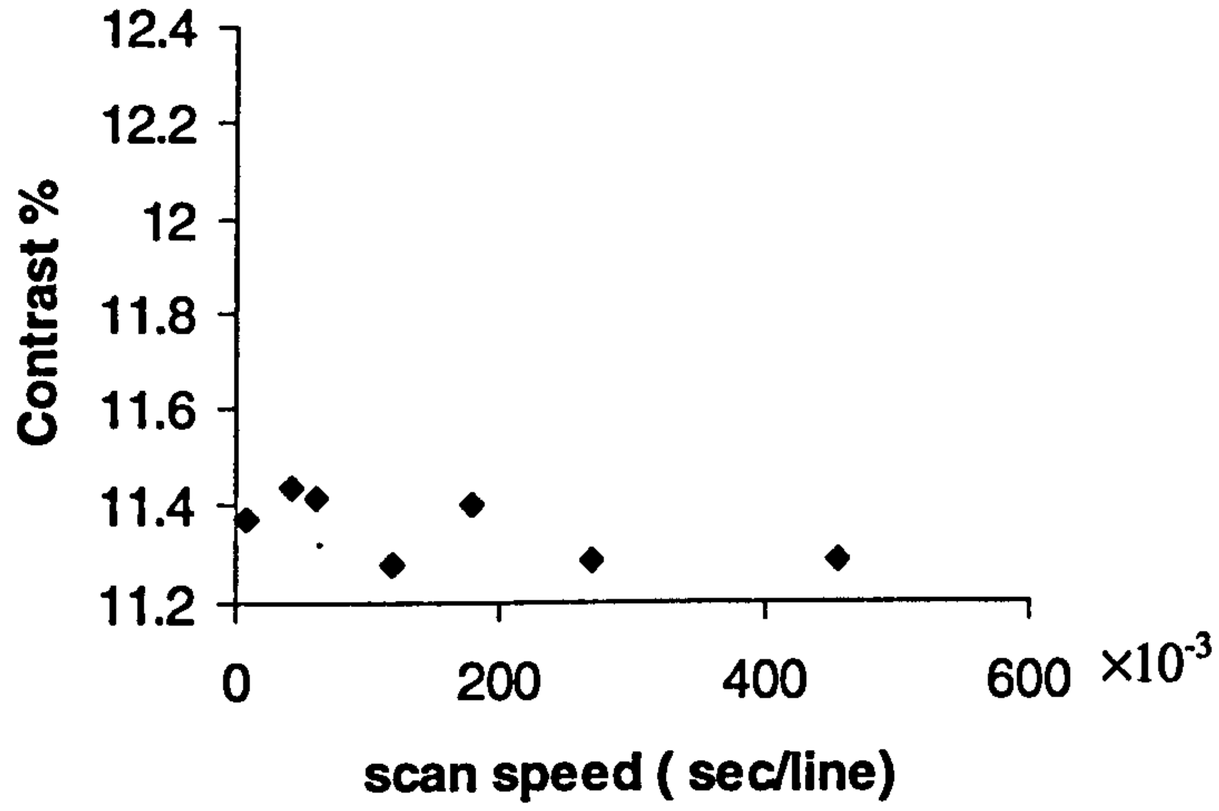

Figure (6.8) The contrast as a function of scan speed for the Durham sample showing nearly a constant value at different scan speeds.

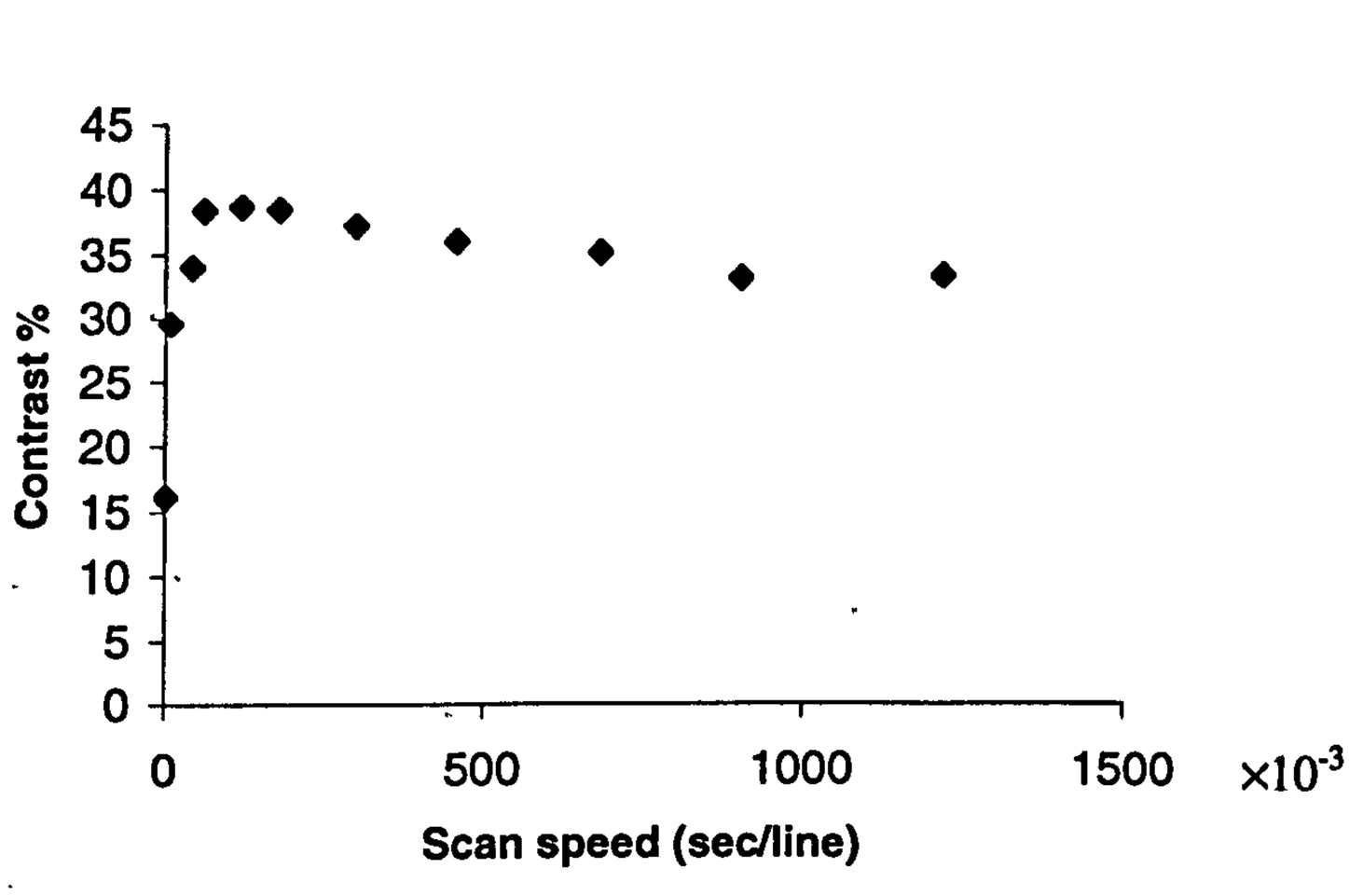

Figure (6.9) Contrast as a function of scan speed from fresh ISI sample.

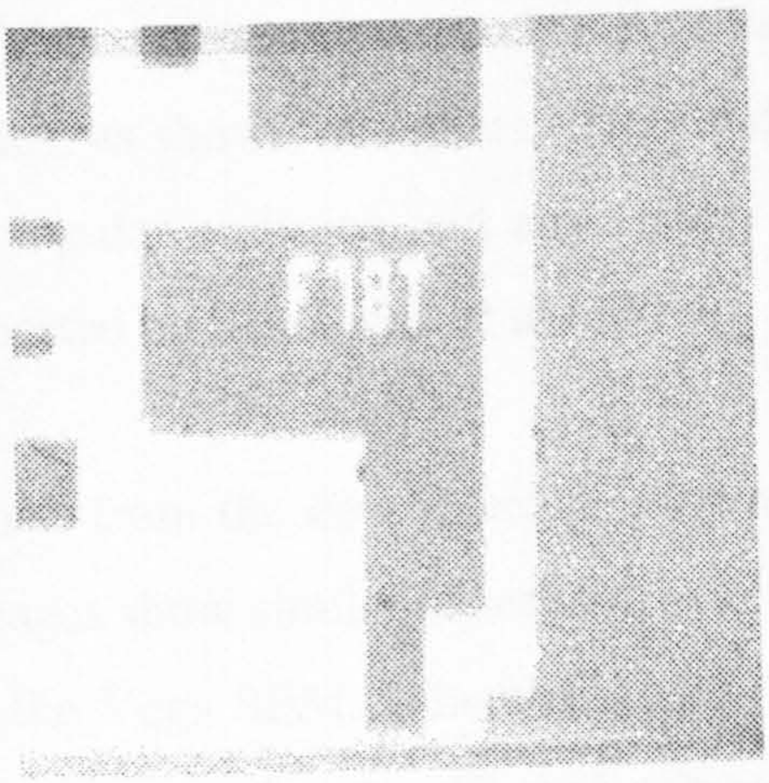

Scanning rate = 7.8×10^{-3} s/line

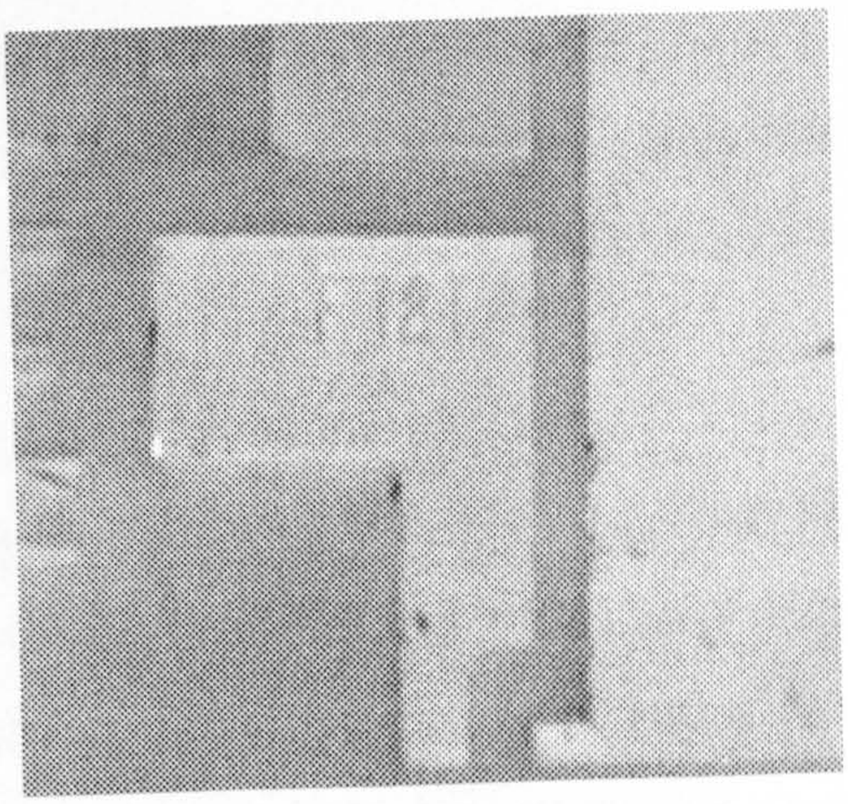

Scanning rate = 59.9×10^{-3} s/line

Scanning rate = 177.18×10^{-3} s/line

Scanning rate = 455.73×10^{-3} s/line

Figure (6.10) SE images collected at different scan speeds to show SE dopant contrast dependence on scan speed.

An interesting phenomenon was observed at low beam energy using either of the two detectors, the E-T detector and a Through-the-lens detector (TLD). For a given beam current, SE images collected by scanning the electron beam at slow scan speeds (90 secs/frame) reveal new patterns in the structures in comparison to collecting the images at TV rates (where several frames have been integrated to improve the signal to noise ratio), as shown in figures (6.11) and (6.12). Therefore, this eliminates any effects due to angular emission and any energy shift of the SE caused by extra energy filters as reported by Schonjahn et al (2003).

Apart from the new structure shown clearly at slow scan speeds in the FESEM, these images show similar observations to the previously reported results that have been made in the Vega SEM. Whereby figure (6.12) shows higher contrast of p^+ and n^+ doped Si compared with n-type doped substrate at slow scan speeds. However, this contrast is inverted at fast scan speed.

The SRL sample that has been investigated in the Serion FESEM is likely to have a natural oxide layer of only 2-3 nm in thickness. Therefore, our belief is that electron injection in the existence of an oxide layer leads to such interesting observations. Although further work is required to develop an understanding of this contrast which is essential for a quantitative understanding of dopant profiling using LVSEM, at this stage after estimation of surface layer using XPS it is possible to develop a mechanism that leads to contrast reversal as a function of electron dose injection. It is believed that the surface structure combined with electron injection dose may lead to such behaviour. The proposed mechanism will be discussed in details in section (6.6).

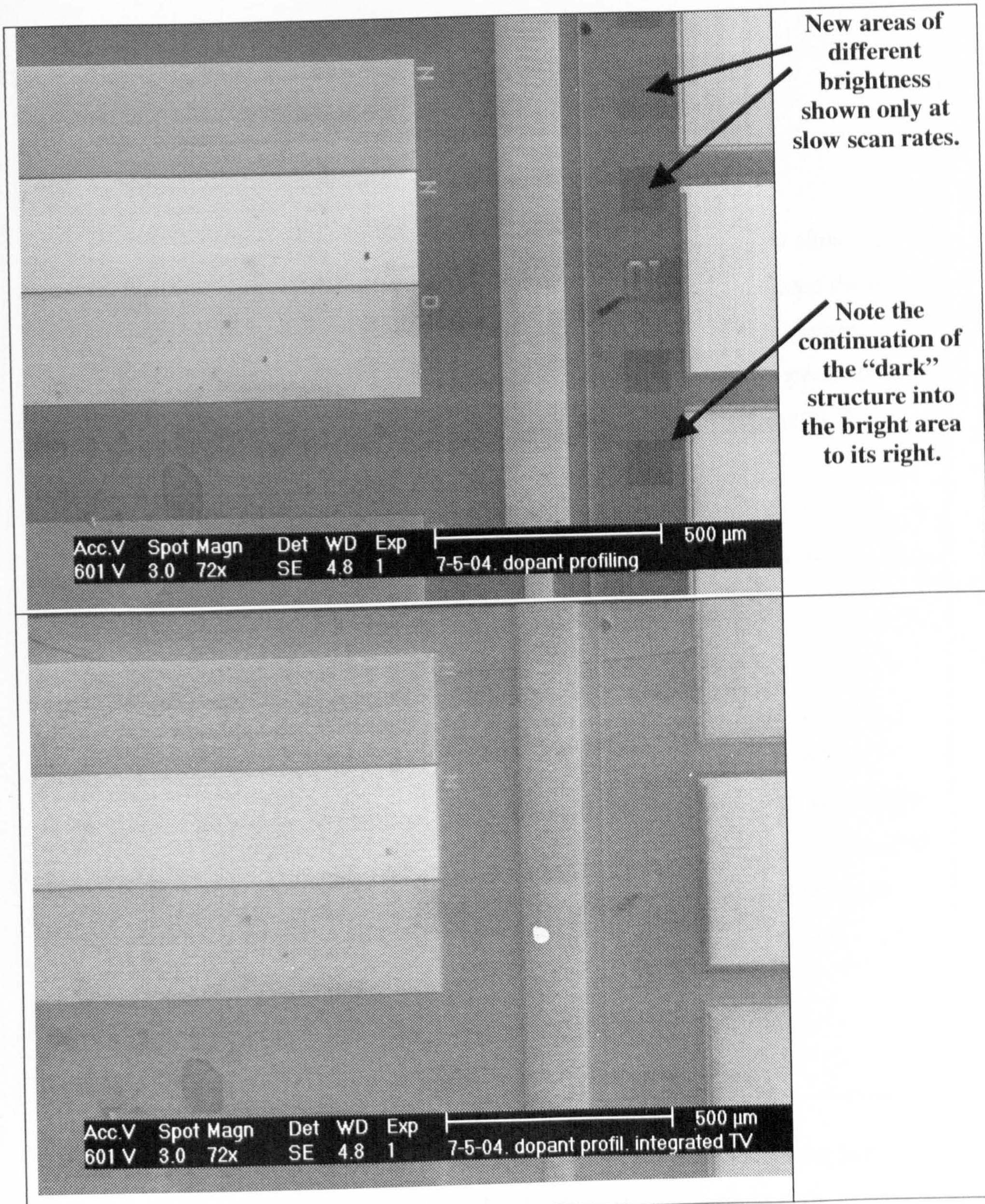

Figure (6.11) The effect of the speed of the scan on the SE contrast in the Serion FESEM. (a) Showing the appearance of well defined structures, indicated by arrows, as the beam is scanned slowly. (b) Does not show the same structures even though the image has approximately the same magnification and the same beam current.

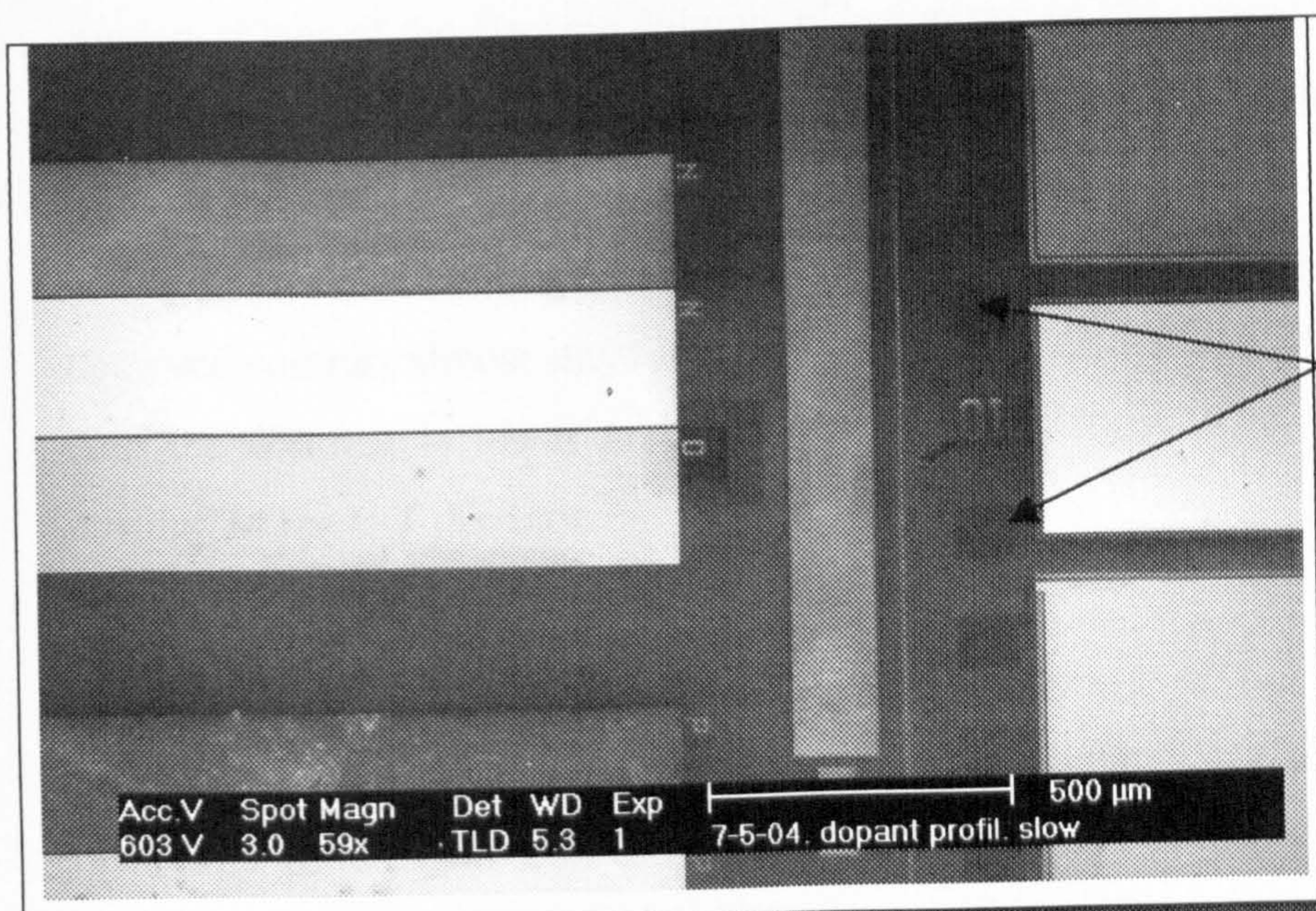

Figure (6.12) Scan speed effect on SE contrast using TLD detector, in the Serion FESEM. Some areas of the sample can be seen clearly only at slow scan speeds as shown in (a) while this pattern only can be seen in (b).

(6.4) Working Distance Effect on SE Dopant Contrast

Working distance is defined as the distance between the specimen and the final condenser lens of the electron column. p^+/n contrast of ISI sample has been examined in the Vega SEM at different values of the working distance. The measurements have been taken at the optimal operating conditions; beam energy of 1keV, slow scan speed of ~ 177.18×10^{-3} s/line and high beam current of ~2090pA. Figure (6.13) indicates that the observed contrast almost stays constant for working distances within the range 6-14mm. And the contrast is lower at smaller working distances. This might depend on the position of the E-T detector.

(6.5) Oxygen Adsorption on Si

Most frequently the semiconductor surface is prepared by chemical etching, this invariably produces a thin oxide layer of thickness 1-2 nm, the precise nature and thickness depend on the exact method of preparing the surface (Rhoderick and Williams, 1988). Oxygen adsorbed atoms or monolayers may change the amount of band bending at the semiconductor surface by changing the surface state structure. This change may cause electron flow between the adsorbent and the surface states, removing old surface states or introducing new surface states into the band gap (Zangwill, 1988). However, no quantitative data are available with regard to the oxide thickness.

In the case of Si(111), it is established that oxygen adsorption will increase the Si work function, indicating that it is negatively charged with significant charge transfer from the surface occurring. On the one hand, if a relatively thin layer of oxide is sandwiched between a metal and Si, this layer will change the potential barrier of the Si due to the creation of surface states followed by charge transfer which results in negative surface charge. Such an insulating film is often referred to as an interfacial layer. The electrical behaviour of this interfacial layer is not clear, it may be considered to be an insulator, even though it is so thin, of the order of 1nm, and charging effect is the unique way to predict the insulator behaviour. However, Chang and Nixon (1967) have reported that if this layer was completely penetrated by an electron beam, it behaves like a conductor at the moment it is bombarded by the electron beam. Moreover, Rhoderick and William (1988) have shown that the presence of an oxide layer may affect m-s contact whereby

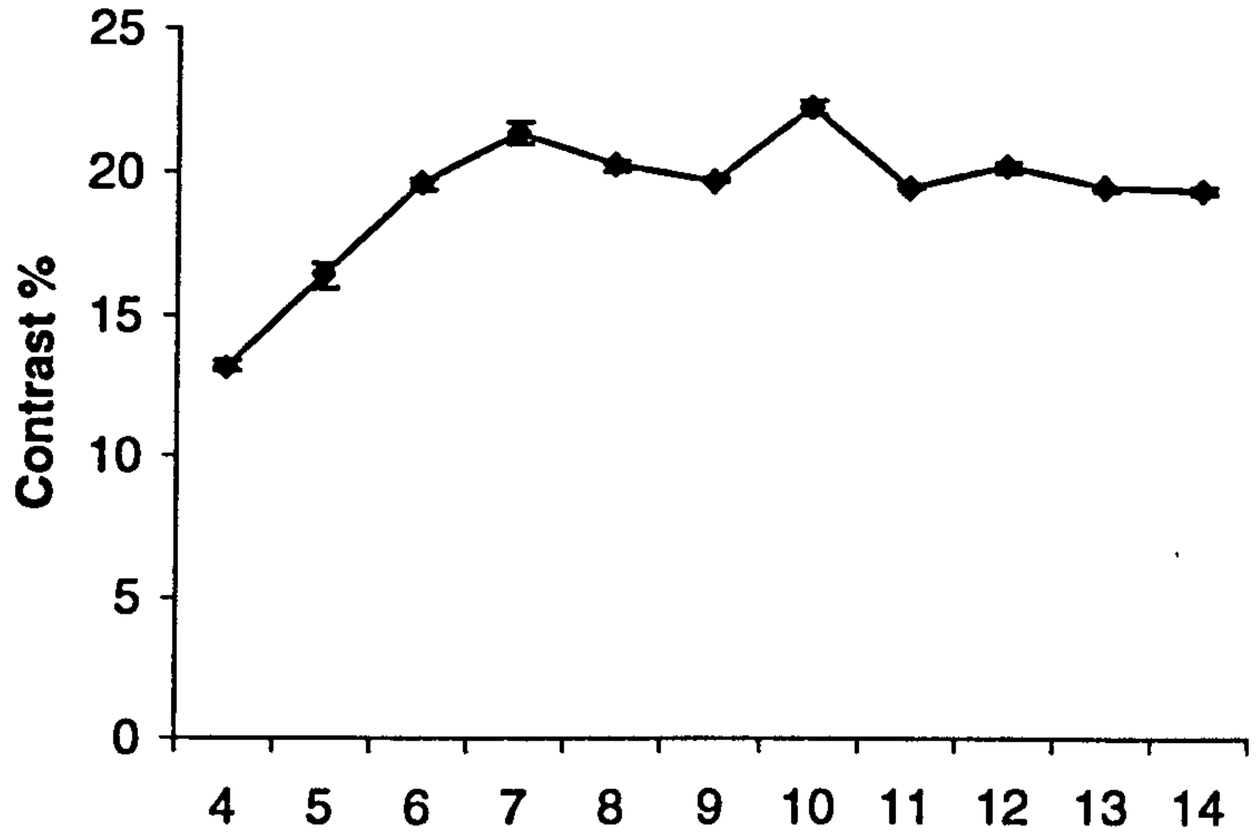

Figure (6.13) Plot of C_p^+/n versus working distance obtained with the E-T detector in the Vega SEM, showing lower contrast for smaller working distances.

contact will be insensitive to the metal work function.

Originally it was believed that oxygen adsorption on Si charges the surface negatively during the electron beam bombardment. Therefore, this negative charge is expected to produce bright-doped Si areas in the SE imaging. In this study, however, imaging doped Si samples with thin layer of oxide has shown an interesting behaviour as a function of beam energy (chapter 5) and electron dose.
So what can be expected to happen in case if 2-3 monolayers of oxide layer sandwiched between differently doped Si regions and quasi metallic layer of C?

(6.6) Discussions

The results shown in this chapter show that SE dopant contrast depends critically on the surface condition of the sample under investigation and it is shown that the oxidation of the surface results in a significant change in the SE dopant contrast.
The oxide layer of several monolayers will create surface states within the forbidden gap. In addition to the extrinsic surface states due to dopant atoms; donor surface states are filled with positive charge when ionized and acceptor states are filled with negative ions. Therefore, electrons from the conduction band may flow to the available states and will put an additional negative charge at the n-type surface. This accumulation of negative charge into the surface will retard any SE emission at zero point (when no electron beam impinged into the surface) due to the negatively charged surface. As a result to charge transfer, the Fermi level must move down to compensate charge transfer and the created surface states will bend the bands up in n-type.

On the other hand, electrons may flow from the valence band to fill in the empty surface states in the p-type Si, resulting in negative surface charge and the Fermi level moves up to compensate charge transfer. Hence there is no emission at the zero point from p^+doped Si.

Apart from surface states within energy band gap caused by donor or acceptor ions and oxide adsorption onto Si, electron beam irradiation can create surface defects at the SiO_2- Si interface even at low beam energy, e.g. 1kV. These surface defects called fast surface states increase the recombination velocity (KroniK and Shapira, 1999).

At low electron dose the incident electrons will generate low number of electron-hole pairs, which recombine with the created surface states. Since Si is indirect semiconductor, charge carrier recombination occurs within localised energy states in the forbidden energy gap; at very low electron-dose the generated pairs will recombine part of the induced surface charge. This is due to the recombination of the generated minority carriers in the surface with the surface induced charge. Because there is an abundance of electrons in n-type Si, as soon as a generated hole is captured by a recombination centre, an electron will immediately be captured by the same centre to complete the recombination process. This may results in a reduction of the surface negative charge on n doped Si. Therefore, in n doped Si SE emission starts after a threshold point of the electron dose. The threshold point of the electron dose depends on charge density of the surface states. On the other hand, extra negative charge accumulated on the p^+ doped Si which retards SE emission. As a result, no SE emission can be detected from p^+ doped region at very low electron dose.

With increasing electron-dose value above the threshold dose by increasing either the magnification, scan time or the beam current, the generated e-h pairs recombine with the rest of the created negative surface charge on n-type Si. Therefore, n doped areas exhibit higher SE contrast compared with p^+ doped regions. This is seen as reversal of contrast. There are two factors that may contribute into this situation;

1- Number of electrons in n-type valence band is higher than its equivalent number of electrons in p^+ doped regions.

2- If the surface states recombined, the filled donor states will accelerate SE emission generated due to direct inelastic scattering between incident electron beam with valence band electrons in n-type Si. On the contrary, the acceptor surface states in p^+ doped region will retard SE emission from valence band.

At high electron dose, the created electron-hole pairs will be captured by the empty surface levels; in n-type Si the conduction band is filled by electrons (original + created) so some of them will fill the upper surface states while the lower surface states will be filled with holes. Therefore the created electric field will retard SE emission from valence band of n-type Si. On the contrary to the created electric field in p^+ doped Si which accelerate SE emission to the vacuum. As a result, p^+ doped areas reflect higher SE yield to the vacuum compared with n-substrate.

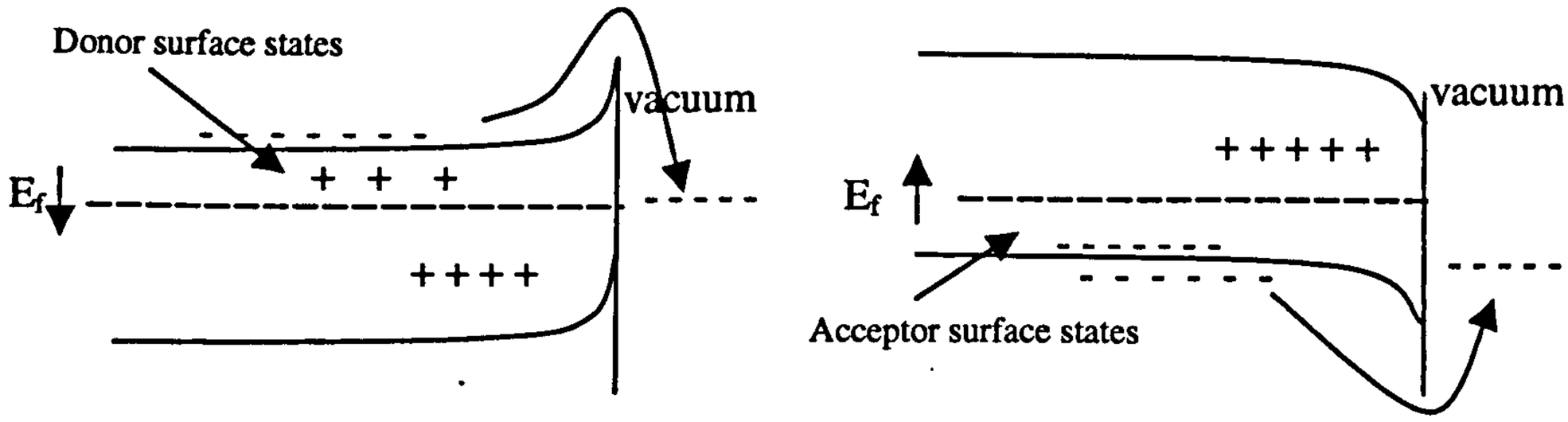

n-type Si

p^+ doped Si

Figure (6.14) Surface charge movement and surface states distribution within band gap followed by Fermi level movement to compensate charge transfer.

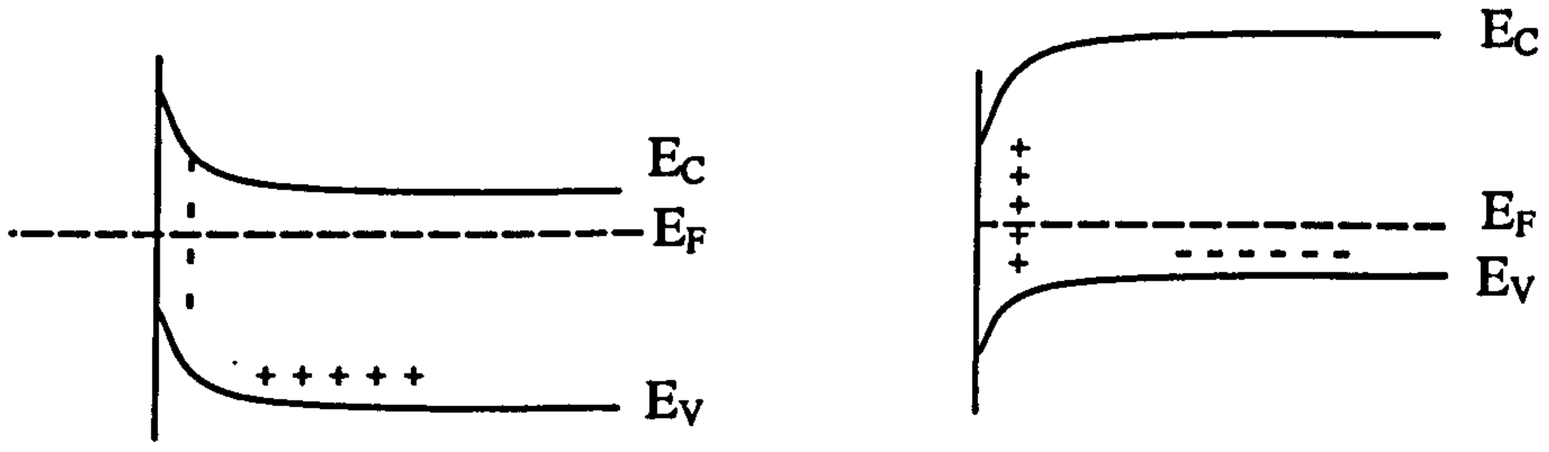

n-type Si

p^+ doped Si

Figure (6.15) At high injection level, the majority excess carriers in n-type Si retards the generated SEs, while the majority excess carriers in p^+ doped Si accelerate the generated SEs to the vacuum.

(6.7) Conclusions

In order to understand electron dose effect on SE dopant contrast in the SEM, the SE contrast from a Si p^+/n and n^+/n structures as a function of magnification, beam current and scan time have been studied. The results show that SE contrast is sensitive function to the surface structure.

In a well-cleaned Si surface, the contrast has shown strong dependence on beam current whereby SE contrast increases at high beam current. In contrast to its dependence on magnification, the highest contrast is observed at low magnification. On the other hand, SE contrast is almost independent of the variation of scan speed.

If the surface is left with few monolayers of oxide adsorbed onto the Si surface, then the presence of surface states within the forbidden gap due to oxide adsorption onto the Si surface must play a role in SE emission. Irradiating the surface with low energy electron beam of different electron dose values will excite the semiconductor, and the pronounced contrast has shown an interesting behaviour as a function of electron dose injection. It is found that the results can be divided into two regimes;

At low electron dose ($\leq$ 3360 e/line. μm^2), an inverted contrast is obtained whereby p^+/n and n^+/n doped Si exhibit an inverted contrast (p^+ and n^+ doped regions appear darker than n doped Si). At low electron dose, low number of electron-hole pairs is generated. The generated minority carriers will recombine the induced surface charge within the energy band gap, after partial recombination, the SE emission starts with n appear brighter than p^+ in the SE image. The emitted SE, in this case, is produced due to the direct inelastic scattering with valence band electrons.

High electron dose can be obtained by going to higher magnification, slow scan speeds or higher beam current. At such high electron dose, the generated e-h pairs per unit area are increased at the same interaction volume. Therefore, part of the created carriers will recombine with each other within the surface states, rest of the carriers may create opposite electric field in p^+ and n doped Si, whereby the created electric field in p^+ accelerate the generated SE to the surface and retard SE emission in n-type Si.

In contrast to electron dose effect on SE contrast, studying contrast as a function of working distance has shown that the contrast is almost constant for wide range of working distances, which is indicative of the weak dependence on angular emission.

Chapter 7: Effect of Barrier Height Variations on SE Dopant Contrast

(7.1) Introduction

The physical mechanism responsible for the SE dopant contrast is not fully understood. However, several hypotheses (models) have been suggested. Formation of m-s contact of barrier height based on the difference between the metal work function and electron affinity of the semiconductor is one of the mechanisms which is suggested to be responsible for this contrast. In order to investigate the validity of the m-s contact model on SE contrast, new experiments were carried out to clarify the effect of barrier height variations on the obtained contrast.

It is known, that the situation where the atoms, which behave as donors or acceptors, diffuse into the semiconductor, or that electrically active defects are created, results in change of the effective density of dopants in the semiconductor. If the dopant density increases, (the semiconductor becomes degenerate) the barrier gets thinner. On the other hand, if the surface layer is doped with impurities of the opposite type to those in the substrate, the effective dopant density decreases and is expected to cause an increase in the barrier height for carriers moving between the semiconductor and the metal. This situation arises in Al/Si (111) diodes following annealing treatments. However in case of Al/Si(100) hydrogen plasma has been used widely to increase the Schottky barrier height between the Al metal and the hydrogenated amorphous layer.

The aim of this chapter is to further investigate potential barrier height variations on SE dopant contrast in Si, by heat treatment of Al/Si diodes. This experiment has been repeated on a wide range of doped Si structures. Although it has already been found that potential barrier variation altered the contrast by depositing candidate materials of work functions lower and higher than that of Si, it is important to carry on such investigations to provide comprehensive or proper understanding of this behaviour. Finally, new experiments have been carried out by estimating the barrier height variations using KPM.

(7.2) Review of Barrier Height Variations

Many practical applications require control of the barrier height of a rectifying contact. Arizumi et al (1969) suggested a simple method by using alloys of noble metals to make contacts onto Si. By this method they were able to obtain a linear variation of barrier

height with composition, but the practical application of this principle requires extremely careful control of the composition of the alloy.

Another method to control the barrier height of Si is by exposure of the semiconductor surface to oxygen before evaporation of the metal. It is suggested that the modification of the barrier height is due to the creation of interface states. Montgomery et al (1981) have reported that exposure of indium phosphide to hydrogen sulphide causes lowering of the barrier height and producing ohmic contacts. They suggested that the change in barrier height is caused due to doping the surface layer in the manner proposed by Shannon (1974).

The most practicable method that has been reported to control barrier height seems to be that of Shannon (1974, 1976), who has used the principle of incorporating highly doped surface layers to show that the effective barrier height of a Schottky barrier can be controlled over quite a wide range. It is found that incorporating oppositely doped surface layer to the substrate increased the height of the Schottky barrier formed between Ni and p- type Si diodes by implanting 5 keV antimony ions with high doses. However, implanting n-type Si with 5 keV antimony ions resulted in a reduction of the barrier height between Ni and n-type Si at high dose. Figure (7.1) shows the effective barrier height between Ni and p-n Si substrates as a function of surface concentration of 5 keV antimony ions.

Many structures in integrated circuits require both Schottky barrier diodes and Ohmic contacts to be made using a single metal evaporation (Basterfield et al, 1975). Al-Si contacts are one of the most favourable contacts to be used for good Ohmic and Schottky contacts with Si. Thus many attempts have been carried out to control the barrier height of Al/Si contacts such as annealing. Chino (1973) has shown that there is a change in the barrier height of Al-nSi(111) Schottky barrier diodes after heat treatment, whereby the potential barrier increases clearly as the heating temperature rises above 450°C. On the other hand, Card (1975) has observed that the behaviour of the Al-pSi contact is complementary to that of the Al-n Si contact with barrier height decreasing due to annealing over the same temperature range, as shown in figure (7.2).

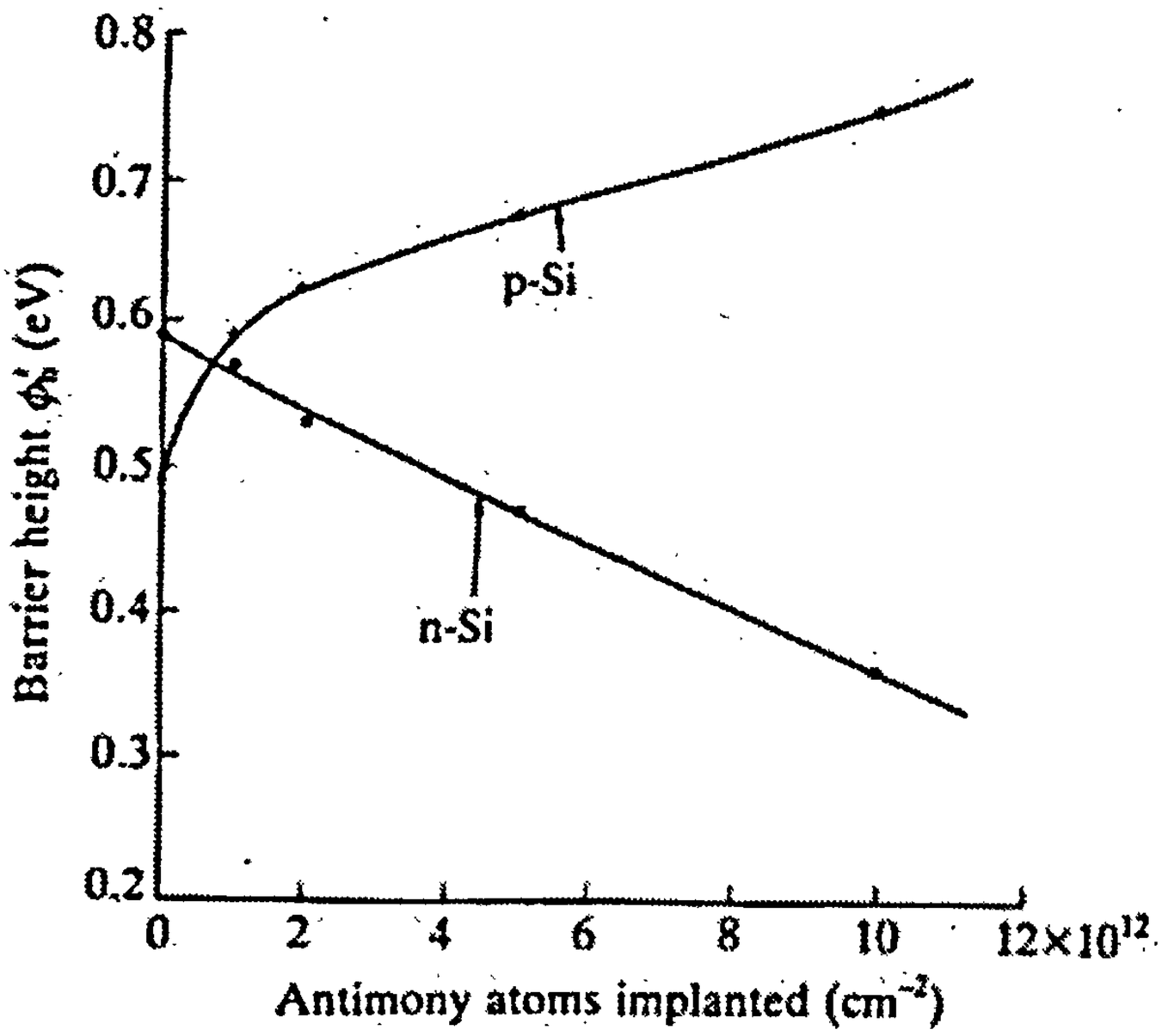

Figure (7.1) Effective barrier height for holes in p-type substrates and electrons in n-type substrates as a function of the number of antimony atoms (ions) implanted at 5keV, Shannon (1974).

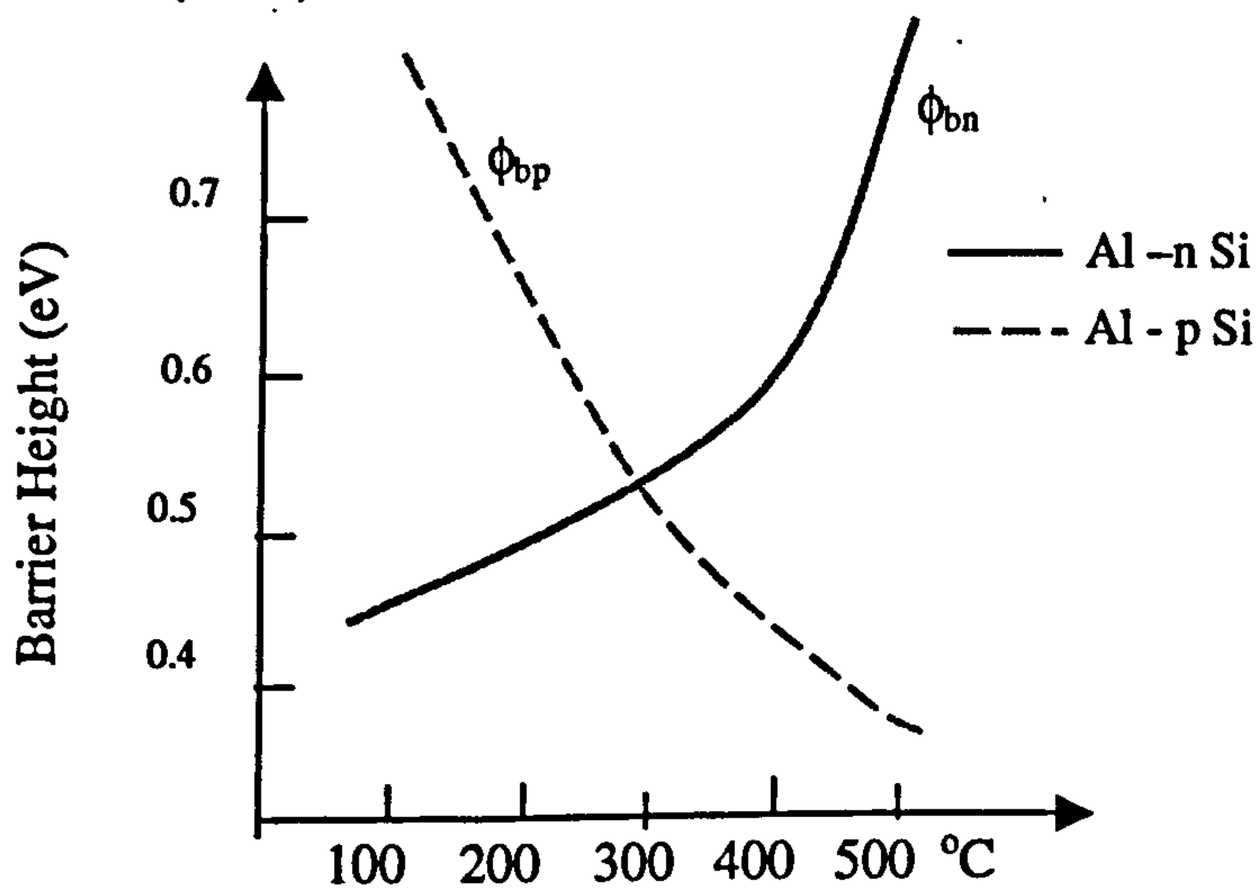

Figure (7.2) Barrier height of Al contacts to n-type Si and p-type Si, as a function of annealing temperature, Card (1975).

The variation of barrier height between Al and Si can be explained due to solid solubility of Al into Si; at temperatures around 500°C, Si is taken up into solid solution by the Al to an amount determined by the solubility limit at the particular temperature. On cooling, an interfacial layer of Si that contains Al atoms is formed between the Si and Al. This layer of Si is doped p-type, because Al is an acceptor. So, the net space charge density is negative near the Al/Si-Al interface, and the bands become bent downwards as shown in figure (7.3). While in the case of p-type Si, the Al doped layer causes the depletion region to become narrower, so that the effective barrier height is reduced. Further no change in barrier height in case of Al/ p^+ doped Si contact was reported. The modification of the barrier height between Al and Si agrees with Shannon's principle.

Apart from low energy ion implantation and heat treatment, exposure to hydrogen plasma etching increases the Schottky barrier heights of Al/n-Si contact. The Schottky barrier height increases constantly with an increase in an applied rf power or hydrogen concentration in the plasma (Iwakuro et al, 1991). It is found that exposure of the Si surface to hydrogen plasma produced a hydrogenated amorphous layer in the Si substrate. Therefore, the increase in the Schottky barrier height is attributed to the formation of the Schottky barrier at the interface between the Al metal and the hydrogenated amorphous layer (hydrogen- absorbing zone in Si),(Iwakuro et al, 1993).

.

Silicides play an important role in IC technology due to the most reliable and reproducible Schottky barriers (Taubenblatt et al, 1982). It is shown that a reaction between Ti and the Si oxide leads to the formation of small quantities of Ti silicide. Later De Bosscher et al (1986) investigated the influence of silicide formation on the barrier height of Ti/Si Schottky barriers. It is found that contribution of the silicide formation of the barrier height is strongly dependent on the pre-evaporation treatment such as HF dips and annealing. It also depends on the substrate temperature T_S during evaporation of the metal (Iwami and Hiraki, 1982). De Bosscher et al (1986) found that increasing T_S up to 450°C during Ti evaporation has led to a reduction of the barrier height between Ti and p-Si. However, a slight increase of the barrier height between Ti and n-Si has been reported in this range of temperatures.

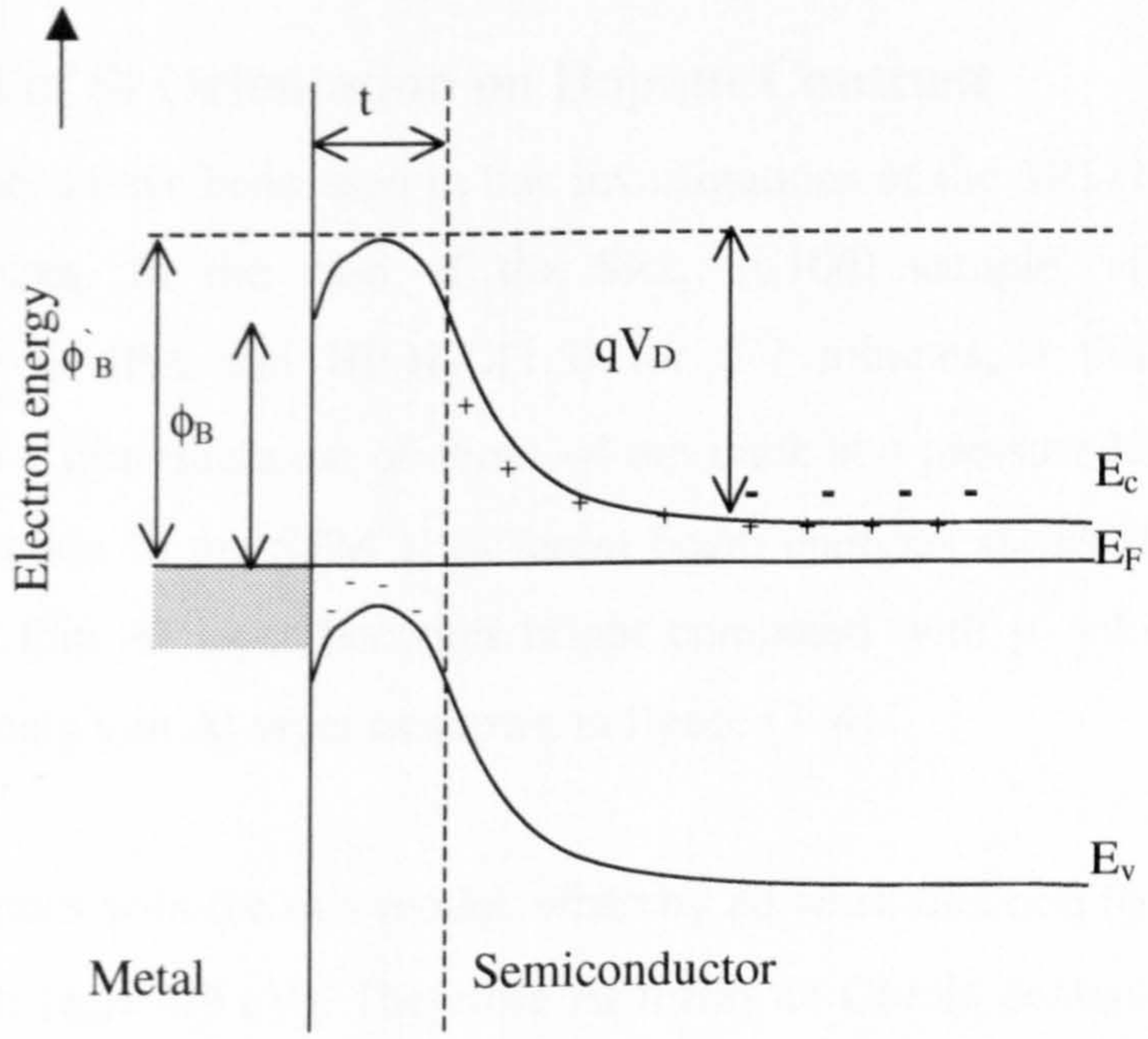

Figure (7.3) Band diagram of Al –Si contact after heat treatment, ϕ_B is the barrier height at the surface without any Si precipitation, t is the thickness of the recrystallised layer required to give a band bending V_D from the potential maxima ϕ'_B (Basterfield et al, 1975).

The sensitivity of barrier height to Si surface orientation has not been reported in an explicit way (Card 1975, Iwakuro et al 1991, Horvath et al 2002). However, Al deposition on different Si orientation exhibits different contacts. Therefore, SE contrast of different contacts by using different Si orientation should be different according to m-s model. This effect is presented in the next section.

(7.3) Effect of Si Orientation on Dopant Contrast

Many specimens have been used in this investigations of the SRL(100) and ISI(111) Si doped structures. In the case of the SRL Si(100) sample, after initial cleaning ultrasonically in IPA and HF:H_2O(1:5) for 5-7 minutes, a thin layer of Al was evaporated to a film thickness of about ~4 nm thick at a pressure less than 4×10^{-6}mbar. Sample inspection in the SEM at different beam energies shows that n-type substrate covered with thin Al layer becomes bright compared with p^+ which becomes darker after depositing a thin Al layer as shown in figure (7. 4).

This result agrees with the m-s model, whereby Al work function (ϕ_{Al}= 4.3 eV) is lower than that of Si (ϕ_{Si}= 4.9 eV). Therefore Al forms an Ohmic contact with n-type Si and Schottky contact with p^+ doped region (Horvath et al, 2002). As a result, Al on n-type doped Si appears to show higher contrast compared with Al on p^+. Or it can be understood simply as following both of them Schottky contacts with different potential barrier, the potential barrier on p^+ doped region is higher than that on n-type Si. Thus Al/n-type exhibits higher contrast compared with Al/p^+. Similarly, p^+ doped region should be brighter than n-type, where there is Carbon natural layer. This can be seen in figure (7.4). This result agrees with Cr case ($\phi_{Cr} < \phi_{Si}$) where deposition of a metal of work function lower than that of Si caused contrast inversion (Jayakody, 2003).

On the other hand, depositing a thin layer of the same thickness of Al ~ 4nm thick on top of ISI Si(111) sample has shown non expected contrast as shown in figure (7.5), whereby Al on p^+ appears brighter than Al on n doped Si. .

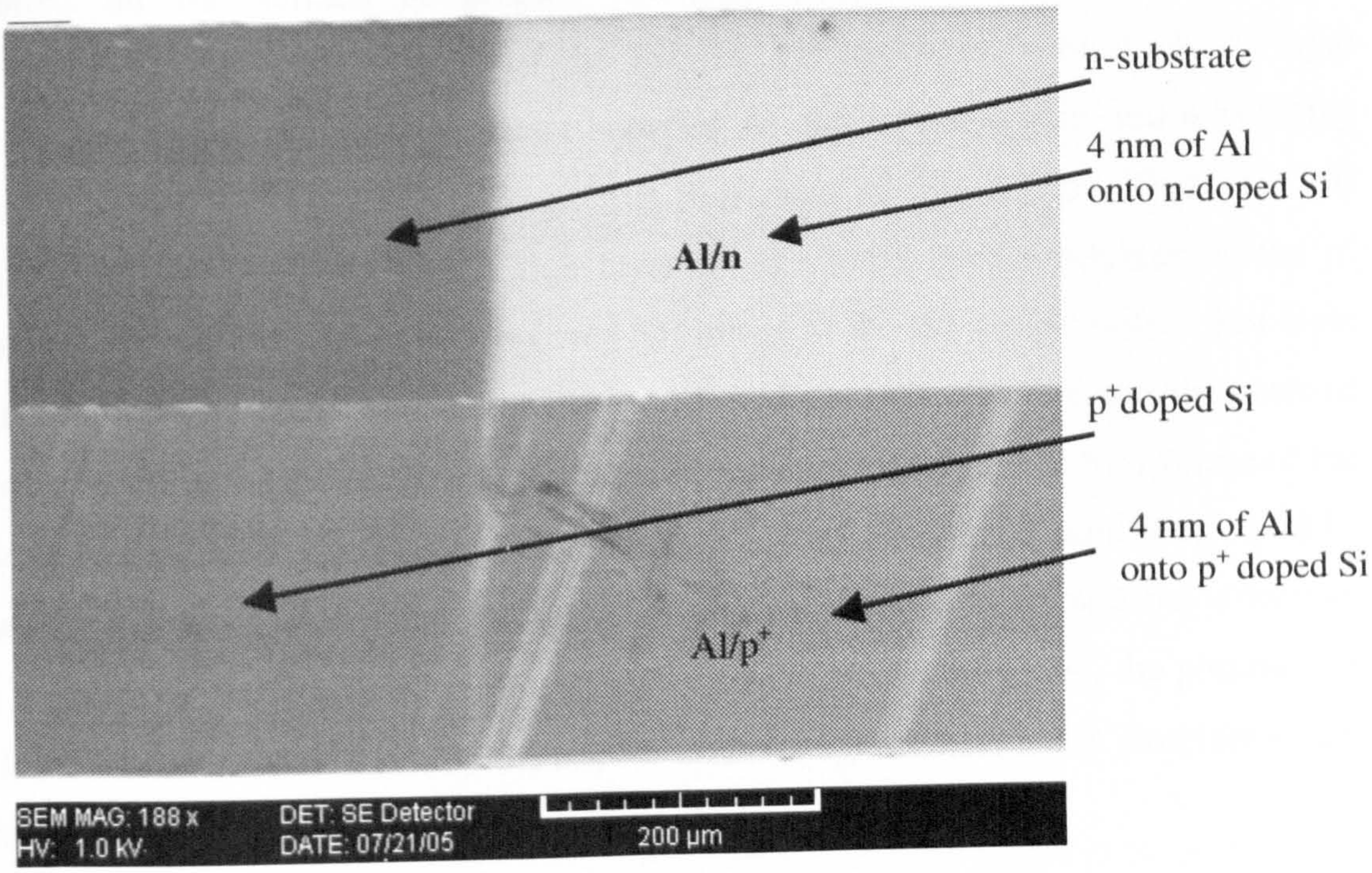

Figure (7.4) SE image of SRL sample, part of p^+ and n doped Si covered with thin layer of Al ~4nm thickness.

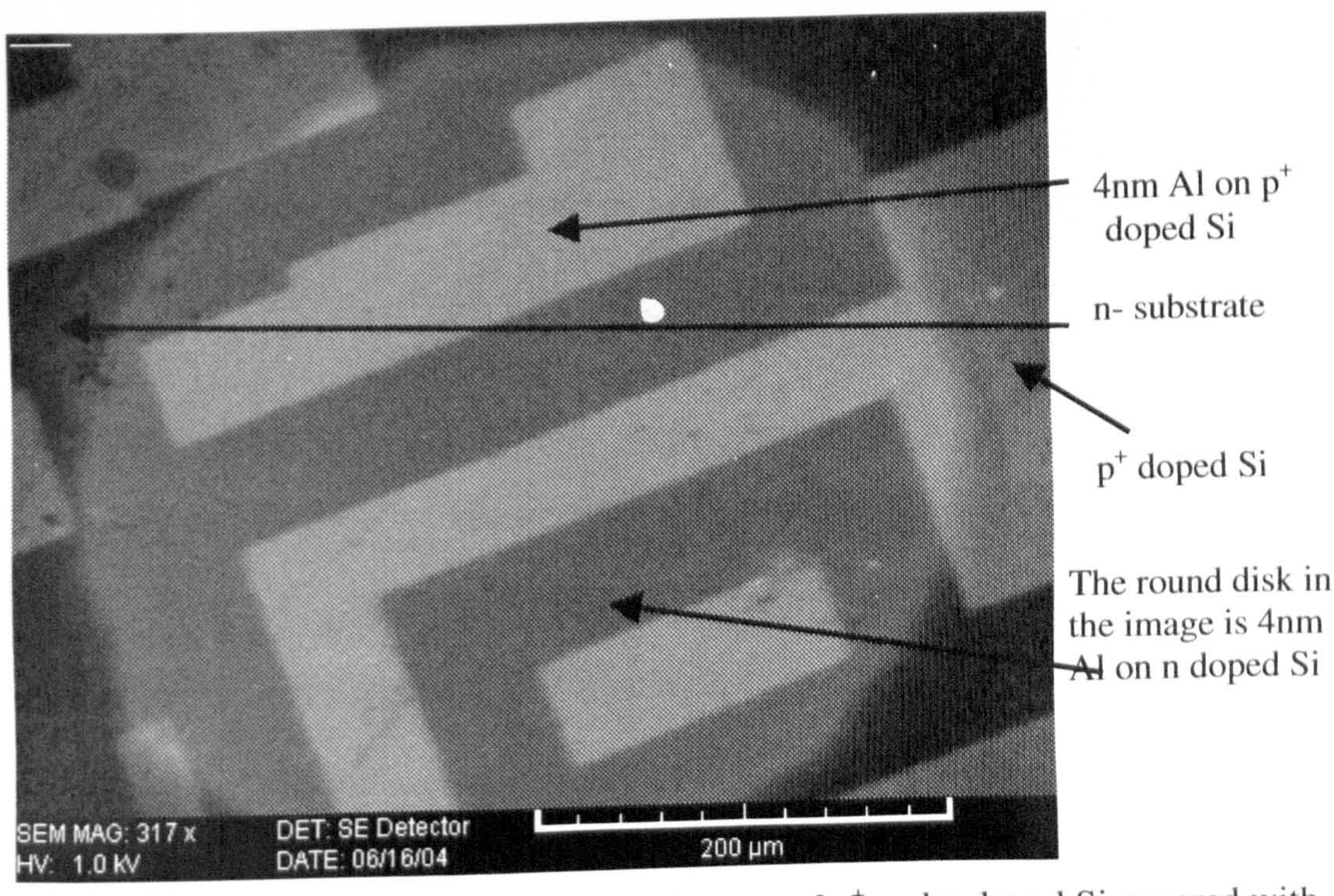

Figure (7.5) SE image of ISI Si(111) sample, part of p^+ and n doped Si covered with thin layer of Al ~4nm thickness.

In order to test contact type between Al and ISI Si(111) a thick Al layer of ~100nm was deposited on the surface to prepare this structure to current / voltage (I/V) measurements. I/V measurements of the ISI Si(111) specimen with thick Al layer indicate that there is an Ohmic contact between Al and n-type region and a Schottky contact between Al and p^+ doped region as illustrated in figure (7.6). Therefore, SE images of doped Si coated with a thin layer of Al should appear brighter on the p^+ region than on the n-type region. However, SE image of the ISI sample with a thin layer of Al = 4nm thick, shows that the contrast of the Al covered structure and the contrast of the structure without any coverage are similar as shown in figure (7.5). In spite of the difference of the work function between Al and C. This unexpected behaviour could be related to a residual oxide layer in between the deposited Al layer and the substrate. This layer might be very thin to influence I/V measurements. However, the presence of this layer and its influence on the SE dopant contrast agrees with MOS structure effect on the SE contrast as reported in chapter 5.

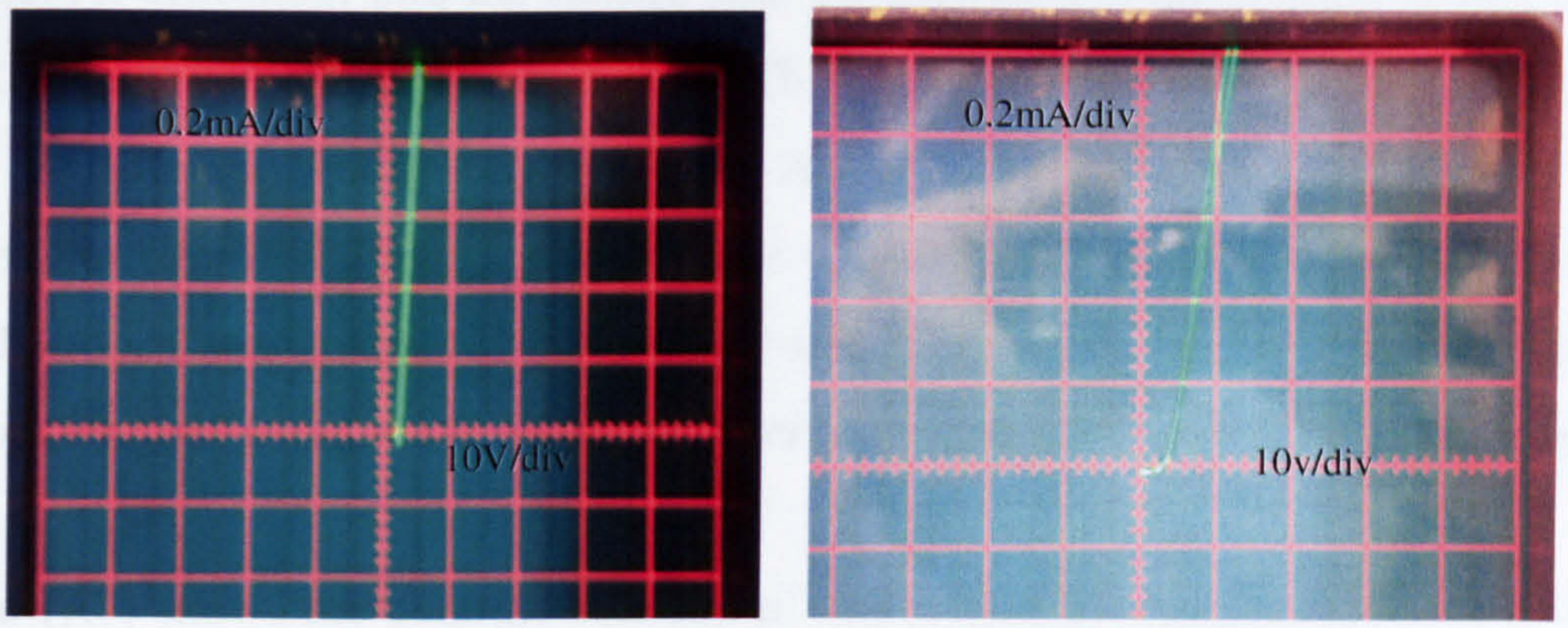

(a) (b)

Figure (7.6a) I/V measurements in the forward bias; a-Al on p^+, b-Al on n.

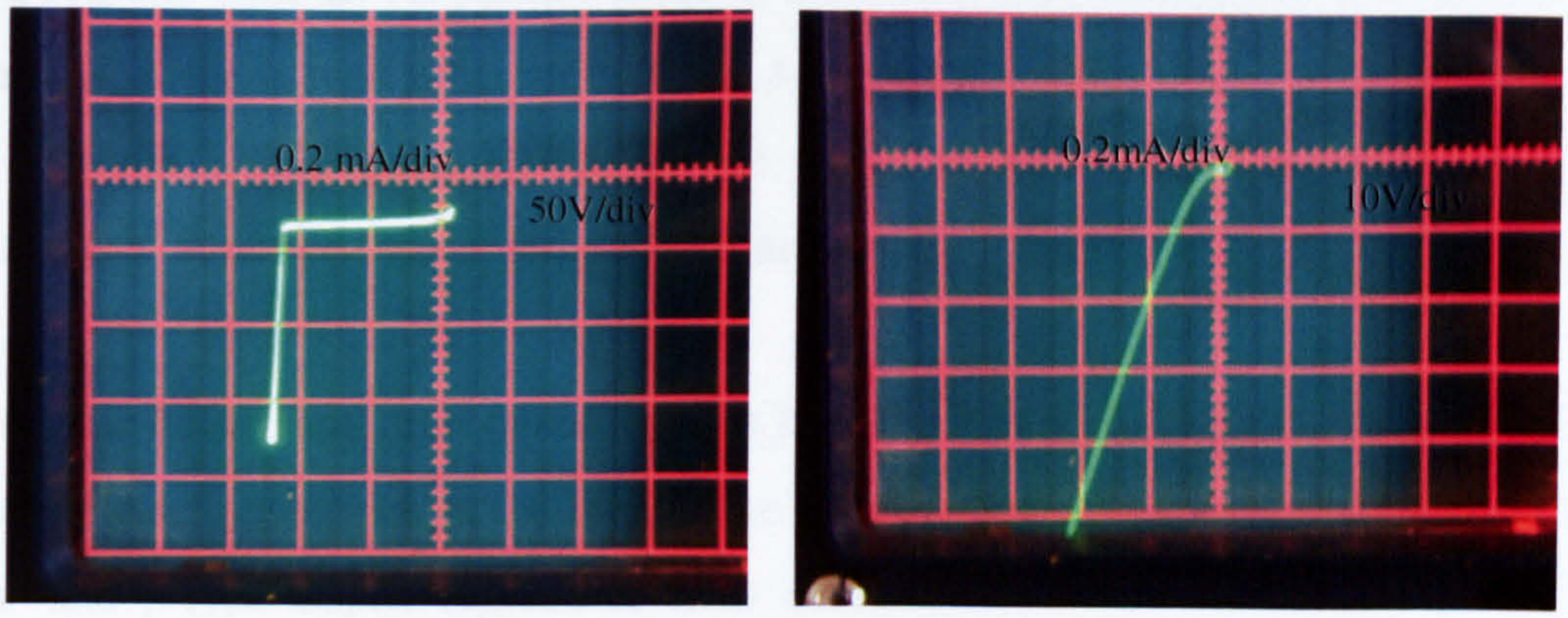

(c) (d)

Figure (7.6b) I/V measurements in the reverse bias;

c- Schottky contact between Al and p^+. d- An Ohmic contact between Al and n

(7.4) Annealing Effect on SE Dopant Contrast

In order to study annealing effect on SE dopant contrast, the ISI sample was first ultrasonically cleaned in IPA and then dipped in HF to remove any native oxide on the surface. Al deposition into the surface was done through a metal mask to give several circular contacts (~0.42 mm diameter). The sample was then inspected in the Vega SEM at different accelerating voltages. An E-T detector was used for SE image collection. After initial imaging the sample was then annealed in a 10% Hydrogen and 90% Nitrogen atmosphere to 500°C for 10 min. The sample was allowed to cool down to room temperature in the forming gas prior to loading into the SEM for SE imaging.

Figure (7.7) shows the contrast between p^+ and n-type Si regions that have a thin Al film of the order of 7 nm deposited on it. These images were collected with a beam of 1 keV incident electrons. These images clearly show the contrast between the n- and p^+-doped regions with an Al surface layer is increased after annealing. It is clear that the brightness of the n-type substrate with an Al surface layer is much higher than its value after annealing. This indicates that the SE yield from the n-type region is reduced as a result of the increased barrier height after heating the sample.

The sample before and after annealing has been imaged in the Vega SEM with different primary electron energies in the range 1 keV to 10 keV. The contrast obtained between the n- and p-type doped regions at each incident electron beam energy is used as a measure of the SE yield from these two regions. The contrast values are calculated from the digitally analysed images according to the expression (2.5). Figure (7.8) shows annealing effect on SE intensity of Al covered Si structure, obviously annealing caused a significant reduction of the SE intensity of Al covered n/Si structure compared with a slight increase of the SE intensity of Al covered p^+/Si structure. As a result, the intensity difference after annealing is larger than before annealing. This increase of the SE intensity difference after annealing causes enhancement of the contrast as shown in figure (7.9). In addition, it shows a shift of the contrast peak to lower beam energy after annealing. The shift of the contrast peak may imply a reduction of the Al layer thickness due to the heat treatment.

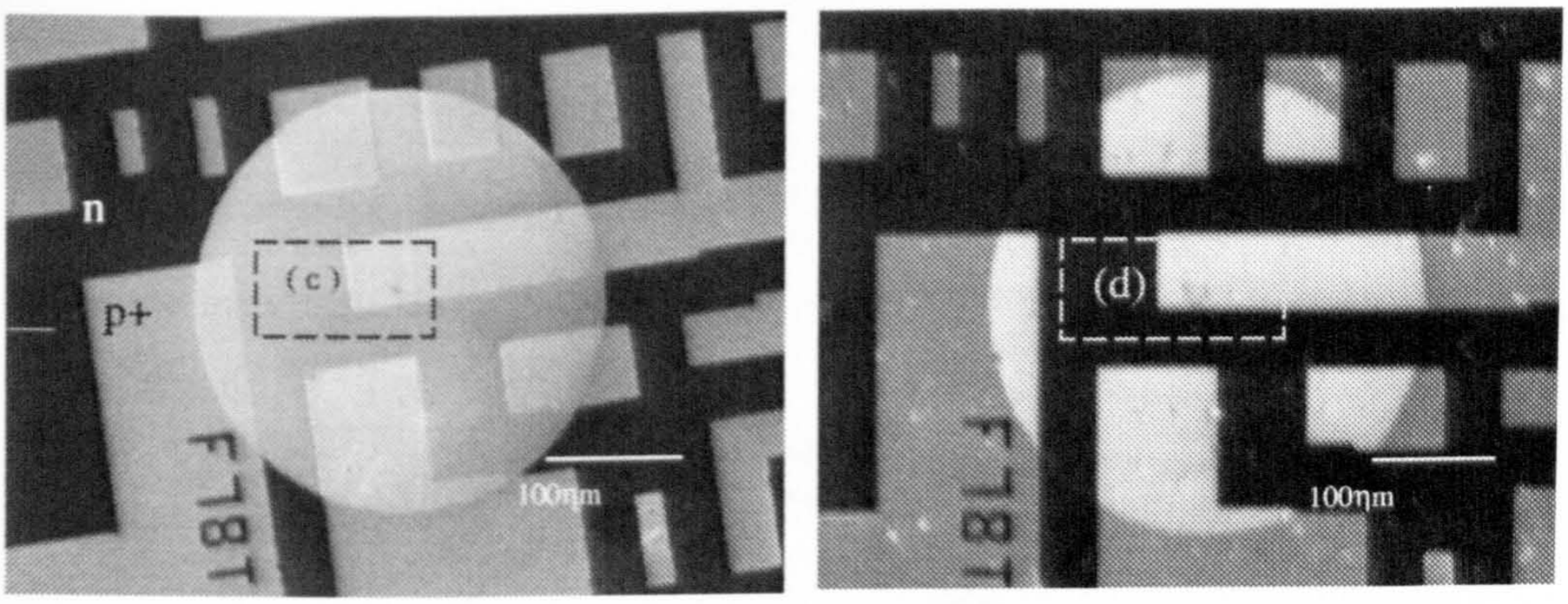

Figure (7.7) (a) Room temperature. (b)After annealing to 500°C for 10 minutes.

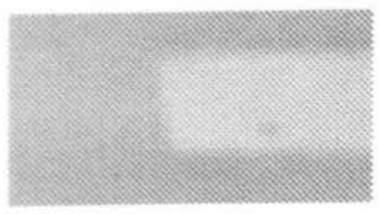

Before annealing

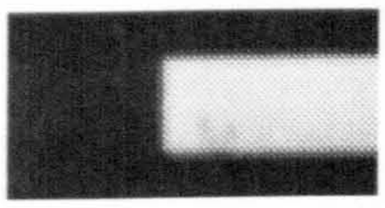

After annealing

The above images are the marked areas (c) and (d) of Al covered Si structures that have been extracted from images (7.7a) and (7.7b) respectively.

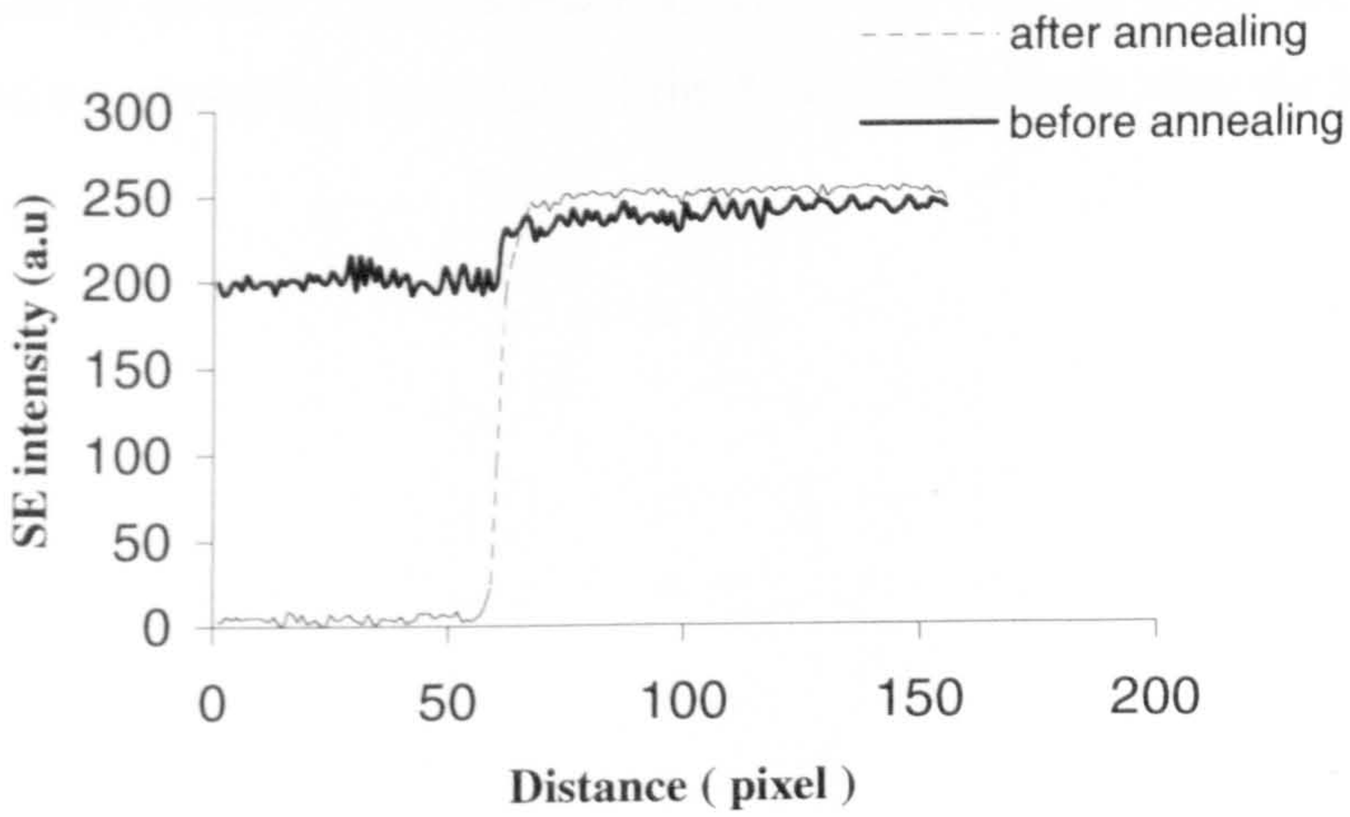

Figure (7.8) SE intensity profile extracted from the SE images of the marked areas c and d shown above. SE intensity collected from Al on n substrate at points below 60 pixel shows less emission from Al on n doped Si after annealing compared with SE intensity of the same area before annealing. The intensity difference after annealing is larger than before annealing

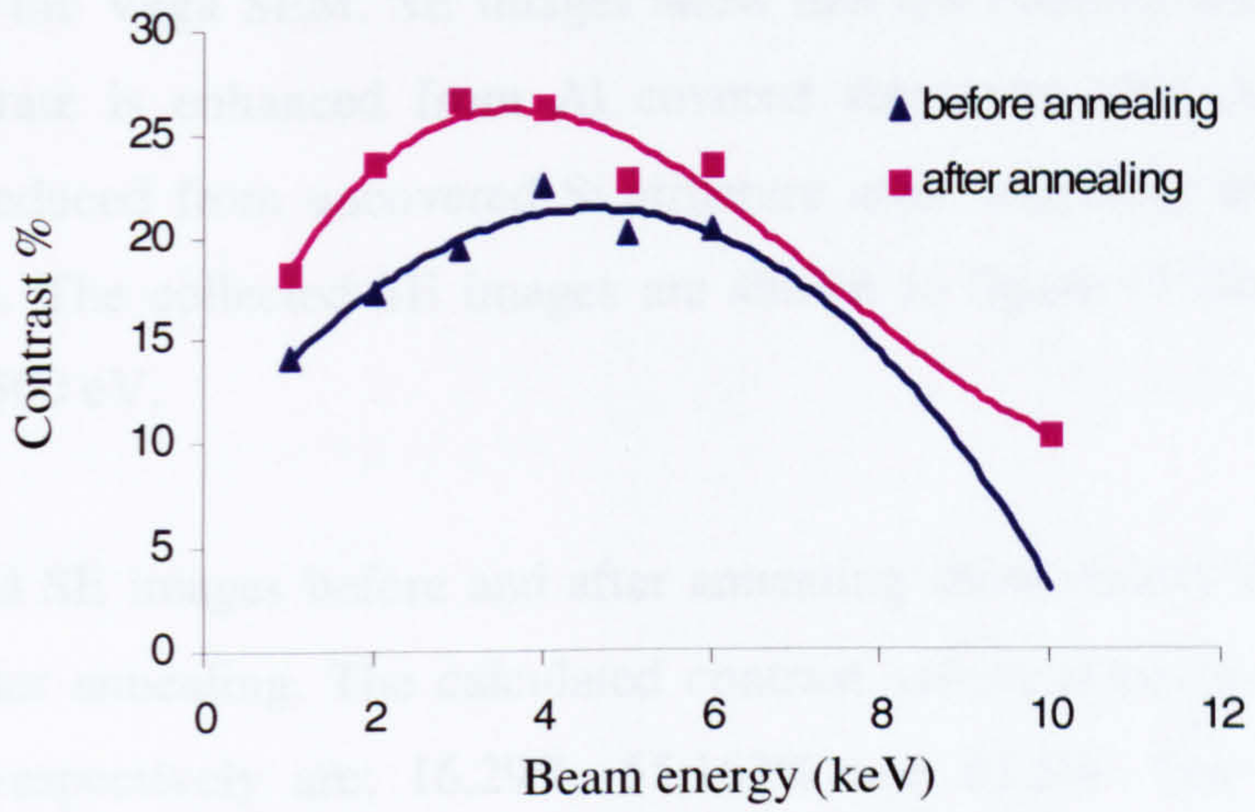

Figure (7.9) The contrast as measured from images taken at different accelerating voltages before and after annealing. Note the enhanced contrast after annealing. Moreover, the contrast curve shows a peak at about 3-6 kV before annealing, while the peak is shifted to lower beam energy (2-5kV) after annealing. The peak shift to lower beam energy after annealing could be related to a reduction of the Al layer thickness after the heat treatment.

To study annealing effect on SE dopant contrast at different temperatures, a new ISI Si (111) sample has been cleaned in a similar way and a thin Al layer was deposited onto the surface using a metal mask, the thickness of the Al layer ~ 4nm. Then the sample was taken to the polaron annealer to be heated in a forming gas at 200°C and 500°C each, separately. After allowing cooling down in the forming gas, the sample has been inspected in the Vega SEM. SE images show that the contrast between the p^+ and n-doped substrate is enhanced from Al covered structures after annealing. However, contrast is reduced from uncovered Si structure after annealing at the same range of temperatures. The collected SE images are shown in figure (7.10). These images are collected at 500 eV.

The collected SE images before and after annealing show clearly that the contrast has enhanced after annealing. The calculated contrast values at room temperature, 200°C and 500°C respectively are; 16.29%, 55.162% and 67.5%. The calculated contrast values show that SE contrast has enhanced significantly after annealing at 200 °C and this may be attributed to reduction of the original SiO_2 by the Al and penetration at least in certain regions. However, annealing at 500°C does not cause similar contrast enhancement. Because the same penetration happened in the first stages of heating to 500 °C.

Annealing effect on SE dopant contrast has been carried out on different doped Si structures such as Durham Si(111). A fresh Durham Si sample has been cleaned and covered by a thin Al layer of thickness ~ 5nm. In this experiment three pieces of Durham sample have been utilised in order to avoid extra carbon deposition on the surface during each SEM investigation. SE images collected from this sample have been carried out at room temperatures, after annealing at 300°C and finally after annealing at 500°C in a forming gas.

The collected SE images shown in figure (7.11) indicate that SE image of the as inserted surfaces (i.e. with no Al coverage) exhibits very weak contrast. However, covering the surface with thin layer of Al ≈ 5 nm has enhanced the contrast. Moreover, these images confirm that annealing has enhanced the SE contrast of Al covered Durham Si structure.

(a) SE images of Al covered ISI sample collected at 500eV before any annealing.	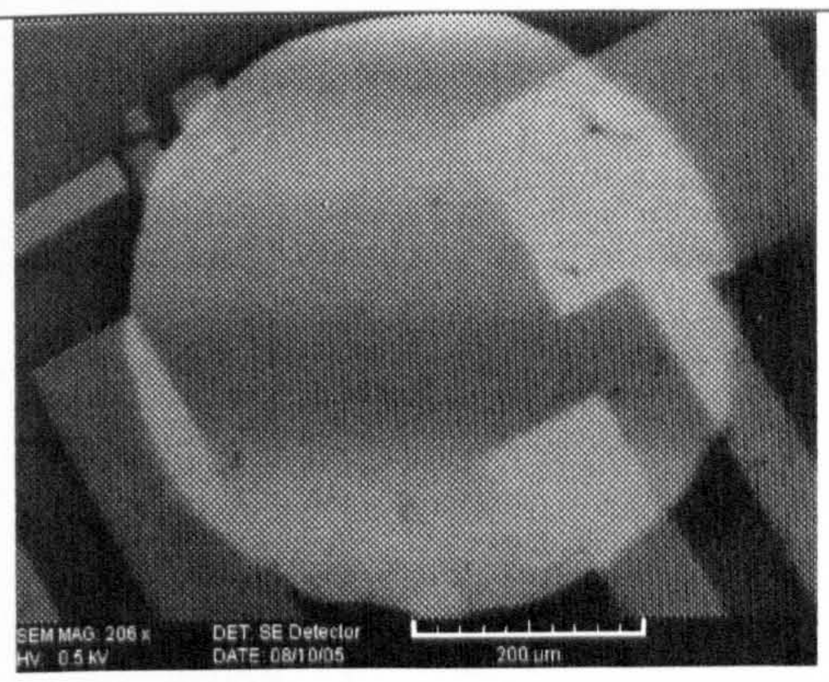
(b) SE image of the same area after annealing at 200°C.	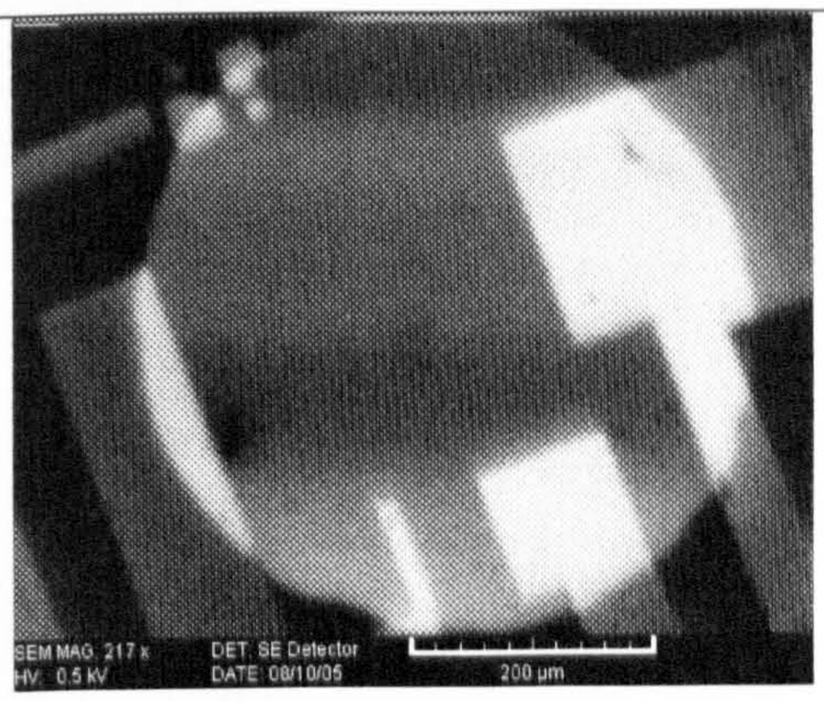
(c) SE image collected after annealing at 500°C.	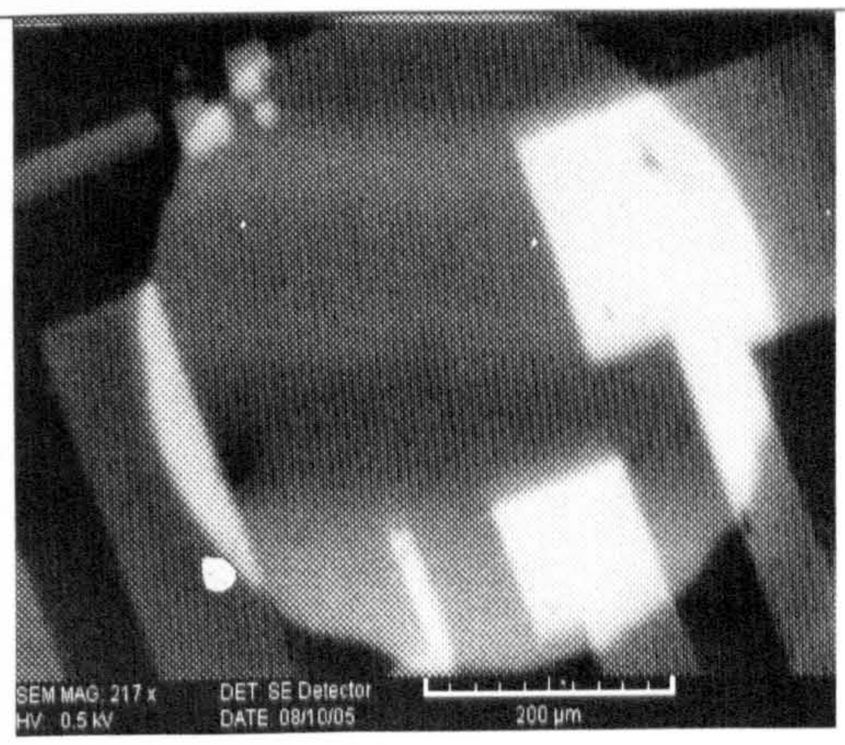

Figure (7.10) SE images collected of ISI Si (111) sample covered with 4nm of Al annealed at different temperatures.(a) at room temperature, then the sample annealed in a forming gas at 200°C for 20 min, followed by inspection in the Vega SEM and the collected image is shown in (b). The sample was further annealed at 500°C for 20 min and then investigated in the SEM under the same parameters, the collected SE image in this case is shown in (c).

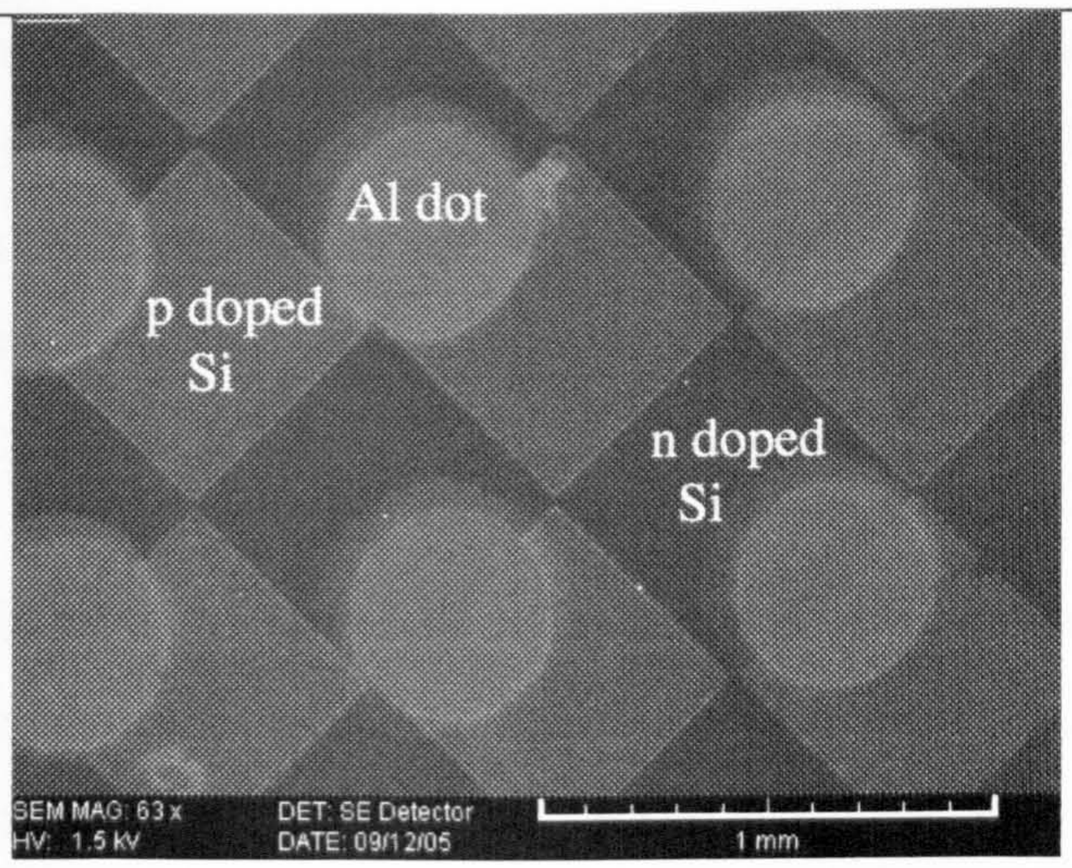	(a) Without annealing, the SE contrast within the Al covered layer is negligible.
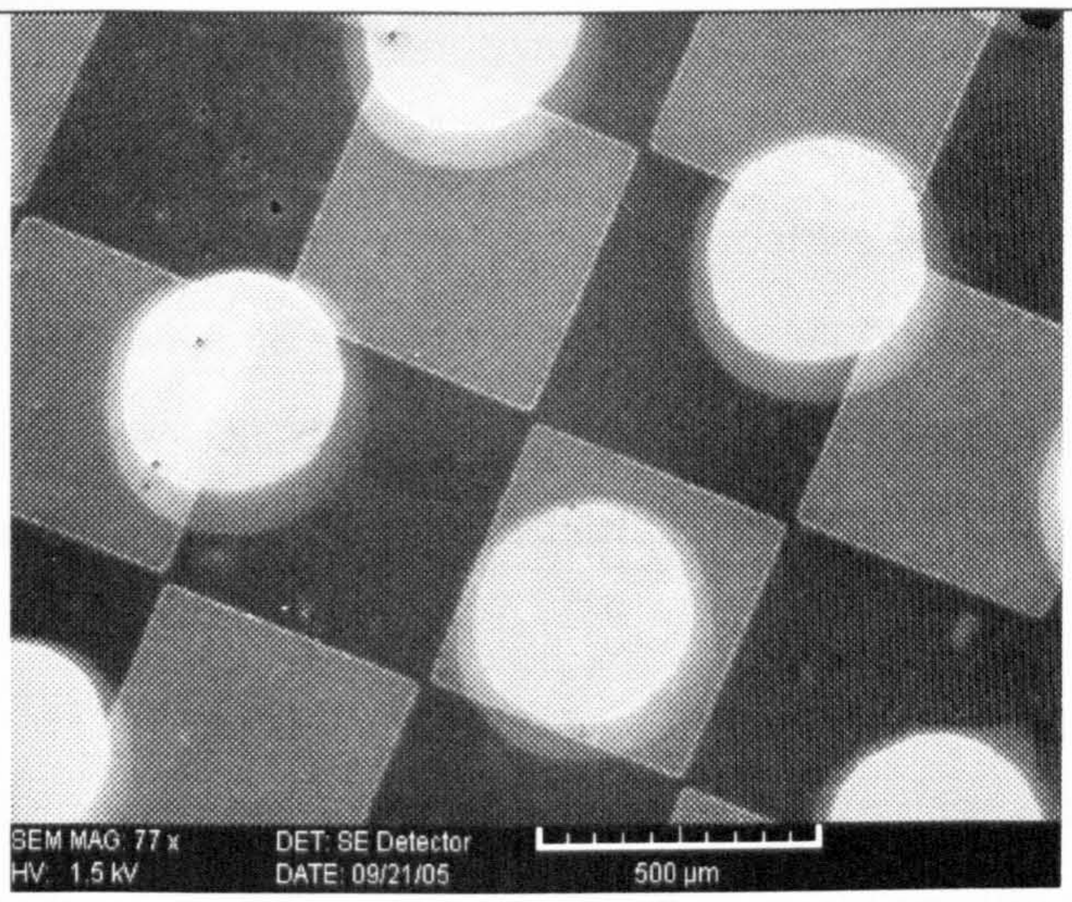	(b) After annealing at 300°C, some contrast can be seen especially within the thin shadow areas.
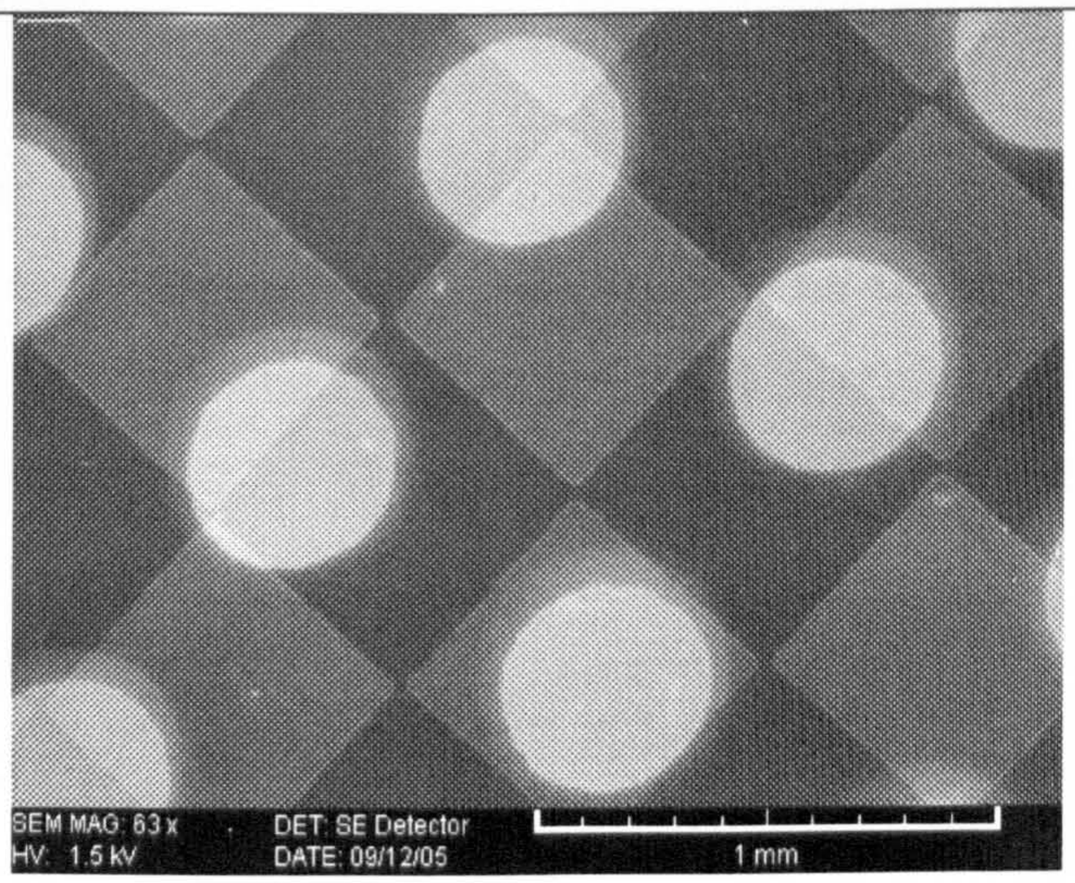	(c) After annealing at 500°C, enhanced contrast can be seen within Al covered structure. On the other hand, a reduced contrast is obtained from uncovered doped Si surface.

Figure (7.11) SE images of Durham Si(111) collected at room temperature, after annealing at 300°C and after annealing at 500°C respectively. Different areas have been investigated to avoid deposition extra carbon in each investigation.

On the other hand, annealing has decreased the contrast significantly between p^+ and n doped Si regions without Al coverage after annealing at 500°C. Digital contrast profiles across the p^+/n junction were obtained for images taken at room temperature and after annealing at various temperatures showing alteration of SE intensity by heat treatment as shown in figures (7.12a) and (7.12b).

It is believed that contrast reduction after annealing of uncovered Si structure caused by contaminant adsorption into Si surface. Annealing the sample in non evacuated system will increase the adsorption into the surface such as O, H, C which will mask the contrast gradually. To investigate the effect of the adsorbent adlayer on the SE contrast, Argon ion sputtering was performed to remove the first few layers of the surface. The use of low energy ion sputtering enables to minimise the damage. After gentle etching of the annealed sample at 500°C by Argon ions for 15 sec, SE imaging of the sputtered sample was performed to compare the SE dopant contrast before and after sputtering. Imaging the sputtered surface has shown that contrast level has been restored as shown in figure (7.13).

Moreover, sputtering has removed the shadow area of Al, this confirms that etching has removed the few upper adsorbed monolayers which reduced the contrast.

The main purpose of performing the Al annealing experiments is to investigate whether contrast inversion could be obtained due to the inverted potential barrier height between Al thin layer and differently doped Si region or not. Although SE intensity is reduced from Al/n-type Si due to increasing barrier height, inverted contrast has not been obtained of both ISI and Durham Si samples. Therefore it was suggested to study annealing effect on SRL Si sample whereby this sample includes an oxide layer below the p^+ doped region. This means this area of the sample is similar to the sample that was used by Card (1975). In addition, an inverted contrast is obtained from this sample at room temperature, i.e Al on n appears higher contrast compared with Al on p^+.

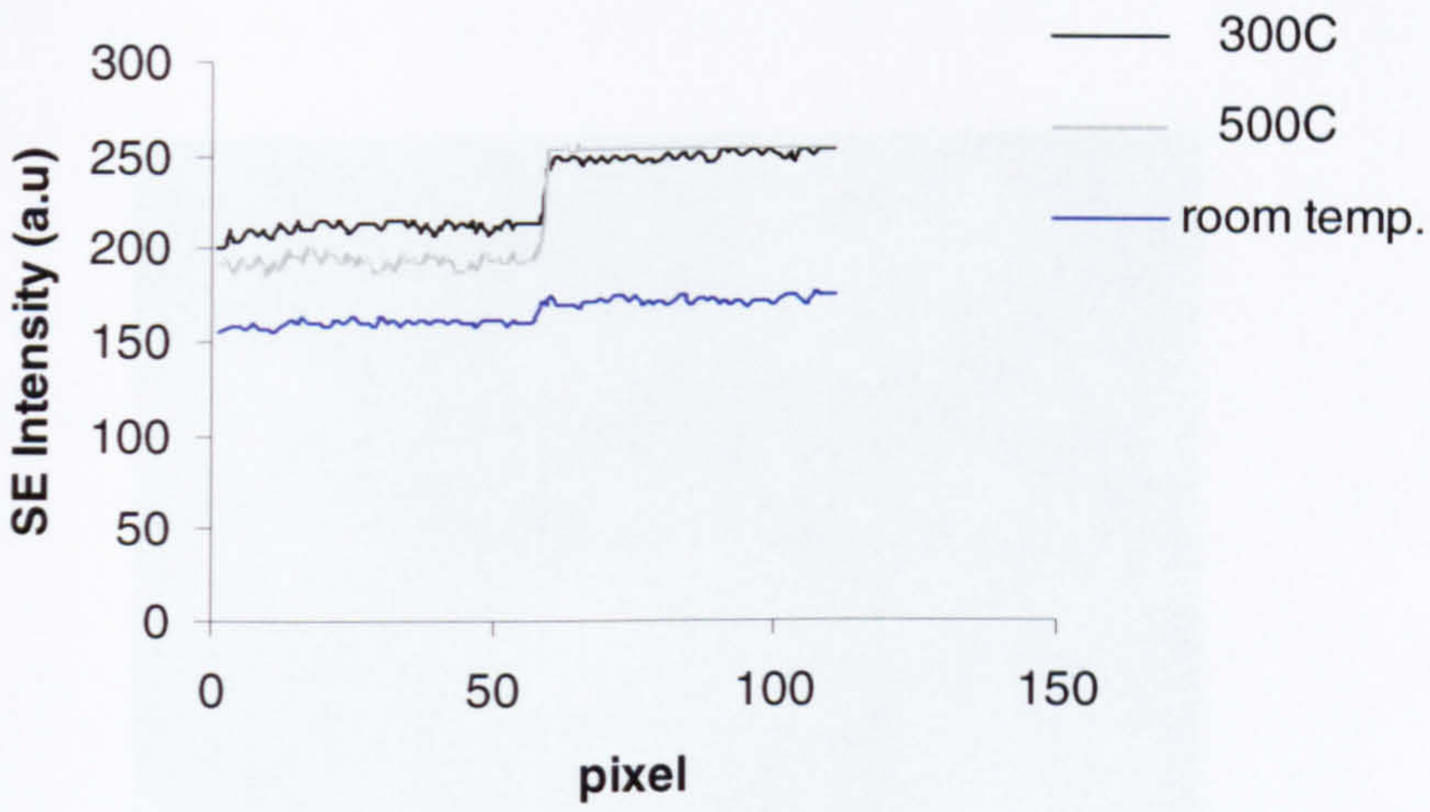

Figure (7.12) (a) One dimensional intensity profile of Durham Si(111) extracted from the SE images shown in figure(7.11), notice changes of SE intensity of both covered p and n doped regions due to annealing.

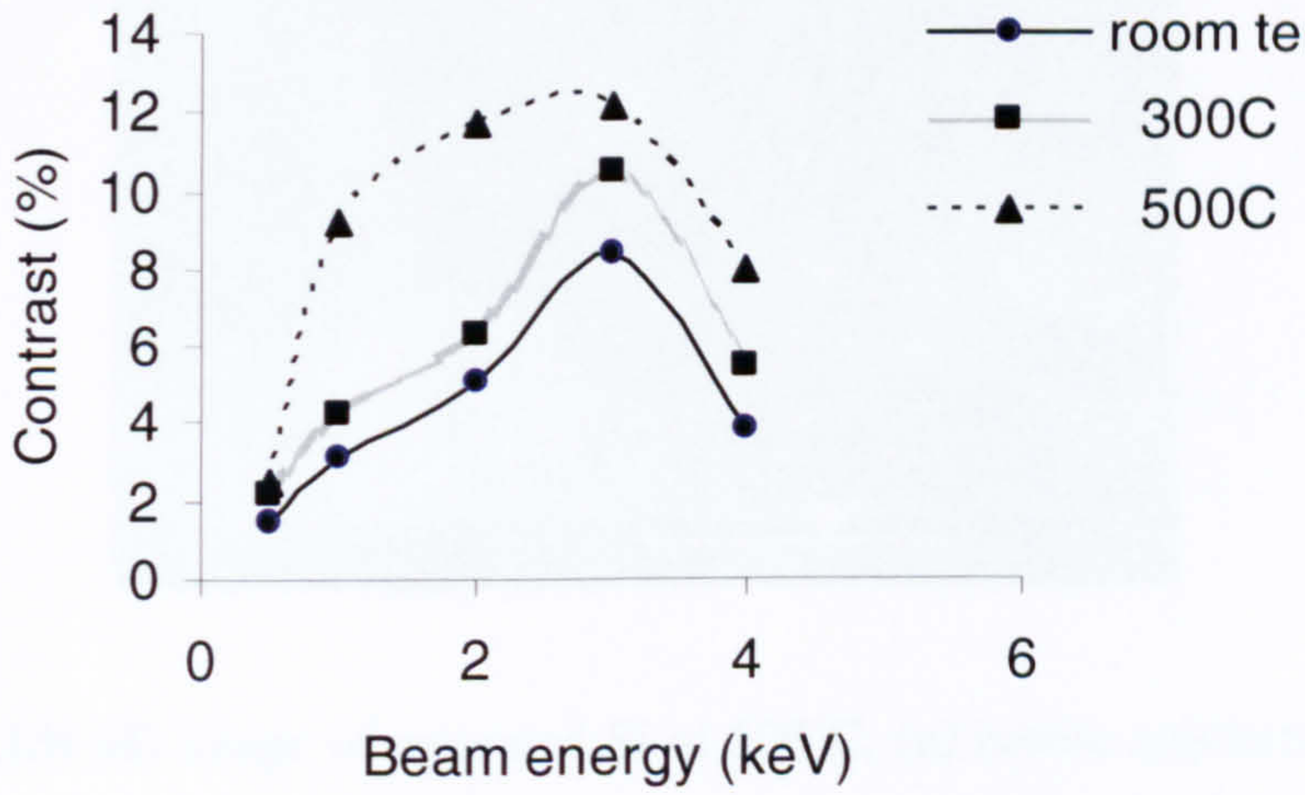

Figure (7.12) (b) The contrast as measured from images taken at different accelerating voltages before and after annealing. Note the enhanced contrast after annealing. In addition, it shows a peak shift to lower beam energy after annealing at 500°C, while it does not show a similar shift after annealing at 300°C.

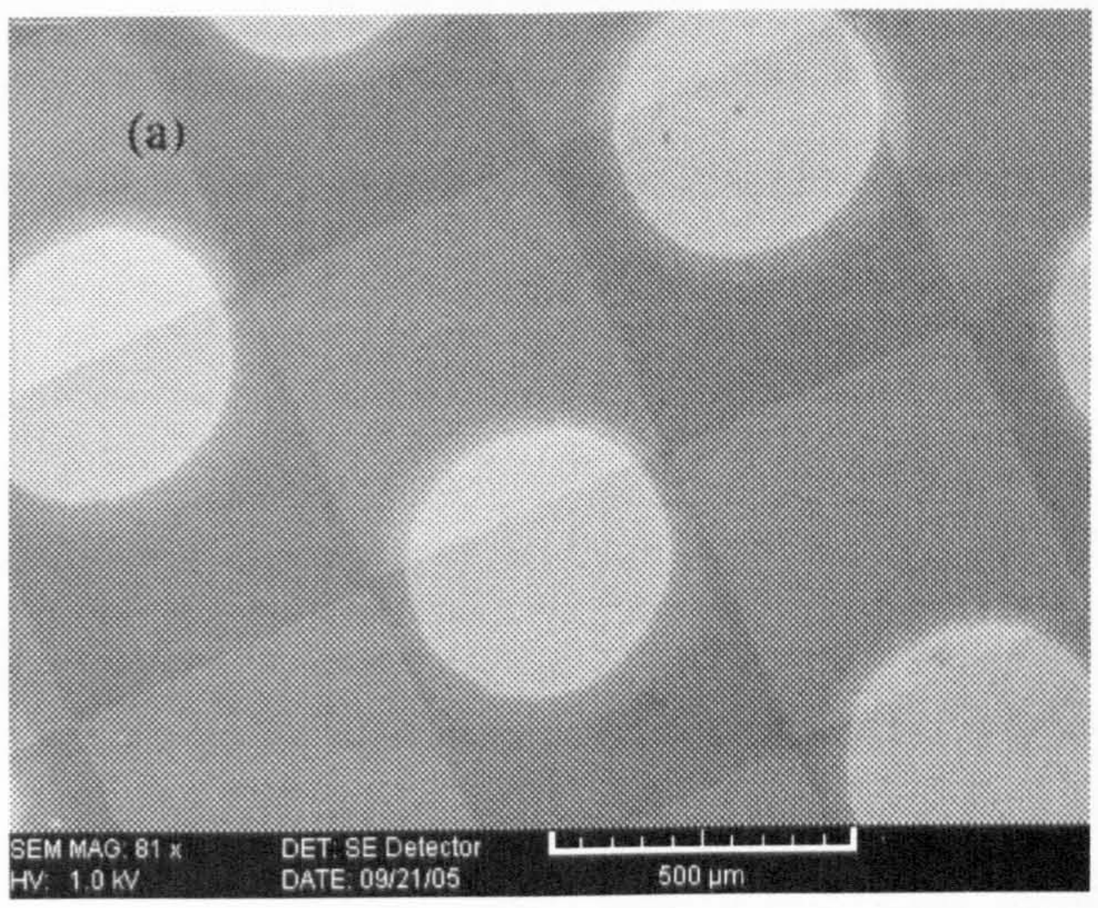

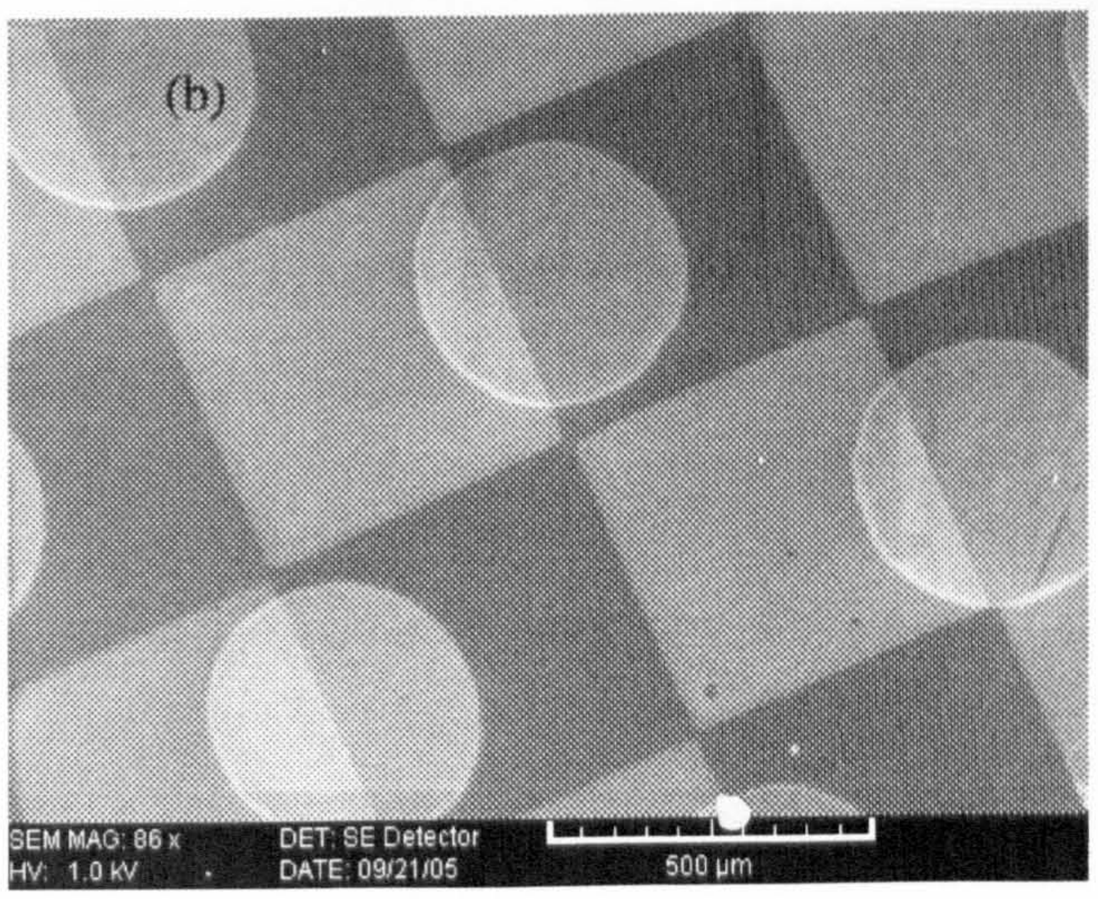

Figure (7.13) SE image of annealed Si at 500°C, (a) before sputtering.(b) after sputtering with argon ions, obviously the contrast has enhanced after removing the adsorbed adlayer.

Annealing effect on SE contrast has been studied on SRL Si sample using Al thin layer ~ 4nm, a comparison between SE images collected before and after annealing at 500°C show that SE contrast of Al covered structure is inverted after annealing as shown in figure (7.14). The contrast reversal that is obtained on the SRL sample supports the idea that SE dopant contrast is sensitive to barrier height variation. While the enhanced contrast that has been obtained from both ISI and Durham Si samples due to annealing needs further investigation to identify the factor behind this unexpected behaviour. Therefore, it was suggested to study potential barrier variation between Al and differently doped Si region using KPM.

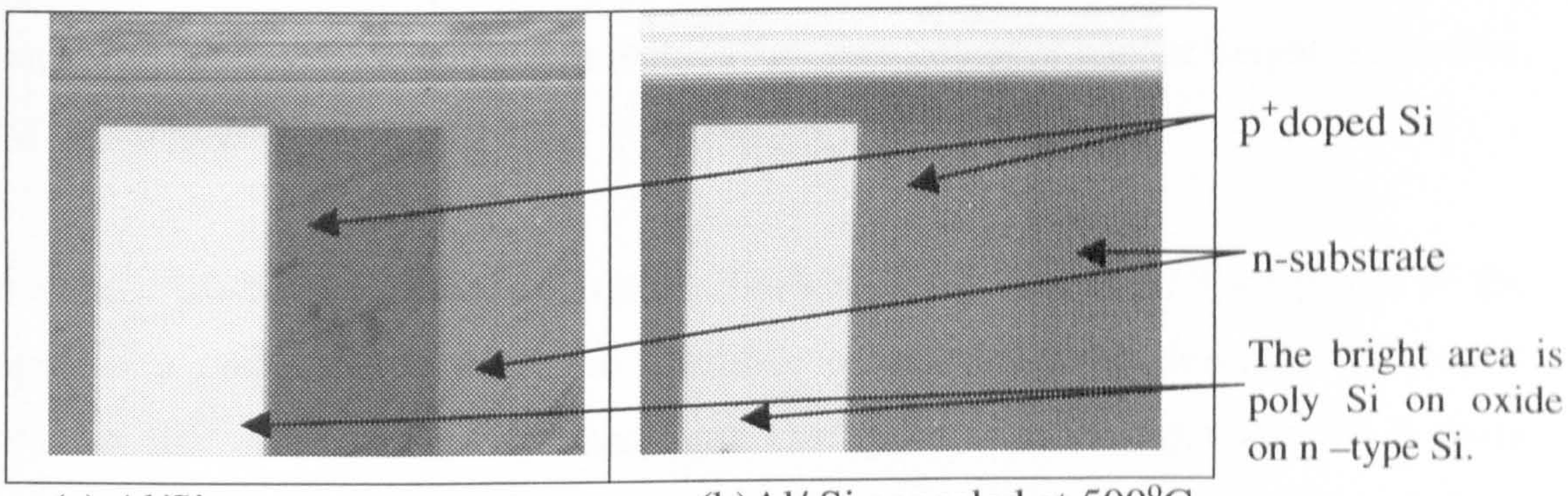

(a) Al/Si at room temperature (b)Al/ Si annealed at 500°C

Figure (7.14) SE images of SRL Si sample covered with 4nm Al collected at 1kV in the Vega SEM, showing that Al/ Si contrast has been inverted due to heat treatment. Moreover, contrast after annealing is lower than contrast obtained without annealing.

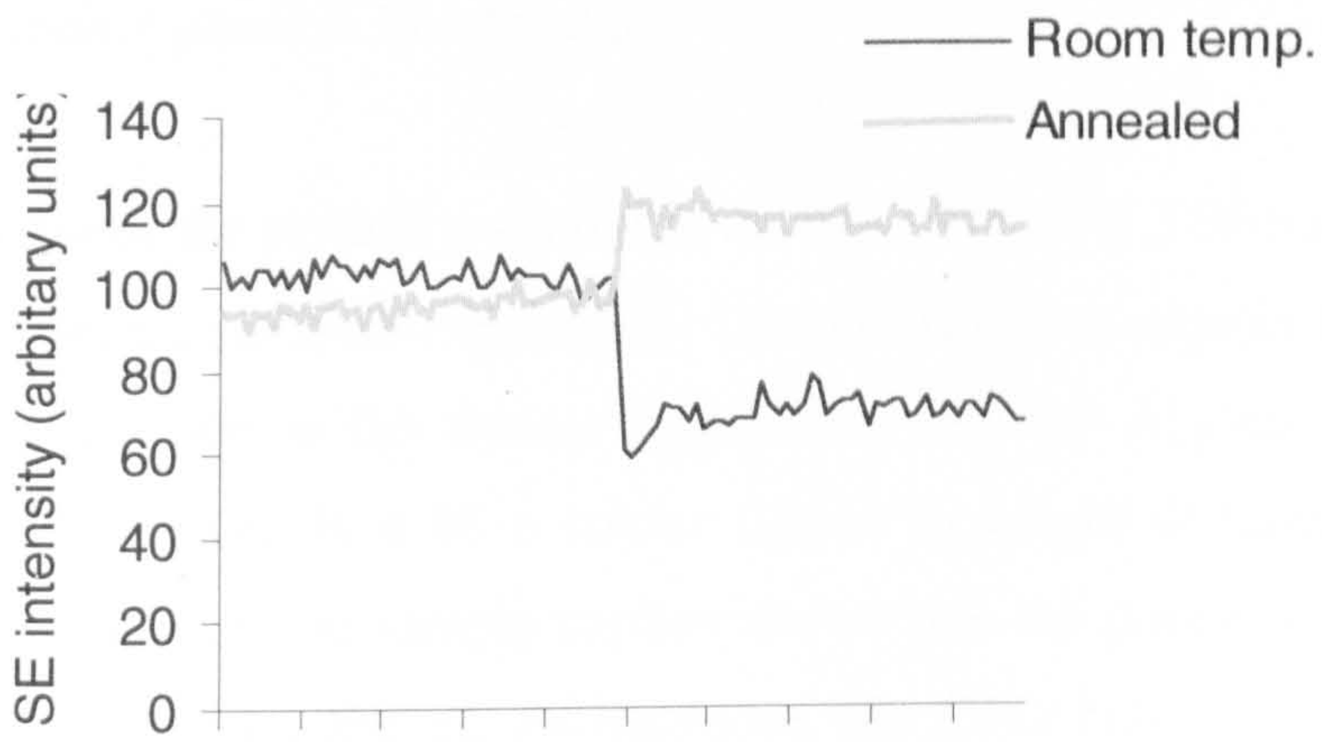

Figure (7.15) One dimensional intensity profile of SRL Si sample extracted from the SE images shown in figure (7.14), notice changes of SE intensity of both covered p^+ and n doped region due to annealing.

(7.5) Kelvin Probe Microscopy

Research has been carried out using a Kelvin Probe Microscope (KPM) in order to measure barrier height variations of Al covered patterned Si structure between room temperature and after annealing. These measurements were performed in order to investigate the effect of the barrier height variation on the SE dopant contrast. The barrier height between a metal and a semiconductor is usually estimated from changes in electrical current or capacitance when a bias voltage is applied to the interface. However, for the specimens that have been prepared in this study with few nanometres of Al layer has been deposited into Si surface, it is not possible to use I/V or Capacitance-Voltage (CV) measurements to measure potential barrier height. Therefore, KPM was utilised for this purpose.

The sample for the KPM investigation is Durham Si(111) sample. Two pieces of the sample were prepared following the specimen preparation steps described in section (7.4) with 5nm Al thickness deposited on it. One piece of the sample was left at room temperature while the second piece was annealed at 500°C and then both of them transferred to the KPM system. The Al dots are easily detected by the probe because their work function is different from that of the Si. A contact potential difference(CPD) map of a lateral Al/Si(111) interface is shown in Figures (7.16) and (7.17), before and after annealing respectively. Both of these images were taken with lights off in the laboratory to reduce possible interference.

Figure (7.16) shows the surface potential in an area of (2.88×3.96 mm^2) on the sample prepared for room temperature experiment. The p-doped area appears towards the top of the image, p-n junction in the middle (horizontal) and the Al dots are shown in the lower part of the image in a blue colour (lower in height difference). The surface potential distribution on the sample surface shows that the potential on the Al film is much lower than that on the Si. Furthermore, the CPD between p and n doped Si regions amounts to approximately 70 mV.

As can be seen from figure (7.16) of the potential distribution, the potential across the Al film and Si boundary does not show a sharp change. This gradual change around the boundaries indicates that the surface potential may have a spreading effect on the Si surface around the Al film (Nie et al, 1997). Or that may be due to the poor spatial

resolution of the KPM. Potentials on the Al film surfaces around the Si are much higher than those on the Al film far from the Si substrate. We can estimate the contact potential between the Al dots and n doped Si without annealing to be in the range of (142-154) meV. While the extracted contact potential between the Al dots and p doped Si without annealing is in the range of (220-225) meV. Therefore, the measured values of the potential barrier from KPM are comparable with potential barrier values deduced from I/V measurements of Card (1975), whereby barrier height between Al and p doped Si is larger than that between Al and n doped Si. By considering potential barrier effect on SE dopant contrast, Al/n should appear with a higher brightness compared with Al/p in SE image without any heat treatment.

On the other hand, potential barrier measurements that have been extracted from surface potential distribution shown in figure(7.17) of annealed sample at 500°C show that; annealing has increased contact potential between Al and n substrate to the range (173 - 200) meV. While the extracted contact potential between Al and p doped Si shows complimentary behaviour with a significant reduction to the range (81 - 90) meV. By considering the measured contact potential, obviously, contact potential reduction between Al and p doped Si is larger than contact potential rise between Al and n doped Si. According to the measured values of the potential barrier after annealing at 500°C, it is expected that the Al/p should appear brighter than Al/n.

In spite of the agreement between I/V and KPM measurements at room temperature and after annealing at 500°C, SE image of Al covered structure without annealing shows an inverted contrast to what is expected. This irregular behaviour of the Durham Si sample can be explained due to presence of an oxide layer on top of the Si layer, this layer might not affect I/V and KPM measurements, but it affects SE emission due to forming MOS structre as has been discussed in chapter 5.

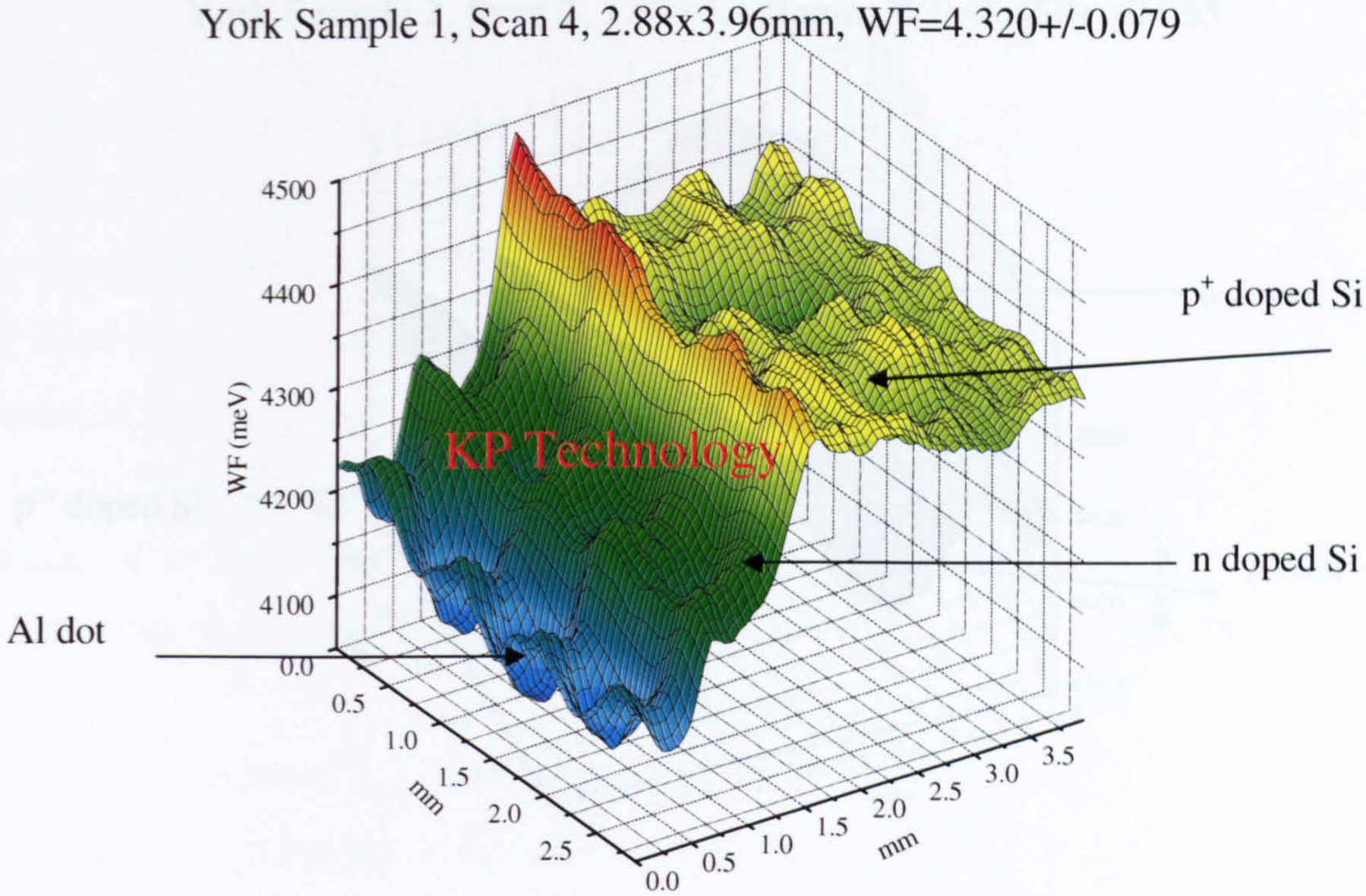

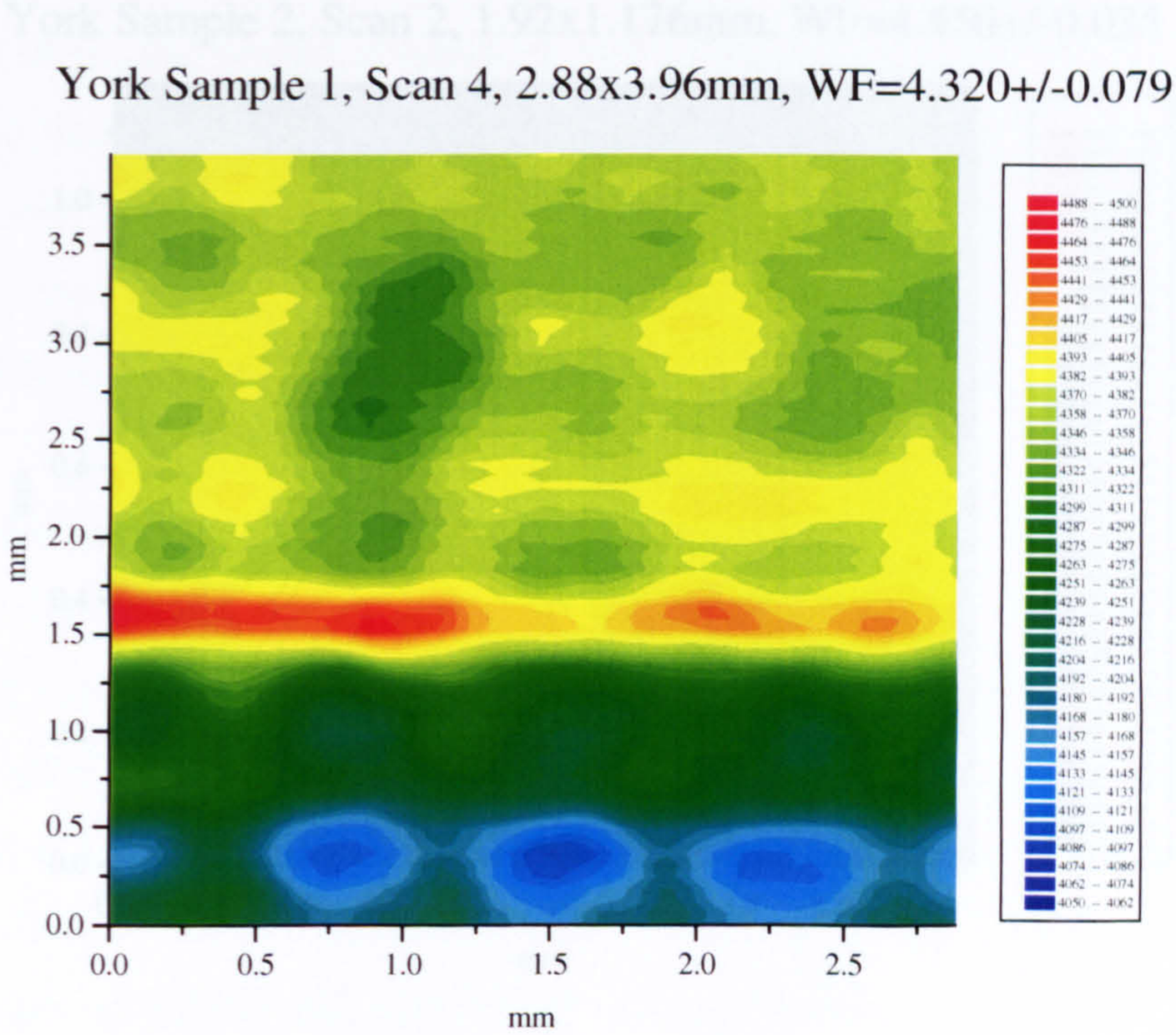

Figure (7.16) Surface potential distribution of Al on top of Durham Si(111) sample before annealing.

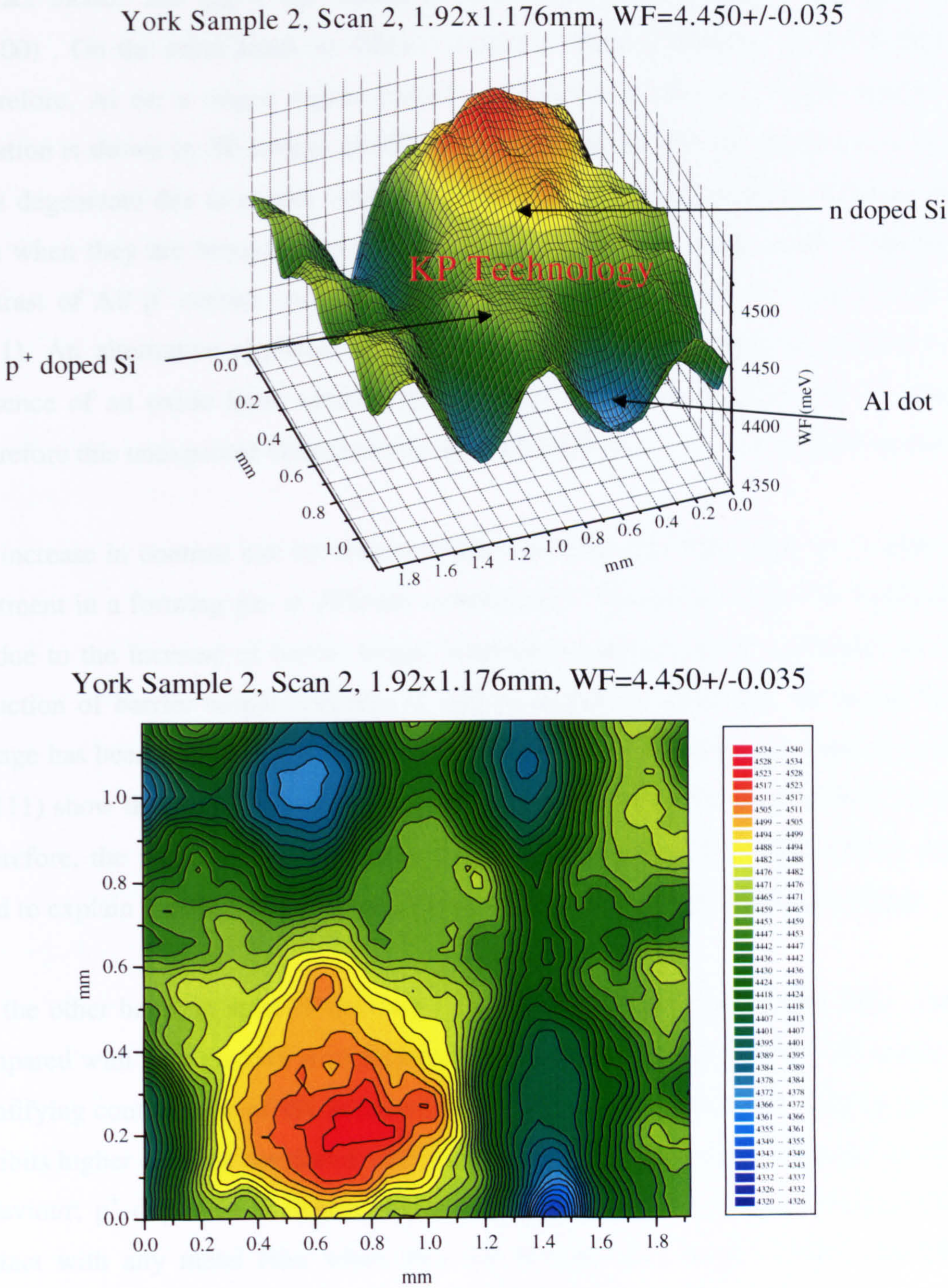

Figure (7.17) Surface potential distribution of Durham Al/Si sample after annealing at 500° C.

(7.6) Discussion of Results

The observed contrast within the Al covered structures can be explained by the M-S contact model. For $\phi_{Al} < \phi_{Si}$, Schottky barriers are formed between Al and p-type Si(100) . On the other hand, an Ohmic contact is formed between Al and n-type Si. Therefore, Al on n doped region appears brighter than Al on p doped region, this situation is shown by SE images of SRL Si presented in figure (7.4). However, p^+ doped Si is degenerate due to excess carriers, which makes an ohmic contact with any metal film when they are brought into contact. Thus, this ohmic contact leads to higher SE contrast of Al/ p^+ contact compared with Al/n contact as shown in figures (7.5) and (7.11). An alternative explanation is that such a behaviour might be related to the presence of an oxide layer sandiwiched between the semiconductor and Al adlayer. Therefore this unexpected behaviour can be explained due to MOS structure formation.

An increase in contrast can be observed between Al/p^+ and Al/n areas of Si after heat treatment in a forming gas at different temperatures. This increase can be explained to be due to the increase of barrier height between Al and n type Si combined with the reduction of barrier height between Al and p^+ doped Si. Although, no barrier height change has been reported between Al and p^+ doped Si, KPM measurements of Durham Si(111) show that annealing causes reduction of contact potential within Al/p^+ contact. Therefore, the metal to semiconductor model suggested by El-Gomati (2001) can be used to explain the observed contrast before and after annealing of SRL Si sample.

On the other hand, in spite of measuring higher contact potential within Al/p^+ contact compared with Al/n contact at room temperature using KPM of Durham Si sample and identifying contact type of ISI Si sample using I/V measurements, SE imaging of Al/p^+ exhibits higher contrast compared with Al/n. There are two possible explanations of this behaviour; p^+ doped Si is degenerate due to excess carriers, which makes an ohmic contact with any metal film when they are brought into contact. Thus, this ohmic contact leads to higher SE contrast of Al/ p^+ contact compared with Al/n contact. Therefore, appearance of Al/p^+ is brighter than Al/n at room temperature is reasonable. The question now if it is accepted that p^+ is degenerate and forms an ohmic contact with Al, why KPM and I/V measurements do not show this? The answer might be related to a residual thin layer of oxide existing on the Si surface which affect KPM resolution and then the measured contact potential. Therefore, SE contrast of Al covered Si structure is

dominated by the MOS model at room temperature.

Although both Al/Durham Si structure and Al/ISI Si structure show unexpected behaviour at room temperature, SE contrast behaviour still depends on surface structure (i.e surface condition, El-Gomati et al, 2001). This diverted behaviour occurs in covalently bonded semiconductors like Si (the main material of this study). In this material, the barrier height is almost independent of ϕ_m due to the presence of localized surface states that are continuously distributed in energy within the forbidden gap. These states try to pin the Fermi level at the surface and thus influence the barrier height at equilibrium.

A reduction in the contrast has been observed between p^+ and n areas of Si after annealing in a forming gas at 500°C. This reduction can be explained to be due to adsorption of atoms or molecules onto Si surface. The adsorbed molecules onto Si after annealing at 500°C have masked the contrast, which results in a reduced contrast. Adsorption effect on SE contrast has been investigated by gentle argon ion sputtering in a Plasma Etcher instrument. The collected SE images after sputtering show that SE contrast is restored after sputtering.

A second possibility is that adsorbed atoms or molecules can have a significant influence on the electronic structure of a surface by changing the amount of band bending. The adsorbed molecules are almost C, H and O, cleaning the surface with a gentle ion gun predicts that the thickness of the adsorbed layer on Si is ~3nm. Although with such a layer there is little information about the change in the band bending, it is suggested that adsorbed molecules can form surface states that are located in the band gap and can pin the Fermi level to a near mid-gap position at the surface. These surface states can trap free carriers from the bulk material resulting in a charge accumulation region at the surface and associated band bending (Sealy et al, 2000). It was shown that band bending causes reduction of SE dopant contrast (Sealy et al, 2000).

(7.7) Conclusions

SE imaging of Al covered Si structures has been performed on different Si samples. It has been shown that the observed contrast can be explained by the M-S contact model.

The effect of heat treatment on the electrical behaviour of Al/Si contacts has been used to study the effect of barrier height variation on the SE dopant contrast by annealing the prepared samples to different temperatures. Analysis of the collected SE images shows enhanced contrast of Al covered structures after annealing caused by increasing the barrier height between Al and n-type Si combined with reduction of the barrier height between Al and p doped Si. Contact potential variation due to annealing has been extracted from surface potential map that has been taken using KPM. Moreover, an inverted contrast of Al covered structure has been obtained due to heat treatment, this result shows dependence of the SE contrast on the barrier height.

On the other hand, it has been found that the uncovered annealed surface at 500°C gives rise to a reduced SE contrast from the doped regions. The reduction in the observed SE contrast can be explained as a result of adsorption onto Si surface at the time the sample has been handled in air. This effect has been further investigated by sputtering the annealed sample by low energy argon ions. SE images show that sputtering restores SE contrast level as a result of the removal of the adsorbed layer from the surface. The SE contrast from doped Si is complicated as a result to its high sensitivity to contact formation and band bending at the surface.

The results presented here show dependence of the SE contrast of doped semiconductors on the surface structure. Whereby an inverted contrast has been obtained due to inversion of the barrier height and explained simply by m-s contact model. In addition, the inverted behaviour of Al covered Si structure has been explained due to oxide adsorption into Si surface which provides further support for surface structure effect on SE dopant contrast.

Chapter 8: Summary and Further Work

(8.1) Summary

Dopant contrast from a variety of Si structures that have been differently doped (n- and p-type) has been observed and systematically studied in this thesis. Some clarification of the dopant contrast mechanism has been obtained. This has required a study of the effects of surface structure on the contrast.

It has been shown elsewhere that SE dopant contrast is quite sensitive to the surface composition, and M-S contact is the dominant contrast mechanism in high vacuum environment (El-Gomati et al, 2004). To further investigate the effects of surface structure on SE dopant contrast, differently doped Si surfaces were investigated. It was found that the SE dopant contrast is strongly dominated by the surface structure. Therefore, the XPS has been utilised for the first time to identify the surface composition of doped Si surface. Results have shown that with oxidation of the freshly cleaned Si surface and the presence of surface states, contrast was altered as function of beam energy and electron dose. Therefore, the opportunity to directly discriminate between n-and p-type dopant using SE contrast is lost in this case. However, this result is consistent with M-S contact model whereby an existing oxide layer may produce a MOS structure. And a new model has been developed to explain the altered SE dopant contrast behaviour.

The electron dose effect on SE dopant contrast also revealed new contrast behaviour as a function of electron injection level. This b haviour can not be easily explained with M-S contact. In this case it is believed that changes of SE dopant contrast behaviour are mainly dominated by surface state occupation, due to oxide adsorption. The process of introducing excess electrons to the semiconductor would imply a movement of the Fermi level. It is found that the results can be divided into two regimes. At low electron dose, a low number of electron-hole pairs is generated. The generated minority carriers will recombine with the induced surface charge within the energy band gap, after partial recombination, the SE emission starts with n-type doped regions appearing brighter than the p^+ -type doped regions in the SE image. The emitted SE, in this case, is produced due to the direct inelastic scattering with valence band electrons.

At high electron dose, the generated e-h pairs per unit area are increased at the same interaction volume. Therefore, part of the created carriers will recombine with each

other within the surface states, the rest of the carriers may create opposite electric field in p^+ and n doped Si, whereby the created electric field in p^+ accelerate the generated SE to the surface and retard SE emission in n-type Si.

The effect of heat treatment on the electrical behavior of Aluminum/Silicon (Al/Si Schottky junctions) is used to study the impact of barrier height variation on SE dopant contrast by annealing at different temperatures. In this study, the variation of the Schottky barrier height has been detected as an inverted contrast between Al on p^+ and Al on n-type doped region of SRL sample in the SE imaging. However, the variation of the barrier height has caused an enhanced contrast of ISI and Durham samples between Al on p^+ and Al on n-type Si doped regions. The inverted contrast of SRL sample as well as the enhanced contrast of ISI and Durham samples have been attributed to a decrease in the SE yield of Al/n-type Si contact combined with an increase of the SE emission of Al/p-type Si contact. In this case it is believed that changes in contrast can be understood in terms of changes in barrier height within Al/Si contact due to annealing. Whereby annealing causes an increase in the Schottky barrier height between Al and n-type Si and a complimentary reduction of the barrier height between Al and p-type Si.

Annealing experiments also revealed some changes in the contrast after annealing to 500°C in a forming gas (non evacuated system). These changes could be explained due to molecular adsorption onto the Si surface. Adsorption may increase surface band bending. Further investigation of these changes was carried out by sputtering the surface with argon ions. It is found that the contrast could be restored by sputtering. This supports Sealy's argument (2000) by showing that surface band bending such that caused by molecular adsorption leads to reduction of SE dopant contrast.

The results of this thesis indicate a dependence of the contrast on the surface structure, whereby the presence of surface states and oxidation of the freshly prepared Si surface are two factors that have altered the absolute value of the contrast. Therefore, it is not possible to directly discriminate between differently doped regions. However, it is possible to distinguish between differently doped regions if the surface structure of the sample has been analysed using XPS or AES, then analysing the image according to the used electron beam energy and the electron dose. Over all, a new model has been

proposed to understand the SE dopant contrast mechanism. This model is based on experimental results deduced from surface analysis data. However, the exact contrast mechanism still requires further verification.

(8.2) Further Work

Since this study is mainly concentrated on studying surface condition effects on SE dopant contrast, therefore, some experiments have been planned to run to study the effect of surface contact potential on SE dopant contrast such as silicide formation effect on SE dopant contrast. In this case Durham Si(111) sample has been used, the sample is degreased in boiling trichloroethylene, acetone and methanol consequently. Then the sample is dipped in HF. After initial cleaning, the sample had a low temperature anneal cycle by soaking it at 530°C and cooling under an inert atmosphere. The Ti was evaporated on the Si substrate once at room temperature to a film thickness of about ~5 nm thick at a pressure less than 4×10^{-6}mbar. Another piece of the same sample has been covered with similar Ti layer thickness; the Si substrate at this time was at 430°C. The value of T_S was measured by means of a thermocouple near to the substrate. Evaporation on a hot substrate has been reported as a developed method to favour silicidation (De Bosscher et al, 1986). Ti makes a Schottky contact with p doped Si at room temperature and Ohmic contact with n-type Si. Therefore, SE imaging of Ti covered Si structure at room temperature should show Ti/n Si in higher brightness compared with Ti/p Si. However, SE imaging does not show an intensity difference between Ti/n-type and Ti/p-type Si as shown in figure (8.1).

According to De Bosscher et al (1986), for high T_S=430°C low barrier height is found between Ti and p doped Si and almost constant barrier height is found between Ti and n doped Si. This change of the Schottky barrier height with T_S has been explained due to the reaction wherein Ti converts Silicon oxide into titanium oxide and titanium silicide. In addition, it has been found (Taubenblatt et al, 1982) the required temperature T_S to complete the conversion at the interface depends on the thickness of the oxide layer. Therefore, in order to correlate the effect of the barrier height on SE contrast further measurements are required to analyse the interfacial layer by using Auger measurements. However, due to the limited time of this study it was not possible to run such measurements.

In addition, SE imaging of the second sample shows an increase of SE intensity of both Ti/n and Ti/p by the same amount as shown in figure (8.2). This result does not agree with the expected behaviour due to the reduction of the barrier height within Ti/p Si as a result to silicide formation. Unfortunately this attempt has not been successful due to missing surface structure investigation in order to know the factors responsible about this unexpected behaviour.

(8.3) Suggestion for Further Work

Results obtained in this research combined with obtained results by many researchers indicate that there is much work remaining in this area of research before accepting the SEM as a quantitative technique for dopant profiling by the SIA. A full understanding of the contrast mechanism requires more research and further experimental verification of wide range of samples (of different orientation, dopant concentrations, and materials other than Si).

Although the obtained results of this research and of many previous studies show dependence of the SE relative measurements on dopant type and concentration level, it is not possible to extract dopant concentration profile. Moreover, with SEM alone the obtained results are still far from being quantitative in spite of monotonic contrast dependence on dopant concentration. i.e till this stage it is not possible to directly extract dopant concentration profile from direct SE intensity measurements. Therefore, it is suggested to perform relative measurements of the SE intensity combined with theortical calculation taking in consider the parameter which its influence on SE intensity is under investigation, then calibrating the results using SIMS. This calibration may help to develop a formula enable of extraction of the dopant concentration.

Due to the large effect of contamination on SE dopant contrast, and due to existing adsorbed layer of an oxide onto the semiconductor surface (particularly with Si), whereby preliminary experiments on the dopant contrast showed that the SE contrast can be altered from the doped regions in the presence of a relatively thick oxide layer on the surface. It is crucial to eliminate adsorbed layer effect on contrast. This would help to clarify the contrast mechanism in absence surface adlayers. Further experiments should be carried out in the UHV conditions.

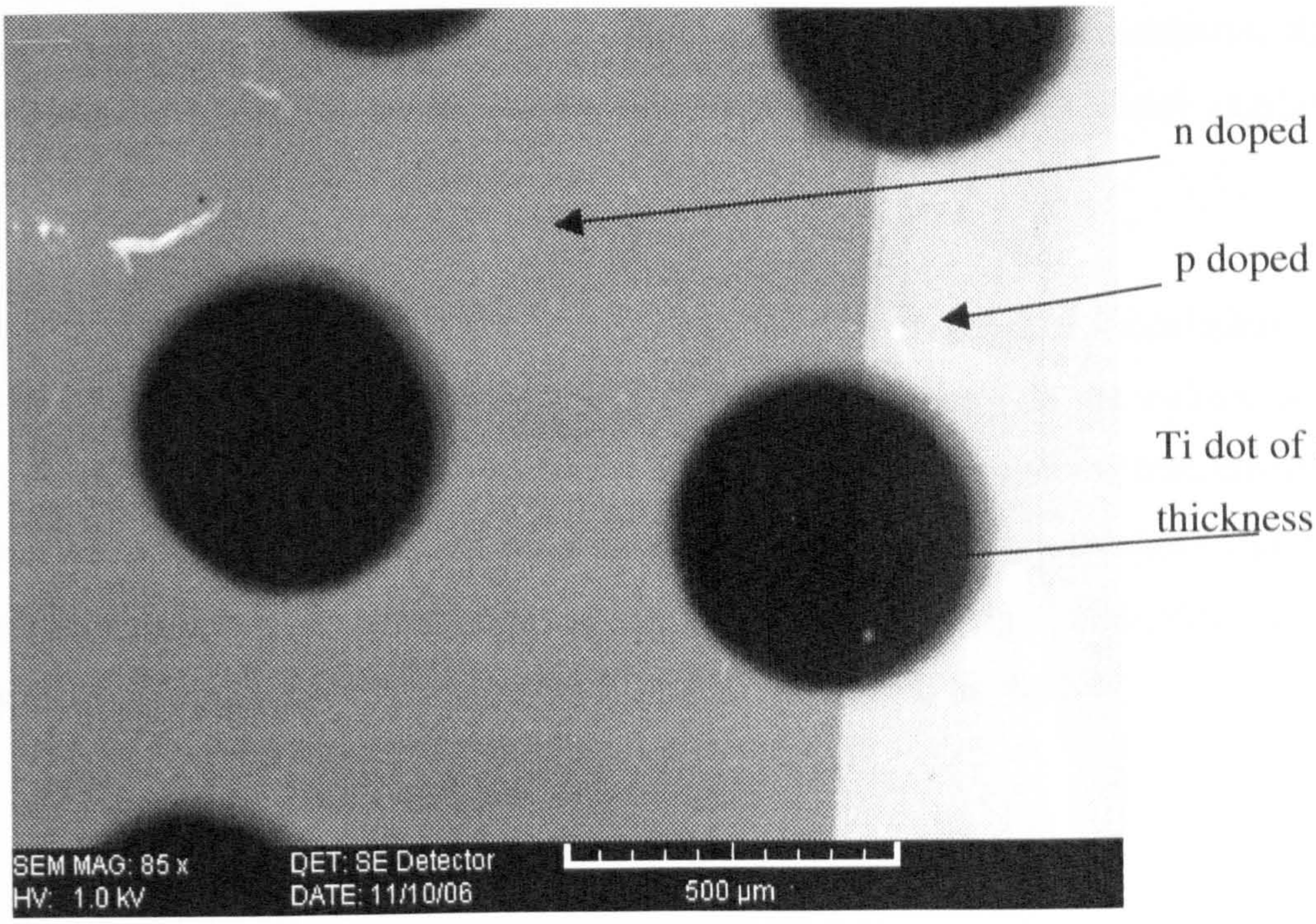

Figure (8.1) SE of Durham Si sample with Ti spots at room temperature.

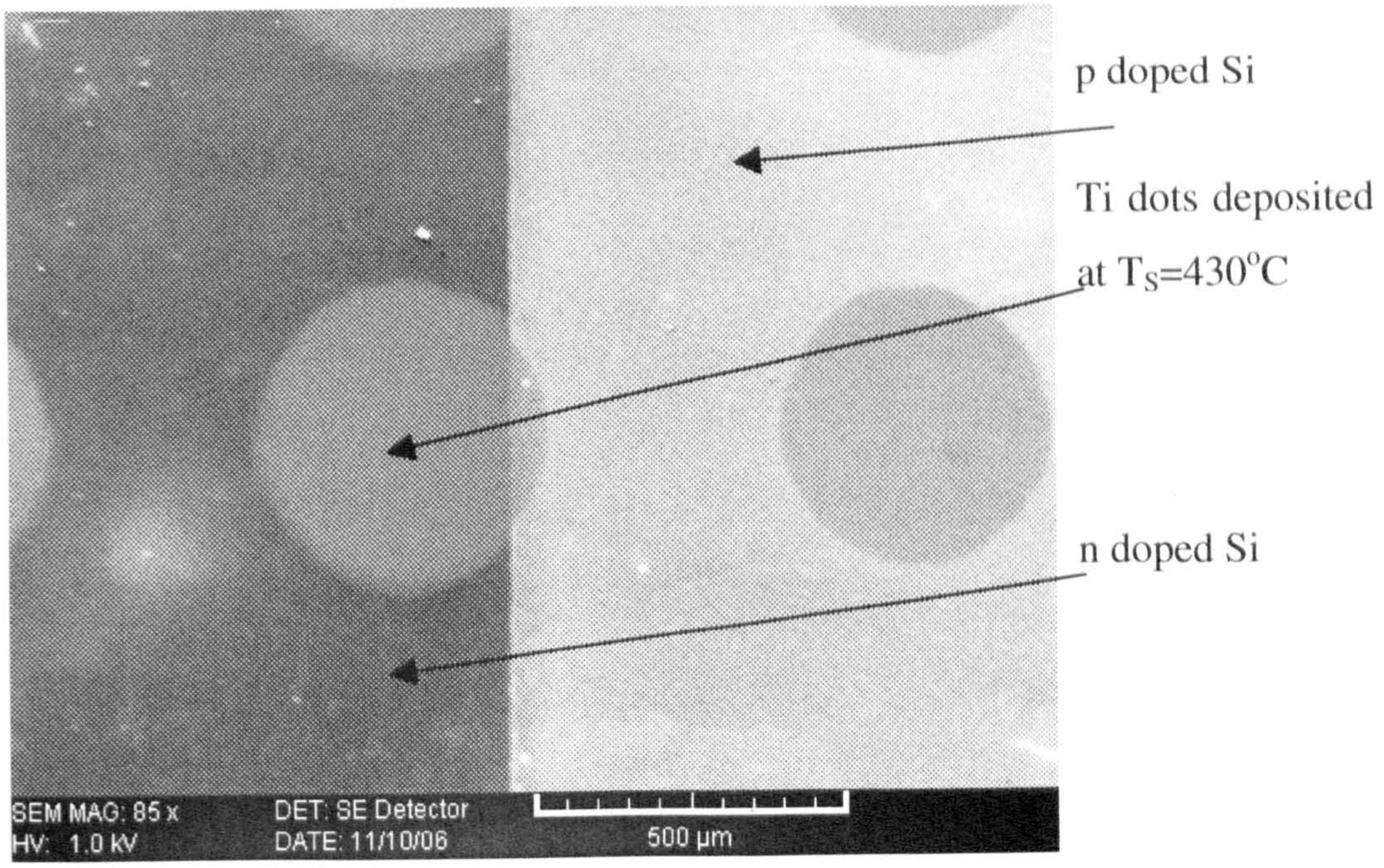

Figure (8.2) SE of Durham Si sample with Ti spots deposited at T_S=430°C.

These experiments must be performed in a dedicated AES with high resolution SE energy analyser. Small shifts in the energy distribution on differently doped regions would help to clarify the contrast mechanism.

One further area of research for SEM dopant profiling is theoretical calculation of surface charge effects. To completely understand what is happening on the surface of a p-n junction requires calculations of surface charge distributions, sub-internal electric field and surface states, as well as simulations of Fermi level movements during impinging the surface with electron beam of a particular energy then simulating secondary electron trajectories from different areas of the sample surface.

References

Assa'd A. **The Effect of Energetic Backscattered Electrons in Quantitative Multispectral Analysis**, D. Phil Thesis, University of York, 1995

Assa'd A. M. D. and El-Gomati M. M. "Backscattering coefficient for low energy electrons", Scanning Microsc.**12** (1), (1998), pp.185-191

Ambridge T. and Wakefield B. "Probe beam microanalytical techniques for electronic and optical materials and device research", Br Telecom Technol. J. **3**(1), (1985)

Angermann H. Dittrich Th. And Flietner H. "Investigation of native-oxide growth on HF treated Si(111) surfaces by measuring the surface-state distribution", Appl. Phys. A: Materials Sci. and Proc. **59**(2), (1994) pp.193-197

Arizum T. Hirose M. and Altaf N. "Au-Cu Alloy and Ag-Cu Alloy-Silicon Schottky Barriers", Jap. J. Appl. Phys. **8**(11), (1969) pp.1310 -1313

Basnar B. Golka S. Gornik E. Harasek S. Bertagnolli E. Schatzmayr M. and Smoliner J. "Calibrated scanning capacitance microscopy investigations on p-doped Si multilayers", J. Vac. Sci. Technol. B **19**(5), (2001) pp.1808-1812

Basterfield J. Shannon J. M. and Gill A. "The nature of barrier height variations in alloyed Al-Si Schottky barrier diodes", J. Solid-St. Electron. **18** (1975) pp. 290-291

Blaise G. in: 4th International conference on electric charges in Non-Conductive Materials, France, Vide Sci. Tech. Appl. Suppl. 275 (2001).

Briggs D. and Seah M. P. **Practical Surface Analysis,** V (1); Auger and X-ray Photoelectron Spectroscopy, John Wiley, Chichester (1996)

Burrows V. A. Chabal Y. J. Higashi G. S. Raghavachari K. and Christman S. B. "Infarad spectroscopy of Si(111) surfaces after HF treatment: hydrogen termination and surface morphology", Appl. Phys. Lett. **53** (1988) pp.998-1000

Buzzo M. Ciappa M. and Fichtner W. "Imaging and dopant profiling of silicon carbide device by secondary electron dopant contrast", IEEE Transactions on Device and Material Reliability, **16**(2), (2006) pp.203-212

Card H. C. "Thermally–induced changes in barrier heights of Aluminum contacts to p- and n-type silicon", J. Solid-St. Communications **16** (1975) pp. 87-89

Castell M. R. Simpson T. W. Mitchell I. V. Perovic D. D. and Barrbeau J. M. "Deactivation and diffusion of boron in ion implanted silicon studied by secondary electron imaging", Appl. Phys. Lett. **74**(16), (1999) pp.2304-2306

Chang T. H. P. and Nixon W. C. "Electron beam induced potential contrast on unbiased planar transistors", Solid- St. Electron. **10** (1967) pp.701-702

Chino K. "Behavior of Al-Si Schottky barrier diodes under heat treatment", J. Solid-St. Electron. **16** (1973) pp.119-121

Cooke G. A. Dowsett M. G. Hill C. Pearson P. J. and Walton A. J. "Comparison between computer simulation and direct secondary ion mass spectrometry measurement of lateral dopant distributions", J. Vac. Sci. Technol. B **12**(1), (1994) pp. 243-246

De Bosscher W. Van Meiraeghe R. L. Hanselaer P. L. Caenepeel L. Laflere W. H. and Cardon F. "The influence of silicide formation on the barrier height of Ti/Si Schottky barrier", Semicond. Sci. Technol. **1**(1986) pp. 376-382

De Wolf P. Clarysse T. Vandervorst W. Snauwaert J. and Hellemens L. "One and two dimensional carrier profiling in semiconductors by nanospreading resistance profiling", J. Vac. Sci. Technol. B **14**(1), (1996) pp.380-385

De Wolf P. Stephenson R. Trenkler T. Clarysse T. Hanstchel T. and Vandervorst W. "Status and review of two-dimensional carrier and dopant profiling using scanning probe microscopy", J. Vac. Scin. Technol. B **18**(1), (2000) pp.361-368

Dowsett M. G. and Cooke G. A. "Two dimensional profiling using secondary ion mass

spectrometry", J. Vac. Sci. Technol. B **12**(1), (1992) pp.353-357

Duhayon N. Eyben P. Fouchier M. Clarysse T. Vandervorst W. Álvarez D. Schoemann S. Ciappa M. Stangoni M. Fichtner W. Formanek P. Kittler M. Raineri V. Giannazzo F. Goghero D. Rosenwaks Y. Shikler R. Saraf S. Sadewasser S. Barreau N. Glatzel T. Verheijen M. Mentink S. A. M. Sprekelsen M. Maltezopoulos T. Wiesendanger R. and Hellemans L. "Assessing the performance of two-dimensional dopant profiling techniques", J. Vac. Sci. Technol. B **22**(1), (2004) pp.385-393

El-Gomati M. M. and El Bakush T. A. "Sources of internal scattering of electrons in a cylindrical mirror analyser (CMA)", Surf. Interface. Anal. **24** (1996) pp.152-162

El-Gomati M. M. and Mathew J. A. D. "Scanning low energy loss microscopy (SLEEM)", J. Micros. **147** (1998) Pt2, pp.137-147

El-Gomati M. M. Mullerova I. Frank L. "Combination of scanning Auger and very low energy electron microscopy", Proceeding of the International Centennial Symposium on the Electron, Cambridge (1997) pp.326-333

El-Gomati M. M. Wells T. C. R. Frank L. Mullerova I. "On the imaging of semiconductor doping using low energy electron microscopy", 12th Eur. Congr. El. Microscopy, Brno, **2** (2000) pp.635-636

El-Gomati M. M. and Wells T. C. R. "Very-Low energy electron microscopy of dopped semiconductors", J. App. Phys. Lett. **79** (2001a) pp.2931-2933

El-Gomati M. M. and Wells T. C. R. "Imaging doped regions in a semiconductor with very low energy SEM and Auger electrons", Electron Microscopy and Analysis Group conference, EMAG 2001, Dundee, No **168** (2001b) pp.489-492

El-Gomati M. M. Wells T. C. R. and Jayakody G. H. "Very low energy electron

microscopy of doped semiconductors", Microscopy of Semiconducting Materials conference, Oxford, No **169** (2001) pp.435-438

El-Gomati M. M. Wells T. C. R. Mullerova I. Frank L. and Jayakody H. "Why is it that differently doped regions in semiconductors are visible in low voltage SEM?", IEEE Transactions on Electron Devices **51**(2),(2004) pp.288-292

El-Gomati M. Zaggout F. Jayacody H. Tear S. and Wilson K. "Why it is possible to detect regions of semiconductors in low voltage SEM: a review and update", Surf. Interface Anal. **37** (2005) pp.901- 911

Elliott S. L. **Dopant Profiling with the Scanning Electron Microscope,** PhD Thesis, (2001) University of Cambridge, UK.

Elliott S. L. Broom R. F. and Humphreys C. J. "Dopant profiling with the scanning electron microscope- A study of Si", J. Appl. Phys. **91**(11), (2002) pp.9116-9122

Elliott S. L. Broom R. F. and Humphreys C. J. "Enhanced SEM doping contrast on an H-passivated silicon surface", EUREM 12, Brno, Czech Republic (2000) pp. 609-610

Farrow R. C. Maher D. M. Ellington M. B. Katz A. and Weir B. E. J. Scanning Microsc. 13 Suppl.1 (1991) I-45

Feenstra R. M. Yu E. T. Woodall M. Kirchner P. D. Lin C. L. and Pettit G. D. "Cross-sectional imaging and spectroscopy of GaAs doping superlattice by scanning tunneling microscopy", Appl. Phys. Lett. **61** (1992) pp.795-797

Frank L., Müllerová I. El-Gomati M. M. and Jayakody H. Proceedings Japanese-Polish Joint Seminar on Material Analysis, Toyama, (2002) p.9

Frank L. and Müllerová I. "Strategies for low and very low energy SEM", J. Electron Microsc. **48** (1999) pp. 205-219

Frank L. Müllerová I. Faulian K.and Bauer E. "The scanning low-energy electron

microscope: first attainment of diffraction contrast in the scanning electron microscope". Scanning, **21** (1999) pp. 1-13

Frank L. Müllerová I. and El Gomati M. M. "A novel in-lens detector for electrostatic scanning LEEM mini-column", Ultramicroscopy, **81** (2000) pp.99-110.

Frank L. Müllerová I. Dimitrii A. Gloskovskii A. Neppjko S. A. Elmers Hans-J. and Schonhense G. "The origin of contrast in the imaging of doped areas in silicon by slow electrons", J. Appl. Phys. **100**(2006) pp. 093712(1-5)

Frank L. "Advances in scanning electron microscopy", in: Advances in Imaging and Electron Physics, ed. P. W. Hawkes, **123**, Elsevier (2002), pp. 327-373.

Frank L. Matsuda K. Hrnčiřík P. and Müllerová I. "Low energy contrast of metal matrix composite in SEM". Microscopy and Microanalysis **9** [Sup. 3] (2003) pp. 328-329.

Frank L. Zadražil M. and Müllerová I. "Scanning electron microscopy of nonconductive specimens at critical energies in a cathode lens system", Scanning, **23** (2001) pp 36-50.

Futamoto M. Hanbucken M. Harland C. J. Jones G. W. and Venables J. A. "Visualisation of submonolayers and surface topography by biased secondary electron imaging: Application to Ag layers on Si and W surfaces", Surf. Sci. **150** (1985) pp.430-450

Goeckner M. J. Felch S. B. Fang Z. Oberhofer A. Chia V. K. F. Mount G. R, Poulakos M. and Keenan W. A. "Profiling of ultrashallow junctions", J. Vac. Sci. Technol. B **18**(1) (2000) pp.472-476

Goldstein J. I. Newbury D. E. Echhlin P. Joy D. C. Fric C. and Lifshin E. **Scanning Electron Microscopy and X-Ray Microanalysis** (1981), Plenum Press, NewYork.

Grasserbauer M. and Werner H. J. "X-ray photoelectron spectroscopy (XPS)", in Analysis of Microelectronic Materials and Devices, Pireaux J. J. and Sporken R. J. Wiley, Chichesterter (1991) pp.111-115

Heimbrook L. A. Baiocchi F. A. Bittner T. C. Geva M. Luftman H. S. and Nakahara S. "Practical prospective of shallow junction analysis", J. Vac. Sci. Technol. B **14** (1996) pp.202-212

Heintze M. Catana A. Schmid P. E. Levy F. Stadelmann P. and Weiss P. J. Appl. Phys. **23** (1990) pp.1076-1081

Henning A. K. Hochwitz T. Slinkman J. Never J. Hoffmann S. Kaszuba P. and Daghlian C. "Two-dimensional surface dopant profiling in silicon using scanning Kelvin probe microscopy", J. Appl. Phys. **77** (1995) pp.1888 -1896

Hellemans L. "Assessing the performance of two-dimensional dopant profiling techniques", J. Vac. Sci. Technol. B **22**(1), (2004) pp.385-393

Horvath Z. J. Adam M. Szabo I. Serenyi M. and Tuyen V. Van, "Modification of Al/Si interface and Schottky barrier height with chemical treatment", Appl. Surf. Sci. **190** (1), (2002) pp. 441-444

Iwakuro H. Inoue T. and Kuroda T. "High-barrier Schottky diodes on n-type Si(100) due to hydrogen plasma", Jpn. J. Appl. Phys. **30** (1991) pp. L255-L257

Iwakuro H. Tokonami M. Kuroda T. Tamaki S. and Kitatsuji Y. "Interfacial layers of high-barrier Schottky diode of Al/n-type (100)Si exposed to H_2 plasma", Jpn. J. Appl. Phys. **32** (1993) pp. 5487-5495

Iwami M. and Hiraki A. Jpn. J. Appl. Phys. **53**(1982) p. 6308

Jaeger R. C. **Introduction to Microelectronic Fabrication** (1988), Addison Wesley, Canada

Jayakody G. H. **Low and Very Low Voltage SEM Contrast from Doped Semiconductors,** Ph.D Thesis, University of York, 2003

Jayakody G. H. and El-Gomati M. M. "SE dopant contrast in LVSEM: The effects of

surface and vacuum conditions", Inst. Phys. Conf. Ser. No179, EMAG (2003), Oxford

Johnson M. B. Albrektsen O. Feenstra R. M. and Salemink H. W. M. "Direct imaging of dopants in GaAs with cross-sectional scanning tunnelling microscopy", Appl. Phys. Lett. **63** (1993) p.2923

Johnson M. B. Meier H. P. and Salemink H. W. M. "Dopant and carrier profiling in modulation-doped GaAs multilayers with cross-sectional scanning tunnelling microscopy", Appl. Phys. Lett. **63** (1993) pp.3636-3638

Joy D. C. "Beam interactions, contrast and resolution in the SEM", J. Microscopy, **136** (1984) pp.241-258

Joy D. C. "Resolution in low voltage scanning electron microscopy", J. Microscopy, **140** (1985) pp. 283-292

Joy D. C. "Low voltage scanning electron microscopy", Proceedings EMAG **87**(1987)

Joy D. C. "Control of charging in low voltage SEM", J. Scanning, **11** (1988) pp.1-4

Joy D. C. Joy C. S. and Bunn R. D. "Measuring the performance of scanning electron microscope detectors. Scanning, **18** (1996) pp.533-538

Kazemian P. Rodenburg C. and Humphreys C. J. "Effect of experimental parameters on doping contrast of Si p-n junctions in a FEG-SEM", Microelectronic Engineering 73-74: 948-953 Sp. Iss. SI June 2004

Kazemian P. Schonjahn C. Humphreys C. J. "Quantitative doping contrast profiling of p-n junctions in Si with the scanning electron microscope", Institute of Physics conference Series, **180** (2003) pp.590596

Kikukawa A. Hosaka S. and Imura R. "Silicon pn junction imaging and characterizations using sensitivity enhanced Kelvin probe force microscopy," Appl.

Phys. Lett. **66** (1996) p.3510

Kopanski J. J. Marchiando J. F. and Rennex B. G. "Comparison of experimental and theoretical scanning capacitance microscope signals and their impact on the accuracy of determined two-dimensional carrier profiles", J. Vac. Sci. Technol. B **20**(5), (2002) pp. 2101-2107

Kordic S. Van Loenen E. J. and Walker A. "Two-dimensional imaging of cleaved Si p-n junctions with 30-nm resolution using a UHV scanning tunnelling microscope", IEEE Electron Device Lett. **12** (1991) pp.422-424

Kronik L. and Shapira Y. "Surface photovoltage phenomena: theory, experiment and applications", Surf. Sci. Reports. **37** (1999) pp.1-206

Lappacher C. Zerweck U. Teich S. Beyreuther E. Otto T. Grafstrom S. and Eng L. M. "FM demodulated Kelvin probe force microscopy for surface photovoltage tracking", Nanotechn. **16** (2005) S1-S6

Lenc M. and Müllerová I. "Electron optical properties of a cathode lens", Ultramicroscopy, **41** (1992) pp. 411-417

MaÈckel R. BaumgaÈrtner H. and Ren J. "The scanning Kevin microscope", Rev. Sci. Instrum. **64** (1993) pp. 694-699.

McGuire G. E., **Auger Electron Spectroscopy Reference Manual** (1979), Plenum, New York

Merli P.G. Corticelli F. and Morandi V. "Images of dopant profiles in low–energy scanning transmission electron microscopy", Appl. Phys. Lett. **81**(24), (2002) pp.4535-4537

Montgomery V. Williams R. H. and Rsivastava G. P. "The influence of adsorbed layers in controlling Schottky barriers", J. Phys. C: Solid- St. Phys **14**, (1981) L191

Morita M. Ohmi T. Hasegawa E. Kawakami M. and Ohwada M. "Growth of native oxide on a silicon surface", J. Appl. Phys. **68**(3), (1990) pp. 1272-1281

Müllerová I. "Imaging of specimens at optimized low and very low energies in scanning electron microscopy", Scanning Microscopy, **13**(1), (1999) pp.7-22

Müllerová I. El-Gomati M. M. and Frank L. "Imaging of the boron doping in silicon using low energy SEM", Ultramicroscopy, **93** (2002) p.223.

Müllerová I. and Lenc M. "Some approaches to low voltage scanning electron microscopy", Ultramicroscopy, **41** (1992a) pp. 399-410.

Müllerová I. and Lenc M. "The scanning very-low energy electron microscope (SVLEEM)", Mikrochim Acta [Suppl] **12** (1992b) pp. 173-177.

Müllerová I. and Frank L. "Multidimensionality of the scanned imaging with very low energy electrons", G.I.T. Imaging and Microscopy **2** (2), (2000) pp. 20-23.

Munakata C. and Shimizu H. "Fixed oxide charge in n-type silicon wafers studied by ac surface photovoltage technique", Semicond. Sci. Technol. **15** (2000) pp. 40-43

Nabhan W. Equer B. Broniatowski A. and De Rosny G. "A high-resolution scanning Kelvin probe microscope for contact potential measurements on the 100nm scale", Rev. Sci. Instrum. **68**(1997) pp. 3108 -3111

Nie H.Y. Horiuchi K. Yamauchi H. and Masai J. "Local surface potential measurement of Pd/GaAs contact and anodized aluminum films using scanning probe microscopy", Nanotechno, **8** (1997) A24-A31.

Ogura K. "Observation of $GaAs/Al_xGa_{1-x}As$ superlattice by backscattered electron image obtained with an ultrahigh-resolution SEM", JEOL news, **29E** (2), (1991) pp.26-31

Ogura K. Ono A. Franchi S. Merli P. G. and Migiori A. "Observation of GaAs/AlAs

superlattice structures in both secondary and backscattered electron imaging modes with ultrahigh resolution scanning electron microscope", Proceedings of the XIIth International Congress for Electron Microscopy, (1990), San Francisco.

Paden R. S. and Nixon W. C. "Retarding field scanning electron microscopy", J. Sci. Instrum. **1** series2 (1968)

Park R. L. and Den Boer M. L. **In chemistry and Physics of Solid Surfaces** (1977), eds. Vanselow and Tong, Claveland: CRC, pp.191-203

Parker J. H. and Warren R.W. "Kelvin device to scan large areas for variations in contact potential", Rev. Sci. Instrum. **33** (1962) pp. 948-950.

Pawley J. B. "Practical aspects of high-resolution LVSEM", Scanning, **12** (1990) pp.247-252

Perovic D. D. Castell M. R. Howie A. Lavoie C. Tiedje T. and Cole J. S. W. "Field – emission SEM imaging of compositional and dopping layer semiconductor superlattices", Ultramicroscopy, **58** (1995) pp.104-113

Perovic D. D. Turan R. and Castell M. R. "Quantitative imaging of semiconductor doping distributions using a scanning electron microscope", The Int. centennial Symposium on the Electron (IOM Communications, London) (1998) pp. 258-265

Peters K. P. "Generation, collection and properties of an SE(1) enriched signal suitable for high resolution SEM on bulk specimens", Proc. of Asilomar Conf. (1982) New York

Pireaux J. J. and Sporken R. edited by Grasserbauer M. and Werner H. W. **Analysis of Microelectronic Material and Devices**, ch(2.1), Wiley (1991).

Poate J. M. Milo J. "Thin films interdiffusion and reactions", edited by Poate, Milo J. Tu K. W. and Mayer J. W. New York Chichester Wiley (1987)

Prutton M. and El Gomati M. M. **Scanning Auger Euger Electron Microscopy,**

Chichester, Wiley (2006)

Rau W. D. Schwander P. Baumann F. H. Hoppner W. and Ourmazd A. "Two dimensional mapping of the electrostatic potential in transistors by electron holography", Phys. Rev. Lett. **82** (12), (1999) pp. 2614-2617

Reimer L. **Scanning Electron Microscopy** (1985), Springer, Berlin.

Reimer L. **Scanning Electron Microscopy** (1998), (2nd edn), Springer, Berlin.

Reimer L. and Tolkamp C. "Measuring the backscattering coefficient and secondary electron yield inside a SEM, Scanning, **3**(1980) p. 35

Rhoderick E. H. and Williams R. H. **Metal–Semiconductor Contacts** (1988), (2nd edn), Oxford, Clarendon press, ch.5

Sar-El H. Z. "Cylindrical capacitor as an analyzer I. Nonrelativistic part", Rev. Sci. Instrum. **38** (1967) pp.1216-1210

Schonjahn C. Broom R. F. Humphreys C. J. Howie A. and Mentink S. A. M. "Optimizing and quantifying dopant mapping using a scanning electron microscope with a through-the –lens detector", Appl. Phys. Lett. **83**(2), (2003) pp. 293-295

Schonjahn C. Humphreys C. J. and Glick M. "Energy-filtered imaging in a field emission scanning electron microscope for dopant mapping in semiconductors", J. Appl. Phys. **92** (12), (2002) pp.7667-7671

Schroeder D. K. **Semiconductor Material and Device Characterization,** (1990), Wiley, New York

Seah M. P. "Measurement: AES and XPS", J. Vac. Sci. Technol. A **3**(3), (1985) pp.1330- 1337

Sealy C. P. Castell M. R. Reynolds C. L. and Wilshaw P. R. "Application of secondary

electron dopant contrast imaging to InP/ InGaAsP laser structures", Inst. Phys. Conf. Ser.157 (1997) pp.561-564

Sealy C. P. Castell M. R. and Wilshaw P. R. "Mechanism for secondary electron dopant contrast in the SEM", J. Elec. Microsc. **49**(2), (2000) pp. 311-321

Seiler H. "Secondary electron emission in the scanning electron microscope". J. Appl. Phys. **54** (11): R1-R18 (1983).

Shannon J. M. "Increasing the effective height of a Schottky barrier using low energy ion implantation", Appl. Phys. Lett. **25**(1), (1974) pp. 75-77

Shannon J. M. "Control of Schottky barrier height using highly doped surface layers", J. Solid-St. Electron. **19** (1976) p.537

Sheng T. T. and Marcus R. B. "Delineation of shallow junctions in silicon by Transmission Electron Microscopy", J. Electrochem. Soc. **128** (1981) pp. 881-884

Shimizu R. "Secondary electron yield with primary electron beam of kilo-electron volts", J. Appl. Phys. **45** (1974) pp.2107-2111

Siegbahn K. Norlding C. Fahlhan A. Nordberg R. Hamrin K. Hedman J. Johansson G. Bergmark T. Karlsson S. E. Lindgren J. and Lindberg B. *ESCA* , " Atomic, molecular and solid state structure studied by means of electron spectroscopy", Almqvist and Wiksells, Uppsala(1967)

Stewart R. L. "Insulating films formed under electron and ion bombardment", Phys. Rev. **45** (1934) pp.488-490

Stradling R. A. and Klipstein P. C. **Growth and Characterisation of Semiconductors.** (1990) Adam Hilger, Bristol

Streetman Ben G. **Solid State Electronic Devices** (1995), New Newsy, pp. 80-81.

Subrahmanyan R. "Methods for the measurement of two-dimensional doping profiles", J. Vac. Sci. Technol. B **10**(1), (1992) pp.358-367

Sze S. M. **Physics of Semiconductor Devices** (1981), (2nd edn). J. Wiley& Sons: New York

Sze S. M. **Semiconductor Devices-physics and technology** (1985), Wiley press, NewYork.

Tanimoto M. and Vatel O. "Kelvin probe force microscopy for characterization of semiconductor devices and processes", J. Vac. Sci. Technol. B **14**, (1996) pp. 1547-1551

Taubenblatt A. M. and Helms C. R. "Silicide and Schottky barrier formation in the Ti-Si and the Ti-SiOx -Si systems", J. Appl. Phys. **53** (9), (1982) pp.6308-6315

Thomas Ch. Joachimsthaler I. Heiderhoff R. and Balk L. J. "Electron-beam-induced potentials in semiconductors: calculation and measurement with with an SEM/SPM hybrid system", J. Phys. D. Appl. Phys. **37**(2004) pp. 2785-2794

Turan R. Perovic D. D. and Houghton D. C. "Mapping electrically active dopant profiles by field emission scanning electron microscopy", Appl. Phys. Lett. **69** (11), (1996) pp.1593-1595

Twitchett A. C. Dunin-Borkowski R. E. and Midgley P. A. "Quantitative electron holography of biased semiconductor devices", Phys. Rev. Lett. **88** (23), (2002) pp.238302(1-4)

Tyagi M. S. **Introduction to semiconductor materials and devices** (1991) Wiley, Canada, ISBN 0-471-60560-3

Vandervorst W. Clarysse T. Vanhellemont J. Rodriguez A. R. "Two-dimensional carrier profiling", J. Vac. Sci. Technol. B **10**(1), (1992) pp. 449-455

Vandervorst W. Clarysse T.and Smith H. E. "Influence of the substrate doping level on spreading resistance profiling", J. Vac. Sci. Technol. B **14**(1), (1996) pp. 404-407

Vandervorst W. Eyben P. Callewaert S. Hantschel T. Duhayon N. Trenkler M. Xu. and Clarysse T. "Towards routine quantitative two-dimensional carrier profiling with scanning spreading resistance microscopy", Characterisation and Metrology for ULST Technology: (2000) International conference, pp.613-619

Vatel O. and Tanimoto M. "Kelvin probe force microscopy for potential distribution measurement of semiconductor devices", J. Appl. Phys. **77**(6),(1995) pp.2358-2362

Venables D. and Maher D. M. "Quantitative two dimensional dopant profiles obtained directly from secondary electron images", J. Vac. Sci. Technol. B **14**(1), (1996) pp. 421-425

Venables D. and Jain H. and Collins D. C. "Secondary electron imaging as a two-dimensional dopant profiling technique: Review and update", J. Vac. Sci. Technol. B **16**(1), (1998) pp.362-366

Williams C. C. Annual Review of Materials Science, 1999, **29**; 471-504 (Volume publication date August 1999) (doi: 10.1146/ annurev.matsci.29.1.471)

Williams C. C. Slinkman J. Hough W. P. and Wickramasinghe H. K. "Lateral dopant profiling on a 100 nm scale by scanning capacitance microscopy", J. Vac. Technol. A **8** (2), (1990) pp. 895-898

Woodruff D. P. and Delchar T. A. **Modern Techniques of surface Science**, (1990), (2^{nd} edn), Cambridge University Press, Cambridge

Yu E. T. Johnson M. and Halbout J. M. "Electrical profiling of Si (001) p-n junctions by scanning tunneling microscopy", Appl. Phys. Lett. **61** (2), (1992) pp. 201-203

Zaggout F. and El-Gomati M. "The effect of barrier height variations in Alloyed Al-Si Schottky barrier diodes on secondary electron contrast of doped semiconductors", Proc.

of the 14th Conference of Microscopy of Semiconducting Materials, Oxford (2005) pp.523-526

Zangwill A. **Physics at Surfaces** (1988), Cambridge University Press, Cambridge.

http://www.jhu.edu/~chem/fairbr/surfacelab/xps.html